NUMERICAL SIMULATION OF FREE CONVECTIVE HEAT TRANSFER FROM A SPHERE

by

FARAMARZ GEOOLA, M.Sc.(Eng.), D.I.C.

May, 1976

A thesis submitted for the degree
of Doctor of philosophy of the
University of London

Department of Chemical Engineering
and Chemical Thecnology,
Imperial College of Science and
Technology,
London, S.W.7

ABSTRACT

A theoretical study of time-dependent free convective heat transfer from a solid sphere to an incompressible Newtonian fluid has been carried out for Grashof numbers between 0.05 and 12500 and for Prandtl numbers of 0.72, 10, and 100.

The time-dependent Navier-Stokes equation for axisymmetric flows was expressed in terms of a time-dependent vorticity transport equation and a stream function equation. These equations together with the time-dependent energy equation were transformed from polar space to rectangular space. These three equations were then solved simultaneously.

For purposes of computation, the equations which were elliptic second-order partial differential equations with respect to space variables and parabolic with respect to time, were replaced by appropriate finite-difference approximations in which an upwind differencing scheme was applied to the convective terms of the transport equations. The time-dependent energy equation and the time-dependent vorticity transport equation were solved using Peaceman and Rachford's alternating direction implicit method and the stream function equation was solved using point iterative successive over-relaxation.

A computer programme was developed to solve the finite-

difference equations for a wide range of Grashof and Prandtl numbers. The solutions, which were obtained in the form of distributions of temperature, vorticity and stream function, were used to calculate the local and average Nusselt numbers, the surface pressure and the drag coefficients.

Numerical solutions were obtained for Grashof numbers of 0.05, 1, 10, 25, 50 and 125 for a Prandtl number of 0.72. Solutions were also obtained for Grashof numbers of 1250 and 12500 for a Prandtl number of 10; and for a Grashof number of 50 and a Prandtl number of 100.

From the late-time steady state solutions it was observed that even at extremely low Grashof numbers, weak convection processes were present in the region close to the outer boundary. However, it was found that even at moderate Grashof numbers the dominant mode of vorticity transport close to the surface of sphere was by diffusion. For all the solutions obtained it was observed that during the early stages of simulation the dominant mode of vorticity transport was by diffusion and that heat transfer took place largely by unsteady state conduction. The drag coefficients reached their late-time steady state values in a shorter time than the other quantities and the local Nusselt numbers took the longest time to reach their late-time steady state values. The late-time steady state values obtained for the average Nusselt number were found to be in reasonable agreement with the experimental measurements obtained by previous workers.

To Hadji Agha and Maman

ACKNOWLEDGEMENTS

I would like to express my sincere thanks and gratitude to Dr. A.R.H. Cornish for his constant interest, guidance and encouragement throughout the course of this study.

The studentship award received from the Reza Pahlavi Cultural Foundation is gratefully acknowledged.

Thanks are also due to the staff of Chemical Engineering and Chemical Technology Department Computer Service and to the staffs of the Imperial college and University of London Computer Centres for their willing help and assistance in running the computer programme.

Thanks are also extended to all my Imperial College colleagues, especially Mr. A.A. Ghandi and Mr. D. Abi-zadeh for their friendship and for the many useful discussions I had with them and for their criticisms.

Finally, I must express my profound appreciation to the members of my family, Farhad, Sina, Nahid and, in particular, to my parents for their encouragement, patience and generous help in many ways.

Faramarz Geoola

LIST OF CONTENTS

PAGE

LIST OF SYMBOLS

SYMBOL	EXPLANATION OR DEFINING EQUATION
a	Coefficient defined by equation (3.3.41)
a_{1i}, a_{2i}, a_{3j}, a_{4j}, a_{5ij}	Coefficients in equation (3.5.3)
$\overline{A}$	Arbitrary vector quantity
b_{1i}, b_{2i}	Coefficients defined by equations (3.3.37) and (3.3.38)
b_{3j}, b_{4j}	Coefficients defined by equations (3.3.39) and (3.3.40)
$\overline{B}$	Arbitrary vector quantity
c_i	Coefficient defined by equation (3.3.67)
C_{DF}	Viscous or friction drag coefficient defined by equation (C.3.1)
C_{DP}	Pressure or form drag coefficient defined by equation (C.2.1)
C_{DT}	Total drag coefficient
C_P	Specific heat at constant pressure
C_R	Coefficient defined in equation (3.3.43)
C_{1i}, C_{2i}, C_{3i}	Coefficients defined by equations (3.3.27), (3.3.28) and (3.3.29)
C'_{1i}, C'_{2i}, C'_{3i}	Coefficients defined by equations (3.3.33), (3.3.34) and (3.3.35)
C_{1j}, C_{2j}, C_{3j}	Coefficients defined by equations (3.3.24), (3.3.25) and (3.3.26)

SYMBOL	EXPLANATION OR DEFINING EQUATION
C'_{1j}, C'_{2j}, C'_{3j}	Coefficients defined by equations (3.3.30), (3.3.31) and (3.3.32)
C_{4ij}	Coefficient defined by equation (3.3.36)
D	Differential operator defined by equation (E.3.2)
D_F	Skin friction drag force defined by equation (C.3.2)
D_P	Pressure drag force defined by equation (C.2.2)
D_T	Total drag force
$D_i^{n+\frac{1}{2}}$	Coefficient defined by equation (3.3.23)
D_j^n	Coefficient defined by equation (3.3.21)
$\bar{e}_1$, $\bar{e}_2$, $\bar{e}_3$	Unit tangent vector in the directions X_1, X_2 and X_3
E	Specific internal energy
E^2	Differential operator defined by equation (2.5.9)
E_+^2	Differential operator defined by equation (2.5.9)
$\bar{F}$	Body force vector
F_r, F_Θ, F_Φ	Components of body force in the r, Θ and Φ - directions
F_{1i}, F_{2i}, F_{3i}	Coefficients defined by equations (3.3.56), (3.3.57) and (3.3.58)

SYMBOL	EXPLANATION OR DEFINING EQUATION
F'_{1i}, F'_{2i}, F'_{3i}	Coefficients defined by equations (3.3.62), (3.3.63) and (3.3.64)
F_{ij}, F_{2j}, F_{3j}	Coefficients defined by equations (3.3.53), (3.3.54) and (3.3.55)
F'_{1j}, F'_{2j}, F'_{3j}	Coefficients defined by equations (3.3.59), (3.3.60) and (3.3.61)
$\bar{g}$	Gravitational acceleration vector
g_r, g_Θ	Components of the gravitational acceleration in the r and Θ directions
G	Modified vorticity defined as $G = \zeta r \sin\Theta$
G^*	Dimensionless Modified vorticity (GR/ν)
Gr	Grashof number based on the radius of the sphere $G = \frac{R^3 \beta g(T_s - T_\infty)}{\nu^2}$
Gr_d	Grashof number based on the diameter of the sphere $Gr_d = \frac{(2R)^3 \beta g(T_s - T_\infty)}{\nu^2}$
h	Mesh size in the Z-direction
$\bar{h}$	Average or overall heat transfer coefficent
h_1, h_2, h_3	Scale factors in the directions X_1, X_2 and X_3
$h(\Theta)$	Local heat transfer coefficient
h_{3ij}	Function defined in equation (3.3.43)
IN1	Number of mesh lines in the Z-direction

SYMBOL	EXPLANATION OR DEFINING EQUATION
JN1	Number of mesh lines in the Θ direction
k	Mesh size in the Θ direction
k_T	Thermal conductivity
K_o	Dimensionless pressure coefficient at the front stagnation point
K_Θ	Local dimensionless pressure coefficient
K_π	Dimensionless pressure coefficient at the rear stagnation point
KG_{ij}	Coefficient defined by equation (3.3.44)
KT_{ij}	Coefficient defined by equation (3.3.43)
n_1	Exponent of Gr in equation (4.12.1)
n_2	Exponent of Pr in equation (4.12.1)
$\overline{Nu}$	Average or overall Nusselt number defined by equation (D.2.7)
Nu_Θ	Local Nusselt number defined by equation (D.1.4)
P	Pressure
P_{ij}	Ageneral working variable
Pr	Prandtl number ($C_p\mu/k_T=\nu/\alpha$)
$\overline{q}$	Heat flux vector
q_r, q_Θ , q_Φ	Components of heat flux in the r, Θ and Φ - directions

SYMBOL	EXPLANATION OR DEFINING EQUATION
Q_T	Heat flow rate
(r, θ, ϕ)	Spherical polar coordinates
r^*	Dimensionless radial coordinate (r/R)
r_∞	Radius of the outer boundary
R	Radius of the sphere
Ra	Rayleigh number based on the radius of the sphere (Ra = GrPr)
Ra_d	Rayleigh number based on the diameter of the sphere ($Ra_d = Gr_dPr$)
$R_i^{n+\frac{1}{2}}$	Coefficient defined by equation (3.3.52)
R_j^n	Coefficient defined by equation (3.3.50)
S	Surface area
t	Time
t^*	Dimensionless time $(\frac{t\nu}{R^2})$
T	Temperature
T^*	Dimensionless temperature $(\frac{T-T_\infty}{T_s-T_\infty})$
u_1, u_2, u_3	Velocity components in the X_1, X_2 and X_3 - directions
u_r, u_θ, u_ϕ	Velocity components in the r, θ and ϕ - directions
u_r^*, u^*_θ	Dimensionless velocity components in the r and θ - directions $(\frac{u_r R}{\nu}, \frac{u_\theta R}{\nu})$
u_z, u_θ	Velocity components in the z and θ directions

SYMBOL	EXPLANATION OR DEFINING EQUATION
$\bar{U}$	Velocity vector
W	A general continuous function
X_1, X_2, X_3	Orthogonal curvilinear coordinates
X_i	Coefficient defined by equation (3.3.42)
Y_1, Y_2, Y_3	Rectangular cartesian coordinates
Y_2	Distance of a point from the axis of symmetry Y_3
Y_3	Axis of symmetry
Z	Modified coordinate defined as $Z = \ln r^*$

GREEK SYMBOL

α	Thermal Diffusivity $(k_T/\rho C_p)$
Δ	Difference operator defined by equation (E.3.1)
ε_G	Convergence criterion for the surface vorticity
ε_T	Convergence criterion for the temperature along the axis of symmetry
ε_ψ	Convergence criterion for the stream function
$\varepsilon_{W^n_{i,j}}$	The error of approximation defined by equation (3.5.1)
ζ	Vorticity

GREEK SYMBOL	EXPLANATION OR DEFINING EQUATION
ζ^*	Dimensionless vorticity ($\zeta R^2/\nu$)
Θ	Angular coordinate
μ	Fluid viscosity
ν	Fluid kinematic viscosity
ρ	Fluid density
τ	Stress term in a Newtonian fluid
Φ	Coordinate representing the angle of rotation about the axis of symmetry Y_3
φ	Arbitrary scalar quantity used in appendix A
Φ_D	Rate of heat generation per unit volume by viscous dissipation
ψ	Stream function
ψ^*	Dimensionless stream function ($\psi/\ \nu R$)
$\bar{\omega}$	Vorticity vector
ω_G	Relaxation factor for the surface vorticity
ω_T	Relaxation factor for the temperature along the axis of symmetry
ω_Z	Weighting factor defined in equation (3.2.11)
ω_Θ	Weighting factor defined in equation (3.2.12)
ω_ψ	Relaxation factor for the stream function

GREEK SYMBOL	EXPLANATION OR DEFINING EQUATION
∇	Vector operator 'del'
SUBSCRIPT	
i	Mesh point index in the Z-direction (figure 3.2.1)
j	Mesh point index in the θ-direction (figure 3.2.1)
i,j	Indices of a mesh point in the flow region (figure 3.2.1)
r	r - direction
S	Sphere surface
Z	Z - direction
∞	Outer boundary condition
SUPERSCRIPT	
n	nth time-step
r	rth iteration
*	Dimensionless variable
$\_$	Vector quantity

LIST OF FIGURES

LIST OF TABLES

CHAPTER 1

INTRODUCTION AND LITERATURE SURVEY

1.1 INTRODUCTION

The process of heat transfer by free convection is encountered frequently in industrial applications such as steam boilers, digesters, furnaces, as well as being a mode of transfer by which heat losses from pipes, boilers, etc. takes place. In general, free convective heat transfer becomes an important mode of heat transer in any situation in which a hot body is immersed in an otherwise stationary medium or in any moving medium in which changes of density induced by temperature gradients will disturb appreciably the fluid motion.

Because of its considerable importance in many engineering applications the fundamentals of mass or heat transfer from solid particles, drops, or bubbles to a continuous fluid phase have long attracted the attention of investigators. The study of mass and heat transfer from a single sphere together with the associated fluid dynamics has been used as a first step in the analysis of multiparticle systems.

For many engineering design problems, experimental correlations are available for the prediction of average heat or mass transfer rates. However, the optimum design of chemical process equipment requires an understanding of the basic mechanisms of heat, mass, and momentum transfer which these correlations do not provide. Such detailed knowledge could be provided in part by extensive experimentation but in many cases it could only be obtained or

supplemented from a study of the solutions of the equations which describe heat, mass, and momentum transfer. Such solutions would not only provide fundamental insight into transport processes but also increase our ability to analyse and solve complex engineering problem.

The theoretical problem of free convective heat transfer from the surface of a body can be expressed using the equations which describe the conservation of momentum, mass, and energy. These equations form a complex set of interdependent partial differential equations which are very difficult to solve. Because of the complexity of these equations it has nearly always been necessary to simplify them by the introduction of simplifying assumptions.

When the changes in the density of the fluid which arise because of temperature variations are very small, the equations of motion and continuity can be solved independently of the energy equation and the solutions used in order to solve the energy equation. This is the usual situation which arises under conditions of forced convection. However, free convection differs from forced convection in that the buoyancy term which appears in the equation of motion, gives rise to, or disturbs, fluid motion. In this case, the energy equation has to be solved simultaneously with the momentum and continuity equations.

The set of interdependent partial differential equations which describes free convective heat transfer is non-linear and it is not possible to find exact analytical solutions even when the fluid is Newtonian. Hence, solutions must be

obtained numerically.

Methods of solving non-linear partial differential equations, in contrast to those for linear equations, are not highly developed.

In fluid dynamics and heat transfer problems the dependent variables are generally functions of three space variables and a time variable. If it is supposed that at large times a steady state is reached such that the dependent variables no longer depend on time and that this steady state is of primary interest, then there are two alternative methods of attacking the problem; the steady state equations can be solved directly or the unsteady state equations can be solved as a function of time and the solutions obtained up to and including sufficiently large time values of the time variable. In the steady state method the dependent variables are dependent only upon the space variables. In the time-dependent method, the equations are written as an initial value problem in which the dependent variables are calculated as functions of space and time.

Roache (1972) has summarised the comparison between the iterative steady state and time-dependent methods as fallows:

"Some steady state methods, with under - and over - relaxation adjustments being equivalent to time-step changes. Most steady state iterative methods are at least analogous to time-dependent methods. In any case, the analogy illustrates that steady state iterative methods can not be presumed to be

stable, and should be analysed for stability through the von-Neumann analysis". Roache also pointed out that "the explicit time-dependent methods; ....., are less suceptible to non-linear instabilities and are thereby less sensitive to initial conditions. The time-dependent formulation offers the flexibility of obtaining the transient solution if it should be desired; more important, it does not presume the existence of a steady state solution, which indeed may not exist. There is a philosophical and even aesthetic attraction in modelling the actual physical process which is, after all, fundamentally time-dependent". Proof of the existence of solutions is somewhat less of a problem if an unsteady state method is used: this method has proved to be generally successful for viscous flow problem. Since there is some confidence in the validity of the time-dependent equations of motion and energy, one is inclined to believe that a numerical solution which proceeds from a physically reasonable initial condition also has validity.

In view of the difficulties involved in solving non-linear partial differential equations together with reasons given above, the unsteady method was used throughout this work.

The numerical solution of the equations which describe time-dependent free convective heat transfer from a sphere is one of the most challenging problems in numerical analysis. However, the availability of high capacity computers invites

further consideration of the problem so that the present study is timely.

The particular problem which is studied in this thesis was initiated in order to make a theoretical investigation of time-dependent free convective heat transfer from a solid sphere to a Newtonian fluid.

The equation of motion for an incompressible Newtonian fluid is the well known Navier-Stokes equation. Since the flow around a solid sphere is axisymmetric the problem is two-dimensional so that the Navier-Stokes equation can be combined with the continuity equation and expressed in the form of a stream function equation and a time-dependent vorticity transport equation. The stream function, vorticity transport, and energy equations are solved simultaneously. As is shown later in this thesis, the energy equation is of the same classification as the vorticity transport equation so that both equations can be solved using the same method.

The method of solution is numerical; a set of finite-difference equations are obtained by the expansion of the terms in the original partial differential equations using Taylor's series. Each finite-difference equation relates the values of the dependent variables, such as vorticity, stream function, and temperature to the values of the same variables at the neighbouring mesh points. The vorticity transport and energy equations are solved using Peaceman and Rachford's alternating direction implicit, (ADI), method

(1955). Although, the method chosen complicates the updating of the vorticity and temperature fields with respect to time, it has good numerical stability and is known to be accurate and economical in computational time in comparison with other explicit or iterative implicit methods. The sets of simultaneous algebraic equations obtained by application of the method are solved using Thomas's elimination method as presented by Lapidus (1962). The stream function equation is solved using point iterative successive over relaxation, (SOR).

It is difficult to estimate the accuracy of the solution procedure because of the complexity of the equations. At present a complete error analysis of the solution is not possible. However, the forms of the errors introduced are known and a qualitative estimate of the accuracy of the solutions can be obtained by comparing the late-time steady state results with the experimental and theoretical steady state results obtained by previous workers. The late-time steady state average Nusselt numbers were found to be in reasonable agreement with the experimental results obtained by Mathers et al (1957) and yuge (1960).

A computer programme is developed in this thesis in order to solve the finite - difference equations. The distributions of temperature, stream function and vorticity which are obtained are used to calculate the local and average Nusselt numbers, the pressure distribution on the surface of sphere, and the viscous, pressure, and total drag coefficients. The computer

programme is used to obtain the time-dependent free convective heat transfer rate from a solid sphere for Grashof numbers (based on the radius of the sphere) between 0.05 and 12500 and for Prandtl numbers of 0.72, 10, and 100. These solutions were obtained using a CDC7600 digital computer.

1.2 NUMERICAL SIMULATION OF FLUID DYNAMICS

Lamb (1932) has expressed the view that theoretical fluid dynamics began with the theory of potential flow of an ideal incompressible fluid. Development of this theory extended over a long period of time during which a large class of flows was successfully analysed. However, according to the Euler - d'Alembert paradox (Birkhoff 1968), the total drag force exerted on a solid object placed in a potential flow is zero.

Theoretical analyses of viscous flows were first developed by Navier (1822) and by Stokes (1845). One of the results of their work was the development of the equation which expresses the conservation of momentum for a viscous flow. This equation, which is known as the Navier-Stokes equation, shows the importance of the viscous terms and why the potential flow theory is unable to predict drag forces correctly. However, for a long time after its development, because of its non-linear character the Navier-Stokes equation was unsolvable except for a few simplified cases.

Stokes (1851) succeeded in solving the Navier-Stokes equation for the case of very slow motion, 'creeping flow',

past a sphere. He obtained his solution by neglecting the inertial or non-linear terms.

Prandtl (1904) showed how flows of high Reynolds numbers could be analysed. He hypothesized that the flow about a solid body at high Reynolds numbers could be divided into two regions: a very thin region, or boundary layer, near the solid body in which the viscous effects are important, and a region outside this boundary layer in which the effects of viscosity are unimportant and potential flow theory applies. With the aid of this hypothesis, Prandtl succeeded in reducing the Navier-Stokes equation to a more easily solvable form. The resulting equation is known as the boundary layer equation.

At high Reynolds, Grashof, and Prandtl numbers, the simplifying assumptions of boundary layer theory have been used successfully to obtain solutions of both the Navier-Stokes equation and the energy equation. Excellent discussions of the theory and its applications are given by Schlichting (1968).

The very nature of the boundary layer equations limits their applicability to flows with a predominant direction so that they cannot be used to predict the flow pattern within the recirculatory wake behind a bluff body. Also, flows at intermediate Reynolds or Grashof numbers cannot be analysed by use of boundary layer theory because the effects of viscosity are not confined to a thin region close to the body. Further, at intermediate Reynolds and Grashof numbers the Navier-Stokes equation cannot be linearised by neglect

of the inertial terms.

It follows from the above, that for intermediate Reynolds or Grashof numbers, the Navier-Stokes equation cannot be simplified. Thus analytical solutions cannot be obtained and solutions must be obtained by numerical means.

In 1910, Richardson presented a paper to the Royal Society which may be considered to be the cornerstone of modern numerical analysis of partial differential equations. He devised an iterative method of obtaining solutions of Laplace's equation and of the biharmonic equation. He obtained error estimates and gave an accurate method of extrapolating solutions towards zero mesh size. In Richardson's iterative method for solving elliptic equations, each point in the mesh is made in turn to satisfy the finite - difference equation involving 'old' values at neighbouring points obtained from the previous iteration.

In 1918, Liebmann showed how the convergence rate could be improved greatly merely by using 'new' values as soon as they become available. An early rigorous mathematical treatment of convergence and error bounds for iterative solutions of elliptic equations by Liebmann's method was given by Phillips and Wiener in 1923.

It can be said that the first numerical solution of the partial differential equations for a viscous fluid dynamics problem was given by Thom in 1928. Thom solved the time-independent Navier-Stokes equation numerically for viscous

fluid flow past a cylinder at a Reynolds number of 10.

The first of the implicit methods, which for multidimensional problems require iterative solutions at each time step, was the Crank-Nicolson method published in 1947. In 1953, Dufort and Frankel presented their 'leapfrog' method for solving parabolic equations. Their method allows for arbitrarily large time steps (in the absence of convective terms) and has the advantage of being fully explicit.

In the mid-fifties, Peaceman and Rachford (1955) and Douglas and Rachford (1956) presented efficient implicit methods allowing arbitrarily large time steps for solving parabolic equations. These methods which are known as 'alternating direction implicit', (ADI), methods, have also been applied to elliptic equations. Alternating direction implicit methods are probably the most popular methods used for solving incompressible flow problems expressed in terms of the vorticity transport equation.

The development of digital computers has motivated further development of numerical simulation of fluid dynamics. Progress has been remarkable, both in the development of numerical techniques and in the range and variety of the different types of problems analysed. Notwithstanding this rapid development, no general numerical method for solving the Navier-Stokes equation has so far emerged. This can be attributed partly to a lack of the methods of effective error analysis of the solutions. Error analysis could form a basis for the

classification of methods (Rafique 1971).

The following section surveys existing solution for free convective heat transfer from a solid sphere.

1.3 LITERATURE SURVEY:
FREE CONVECTIVE HEAT TRANSFER FROM A SOLID SPHERE

Considerable previous effort has been given to the study of free convective heat and mass transfer. These studies have been analytical as well as experimental.

Most of the studies of free convective heat transfer have investigated heat transfer from flat plates and cylinders; relatively little work has been undertaken on transfer from sphere and particles.

As far as this author is aware, no numerical or analytical studies of time-dependent or time-independent free convective heat transfer from a solid sphere at moderate and low Grashof numbers has been carried out other than described in this thesis. The results of a few experimental studies are, however, available in which the average heat transfer coefficients were determined but the flow patterns and the temperature distributions about the body were not measured.

1.3.1 Theoretical and Experimental Studies at Low and Moderate Grashof Numbers

Mahony (1956) made a theoretical study of time-independent

free convective heat transfer for small Grashof numbers from spheres and thin wires by perturbing the steady state conduction solution. He did not determine the flow field. However, by considering the magnitudes of the various terms in the Navier-Stokes and energy equations, he was able to deduce for small Grashof numbers that convection is negligible in comparison with conduction near the body, but that it becomes as important as conduction at large distances from the body. He then concluded that for small distances from the body, i.e. for distances that are small in comparison with the dimensions of the body, the use of the conduction equation yields correct heat transfer rates. However, for large distances from the body, the heat transfer rate must be calculated from the solutions of the complete equations.

Farzetdinov (1958) proved that the solutions of the steady state equations for free convective heat transfer are unique. He obtained this result for small Grashof numbers by perturbing the steady state conduction solution.

Hossain (1966) used a perturbation analysis to study steady state laminar free convection flow and heat transfer around an isothermal sphere for Grashof numbers in the range between zero and unity and for Prandtl numbers of about unity. Solutions of the governing equations were expressed in series form with the Grashof number itself taken as the perturbation parameter. The expressions were as follows:

stream function:

$$\psi^* = Gr\psi_1^*(r,\Theta)e^{-\frac{rGr}{4}(2+\cos\Theta)} + Gr^2\psi_2^*(r,\Theta)e^{-\frac{r^3Gr}{4}(2+\cos\Theta)} + \ldots \quad (1.3.1)$$

temperature:

$$T^* = T_o^*(r,\Theta)e^{-\frac{rGr}{4}(2+\cos\Theta)} + GrT_1^*(r,\Theta)e^{-\frac{r^3Gr}{4}(2+\cos\Theta)} + \ldots. \quad (1.3.2)$$

where, ψ^* and T^* are the dimensionless stream function and temperature; Gr is the Groshof number based on the radius of the sphere, and r and Θ are the dimensionless spherical polar coordinates. He obtained the following relationship between the average Nusselt number, $\overline{Nu}$, the Grashof number, Gr, and the Prandtl number Pr;

$$\overline{Nu} = 2 + Gr + Gr^2(0.139-0.4519Pr+1.1902Pr^2) \quad (1.3.3)$$

where the first term represents the Nusselt number which arises from the contribution made by pure conduction in the absence of convective effects.

Hossain found that the thickness of disturbed region was very large for Grashof numbers slightly greater than zero but that it decreased with increasing Grashof number. He stated that the perturbation approach to free convection problems is only applicable when the value of the Grashof number is less than unity. At higher Grashof numbers he found that the expressions he had used for the stream function and temperature were highly singular at regions far away from the surface of the body.

Fendell (1968) used a perturbation analysis to study steady state free convection about a small heated isothermal sphere. He found that in an unbounded medium, an ordinary perturbation expansion in the Grashof number leads to unbounded velocities far from the sphere. However, he predicted that recirculating flow will occur within the region contained between a heated inner sphere and a concentric cold outer sphere when the ratio of the radius of the outer sphere to that of the inner sphere is less than the Grashof number, based upon the diameter of the heated sphere, raised to the minus one-half power. The fluid adjacent to the heated sphere rises while that adjacent to the outer sphere falls. Under these circumstances the problem of the existence of singularities in the velocity and temperature profiles does not exist. By using inner - and - outer matched asymptotic series expansions he was able to show that although diffusive transport is dominant near the heated sphere, convective transport is dominant away from the sphere. Fendel did not make any calculations of the flow field.

Numerous experimental studies of free convection at very low and moderate Grashof numbers have been carried out; principally for flat plates and horizontal cylinders. However, only average values of the Nusselt number have been presented. Jakob (1949), McAdams (1954), and Gebhart (1961) reviewed correlations of the experimental data.

Meyer (1937) carried out a few experiments with a silver sphere in air at atmospheric pressure for Grashof numbers between 100 and 1000. For low Grashof number, he examined other experimental results for a cylinder and a sphere and concluded that the average Nusselt number as a function of the Grashof number for a sphere was approximately the same as that for a cylinder if the sphere radius was substituted for the cylinder diameter as the characteristic dimension.

Elenbaas (1942) made experimental studies with both a cylinder and a sphere in air at atmospheric pressure. He found that for a sphere, for small, moderate, and large values of the Grashof number, the following relation applies:

$$\overline{Nu}^3 \left(1- \frac{2}{\overline{Nu}}\right)^6 = \frac{Gr_d}{500} \qquad (1.3.4)$$

where Gr_d is the Grashof number based on the diameter of the sphere.

Ranz and Marshall (1952) carried out experiments on evaporating drops at Grashof numbers as low as 1 and presented the following formula:

$$\overline{Nu} = 2 + 0.60\ Gr_d^{1/4}\ Pr^{1/3} \qquad (1.3.5)$$

In addition to their analytical expression for heat and mass transfer from vertical plates, Mathers, Madden, and Piret (1957), presented empirical equations for spheres.

Data for Rayleigh numbers less than 100 were fitted by the following equation:

$$\overline{Nu} = 2 + 0.282\ (Ra_d)^{0.37} \qquad (1.3.6)$$

For Rayleigh number in the range $10^2 < Ra_d < 10^6$ their correlation was:

$$\overline{Nu} = 2 + 0.5\ (Ra_d)^{\frac{1}{4}} \qquad (1.3.7)$$

Tsubouchi and Sato (1960) used thermister particles of approximately ellipsoidal shape in order to study free convection in air. They obtained the following correlation for shperes for Prandtl numbers, Pr, around unity and $10^{-3} < \frac{Gr_d}{27} < 1.5$:

$$\overline{Nu} = 2 + 0.59\ (Gr_d\ Pr)^{\frac{1}{4}} \qquad (1.3.8)$$

Yuge (1960), suggested the following empirical formula for free convective heat transfer from a sphere in air for Grashof numbers, Gr_d, between 1 and 100,000. The Prandtl number is incorporated in the coefficient:

$$\overline{Nu} = 2 + 0.392\ Gr_d^{\frac{1}{4}} \qquad (1.3.9)$$

Hossain (1966) made experimental studies with an isothermal sphere of 1/4 inch diameter. He carried out the experiments by means of a Mach-Zehnder interferometer of 5 inch field. He found the following empirical formula for Grashof numbers between 0.02 and 2.54 and Prandtl numbers

between 125 and 1000.

$$\overline{Nu} = 2 + 1.16\ Gr^{1/4}\ Pr^{1/3} \qquad (1.3.10)$$

1.3.2 Theoretical and Experimental Studies at Large Grashof Numbers

The subject of free convection heat and mass transfer has drawn the attention of many authors in the past. Almost all of the theoretical studies are based on the assumption of the existence of a boundary layer. From the point of view of mathematics, these solutions represent the asymtotic solutions as the parameter Grashof number approaches infinity. Although boundary layer theory is only applicable at reasonably large Grashof numbers, large Grashof numbers are a limiting case of intermediate Grashof numbers and the solutions obtained for intermediate Grashof numbers may be expected to approach the boundary layer solution as the Grashof number is increased. For this reason boundary layer solutions and experimental results obtained for large Grashof numbers will be briefly reviewed.

Yamagata (1943) suggested the following relation from his empirical study of free convective heat transfer from sphere in air for Grashof numbers between 10^5 and 10^8. The Prandtl number is incorporated in the coefficient,

$$\overline{Nu} = 0.421\ Gr_d^{\frac{1}{4}} \qquad (1.3.11)$$

In a series of three theoretical papers, Merk and

Prins (1953-54) discussed and extended approximate solutions of the partial differential equations describing thermal convection in a laminar boundary layer. Extended solutions were obtained for the cases of a sphere and a horizontal cylinder. For Prandtl numbers, Pr, much greater than 1, Merk and Prins derived the following relation for free convective heat transfer from a sphere.

$$\overline{Nu} = 0.558\ (Gr_d\ Pr)^{\frac{1}{4}} \qquad (1.3.12)$$

Garner and Hoffman (1961) measured local rates of mass transfer from solid spheres of various organic acids by a photographic technique. Schutz (1963) gave some measurements of local rates of mass transfer from spheres and horizontal cylinders. He found that for a sphere:

$$\overline{Sh} = 2 + 0.59\ (Gr_d\ Sc)^{\frac{1}{4}} \qquad (1.3.13)$$

where Sc and $\overline{Sh}$ are the Schmidt number, and average Scherwood number, respectively.

Chiang, Ossin and Tien (1964) obtained a solution of the problem of external free convection heat transfer from a sphere with various prescribed thermal conditions on the surface. They obtained exact solutions of the boundary layer equations for the cases of uniform surface temperature and of uniform surface heat flux for a Prandtl number of 0.70. For the case of uniform surface temperature they expressed the local Nusselt number as:

$$Nu = (0.4576 - 0.03402\ \xi^2)\ Gr_d^{\frac{1}{4}} \qquad (1.3.14)$$

where ξ represents the dimensionless coordinate along the body surface.

Sandoval (1965) made accurate measurements of overall rates of mass transfer from benzoic acid spheroids of five different eccentricities dissolving into water. His results seemed to be independent of shape, being correlated by:

$$\overline{Sh} = 0.121\ (Gr_d\ Sc)^{\frac{1}{4}} \qquad (1.3.15)$$

Pandya (1967) made a theoretical investigation of the effect of shape, Schmidt (or Prandtl) number, and composition of system, on laminar free convective mass and heat transfer. He considered spheriods, elliptic cylinders of oblate cross-section, and various axisymmetric similarity flow bodies.

Pandya obtained both exact and approximate solutions of the laminar boundary layer equations in the range $0.7 \leqslant Pr \leqslant 2000$ for heat transfer and $0.7 \leqslant Sc \leqslant 2000$ for mass transfer and found very good agreement between the two types of solution.

Yang and Jerger (1964) attempted to extend the applicability of boundary layer theory to lower Grashof numbers. They made a perturbation analysis for laminar free convection along a vertical plate using the classical boundary layer solution as the zeroth-order approximation. However, the first-order approximation showed that their problem remained within the framework of boundary layer theory and, as a result, their method could not be used to extend boundary layer theory

to lower Grashof numbers.

It is seen that there are many associated problmes and gaps to be filled when attempting general treatments of free convection. The present project has studied transient free convective heat transfer from a solid sphere for Grashof numbers, Gr, in the range between 0.05 and 12500 and Prandtl numbers of 0.72, 10 and 100.

CHAPTER 2

THEORETICAL ANALYSIS

2.1 THE EQUATIONS OF CHANGE

The basic differential equations used here are the 'equations of change' namely the equation of continuity, the equation of motion (Navier-Stokes) and the energy equation. These equations express the basic laws of conservation of mass, momentum, and energy applied to a small control volume within a flowing fluid. These conservation equations are called the 'equations of change', inasmuch as they describe the change of mass, momentum, and temperature with respect to time and position in the system. The derivations of these equations may be found in various standard tests such as Schlichting (1968), Batchelor (1970), Aris (1962), Bird, Stewart and Lightfoot (1960), and Howarth (1956).

It is convenient at this stage, however, to list the main assumptions which are usually made in these derivations:

1. Fluid properties are continuous functions of space and time.
2. The fluid is Newtonian.
3. The fluid is isotropic.

With these assumptions, the governing equations of the transport process of heat may be expressed as follows.

1. The equation of continuity.

The equation of continuity is based on the physical principle of conservation of total mass, and expresses a balance between the rates at which mass enters and leaves a

control volume and the rate at which mass is accumulated, through changes in density, within the control volume. The equation of continuity in vector notation may be expressed as:

$$\frac{D\rho}{Dt} = -\rho(\nabla.\bar{U}) \qquad (2.1.1)$$

where: $\bar{U}$ is the velocity vector

t is time

ρ is density

$\frac{D}{Dt}$ is the substantial derivative

and is defined as: $\frac{D}{Dt} = \frac{\partial}{\partial t} + (\bar{U}.\nabla)$

2. The equation of motion.

The equation of motion is derived from Newton's Second Law of motion and may be expressed as:

$$\rho \frac{D\bar{U}}{Dt} = \bar{F} - \nabla P + \mu\nabla^2\bar{U} + \frac{1}{3}\mu\ \nabla(\nabla.\bar{U}) - \frac{2}{3}\nabla\mu(\nabla.\bar{U})$$

$$+ 2(\nabla\mu.\nabla)\bar{U} + \nabla\mu \times (\nabla\times\bar{U}) \qquad (2.1.2)$$

where: $\bar{F}$ is the body force vector

p is the pressure

μ is the viscosity

Equation (2.1.2) is the general form of the Navier-Stokes equation. The terms of equation (2.1.2) represents forces acting on an element of fluid per unit volume. The term $\rho \frac{D\bar{U}}{Dt}$, represents the inertial forces per unit volume. On the right hand side of equation (2.1.2), the first term, $\bar{F}$, expresses the body force per unit volume, the second term,

∇P , represents the pressure force per unit volume, and the remaining five terms represent the viscous forces per unit volume in which the variations of viscosity are included.

3. The energy equation

The energy equation, based on the laws of thermodynamics, is as follows:

$$\rho\frac{DE}{Dt} = -\nabla.\bar{q} - P(\nabla.\bar{U}) + \Phi_D \qquad (2.1.3)$$

The terms of equation (2.1.3) represent rates of energy gained by an element of fluid per unit volume. In equation (2.1.3), the variable E, represents the specific internal energy, so that the term $\rho\frac{DE}{Dt}$, expresses the rate of gain of internal energy per unit volume. On the right hand side of equation (2.1.3), the term $\nabla.\bar{q}$, represents the rate of input of energy by conduction per unit volume, the second term, $P(\nabla.\bar{U})$, represents the reversible rate of internal energy increase per unit volume by compression, and the last term, Φ_D , represents the irreversible rate of internal energy increase per unit volume arising from viscous dissipation. The specific internal energy, E, can be defined in terms of the state variables; the volume, V ; the pressure P; and the temperature, T, as follows:

$$dE = C_p\, dT - T\,(\frac{\partial V}{\partial T})_P\, dP - PdV \qquad (2.1.4)$$

where C_p is the specific heat at constant pressure.

It follows from the substitution of V by $\frac{1}{\rho}$ and the use

of continuity equation, equation (2.1.1), that equation (2.1.4) can be rewritten as follows:

$$\rho\frac{DE}{Dt} = \rho C_P \frac{DT}{Dt} + \frac{T}{\rho}\left(\frac{\partial\rho}{\partial T}\right)_P \frac{DP}{Dt} - P(\nabla . \bar{U}) \qquad (2.1.5)$$

Fourier's law of heat conduction can be expressed as:

$$\bar{q} = -k_T \nabla T \qquad (2.1.6)$$

where k_T is the thermal conductivity.

By application of equations (2.1.5) and (2.1.6), equation (2.1.3) can now be written as follows:

$$\rho C_P \frac{DT}{Dt} = \nabla.(k_T \nabla T) - \frac{T}{\rho}\left(\frac{\partial\rho}{\partial T}\right)_P \frac{DP}{Dt} + \Phi_D \qquad (2.1.7)$$

In general, the properties of the fluid depend on temperature, T, and pressure P. The density of the fluid can be related to temperature and pressure by an equation of state, which may be expressed as (Batchelor 1970):

$$f(\rho,P,T) = 0 \qquad (2.1.8)$$

The molecular transport coefficients μ, viscosity, and k_T, thermal conductivity, are functions of the local state of the fluid. With density, ρ, and temperature,T, as convenient choices of the two parameters of state, one may write:

$$\mu \equiv \mu(\rho,T) \qquad (2.1.9)$$

$$k_T \equiv k_T(\rho,T) \qquad (2.1.10)$$

Equations (2.1.1), (2.1.2) and (2.1.7) to (2.1.10) together with the initial and boundary conditions are so complicated that they are seldom used in their complete form to solve flow problems. In order to make progress with

the solution of a particular problem, it is generally necessary to introduce simplifying assumptions such that the equations become easier to solve while continuing to describe adequately the particular physical situation.

The case to be analysed here, is that of free convective heat transfer from a solid sphere to a Newtonian fluid. The system is assumed to possess the following characteristics.

(i) The only body force operating is that of gravity.

(ii) It is assumed that temperature variations are not large, so that Boussinesq's approximation can be applied thus enabling the density to be treated as a constant in all terms of the transport equations except the buoyancy term. For the same reason, other fluid properties such as the viscosity, specific heat, and thermal conductivity may also be considered as constants.

(iii) The surface temperature of the solid sphere is uniform and unchanging with time. In practice, such behaviour can be approximated during a substantial portion of the transient period provided the sphere has sufficiently high heat capacity and conductance.

(iv) It is assumed that the heat generated by viscous dissipation is negligible. This is justified when the ratio of Brinkman number to the Peclet number is small and the fluid viscosity is low.

With the above simplifications, equations (2.1.1) and (2.1.2) and (2.1.7) reduce to:

$$\nabla.\bar{U} = 0 \qquad \text{(continuity equation)} \qquad (2.1.11)$$

$$\rho_\infty \frac{D\bar{U}}{Dt} = -\nabla P + \mu_\infty \nabla^2 \bar{U} + \bar{F} \quad \text{(Navier-Stokes equation)} \qquad (2.1.12)$$

$$\rho_\infty C_{P\infty} \frac{DT}{Dt} = k_{T\infty} \nabla^2 T \quad \text{(energy equation)} \qquad (2.1.13)$$

where the subscript ∞ denotes the value of the variable distant from the body.

Appropriate boundary and initial conditions are needed for equations (2.1.11) to (2.1.13). For free convective heat transfer from a solid body immersed in a Newtonian fluid the boundary and initial conditions can be obtained from the following considerations:

Boundary conditions:

(i) There is no slip of the fluid at the surface of solid body.

(ii) The temperature is assumed to be constant and uniform at all points on the surface of the body.

(iii) As the distance from the body increases the dependent variables become asymptotic to their values in the undisturbed stagnant fluid.

Initial conditions:

Two different sets of initial conditions could be used in connection with the problem of the unsteady transfer of heat from a solid body to a stagnant fluid. These two different initial conditions are:

(i) Initially, the fluid is at rest everywhere and

temperature distribution is taken to be that of steady state conduction between the body and the surrounding fluid.

(ii) Initially, the fluid is at rest everywhere and temperature everywhere in the domain is set to a constant value, T^{o}, except on the solid surface where the temperature is set to T_s.

In the present work, however, because of the mathematical difficulties which are associated with the second initial condition, the first initial condition is used exclusively.

2.2 THE EQUATIONS OF CHANGE IN SPHERICAL COORDINATE SYSTEM

The vector forms of the equations of change, that is, equation (2.1.11) for the continuity equation, equation (2.1.12) for the momentum equation, and equation (2.1.13) for the energy equation, are applicable for any orthogonal coordinate system. The objective in this section is to expand these equations, in component form, in a general orthogonal curvilinear coordinate system. This is because depending on the shape of the body, a particular coordinate system may offer a great deal of simplifications of the equations of change when setting up flow problems. For example, in the case of axisymmetric flow around a sphere, the use of spherical polar coordinates, (r,Θ,Φ), facilitates the description of the velocity vector, $\bar{U}$, in terms of two components u_r and u_Θ, rather than in terms of the three

components that would be required if rectangular coordinates were to be used.

The first step in the expansion of the equations in component form for any particular orthogonal coordinate system is to express the vector operators in forms such that the transformation into orthogonal curvilinear coordinates is immediate (see appendix A).

From the vector relationships given in appendix A with the replacement of vectors $\bar{A}$ and $\bar{B}$ by the velocity vector $\bar{U}$ and replacement of the scalar φ by the temperature, T, the following relationships are obtained:

$$(\bar{U}.\nabla)\bar{U} = \tfrac{1}{2}\nabla(\bar{U}.\bar{U}) - \bar{U} \times (\nabla \times \bar{U}) \qquad (2.2.1)$$

$$\nabla^2 \bar{U} = \nabla(\nabla.\bar{U}) - \nabla \times (\nabla \times \bar{U}) \qquad (2.2.2)$$

$$(\bar{U}.\nabla)T = \bar{U}.\nabla T \qquad (2.2.3)$$

However, $\nabla.\bar{U} = 0$ from the continuity equation, equation (2.1.13), so that equation (2.2.2) becomes:

$$\nabla^2 \bar{U} = -\nabla \times (\nabla \times \bar{U}) \qquad (2.2.4)$$

By substitution of the relationships (2.2.1), (2.2.3), and (2.2.4) into equations (2.1.11) to (2.1.13), the following equations are obtained:

The continuity equation:

$$\nabla.\bar{U} = 0 \qquad (2.2.5)$$

The Navier-Stokes equation:

$$\rho_\infty \frac{\partial \bar{U}}{\partial t} + \frac{\rho_\infty}{2}\nabla(\bar{U}.\bar{U}) - \rho_\infty \bar{U} \times (\nabla \times \bar{U}) = -\nabla P - \mu_\infty \nabla \times (\nabla \times \bar{U}) + \bar{F} \qquad (2.2.6)$$

The energy equation:

$$\rho_\infty \; C_{P_\infty}\left(\frac{\partial T}{\partial t} + \bar{U}.\nabla T\right) = k_{T_\infty}\nabla^2 T \qquad (2.2.7)$$

By application of equations (A.2.1) to (A.2.5) of appendix A, equations (2.2.5) to (2.2.7) can be rewritten in terms of the orthogonal curvilinear coordinates X_1, X_2, and X_3 and the corresponding scale factors h_1, h_2, and h_3. The coordinate system chosen is illustrated in figure A.3.1 of appendix A.

In orthogonal curvilinear coordinates the continuity equation, equation (2.2.5), becomes:

$$\frac{1}{h_1h_2h_3}\left[\frac{\partial}{\partial X_1}(h_2h_3u_1) + \frac{\partial}{\partial X_2}(h_1h_3u_2) + \frac{\partial}{\partial X_3}(h_1h_2u_3)\right] = 0 \qquad (2.2.8)$$

The Navier-Stokes equation, equation (2.2.6) becomes:

X_1 - component:

$$\begin{aligned}
&\rho_\infty \frac{\partial u_1}{\partial t} + \frac{\rho_\infty}{2}\frac{\partial}{\partial X_1}(u_1^2 + u_2^2 + u_3^2) \\
&- \frac{\rho_\infty}{h_1h_2h_3}\left\{h_3u_2\left[\frac{\partial}{\partial X_1}(h_2u_2) - \frac{\partial}{\partial X_2}(h_1u_1)\right]\right. \\
&\qquad \left. + h_2u_3\left[\frac{\partial}{\partial X_1}(h_3u_3) - \frac{\partial}{\partial X_3}(h_1u_1)\right]\right\} \\
&= -\frac{1}{h_1}\frac{\partial P}{\partial X_1} - \mu_\infty\left\{\frac{1}{h_2h_3}\left[\frac{\partial}{\partial X_2}\left[\frac{h_3}{h_1h_2}\left[\frac{\partial}{\partial X_1}(h_2u_2) - \frac{\partial}{\partial X_2}(h_1u_1)\right]\right]\right.\right. \\
&\qquad \left.\left. + \frac{\partial}{\partial X_3}\left[\frac{h_2}{h_1h_3}\left[\frac{\partial}{\partial X_1}(h_3u_3) - \frac{\partial}{\partial X_3}(h_1u_1)\right]\right]\right]\right\} + F_1
\end{aligned} \qquad (2.2.9)$$

X_2 - component:

$$\rho_\infty \frac{\partial u_2}{\partial t} + \frac{\rho_\infty}{2} \frac{\partial}{\partial X_2} (u_1^2 + u_2^2 + u_3^2)$$

$$- \frac{\rho_\infty}{h_1 h_2 h_3} \left\{ h_3 u_1 \left[\frac{\partial}{\partial X_2} (h_1 u_1) - \frac{\partial}{\partial X_1} (h_2 u_2) \right] \right.$$

$$\left. + h_1 u_3 \left[\frac{\partial}{\partial X_2} (h_3 u_3) - \frac{\partial}{\partial X_3} (h_2 u_2) \right] \right\}$$

$$= - \frac{1}{h_2} \frac{\partial p}{\partial X_2} - \mu_\infty \left\{ \frac{1}{h_1 h_3} \left[\frac{\partial}{\partial X_3} \left[\frac{h_1}{h_2 h_3} \left[\frac{\partial}{\partial X_2} (h_3 u_3) - \frac{\partial}{\partial X_3} (h_2 u_2) \right] \right] \right. \right.$$

$$\left. \left. + \frac{\partial}{\partial X_1} \left[\frac{h_3}{h_1 h_2} \left[\frac{\partial}{\partial X_2} (h_1 u_1) - \frac{\partial}{\partial X_1} (h_2 u_2) \right] \right] \right] \right\} + F_2 \qquad (2.2.10)$$

X_3 - component:

$$\rho_\infty \frac{\partial u_3}{\partial t} + \frac{\rho_\infty}{2} \frac{\partial}{\partial X_3} (u_1^2 + u_2^2 + u_3^2)$$

$$- \frac{\rho_\infty}{h_1 h_2 h_3} \left\{ h_2 u_1 \left[\frac{\partial}{\partial X_3} (h_1 u_1) - \frac{\partial}{\partial X_1} (h_3 u_3) \right] \right.$$

$$\left. + h_1 u_2 \left[\frac{\partial}{\partial X_3} (h_2 u_2) - \frac{\partial}{\partial X_2} (h_3 u_3) \right] \right\}$$

$$= - \frac{1}{h_3} \frac{\partial p}{\partial X_3} - \mu_\infty \left\{ \frac{1}{h_1 h_2} \left[\frac{\partial}{\partial X_1} \left[\frac{h_2}{h_1 h_3} \left[\frac{\partial}{\partial X_3} (h_1 u_1) - \frac{\partial}{\partial X_1} (h_3 u_3) \right] \right] \right. \right.$$

$$\left. \left. + \frac{\partial}{\partial X_2} \left[\frac{h_1}{h_2 h_3} \left[\frac{\partial}{\partial X_3} (h_2 u_2) - \frac{\partial}{\partial X_2} (h_3 u_3) \right] \right] \right] \right\} + F_3 \qquad (2.2.11)$$

The energy equation, equation (2.2.7) becomes:

$$\rho_\infty C_{P_\infty}\left(\frac{\partial T}{\partial t} + \frac{u_1}{h_1} \frac{\partial T}{\partial X_1} + \frac{u_2}{h_2} \frac{\partial T}{\partial X_2} + \frac{u_3}{h_3} \frac{\partial T}{\partial X_3} \right)$$

$$= \frac{k_{T_\infty}}{h_1 h_2 h_3} \left[\frac{\partial}{\partial X_1} \left(\frac{h_2 h_3}{h_1} \frac{\partial T}{\partial X_1} \right) + \frac{\partial}{\partial X_2} \left(\frac{h_1 h_3}{h_2} \frac{\partial T}{\partial X_2} \right) \right.$$

$$\left. + \frac{\partial}{\partial X_3} \left(\frac{h_1 h_2}{h_3} \frac{\partial T}{\partial X_3} \right) \right] \qquad (2.2.12)$$

To simulate flow around a solid sphere, it is convenient to rewrite the above equations in spherical polar coordinates (see figure 2.2.1) for which:

$$X_1 = r \qquad X_2 = \Theta \qquad X_3 = \Phi$$

and

$$h_1 = 1 \qquad h_2 = r \qquad h_3 = r \sin \Theta$$

The continuity equation:

$$\frac{1}{r^2} \frac{\partial}{\partial r} (r^2 u_r) + \frac{1}{r \sin\Theta} \frac{\partial}{\partial \Theta} (u_\Theta \sin\Theta) + \frac{1}{r \sin\Theta} \frac{\partial}{\partial \Phi} (u_\Phi) = 0 \qquad (2.2.13)$$

The Navier-Stokes equation:

r - component:

$$\rho_\infty \left[\frac{\partial u_r}{\partial t} + u_r \frac{\partial u_r}{\partial r} + \frac{u_\Theta}{r} \frac{\partial u_r}{\partial \Theta} + \frac{u_\Phi}{r \sin\Theta} \frac{\partial u_r}{\partial \Phi} - \frac{u_\Theta^2 + u_\Phi^2}{r} \right]$$

$$= -\frac{\partial P}{\partial r} + \mu_\infty \left[\nabla^2 u_r - \frac{2}{r^2} u_r - \frac{2}{r^2} \frac{\partial u_\Theta}{\partial \Theta} - \frac{2}{r^2} u_\Theta \cot\Theta - \frac{2}{r^2 \sin\Theta} \frac{\partial u_\Phi}{\partial \Phi} \right] + F_r \qquad (2.2.14)$$

Θ - component:

$$\rho_\infty\left[\frac{\partial u_\Theta}{\partial t} + u_r\frac{\partial u_\Theta}{\partial r} + \frac{u_\Theta}{r}\frac{\partial u_\Theta}{\partial \Theta} + \frac{u_\Phi}{r\sin\Theta}\frac{\partial u_\Theta}{\partial \Phi} + \frac{u_r u_\Theta}{r} - \frac{u_\Phi^2\cot\Theta}{r}\right]$$

$$= -\frac{1}{r}\frac{\partial P}{\partial \Theta} + \mu_\infty\left[\nabla^2 u_\Theta + \frac{2}{r^2}\frac{\partial u_r}{\partial \Theta} - \frac{u_\Theta}{r^2\sin^2\Theta} - \frac{2\cos\Theta}{r^2\sin^2\Theta}\frac{\partial u_\Phi}{\partial \Phi}\right] + F_\Theta$$

(2.2.15)

Φ - component:

$$\rho_\infty\left[\frac{\partial u_\Phi}{\partial t} + u_r\frac{\partial u_\Phi}{\partial r} + \frac{u_\Theta}{r}\frac{\partial u_\Phi}{\partial \Theta} + \frac{u_\Phi}{r\sin\Theta}\frac{\partial u_\Phi}{\partial \Phi} + \frac{u_\Phi u_r}{r} + \frac{u_\Phi u_\Theta}{r}\cot\Theta\right]$$

$$= -\frac{1}{r\sin\Theta}\frac{\partial P}{\partial \Phi} + \mu_\infty\left[\nabla^2 u_\Phi - \frac{u_\Phi}{r^2\sin^2\Theta} + \frac{2}{r^2\sin\Theta}\frac{\partial u_r}{\partial \Phi} + \frac{2\cos\Theta}{r^2\sin^2\Theta}\frac{\partial u_\Theta}{\partial \Phi}\right] + F_\Phi$$

(2.2.16)

The energy equation:

$$\rho_\infty C_{P_\infty}\left[\frac{\partial T}{\partial t} + u_r\frac{\partial T}{\partial r} + \frac{u_\Theta}{r}\frac{\partial T}{\partial \Theta} + \frac{u_\Phi}{r\sin\Theta}\frac{\partial T}{\partial \Phi}\right]$$

$$= k_{T_\infty}\left[\frac{1}{r^2}\frac{\partial}{\partial r}\left(r^2\frac{\partial T}{\partial r}\right) + \frac{1}{r^2\sin\Theta}\frac{\partial}{\partial \Theta}\left(\sin\Theta\frac{\partial T}{\partial \Theta}\right) + \frac{1}{r^2\sin^2\Theta}\frac{\partial^2 T}{\partial \Phi^2}\right]$$

(2.2.17)

where,

$$\nabla^2 = \frac{1}{r^2}\frac{\partial}{\partial r}\left(r^2\frac{\partial}{\partial r}\right) + \frac{1}{r^2\sin\Theta}\frac{\partial}{\partial \Theta}\left(\sin\Theta\frac{\partial}{\partial \Theta}\right) + \frac{1}{r^2\sin^2\Theta}\left(\frac{\partial^2}{\partial \Phi^2}\right)$$

(2.2.18)

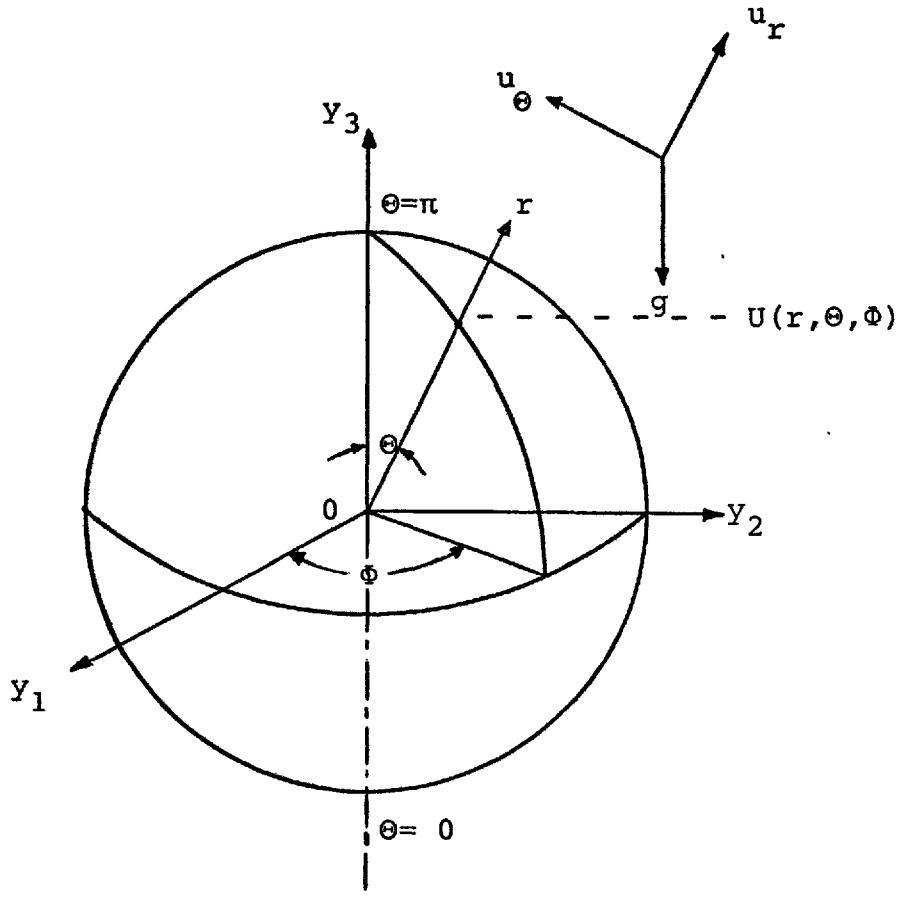

FIGURE 2.2.1 SPHERICAL POLAR COORDINATE SYSTEM

2.3 AXISYMMETRICAL FLOWS

The general three-dimensional equations presented in the previous section, in which the three velocity components depend on all three coordinates, are very difficult to solve even numerically. However, in the case of flows such as axisymmetric flow around a sphere, the equations can be further simplified and the mathematical difficulties encountered in obtaining solutions considerably reduced.

The spherical polar coordaintes (r,Θ,Φ) of the sphere are arranged as shown in figure 2.2.1. As shown in the figure, the coordinate r is normal to the surface of the

body,Θ is parallel to the surface in the flow direction, and Φ is the direction of rotations about the axis of symmetry of the flow. For the particular case of streaming flow past a stationary sphere with no rotation, the flow around the vertical axis is axisymmetric, the component of velocity in the Φ-direction is zero everywhere, and all variables are independent of Φ, that is,

$$u_\Phi = 0 \tag{2.3.1}$$

$$\frac{\partial \bar{U}}{\partial \Phi} = 0 \qquad \frac{\partial T}{\partial \Phi} = 0 \qquad \frac{\partial P}{\partial \Phi} = 0 \tag{2.3.2}$$

Expressing the body force as $\bar{F} = \rho \bar{g}$ and using relations (2.3.1) and (2.3.2), equations (2.2.13) to (2.2.18) can be written as follows:

Continuity equation:

$$\frac{1}{r^2} \frac{\partial}{\partial r} (r^2 u_r) + \frac{1}{r \sin\Theta} \frac{\partial}{\partial \Theta} (u_\Theta \sin_\Theta) = 0 \tag{2.3.3}$$

Navier-Stokes equation:

r - component:

$$\frac{\partial u_r}{\partial t} + u_r \frac{\partial u_r}{\partial r} + \frac{u_\Theta}{r} \frac{\partial u_r}{\partial \Theta} - \frac{u_\Theta^2}{r} = - \frac{1}{\rho_\infty} \frac{\partial P}{\partial r} + \nu_\infty \left[\nabla^2 u_r - \frac{2}{r^2} u_r - \frac{2}{r^2} \frac{\partial u_\Theta}{\partial \Theta} - \frac{2}{r^2} u_\Theta \cot\Theta \right] + \frac{\rho g_r}{\rho_\infty} \tag{2.3.4}$$

Θ - component:

$$\frac{\partial u_\Theta}{\partial t} + u_r \frac{\partial u_\Theta}{\partial r} + \frac{u_\Theta}{r} \frac{\partial u_\Theta}{\partial \Theta} + \frac{u_r u_\Theta}{r} = - \frac{1}{\rho_\infty} \frac{1}{r} \frac{\partial P}{\partial \Theta} + \nu_\infty \left[\nabla^2 u_\Theta + \frac{2}{r^2} \frac{\partial u_r}{\partial \Theta} - \frac{u_\Theta}{r^2 \sin^2\Theta} \right] + \frac{\rho g_\Theta}{\rho_\infty} \tag{2.3.5}$$

Energy equation:

$$\frac{\partial T}{\partial t} + u_r \frac{\partial T}{\partial r} + \frac{u_\Theta}{r} \frac{\partial T}{\partial \Theta} = \alpha_\infty \left[\frac{1}{r^2} \frac{\partial}{\partial r} \left(r^2 \frac{\partial T}{\partial r} \right) + \frac{1}{r^2 \sin\Theta} \frac{\partial}{\partial \Theta} \left(\sin\Theta \frac{\partial T}{\partial \Theta} \right) \right] \qquad (2.3.6)$$

where $\nabla^2 = \frac{1}{r^2} \frac{\partial}{\partial r} \left(r^2 \frac{\partial}{\partial r} \right) + \frac{1}{r^2 \sin\Theta} \frac{\partial}{\partial \Theta} \left(\sin\Theta \frac{\partial}{\partial \Theta} \right)$,

and ν and α are the kinematic viscosity and thermal diffusivity of the fluid, respectively.

The components of the gravitational acceleration in the radial direction, g_r, and angular direction, g_Θ, can be evaluated from figure 2.2.1 as follows:

$$g_r = g \cos \Theta \qquad (2.3.7)$$

$$g_\Theta = -g \sin \Theta \qquad (2.3.8)$$

The pressure, P, can be written as the sum of two pressures:

$$P = P_s + P_d \qquad (2.3.9)$$

where: P_s is the static fluid pressure

P_d is the pressure difference between the static pressure and the pressure when the fluid is in motion.

The static fluid pressure can be derived from equation (2.3.4) as follows

$$0 = - \frac{1}{\rho_\infty} \frac{\partial P_s}{\partial r} + \frac{\rho_\infty g_r}{\rho_\infty} \quad \text{or} \quad P_s = P_o + \rho_\infty g \, r \cos\Theta \qquad (2.3.10)$$

where P_o is a constant. By substitution of equation (2.3.10) into equation (2.3.9) and differentiation with respect to r and Θ, the following relations may be obtained:

$$\frac{\partial P}{\partial r} = \frac{\partial P_d}{\partial r} + \rho_\infty g \cos\Theta \qquad (2.3.11)$$

and

$$\frac{\partial P}{\partial \Theta} = \frac{\partial P_d}{\partial \Theta} - \rho_\infty g\, r \sin\Theta \qquad (2.3.12)$$

By combination of the body force terms, $F_r = \rho g_r$ and $F_\Theta = \rho g_\Theta$, with equations (2.3.11) and (2.3.12), respectively, the following equations can be obtained:

$$-\frac{1}{\rho_\infty}\frac{\partial P}{\partial r} + \frac{\rho g_r}{\rho_\infty} = -\frac{1}{\rho_\infty}\frac{\partial P_d}{\partial r} + \frac{g\cos\Theta}{\rho_\infty}(\rho - \rho_\infty) \qquad (2.3.13)$$

$$-\frac{1}{\rho_\infty}\frac{1}{r}\frac{\partial P}{\partial \Theta} + \frac{\rho g_\Theta}{\rho_\infty} = -\frac{1}{\rho_\infty}\frac{1}{r}\frac{\partial P_d}{\partial \Theta} - \frac{g\sin\Theta}{\rho_\infty}(\rho - \rho_\infty) \qquad (2.3.14)$$

The density, ρ, which is a funtion of temperature T, may be expressed in terms of a Taylor's series expansion relative to the stagnant fluid conditions, ρ_∞, T_∞, as:

$$\rho = \rho_\infty + \left.\frac{\partial \rho}{\partial T}\right|_{T_\infty}(T-T_\infty) + \left.\frac{\partial^2 \rho}{\partial T^2}\right|_{T_\infty}\frac{(T-T_\infty)^2}{2!} + \cdots\cdots$$

thus neglecting second and higher order terms:

$$\rho - \rho_\infty = \left.\frac{\partial \rho}{\partial T}\right|_{T_\infty}(T-T_\infty) \qquad (2.3.15)$$

The coefficient of volumetric expansion is defined by:

$$\beta_\infty = -\frac{1}{\rho_\infty}\left(\frac{\partial \rho}{\partial T}\right)_P\Bigg|_{T_\infty} \qquad (2.3.16)$$

Hence, by substitution of equation (2.3.16) into equation (2.3.15) the following expression can be obtained:

$$\rho - \rho_\infty = -\rho_\infty \beta_\infty (T-T_\infty) \qquad (2.3.17)$$

By substitution of equation (2.3.17) into equations (2.3.13) and (2.3.14) the following equations can be

obtained:

$$-\frac{1}{\rho_\infty}\frac{\partial P}{\partial r}+\frac{\rho g_r}{\rho_\infty}=-\frac{1}{\rho_\infty}\frac{\partial P_d}{\partial r}-g\beta_\infty\cos\Theta\,(T-T_\infty) \qquad (2.3.18)$$

and

$$-\frac{1}{\rho_\infty r}\frac{\partial P}{\partial \Theta}+\frac{\rho g_\Theta}{\rho_\infty}=-\frac{1}{\rho_\infty r}\frac{\partial P_d}{\partial \Theta}+g\beta_\infty\sin\Theta\,(T-T_\infty) \qquad (2.3.19)$$

By substitution of equations (2.3.18) and (2.3.19) into equations (2.3.4) and (2.3.5), respectively, the following equations for the radial direction, r, and the angular direction, Θ, are obtained:

r - component:

$$\frac{\partial u_r}{\partial t}+u_r\frac{\partial u_r}{\partial r}+\frac{u_\Theta}{r}\frac{\partial u_r}{\partial \Theta}-\frac{u_\Theta^2}{r}=-\frac{1}{\rho_\infty}\frac{\partial P_d}{\partial r}$$

$$+\nu_\infty\left[\nabla^2 u_r-\frac{2}{r^2}u_r-\frac{2}{r^2}\frac{\partial u_\Theta}{\partial \Theta}-\frac{2}{r^2}u_\Theta\cot\Theta\right]-g\beta_\infty\cos\Theta\,(T-T_\infty) \qquad (2.3.20)$$

Θ - component:

$$\frac{\partial u_\Theta}{\partial t}+u_r\frac{\partial u_\Theta}{\partial r}+\frac{u_\Theta}{r}\frac{\partial u_\Theta}{\partial \Theta}+\frac{u_r u_\Theta}{r}=-\frac{1}{\rho_\infty}\frac{1}{r}\frac{\partial P_d}{\partial \Theta}$$

$$+\nu_\infty\left[\nabla^2 u_\Theta+\frac{2}{r^2}\frac{\partial u_r}{\partial \Theta}-\frac{u_\Theta}{r^2\sin^2\Theta}\right]+g\beta_\infty\sin\Theta\,(T-T_\infty) \qquad (2.3.21)$$

Now the pressure terms can be eliminated from equations (2.3.20) and (2.3.21) in the following way. Equation (2.3.20) is differentiated with respect to Θ, and equation (2.3.21) is multiplied by r and then differentiated with respect to r. After performing these operations the resultant equations are subtracted from each other and the

following equation obtained:

$$\frac{\partial}{\partial t}\left[u_\Theta + r\frac{\partial u_\Theta}{\partial r} - \frac{\partial u_r}{\partial \Theta}\right] - u_r\left[\frac{\partial^2 u_r}{\partial r \partial \Theta} - r\frac{\partial^2 u_\Theta}{\partial r^2} - \frac{2\partial u_\Theta}{\partial r}\right]$$

$$+ u_\Theta\left[\frac{\partial^2 u_\Theta}{\partial r \partial \Theta} + \frac{2}{r}\frac{\partial u_\Theta}{\partial \Theta} + \frac{\partial u_r}{\partial r} - \frac{1}{r}\frac{\partial^2 u_r}{\partial \Theta^2}\right] + r\frac{\partial u_r}{\partial r}\frac{\partial u_\Theta}{\partial r}$$

$$+ \frac{\partial u_\Theta}{\partial r}\frac{\partial u_\Theta}{\partial \Theta} - \frac{1}{r}\frac{\partial u_\Theta}{\partial \Theta}\frac{\partial u_r}{\partial \Theta} - \frac{\partial u_r}{\partial \Theta}\frac{\partial u_r}{\partial r}$$

$$= \nu_\infty\left[r\frac{\partial^3 u_\Theta}{\partial r^3} + \frac{1}{r}\frac{\partial^3 u_\Theta}{\partial r \partial \Theta^2} - \frac{\partial^3 u_r}{\partial r^2 \partial \Theta} - \frac{1}{r^2}\frac{\partial^3 u_r}{\partial \Theta^3} - \frac{\cot\Theta}{r^2}\frac{\partial^2 u_r}{\partial \Theta^2}\right.$$

$$+ \frac{1}{r^2}\frac{\partial^2 u_\Theta}{\partial \Theta^2} + 3\frac{\partial^2 u_\Theta}{\partial r^2} + \frac{\cot\Theta}{r}\frac{\partial^2 u_\Theta}{\partial r \partial \Theta} + \frac{1}{r^2 \sin^2\Theta}\frac{\partial u_r}{\partial \Theta} + \frac{\cot\Theta}{r^2}\frac{\partial u_\Theta}{\partial \Theta}$$

$$\left. - \frac{1}{r \sin^2\Theta}\frac{\partial u_\Theta}{\partial r} - \frac{1}{r^2 \sin^2\Theta}u_\Theta\right] + g\beta_\infty \cos\Theta \frac{\partial}{\partial \Theta}(T - T_\infty)$$

$$+ g\beta_\infty r \sin\Theta \frac{\partial}{\partial r}(T - T_\infty) \qquad (2.3.22)$$

It is convenient to define a quantity called the stream function. A stream function, ψ, in spherical polar coordinates is defined such that:

$$u_r = -\frac{1}{r^2 \sin\Theta}\frac{\partial \psi}{\partial \Theta} \qquad (2.3.23)$$

and

$$u_\Theta = \frac{1}{r \sin\Theta}\frac{\partial \psi}{\partial r} \qquad (2.3.24)$$

It is clear, by the substitution of u_r and u_Θ from equations (2.3.23) and (2.3.24) into equation (2.3.3), that the continuity equation is satisfied. It is equally clear that the conditions of equations (2.3.1) and (2.3.2) are satisfied as the stream function is independent of Φ.

By substitution of the values of u_r and u_Θ from equations (2.3.23) and (2.3.24) into equations (2.3.22) and (2.3.6), the following equations are obtained:

$$\left\{\frac{\partial}{\partial t} + \frac{1}{r^2 \sin\Theta}\left[\frac{\partial\psi}{\partial r}\left(\frac{\partial}{\partial\Theta} - 2\cot\Theta\right) - \frac{\partial\psi}{\partial\Theta}\left(\frac{\partial}{\partial r} - \frac{2}{r}\right)\right]\right\} E^2(\psi)$$
$$= \nu_\infty E^4(\psi) + \beta_\infty g\left[\sin\Theta\cos\Theta\frac{\partial}{\partial\Theta}(T-T_\infty) + r\sin^2\Theta\frac{\partial}{\partial r}(T-T_\infty)\right] \quad (2.3.25)$$

and the energy equation:

$$\frac{\partial T}{\partial t} + \frac{1}{r^2\sin\Theta}\left[\frac{\partial\psi}{\partial r}\frac{\partial T}{\partial\Theta} - \frac{\partial\psi}{\partial\Theta}\frac{\partial T}{\partial r}\right] = \alpha_\infty\left[\frac{\partial^2 T}{\partial r^2} + \frac{2}{r}\frac{\partial T}{\partial r} + \frac{1}{r^2}\frac{\partial^2 T}{\partial\Theta^2} + \frac{\cot\Theta}{r^2}\frac{\partial T}{\partial\Theta}\right] \quad (2.3.26)$$

where,

$$E^2 = \frac{\partial^2}{\partial r^2} + \frac{\sin\Theta}{r^2}\frac{\partial}{\partial\Theta}\left(\frac{1}{\sin\Theta}\frac{\partial}{\partial\Theta}\right) \quad (2.3.27)$$

Equation (2.3.25) is a non-linear fourth-order partial differential equation, which can not be solved analytically and its solution must generally be obtained numerically.

However, it is more convenient to solve the Navier-Stokes equation as two simultaneous equations in two dependent variables, stream funtion and vorticity.

2.4 VORTICITY TRANSPORT EQUATION

The method used to solve the equation of fluid motion necessitates the expression of the Navier-Stokes equation as a vorticity transport equation. The vorticity in a fluid, $\bar{\omega}$, is a vector quantity having the same nature as anglular velocity. It is defined by:

$$\omega = \text{curl } \bar{U} = \nabla X \bar{U} \tag{2.4.1}$$

The curl of a vector in orthogonal curvilinear coordinate is given in appendix A. Hence the vorticity components in spherical polar coordinates becomes:

$$\omega_r = \frac{1}{r^2 \sin\Theta} \left[\frac{\partial}{\partial\Theta} (r \sin\Theta \, u_\Phi) - \frac{\partial}{\partial\Phi} (r u_\Theta) \right] \tag{2.4.2}$$

$$\omega_\Theta = \frac{1}{r \sin\Theta} \left[\frac{\partial}{\partial\Phi} (u_r) - \frac{\partial}{\partial r} (r \sin\Theta \, u_\Phi) \right] \tag{2.4.3}$$

$$\omega_\Phi = \frac{1}{r} \left[\frac{\partial}{\partial r} (r \, u_\Theta) - \frac{\partial}{\partial\Theta} (u_r) \right] \tag{2.4.4}$$

From equations (2.4.2) to (2.4.4) and from the conditions of axisymmetrical flow , it is clear that since $\omega_r = \omega_\Theta = 0$ for axisymmetric flow, there is only one non-zero component of vorticity, that in the Φ- direction. Denoting ω_Φ by ζ, equation (2.4.4) becomes:

$$\zeta = \frac{1}{r} \left[\frac{\partial}{\partial r} (r u_\Theta) - \frac{\partial}{\partial\Theta} (u_r) \right] \tag{2.4.5}$$

ζ can now be considered as a scalar funtion of r and Θ. Equation (2.4.5) can be expressed in terms of the stream function as follows:

$$\zeta r \sin\Theta = E^2 (\psi) \tag{2.4.6}$$

By substitution of equation (2.4.6) into equation (2.3.25) the vorticity transport equation becomes as follows:

$$\left\{ \frac{\partial}{\partial t} + \frac{1}{r^2 \sin\Theta} \left[\frac{\partial\psi}{\partial r} \left(\frac{\partial}{\partial\Theta} - 2 \cot\Theta \right) - \frac{\partial\psi}{\partial\Theta} \left(\frac{\partial}{\partial r} - \frac{2}{r} \right) \right] \right\} (\zeta r \sin\Theta)$$

$$= \nu_\infty E^2 (\zeta r \sin\Theta) + \beta_\infty g \left[\sin\Theta\cos\Theta \frac{\partial}{\partial\Theta} (T - T_\infty) + r \sin^2\Theta \frac{\partial}{\partial r} (T - T_\infty) \right] \tag{2.4.7}$$

However, it is more convenient to define a modified vorticity, G, as $G = \zeta\, r \sin\Theta$, and to solve the equation in terms of this variable rather than in terms of the vorticity function ζ. Equations (2.4.6) and (2.4.7) when expressed in terms of the modified vorticity, G, are as follows:

Equation (2.4.6) becomes:

$$G = E^2(\psi) \tag{2.4.8}$$

Equation (2.4.7) becomes:

$$\left\{\frac{\partial}{\partial t} + \frac{1}{r^2\sin\Theta}\left[\frac{\partial\psi}{\partial r}\left(\frac{\partial}{\partial\Theta} - 2\cot\Theta\right) - \frac{\partial\psi}{\partial\Theta}\left(\frac{\partial}{\partial r} - \frac{2}{r}\right)\right]\right\}(G)$$
$$= \nu_\infty E^2(G) + \beta_\infty g\left[\sin\Theta\cos\Theta\,\frac{\partial}{\partial\Theta}(T-T_\infty) + r\sin^2\Theta\,\frac{\partial}{\partial r}(T-T_\infty)\right] \tag{2.4.9}$$

where E^2 is given by equation (2.3.27).

2.5 DIMENSIONLESS FORM OF EQUATIONS

It is convenient to render the variables dimensionless. The object is to reduce the number of parameters to a minimum and to group them into dimensionless groups for synthesis, interpretation, and representation of results. A standard technique, for obtaining a suitable dimensionless form, using reference variables, is given by Hellums and Churchill (1961).

For natural convection, the variables in equations (2.3.23) and (2.3.24), (2.3.26), (2.4.6), (2.4.8) and (2.4.9) are made dimensionless by the use of the following dimensionless groups:

$$u_r^* = \frac{u_r R}{\nu_\infty} \quad ; \quad u_\Theta^* = \frac{u_\Theta R}{\nu_\infty}$$

$$r^* = \frac{r}{R} \quad ; \quad t^* = \frac{t\nu_\infty}{R^2} \quad ; \quad \zeta^* = \frac{\zeta R^2}{\nu_\infty}$$

$$G^* = \frac{GR}{\nu_\infty} \quad ; \quad \psi^* = \frac{\psi}{\nu_\infty R} \quad ; \quad T^* = \frac{T - T_\infty}{T_s - T_\infty} \qquad (2.5.1)$$

For convenience, the superscript will be ommitted and dimensionless variables will be used exclusively.

It is also convenient to transform the equations from polar space (r,Θ) to rectangular space (z,Θ) by the following transformation:

$$r = e^z \qquad (2.5.2)$$

The derivation of the appropriate conformal mapping is given in appendix A. It should be noted that the transformation has the advantage that it allows more grid lines to be concentrated near the sphere surface where the gradients are large.

By substitution of dimensionless variables (2.5.1) and by tranformation of $r = e^z$, the system of equations can be rewritten as follows:

The velocity components:

$$u_z = -\frac{1}{e^{2z}\sin\Theta}\frac{\partial\psi}{\partial\Theta} \qquad (2.5.3)$$

$$u_\Theta = \frac{1}{e^{2z}\sin\Theta}\frac{\partial\psi}{\partial z} \qquad (2.5.4)$$

The vorticity transport equation:

$$e^{2z}\frac{\partial G}{\partial t} + \frac{1}{e^z\sin\Theta}\left\{\frac{\partial\psi}{\partial z}\left[\frac{\partial G}{\partial\Theta} - 2\cot\Theta\, G\right] - \frac{\partial\psi}{\partial\Theta}\left[\frac{\partial G}{\partial z} - 2G\right]\right\}$$

$$= e^{2z}E_+^2(G) + e^{2z}Gr\left[\sin\Theta\cos\Theta\frac{\partial T}{\partial\Theta} + \sin^2\Theta\frac{\partial T}{\partial z}\right] \qquad (2.5.5)$$

The stream function equation:

$$e^{2z}G = e^{2z}E_{+}\ (\psi) \tag{2.5.6}$$

The modified vorticity, G:

$$G = \zeta\ e^{2z}\ \sin\Theta \tag{2.5.7}$$

The energy equation:

$$e^{2z}\ \frac{\partial T}{\partial t} + \frac{1}{e^{z}\sin\Theta}\left[\frac{\partial \psi}{\partial z}\ \frac{\partial T}{\partial \Theta} - \frac{\partial \psi}{\partial \Theta}\ \frac{\partial T}{\partial z}\right]$$
$$= \frac{1}{Pr}\left[\frac{\partial^2 T}{\partial z^2} + \frac{\partial T}{\partial z} + \frac{\partial^2 T}{\partial \Theta^2} + \cot\Theta\ \frac{\partial T}{\partial \Theta}\right] \tag{2.5.8}$$

where:

$$e^{2z}E_{+} = \frac{\partial^2}{\partial z^2} - \frac{\partial}{\partial z} + \frac{\partial^2}{\partial \Theta^2} - \cot\Theta\ \frac{\partial}{\partial \Theta} \tag{2.5.9}$$

The dimensionless parameters Gr is the Grashof number $\left[Gr = \frac{R^3 \beta_\infty g(T_S - T_\infty)}{\nu_\infty^2}\right]$ based on the radius of the sphere, R, and Pr is the Prandtl number $\left[Pr = \frac{\mu_\infty C_{P_\infty}}{k_{T\infty}} = \frac{\nu_\infty}{\alpha_\infty}\right]$.

It is important to note that the terms on the right hand side of equation (2.5.8) and the first term on the right hand side of equation (2.5.5), represent the diffusion terms, while the terms on the left hand side of these equations represent the convective terms. The last term on the right hand side of equation (2.5.5), represents the buoyancy term.

Equations (2.5.3) to (2.5.8) are the forms of the governing equations for free convective heat transfer from a solid sphere which, together with the associated boundary and initial conditions given in section 2.6, are to be solved.

2.6 BOUNDARY AND INITIAL CONDITIONS FOR TIME-DEPENDENT FREE CONVECTIVE HEAT TRANSFER FROM A SOLID SPHERE

Before any attempt can be made to obtain a solution of equations (2.5.3) to (2.5.8), the appropriate boundary and initial conditions for the system must be prescribed for each of the dependent variables, ψ, ζ, G, and T.

2.6.1 Boundary Conditions.

The boundary conditions describing free convective heat transfer from a solid sphere for time, t, greater than or equal to zero, are set as follows:

(i) Sphere surface:

On the sphere surface the 'no slip' condition applies. Therefore, the velocity vector, $\bar{U}$, is zero on the surface. Thus, at the sphere surface equations (2.5.3) and (2.5.4) become:

$$\left.\frac{\partial\psi}{\partial\Theta}\right|_s = 0 \ , \quad \left.\frac{\partial\psi}{\partial z}\right|_s = 0 \ , \text{ respectively}$$

since $\dfrac{1}{e^{2z}\sin\Theta}$ can not be zero. Hence at the sphere surface the stream function has a constant value.

Therefore, at the surface of sphere, r=1 or z=0, for $0 \leq \Theta \leq \pi$:

$$\bar{U}\Big|_s = 0; \ \psi\Big|_s = C' \ ; \ \left.\frac{\partial\psi}{\partial z}\right|_s = 0 \ ; \ \left.\frac{\partial\psi}{\partial\Theta}\right|_s = 0; \ \left.\frac{\partial^2\psi}{\partial\Theta^2}\right|_s = 0 \qquad (2.6.1)$$

By application of conditions (2.6.1) to equation (2.5.6), the following relationship for the modified

vorticity, G, at the sphere surface can be obtained:

$$G\Big|_s = \frac{\partial^2 \psi}{\partial z^2}\Big|_s \qquad (2.6.2)$$

In this work the sphere is assumed to have a high thermal conductivity such that it has a uniform temperature T_s, over its entire surface. Also, the sphere is assumed to have a very large thermal capacity so that the surface temperature becomes time independent. Therefore, the temperature condition on the sphere surface is as follows:

$$T\Big|_s = 1 \qquad (2.6.3)$$

(ii) Axis of symmetry.

Along the axis of symmetry, $\Theta = 0$ and $\Theta = \pi$, the 'no cross flow' condition applies. Hence the velocity component in the angular direction, u_Θ, is zero along the axis of symmetry. Also, along the axis of symmetry, $\Theta = 0$ and $\Theta = \pi$, $\sin\Theta$ is zero. Hence from equations (2.5.3) and (2.5.4) it is necessary that:

$$\frac{\partial \psi}{\partial \Theta}\Big|_{\Theta=0,\pi} = \frac{\partial \psi}{\partial z}\Big|_{\Theta=0,\pi} = 0$$

Hence, $\psi\Big|_{\Theta=0,\pi} = C''$

At the front and back stagnation points, the sphere surface and the axis of symmetry coincide, so that at these points:

$$\psi\Big|_s = \psi\Big|_{\Theta=0,\pi} = C' = C'' = \text{constant}$$

For simplicity this constant is usually taken to be zero. Therefore:

$$\psi\Big|_s = \psi\Big|_{\Theta=0,\pi} = 0$$

so that: $\dfrac{\partial^2 \psi}{\partial z^2}\Big|_{\Theta=0,\pi} = 0$

Therefore, the boundary condition for the stream function along the axis symmetry, $\Theta=0$ and $\Theta=\pi$, can be written for all values of z as:

$$u_\Theta\Big|_{\Theta=0,\pi} = 0 \; ; \psi\Big|_{\Theta=0,\pi} = 0 \; ; \; \frac{\partial \psi}{\partial z}\Big|_{\Theta=0,\pi} = 0 \; ;$$

$$\frac{\partial^2 \psi}{\partial z^2}\Big|_{\Theta=0,\pi} = 0 \; ; \; \frac{\partial \psi}{\partial \Theta}\Big|_{\Theta=0,\pi} = 0 \qquad (2.6.4)$$

By application of conditions (2.6.4) to equation (2.5.6) this equation at the axis of symmetry becomes:

$$\frac{\partial^2 \psi}{\partial \Theta^2} - \cot\Theta \frac{\partial \psi}{\partial \Theta} = e^{2z} G \qquad (2.6.5)$$

Using L'Hospital's Law, it can be shown that:

$$\lim_{\Theta \to 0,\pi} \cot\Theta \frac{\partial \psi}{\partial \Theta} = \frac{\partial^2 \psi}{\partial \Theta^2} \qquad (2.6.6)$$

Therefore, equation (2.6.5) becomes

$$0 = e^{2z} G$$

However, along the axis of symmetry, e^{2z} cannot be zero, so that:

$$G\Big|_{\Theta=0,\pi} = 0 \qquad (2.6.7)$$

Along the axis of symmetry, $\Theta=0$ and $\Theta=\pi$, the vorticity condition, ζ, can be obtained from equation (2.5.7).

Along the axis of symmetry both G and sinΘ are zero. Therefore, using L'Hospital's Law, it can be shown that:

$$\underset{\Theta \to 0}{\text{Limit}} \frac{G}{\sin\Theta} = \frac{\partial G}{\partial \Theta} \qquad (2.6.8)$$

However, since the flow is axisymmetrical, $\frac{\partial G}{\partial \Theta}$ is zero, and since e^z can not be zero, then:

$$\zeta\Big|_{\Theta=0,\pi} = 0 \qquad (2.6.9)$$

Since the flow is axisymmetrical and temperature is a continuous function, therefore, at the axis of symmetry, $\Theta=0$ and $\Theta=\pi$:

$$\frac{\partial T}{\partial \Theta}\Bigg|_{\Theta=0,\pi} = 0 \qquad (2.6.10)$$

(iii) Outer boundary:

At large distances away from the sphere surface, all the dependent variables become asymptotic to their values in the undisturbed stagnant fluid. The temperature at the outer boundary is assumed to be constant and time-independent.

Mathematically, the conditions at this boundary are only well defined as r or z tends to infinity. However, because of limitations on computer storage and computation time, numerical integration cannot be made over too large a region, and a finite domain of integration has to be used. This means that any boundary condition is necessarily an approximation. Therefore, the outer boundary condition will be applied at some finite distance from the sphere surface.

For convenience this finite distance will be denoted by $r = r_\infty$ or $z = z_\infty$. The conditions at the outer boundary can now be expressed as:

At $z = z_\infty$:

$$\bar{U} = 0 \; ; \; \psi = 0 \; ; \; G = 0 \; ; \zeta = 0 \; ; \; T = 0 \qquad (2.6.11)$$

2.6.2 Initial Conditions

In free convective heat transfer, since the flow arises because of a density gradient, the medium initially is stationary everywhere and heat is transferred solely by conduction. Therefore, at $t = 0$:

$$\bar{U} = 0 \; ; \; \psi = 0 \; ; \; \zeta = 0 \; ; \; G = 0 \; ; \; T = T^o \qquad (2.6.12)$$

As described earlier, the initial temperature distribution, T^o, in this work, is taken to be that of pure radial steady state conduction between the sphere and the surrounding fluid.

The energy equation for steady state conduction when the surrounding fluid is stagnant is:

$$\nabla^2 T^o = 0 \qquad (2.6.13)$$

Equation (2.6.13) may be expressed in spherical polar coordinates as:

$$\nabla^2 T^o = \left\{ \frac{1}{r^2} \frac{\partial}{\partial r}\left[r^2 \frac{\partial T^o}{\partial r} \right] + \frac{1}{r^2 \sin\Theta} \frac{\partial}{\partial \Theta}\left[\sin\Theta \frac{\partial T^o}{\partial \Theta} \right] + \frac{1}{r^2 \sin^2\Theta} \frac{\partial^2 T^o}{\partial \Phi^2} \right\} = 0 \qquad (2.6.14)$$

now, $\frac{\partial^2 T^o}{\partial \Phi^2} = 0 \quad , \quad \frac{\partial T^o}{\partial \Theta} = 0$

so that; $\frac{1}{r^2} \frac{\partial}{\partial r} \left[r^2 \frac{\partial T}{\partial r} \right] = 0$ (2.6.15)

By application of transformation (2.5.2); equation (2.6.15) becomes:

$$\frac{\partial}{\partial z} \left[e^z \frac{\partial T^o}{\partial z} \right] = 0 \qquad (2.6.16)$$

The solution of equation (2.6.16) with the boundary conditions (2.6.3) and (2.6.11) is as follows:

$$T^o = \left(\frac{e^{z_\infty}}{e^{z_\infty}-1}\right) e^{-z} - \left(\frac{1}{e^{z_\infty}-1}\right) \qquad (2.6.17)$$

2.7 PROPERTIES OF THE PARTIAL DIFFERENTIAL EQUATIONS

The mathematical formulation of most problems in science involving rates of change of dependent variables with respect to two or more independent variables, usually time and position, leads to partial differential equations, either singly or in sets. The three dimensional second order partial differential equations such as those derived in section 2.4, constitute an important class of partial differential equations and are the main concern of the present study.

The maximum possible consideration must be given to the properties of the differential equations to be solved before any numerical solution is attempted. The present set of partial differential equations, vorticity transport equation (3.5.5), stream funtion equation (2.5.6), and

energy equation (2.5.8) is non-linear, second order, and elliptic with respect to the space variables (z,θ). Also equations (2.5.5) and (2.5.8) are parabolic with respect to time. These characteristics classify the problem as being of non-linear, non-stationary kind. (Sommerfield 1949, Forsythe and Wasow 1960, Smith 1965 and Mitchell 1969).

The domain of integration of any of these elliptic partial differential equations is always an area bounded by a closed curve. The boundary conditions usually specify either the value of the function or the value of its normal derivative or a mixture of both at every point on the boundary; such a domain is usually referred to as the flow region. It is generally known (Ames 1965) that a non-linear, non-stationary problem may not have a well-behaved solution for the entire time interval $t \geq 0$. Outside of a finite interval the solution may become 'arbitrary large' or 'split up' by losing its regularity, ceasing to satisfy the equations and beginning to form branches. Moreover, even if a solution exists for all times greater than zero, it may not approach the solution of the stationary problem. In fact, depending on the values of the relevant parameters, a non linear, non stationary boundary value problem can have a unique solution, several solutions, or even no solution at all (Rafique 1971).

In the general case, the questions of existence and uniqueness of the solutions of the equations which describe

time-dependent free convective heat transfer from a solid sphere for a given set of initial and boundary conditions cannot be mathematically answered. However, according to Richtmyer (1967), equations of this kind are of such a nature that if a well-posed state of the physical system is specified at some initial time, $t = t^{o}$, a solution exists for $t \geq t^{o}$ and is uniquely determined by the equations together with the associated boundary conditions and auxilary data.

In view of the above considerations, it has to be assumed that the present formulation of the problem for the time-dependent free convective heat transfer from a solid sphere is well-posed so that it can be further assumed that a solution exists and is unique.

CHAPTER 3

NUMERICAL TECHNIQUE

3.1 INTRODUCTION

The mathematical model consists of a set of partial differential equations, as derived in chapter 2. The first step in the solution of the equations by a finite-difference method is to reduce them from continuous to discrete forms and then to solve the resulting algebraic equations on a digital computer. The details of these steps can be found in standard text books on numerical analysis, such as Smith (1965) and Richtmyer (1967).

The basic method is to expand the terms of the original partial differential equations in Taylor's series. The series are truncated to a reasonable accuracy and a set of finite-difference equations obtained by the replacement of each term by the truncated series. Each finite-difference equation relates the value of a function at any mesh point to the values at neighbouring mesh points. The number of neighbouring points involved depends on the order of the original differential term and on the order of the truncated series expansion. The more accurate the approximation: the greater the number of neighbouring points involved. Thus, a gain in accuracy has to be balanced against an increased number of neighbouring points together with the consequent increased complexity of the finite-difference equations and increased computation time and storage requirements. It is generally accepted that the five point approximation, involving four neighbouring points, is a reasonable compromise between accuracy and computation

requirements.

A number of conditions must be satisfied if the solution of the finite-difference equations is to be a reasonably accurate approximation to the solution of the corresponding partial differential equation. These conditions are referred to as: 'convergence', 'stability', and 'consistency'. These terms will now be described.

The term 'convergence' is understood to mean that the exact solution of the finite-difference equations tends to the solution of the partial differential equation as the increments in time and space tend to zero.

The terms 'stability' and 'consistency' are closely related to 'convergence'. The term stability refers to a property of the finite-difference equations in a computational procedure as the time increment is made vanishingly small. The property is that, as the time increment tends to zero, there is an upper limit, to the extent to which any piece of information, whether present in the initial conditions, brought in through the boundary conditions, or arising from any sort of error in the calculations, can be amplified in the computation without the solution becoming numerically unstable.

The term 'consistency' or 'compatibility', applied to a finite-difference procedure, means that the procedure should, in fact, approximate the solution of the partial differential equation under study, and not the solution of some other partial differential equations. If on the

successive introduction of finer meshes in space as the time-step tends to zero, the finite-difference equations approach the differential equation, the finite-difference formulation is said to be consistent.

Richtmyer (1967) presents a theorem attributed to Lax which states the necessary and sufficient conditions for the convergence of solutions of linear partial differential equations. However, there is no analogous convergence theorem available for non-linear partial differential equations. In the absence of a convergence theorem for non-linear partial differential equations, it can only be assumed that a stable and consistent difference scheme will yield a reasonably accurate solution of the differential problem. Without mathematical proofs the above arguments can never be confirmed but can only be contradicted if the solutions obtained are physically unrealistic.

A further discussion of the stability of the finite-difference equations will be given in a later part of this chapter.

The Navier-Stokes, energy and continuity equations are based on the conservation of momentum, energy, and total mass, respectively. Therefore, the discretization process must not permit undue accumulation of errors in the fluxes when summed over arbitrary groups of cells; including, in particular, the entire field of computation. Ideally, the efflux from one cell to a neighbouring cell should balance

identically the influx into the neighbouring cell from the first cell. The integral of momentum, energy, and mass, over any part of the field of computation will then be conserved. A difference scheme is said to possess the 'conservative property' if it incorporates the above idea (Rafique 1971). Roache (1972) has compared conservative and non-conservative differencing methods and has stated that "experience so far has indicated that conservative systems do generally give more accurate results". In general, the significance of the conservative property is more pronounced in compressible flow problems than in incompressible flow problems. Furthermore, in multi-dimensional fluid dynamics problems the use of differencing methods which achieve conservation of the basic flux quantities such as vorticity or energy are costly in computational requirements.

Finally, there are arguments for and against the application of conservative finite-difference schemes to incompressible flow problems, and the results of numerical tests that have been reported in the literature do not present an entirely one-sided case. In order to avoid both the additional complexity of the finite-difference representation of the partial-differential equations and the increased computational requirements which are associated with the application of conservative differencing methods to multi-dimensional flow problems (Roache 1972), non-conservative finite-difference schemes are used in the present work.

3.2 FINITE-DIFFERENCE REPRESENTATION OF THE DERIVATIVES

The coordinates z and Θ introduced in chapter 2 form a rectangular system of coordinates. The domain over which the equations are to be integrated, the flow region, is represented by a finite number of points or nodes, spaced systematically within the domain. A discretization process is used to represent any of the functions or their derivatives at a general node and to relate them to the corresponding values at neighbouring nodes. The flow region, (z,Θ) plane, is bounded by the straight lines $\Theta=0$, $\Theta=\pi$, $z=0$ and $z=z_\infty$.

Consider the (z,Θ) plane as being divided up into a mesh of length 'h' in z-direction and 'k' in the Θ- direction as in figures 3.2.1 and 3.2.2. It is convenient to introduce the indices i and j in order to locate any point in the flow region at a given time-step, n. The subscripts i and j refer to the z and Θ coordinates respectively, whereas the superscript n refers to the time-level or time-step.

If a funtion $W(z,\Theta,t)$ is a continuous function and has derivatives of all orders, then using Taylor's series expansion, it can be approximated in terms of its values at the neighbouring nodes as follows:

$$W^n_{i+1,j} = \left(1 + h\,\frac{\partial}{\partial z} + \frac{h^2}{2!}\,\frac{\partial^2}{\partial z^2} + \ldots\ldots\right)W^n_{i,j}$$

$$W^n_{i-1,j} = \left(1-h\,\frac{\partial}{\partial z} + \frac{h^2}{2!}\,\frac{\partial^2}{\partial z^2} - \ldots\ldots\right)W^n_{i,j}$$

$$W_{i,j+1} = \left(1+ k\,\frac{\partial}{\partial \Theta} + \frac{k^2}{2!}\,\frac{\partial^2}{\partial \Theta^2} + \ldots\ldots\right)W^n_{i,j}$$

$$W_{i,j-1} = (1-k\frac{\partial}{\partial\Theta} + \frac{k^2}{2!}\frac{\partial^2}{\partial\Theta^2} - \ldots\ldots)W^n_{i,j}$$

$$W^{n+1}_{i,j} = (1+\Delta t\frac{\partial}{\partial t} + \frac{(\Delta t)^2}{2!}\frac{\partial^2}{\partial t^2} + \ldots)W^n_{i,j}$$

$$W^{n-1}_{i,j} = (1-\Delta t\frac{\partial}{\partial t} + \frac{(\Delta t)^2}{2!}\frac{\partial^2}{\partial t^2} - \ldots)W^n_{i,j} \qquad (3.2.1)$$

The function values, W , can be the stream funtion, ψ, vorticity, G, or the temperature, T.

By elimination, approximate expressions for the partial derivatives at the point (i,j) can be found in terms of the neighbouring values as follows:

$$(\frac{\partial W}{\partial z})^n_{i,j} = \partial_i(W^n_{i,j}) + 0(h^2) = \frac{1}{2h}\Delta_i(W^n_{ij}) + 0(h^2)$$

$$= \frac{1}{2h}(W^n_{i+1,j} - W^n_{i-1,j}) + 0(h^2) \qquad (3.2.2)$$

$$(\frac{\partial^2 W}{\partial z^2})^n_{i,j} = \partial_i^2(W^n_{i,j}) + 0(h^2) = \frac{1}{h^2}\Delta_i(W^n_{ij}) + 0(h^2)$$

$$= \frac{1}{h^2}(W^n_{i+1,j} + W^n_{i-1,j} - 2W^n_{i,j}) + 0(h^2) \qquad (3.2.3)$$

$$(\frac{\partial W}{\partial\Theta})^n_{i,j} = \partial_j(W^n_{ij}) + 0(k^2) = \frac{1}{2k}\Delta_j(W^n_{ij}) + 0(k^2)$$

$$= \frac{1}{2k}(W^n_{i,j+1} - W^n_{i,j-1}) + 0(k^2) \qquad (3.2.4)$$

$$(\frac{\partial^2 W}{\partial\Theta^2})^n_{i,j} = \partial_j^2(W^n_{ij}) + 0(k^2) = \frac{1}{k^2}\Delta_j^2(W^n_{ij}) + 0(k^2)$$

$$= \frac{1}{k^2}(W^n_{i,j+1} + W^n_{i,j-1} - 2W^n_{i,j}) + 0(k^2) \qquad (3.2.5)$$

where $0(h^2)$, terms of order h^2, refers to the additional terms with factors h^2, h^3, etc. The derivatives are said to

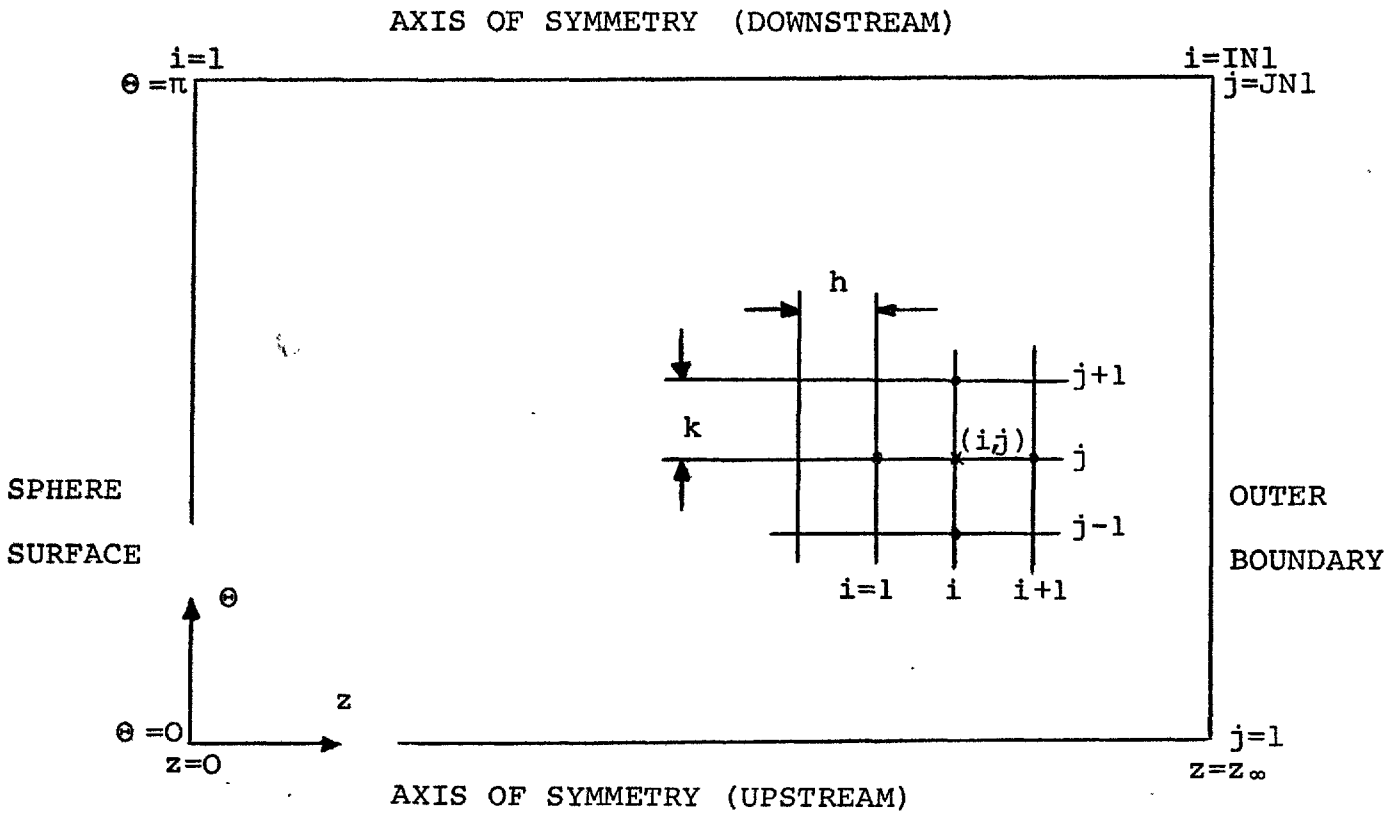

FIGURE 3.2.1 RECTANGULAR GRID COVERING THE FLOW REGION

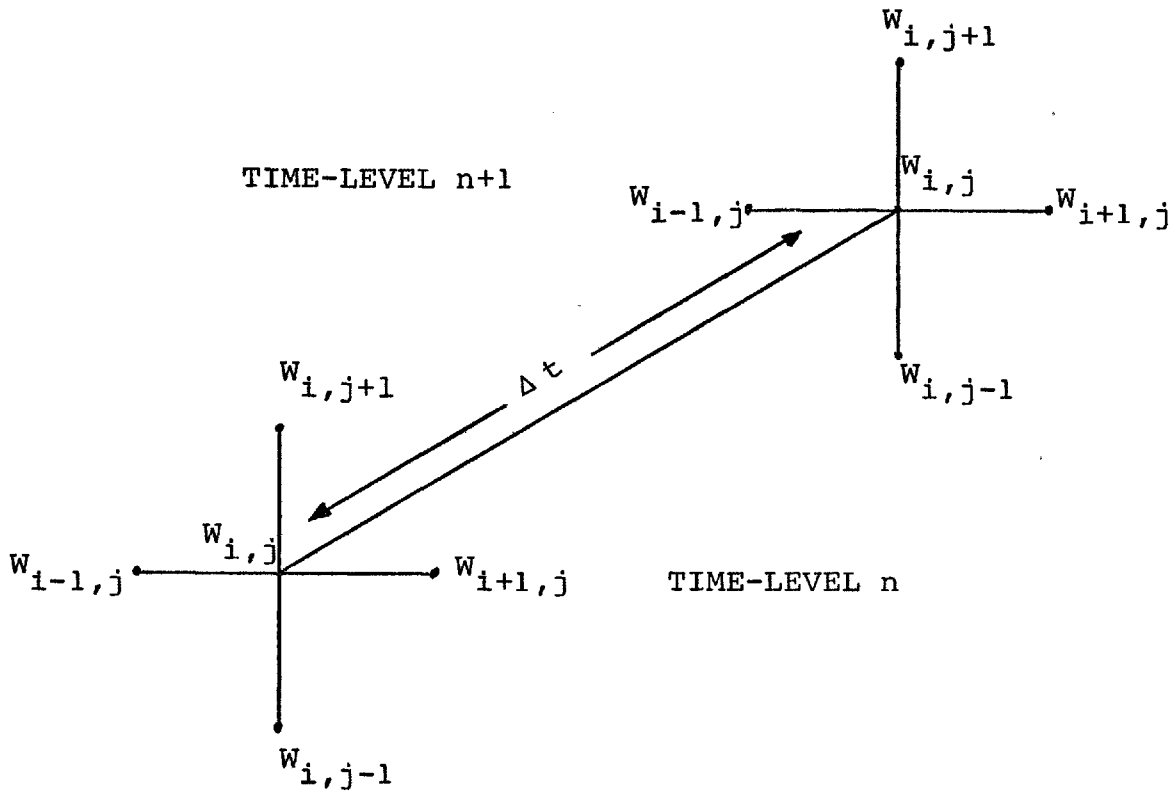

FIGURE 3.2.2 FIVE-POINT COMPUTATIONAL MOLECULE

be approximated at the node (i,j) and at the n time-step. Each derivative approximation is of second order accuracy and is derived using a Taylor's series expansion of the function about the node (i,j) i.e. central differencing is used.

Using the above notations, the second order central difference and first order forward difference schemes for the time derivative can be written as follows:

$$\left(\frac{\partial W}{\partial t}\right)^{n}_{i,j} = \partial_n \left(W^{n}_{ij}\right) + O(\Delta t^2)$$

$$= \frac{1}{2\Delta t}\left(W^{n+1}_{i,j} - W^{n-1}_{i,j}\right) + O(\Delta t^2) \qquad (3.2.6)$$

$$\left(\frac{\partial W}{\partial t}\right)^{n}_{i,j} = \partial_n \left(W^{n+\frac{1}{2}}_{ij}\right) + O(\Delta t)$$

$$= \frac{1}{\Delta t}\left(W^{n+1}_{i,j} - W^{n}_{ij}\right) + O(\Delta t) \qquad (3.2.7)$$

The error which arises because of the difference between the original partial differential equations and their finite-difference forms is known as truncation error. For example, relation (3.2.2) has a truncation error of order h^2 and is interpreted as follows:

$$\lim_{h \to 0} \left(\frac{\partial W}{\partial z}\right)^{n}_{i,j} = \partial_i \left(W^{n}_{i,j}\right) \qquad (3.2.8)$$

or,

$$\lim_{h \to 0} O(h^2) = 0 \qquad (3.2.9)$$

Thus the consistency condition is assumed to be satisfied by each derivative. Therefore, the finite-difference equations derived with the above approximation are assumed to be consistent with the differential equations.

3.2.1 First Upwind Difference Representation of Partial Derivatives of the Convective Terms

The geometrical interpretation of the first partial derivative is that it is the slope, in the direction of the derivative of the tangent plane to the surface. Consider figure 3.2.3. It is required to approximate the slope of tangent XX at the point $Z_{i,j}$ (point C on figure 3.2.3). If a central difference Taylor's series approximation is used the slope of the line XX is approximated by that of line AB. The slope of AB is calculated by taking an arithmetic mean of the slopes of lines AC and CB, that is:

$$\left(\frac{\partial W}{\partial z}\right)^n_{i,j} \simeq \frac{1}{2h}\left(W^n_{i+1,j}-W^n_{i-1,j}\right)=\frac{1}{2h}\left(W^n_{i+1,j}-W^n_{i,j}\right)+\frac{1}{2h}\left(W^n_{i,j}-W^n_{i-1,j}\right) \tag{3.2.10}$$

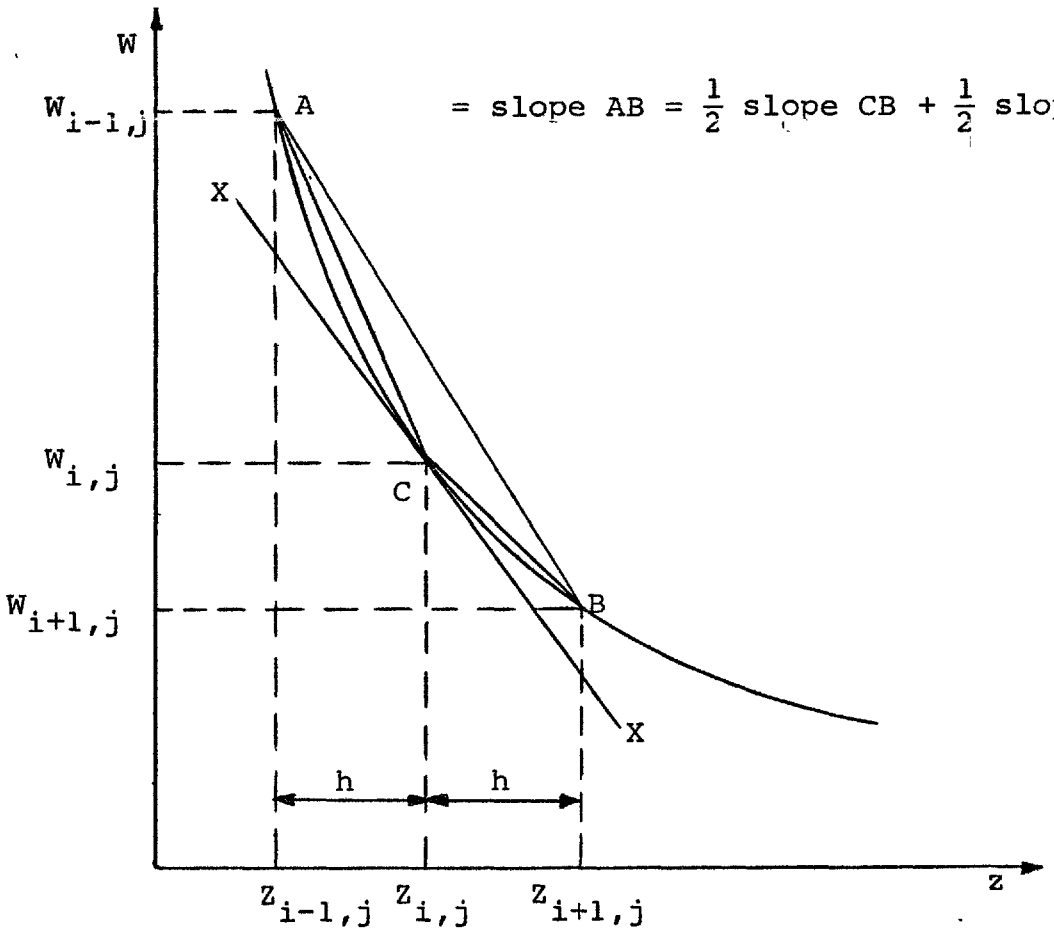

FIGURE 3.2.3 GRADIENT APPROXIMATION

In general, a finite-difference formulation of a flow equation will possess 'the transportive property', as stated by Roache (1972), "if the effect of a perturbation in a transport property is advected only in the direction of velocity". Roache then concluded that "the fact is that the most frequently used methods do not possess this property. All methods which use centered-space derivatives for the advection (convection) terms do not possess this property. The emphasis is on the word 'advected'. A physical perturbation in vorticity will spread in all directions due to diffusion. But it should be carried along only in the direction of the velocity". A lack of the transportive property in a finite-difference representation of a flow equation, may lead to unconditional instability when explicit techniques are used and may cause a poor rate of convergence when implicit techniques are used.

A better and more general approximation would be to use a more flexible representation which adjusts itself to the direction of the velocity. A differencing method which possesses the transportive property and which achieves stability of the convective terms involves the use of one-sided rather than central differences. Using such a scheme, equation (3.2.10) can be rewritten as follows:

$$\left(\frac{\partial W}{\partial z}\right)^{n}_{i,j} = \frac{\omega_z}{h}\left(W^{n}_{i+1,j} - W^{n}_{i,j}\right) + \frac{(1-\omega_z)}{h}\left(W^{n}_{i,j} - W^{n}_{i-1,j}\right) \qquad (3.2.11)$$

where ω_z is a weighting factor. For $\omega_z = 0.5$, equation (3.2.11) will become identical to equation (3.2.10)

The most logical choice of the weighting factor for a particular node would be the 'upstream difference scheme'. In this scheme the terms in which the velocity components apprear as coefficients, the convective terms, are approximated by backward differences if the velocity coefficients are positive. Forward differences, therefore, are used when the velocity coefficients are less than zero. Hence, if the flow direction at point C on figure 3.2.3, is from A to C, then the gradient at point C may be approximated by that of the line AC by setting the weighting factor equal to zero. However, if the flow at C is from B to C, then gradient at C may be approximated by that of the line BC by setting the weighting factor equal to one.

Thus, the one-sided difference is always on the 'upwind' or 'upstream' side of the point at which the first derivative is approximated. It is in this way that upwind differences are used in the present work.

This method has often been used in the past under various names and with different rationales. Meteorologists have long known the stabilizing effect of 'upwind' differencing and have applied it to incompressible and to Boussinesq problems (Lilly 1965: Forsythe and Wasow 1960). Rafique (1971), and Hatim (1975) have referred to it as the 'upstream biased scheme' and they used it at high Reynolds numbers. Forsythe and Wasow (1960) refer to the method as 'difference equations with positive coefficients'.

The variable coefficients, $(-\frac{\partial \psi}{\partial \Theta})$ and $(\frac{\partial \psi}{\partial z})$, of the

convective terms of the vorticity transport equation, equation (2.5.5) and of the energy equation, equation (2.5.8) are connected in direction and magnitude to the velocity components, u_z and u_Θ, by equations (2.5.3) and (2.5.4), respectively.

The upwind difference form of a first order derivative with respect to Θ, using the weighting factor ω_Θ, can be represented as:

$$\left(\frac{\partial W}{\partial \Theta}\right)^n_{i,j} = \frac{\omega_\Theta}{k}\left(W^n_{i,j+1} - W^n_{i,j}\right) + \frac{(1-\omega_\Theta)}{k}\left(W^n_{i,j} - W^n_{i,j-1}\right) \quad (3.2.12)$$

In the remaining part of this chapter the following expressions will be used to express the original partial differential equations in their corresponding finite-difference forms:

$$\left(\frac{\partial W}{\partial z}\right)^n_{i,j} = \partial_i\left(W^n_{ij}\right) + 0(h^2) = \frac{1}{2h}\,\Delta_i\left(W^n_{ij}\right) + 0(h^2)$$

$$= \frac{1}{2h}\left(W^n_{i+1,j} - W^n_{i-1,j}\right) + 0(h^2) \quad (3.2.13)$$

$$\left(\frac{\partial^2 W}{\partial z^2}\right)^n_{i,j} = \partial_i^2\left(W^n_{ij}\right) + 0(h^2) = \frac{1}{h^2}\,\Delta_i^2\left(W^n_{ij}\right) + 0(h^2)$$

$$= \frac{1}{h^2}\left(W^n_{i+1,j} + W^n_{i-1,j} - 2W^n_{i,j}\right) + 0(h^2) \quad (3.2.14)$$

and similarly,

$$\left(\frac{\partial W}{\partial \Theta}\right)^n_{i,j} = \partial_j\left(W^n_{ij}\right) + 0(k^2) = \frac{1}{2k}\,\Delta_j\left(W^n_{ij}\right) + 0(k^2)$$

$$= \frac{1}{2k}\left(W^n_{i,j+1} - W^n_{i,j-1}\right) + 0(k^2) \quad (3.2.15)$$

$$\left(\frac{\partial^2 W}{\partial \Theta^2}\right)^n_{i,j} = \delta_j^2 (W^n_{ij}) + 0(k^2) = \frac{1}{k^2} \Delta_j^2 (W^n_{ij}) + 0(k^2)$$

$$= \frac{1}{k^2} (W^n_{i,j+1} + W^n_{i,j-1} - 2W^n_{i,j}) + 0(k^2) \qquad (3.2.16)$$

$$\left(\frac{\partial W}{\partial t}\right)^n_{i,j} = \delta_n (W^{n+1/4}_{ij}) + 0(\Delta t^2) = \frac{2}{\Delta t} (W^{n+1/4}_{ij}) + 0(\Delta t^2)$$

$$= \frac{2}{\Delta t} (W^{n+\frac{1}{2}}_{i,j} - W^n_{i,j}) + 0(\Delta t^2) \qquad (3.2.17)$$

and finally, the first order partial derivatives in convective terms are approximated as follows:

$$\left(\frac{\partial W}{\partial z}\right)^n_{i,j} = \frac{\omega_z}{h}(W^n_{i+1,j} - W^n_{i,j}) + \frac{(1-\omega_z)}{h}(W^n_{i,j} - W^n_{i-1,j}) \qquad (3.2.18)$$

$$\left(\frac{\partial W}{\partial \Theta}\right)^n_{i,j} = \frac{\omega_\Theta}{k} (W^n_{i,j+1} - W^n_{i,j}) + \frac{(1-\omega_\Theta)}{k}(W^n_{i,j} - W^n_{i,j-1}) \qquad (3.2.19)$$

3.3 FINITE DIFFERENCE REPRESENTATION OF THE EQUATIONS

3.3.1 Discussion of Available Methods

In chapter 2 the form in which the vorticity transport, energy and stream function equations are to be solved was derived. These equations are rewritten below as follows:

vorticity transport equation:

$$e^{2Z} \frac{\partial G}{\partial t} + \frac{1}{e^Z \sin\Theta}\left\{\frac{\partial \psi}{\partial z}\left[\frac{\partial G}{\partial \Theta} - 2\cot\Theta\, G\right] - \frac{\partial \psi}{\partial \Theta}\left[\frac{\partial G}{\partial z} - 2G\right]\right\}$$

$$= e^{2z} E_+^2 (G) + e^{2z} Gr\left[\sin\Theta\cos\Theta \frac{\partial T}{\partial \Theta} + \sin^2\Theta \frac{\partial T}{\partial z}\right] \qquad (3.3.1)$$

energy equation:

$$\mathrm{Pr}\, e^{2z} \frac{\partial T}{\partial t} + \frac{\mathrm{Pr}}{e^{z}\sin\Theta}\left[\frac{\partial \psi}{\partial z}\frac{\partial T}{\partial \Theta} - \frac{\partial \psi}{\partial \Theta}\frac{\partial T}{\partial z}\right]$$

$$= \frac{\partial^2 T}{\partial z^2} + \frac{\partial T}{\partial z} + \frac{\partial^2 T}{\partial \Theta^2} + \cot\Theta \frac{\partial T}{\partial \Theta} \qquad (3.3.2)$$

stream function equation:

$$\frac{\partial^2 \psi}{\partial z^2} - \frac{\partial \psi}{\partial z} + \frac{\partial^2 \psi}{\partial \Theta^2} - \cot\Theta \frac{\partial \psi}{\partial \Theta} = e^{2z} G \qquad (3.3.3)$$

where $G = \zeta e^{z}\sin\Theta$,

and $$e^{2z} E_{+}^{2} = \frac{\partial}{\partial z^2} - \frac{\partial}{\partial z} + \frac{\partial^2}{\partial \Theta^2} - \cot\Theta \frac{\partial}{\partial \Theta}$$

The finite-difference approximation or discretization of equations (3.3.1) to (3.3.3) can formally be expressed as follows:

vorticity transport equation:

$$e^{2z_i}\left(\frac{\partial G}{\partial t}\right)^{n}_{i,j} + \frac{1}{e^{z_i}\sin\Theta_j}\left\{\left(\frac{\partial \psi}{\partial z}\right)^{n}_{i,j}\left[\left(\frac{\partial G}{\partial \Theta}\right)^{n}_{i,j} - 2\cot\Theta_j G^{n}_{i,j}\right] - \left(\frac{\partial \psi}{\partial \Theta}\right)^{n}_{i,j}\left[\left(\frac{\partial G}{\partial z}\right)^{n}_{i,j} - 2G^{n}_{i,j}\right]\right\}$$

$$= \left(\frac{\partial^2 G}{\partial z^2}\right)^{n}_{i,j} - \left(\frac{\partial G}{\partial z}\right)^{n}_{i,j} + \left(\frac{\partial^2 G}{\partial \Theta^2}\right)^{n}_{i,j} - \cot\Theta_j \left(\frac{\partial G}{\partial \Theta}\right)^{n}_{i,j}$$

$$+ e^{2z_i}\,\mathrm{Gr}\left[\sin\Theta_j\cos\Theta_j \left(\frac{\partial T}{\partial \Theta}\right)^{n}_{i,j} + \sin^2\Theta_j \left(\frac{\partial T}{\partial z}\right)^{n}_{i,j}\right] \qquad (3.3.4)$$

energy equation:

$$\Pr e^{2z_i}\left(\frac{\partial T}{\partial t}\right)^n_{i,j} + \frac{\Pr}{e^{z_i}\sin\Theta_j}\left[\left(\frac{\partial \psi}{\partial z}\right)^n_{i,j}\left(\frac{\partial T}{\partial \Theta}\right)^n_{i,j} - \left(\frac{\partial \psi}{\partial \Theta}\right)^n_{i,j}\left(\frac{\partial T}{\partial z}\right)^n_{i,j}\right]$$

$$= \left(\frac{\partial^2 T}{\partial z^2}\right)^n_{i,j} + \left(\frac{\partial T}{\partial z}\right)^n_{i,j} + \left(\frac{\partial^2 T}{\partial \Theta^2}\right)^n_{i,j} + \cot\Theta_j\left(\frac{\partial T}{\partial \Theta}\right)^n_{i,j} \qquad (3.3.5)$$

stream function equation:

$$\left(\frac{\partial^2 \psi}{\partial z^2}\right)^n_{i,j} - \left(\frac{\partial \psi}{\partial z}\right)^n_{i,j} + \left(\frac{\partial^2 \psi}{\partial \Theta^2}\right)^n_{i,j} - \cot\Theta_j\left(\frac{\partial \psi}{\partial \Theta}\right)^n_{i,j}$$

$$= G^n_{i,j}\, e^{2z_i} \qquad (3.3.6)$$

The discretization process is carried out at a typical node i,j in the mesh covering the domain of intergration at the n-th time-step. Time does not appear explicitly in equation (3.3.6) so that the computational procedure to be used must solve equations (3.3.4) and (3.3.5) first in order to obtain values of $G^{n+1}_{i,j}$ and $T^{n+1}_{i,j}$. Equation (3.3.6) is then solved as a Poisson's equation to obtain values of $\psi^{n+1}_{i,j}$. Since the values of $\psi^{n+1}_{i,j}$ are also required in equations (3.3.4) and (3.3.5), the entire step must be repeated until all the three equations are satisfied simulataneously.

Assuming that a suitable mesh is chosen, i.e. h and k are sufficiently small, then the truncation error terms are negligible. Then simple second order explicit finite-difference representations for the equations (3.3.1) and (3.3.2) can be written as follows:

$$e^{2z_i}\partial_n(G^n_{ij}) + \frac{1}{e^{z_i}\sin\Theta_j}\left\{\partial_i(\psi^n_{ij})\left[\partial_j(G^n_{ij}) - 2\cot\Theta_j\, G^n_{ij}\right]\right.$$

$$\left. - \partial_j(\psi^n_{ij})\left[\partial_i(G^n_{ij}) - 2\, G^n_{ij}\right]\right\}$$

$$= \partial_i^2(G^n_{ij}) - \partial_i(G^n_{ij}) + \partial_j^2(G^n_{ij}) - \cot\Theta_j\,\partial_j(G^n_{ij})$$

$$+ e^{2z_i}Gr\left[\sin\Theta_j\cos\Theta_j\,\partial_j(T^n_{ij}) + \sin^2\Theta_j\,\partial_i(T^n_{ij})\right] \quad (3.3.7)$$

and

$$Pr\, e^{2z_i}\partial_n(T^n_{ij}) + \frac{Pr}{e^{z_i}\sin\Theta_j}\left[\partial_i(\psi^n_{ij})\,\partial_j(T^n_{ij})\right.$$

$$\left. - \partial_j(\psi^n_{ij})\,\partial_i(T^n_{ij})\right]$$

$$= \partial_i^2(T^n_{ij}) + \partial_i(T^n_{ij}) + \partial_j^2(T^n_{ij}) + \cot\Theta_j\,\partial_j(T^n_{ij}) \quad (3.3.8)$$

Richtmyer (1967) states that the use of second order time-centered explicit schemes for the representation of diffusion terms (second order linear terms), is unconditionally unstable. Hence, the addition of non-linear terms, for example the convective terms can only make matters worse. Thus the finite-difference approximations represented by equations (3.3.7) and (3.3.8) can not be used. However, explicit schemes with forward time differences and centered space differences are conditionally stable. By the use of such a first order explicit scheme to the vorticity transport and energy equations the following equations are obtained:

vorticity transport equation:

$$e^{2z_i}\partial_n(G_{ij}^{n+\frac{1}{2}}) + \frac{1}{e^{z_i}\sin\Theta_j}\left\{\partial_i(\psi_{ij}^n)\left[\partial_j(G_{ij}^n) - 2\cot\Theta_j\, G_{ij}^n\right] - \partial_j(\psi_{ij}^n)\left[\partial_i^n(G_{ij}^n) - 2\, G_{ij}^n\right]\right\}$$

$$= \partial_i^2(G_{ij}^n) - \partial_i(G_{ij}^n) + \partial_j^2(G_{ij}^n) - \cot\Theta_j\,\partial_j(G_{ij}^n)$$

$$+ e^{2z_i}\,Gr\left[\sin\Theta_j\cos\Theta_j\,\partial_j(T_{ij}^n) + \sin^2\Theta_j\,\partial_i(T_{ij}^n)\right] \qquad (3.3.9)$$

energy equation:

$$Pr\, e^{2z_i}\partial_n(T_{ij}^{n+\frac{1}{2}}) + \frac{Pr}{e^{z_i}\sin\Theta_j}\left[\partial_i(\psi_{ij}^n)\,\partial_j(T_{ij}^n) - \partial_j(\psi_{ij}^n)\,\partial_i(T_{ij}^n)\right]$$

$$= \partial_i^2(T_{ij}^n) + \partial_i(T_{ij}^n) + \partial_j^2(T_{ij}^n) + \cot\Theta_j\,\partial_j(T_{ij}^n) \qquad (3.3.10)$$

Dufort and Frankel (1953) suggested a stable second order explicit scheme. The second partial derivatives were approxiamted in the following manner, (for a general function W):

$$\partial_i^2(W_{ij}^n)_{DF} = \partial_i^2(W_{ij}^n) + \frac{1}{h^2}\left[2W_{i,j}^n - (W_{i,j}^{n+1} + W_{i,j}^{n-1})\right] \qquad (3.3.11)$$

and

$$\partial_j^2(W_{ij}^n)_{DF} = \partial_j^2(W_{ij}^n) + \frac{1}{k^2}\left[2W_{i,j}^n - (W_{i,j}^{n+1} + W_{i,j}^{n-1})\right] \qquad (3.3.12)$$

Therefore, by the use of Dufort and Frankel's scheme, equation (3.3.2) can be written as follows:

$$\Pr e^{2z_i} \partial_n(T^n_{ij}) + \frac{\Pr}{e^{z_i}\sin\Theta_j}\Big[\partial_i(\psi^n_{ij})\ \partial_j(T^n_{ij}) - \partial_j(\psi^n_{ij})\ \partial_i(T^n_{ij})\Big]$$

$$= \partial_i^2(T^n_{ij})_{DF} + \partial_i(T^n_{ij}) + \partial_j^2(T^n_{ij})_{DF} + \cot\Theta_j\, \partial_j(T^n_{ij}) \qquad (3.3.13)$$

The application of Dufort and Frankel's scheme to the vorticity transport equation results in an equation of the same form as equation (3.3.7) except that the second order partial derivatives are expressed by equations (3.3.11) and (3.3.12),

i.e.

$$\partial_i^2(G^n_{ij})_{DF} \quad \text{and} \quad \partial_j^2(G^n_{ij})_{DF}$$

In the absence of non-linear convective terms, the Dufort and Frankel scheme is unconditionally stable. However, in practice, in order to obtain sufficient accuracy, a restriction on the time-step, Δt, has to be imposed.

The use of Dufort and Frankel's scheme requires more computer storage than the conditionally stable simple explicit scheme. The choice between the two schemes is usually made from an assessment of computer time and storage requirements (Rafique 1971).

An implicit scheme requiring the same storage as Dufort

and Frankel explicit scheme is better both for accuracy and numerical stability. A general iterative implicit scheme for solving the vorticity transport and energy equations can be written as follows:

vorticity transport equation:

$$e^{2z_i}\partial_n(G_{ij}^{n+\frac{1}{2}}) + \frac{1}{e^{z_i}\sin\Theta_j}\left\{\overline{\partial_i(\psi_{ij}^n)}\left[\overline{\partial_j(G_{ij}^n)} - 2\cot\Theta_j G_{ij}^n\right] - \overline{\partial_j(\psi_{ij}^n)}\left[\overline{\partial_i(G_{ij}^n)} - 2\,G_{ij}^n\right]\right\}$$

$$= \overline{\partial_i^2(G_{ij}^n)} - \overline{\partial_i(G_{ij}^n)} + \overline{\partial_j^2(G_{ij}^n)} - \cot\Theta_j\overline{\partial_j(G_{ij}^n)}$$

$$+ e^{2z_i}Gr\left[\sin\Theta_j\cos\Theta_j\overline{\partial_j(T_{ij}^n)} + \sin^2\Theta_j\,\overline{\partial_i(T_{ij}^n)}\right] \qquad (3.3.14)$$

energy equation:

$$\Pr\, e^{2z_i}\partial_n(T_{ij}^{n+\frac{1}{2}}) + \frac{\Pr}{e^{z_i}\sin\Theta_j}\left[\overline{\partial_i(\psi_{ij}^n)}\;\overline{\partial_j(T_{ij}^n)} - \overline{\partial_j(\psi_{ij}^n)}\;\overline{\partial_i(T_{ij}^n)}\right]$$

$$= \overline{\partial_i^2(T_{ij}^n)} + \overline{\partial_i(T_{ij}^n)} + \overline{\partial_j^2(T_{ij}^n)} + \cot\Theta_j\overline{\partial_j(T_{ij}^n)} \qquad (3.3.15)$$

where, in general, $\overline{\partial_i(W_{ij}^n)} = \alpha\,\partial_i(W_{ij}^{n+1}) + (1-\alpha)\,\partial_i(W_{ij}^n)$, where α is a weighting factor. All the terms in the above equations are expressed in a similar manner. Equations (3.3.14) and (3.3.15) can be solved by successive over or under-relaxation and, wherever required, the most up to date values of the stream function can be used. Values of the stream

function are obtained by successive over-relaxation sweeps of the stream function equation. The most common value of the weighting factor, α, used is one-half and the scheme is normally called the Crank-Nicolson scheme.

Implicit schemes, especially when applied to the vorticity transport and energy equations for the case of free convective heat transfer from a solid sphere, lead to large sets of non-linear simultaneous equations. This is the real disadvantage of implicit schemes since the solution of large sets of non-linear simultaneous equations is both difficult and time consuming. For these reasons the original alternating direction implicit method, ADI, proposed by Peaceman and Rachford (1955) was adopted.

The alternating direction implicit methods were introduced in companion papers by Peaceman and Rachford (1955) and Douglas (1955). Also known as the method of variable direction, this method makes use of a splitting of the time-step to obtain a multi-dimensional implicit method. The advantage of this approach over the fully implicit methods is that each resulting algebraic equation, although implicit, is only tridiagonal. Therefore, this method requires only the solution of a tridiagonal system such as occurs when the usual implicit methods are applied to one dimensional problems.

This method is unconditionally stable for the linear diffusion equation, as are fully implicit methods. However,

no stability analysis has been made for non-linear partial differential equations such as the vorticity transport and energy equations.

Roache (1972), has given a survey of the early applications of ADI methods to fluid dynamics problems. ADI methods are currently the most popular methods used for viscous problems. In addition to the works surveyed by Roache, Son and Hanratty (1969) used Peaceman and Rachford's alternating direction implicit method to obtain the solution for flow around a circular cylinder. Rafique (1971) used Peaceman and Rachfords alternating direction implicit method to obtain the solution for flow around a solid sphere. Hatim (1975) used Peaceman and Rachford's alternating direction implicit method to obtain the solution of heat transfer from a solid sphere accelerating from rest. The solutions obtained by Son and Hanratty, by Rafique, and by Hatim indicate the suitability of Peaceman and Rachford's alternating direction implicit method for solving the vorticity transport and energy equations. For these reasons, the alternating direction implicit method proposed by Peaceman and Rachford (1955) is used in this work to solve the vorticity transport and energy equations.

3.3.2 Peaceman and Rachford's Alternating Direction Implicit Method.

If a general implicit method of solving equations (3.3.14) and (3.3.15) were to be used, all the derivatives

in the equations would require values of the modified vorticity, G, and temperature, T, at the n+1 time-level. As these values are unknown it would be necessary to solve iteratively large numbers of non-linear algebraic equations. However, if the derivatives in one of the directions were to be approximated at the $n+\frac{1}{2}$ time-level, while the derivatives in other direction were to be approximated at the n-th time-level, the sets of simultaneous equations in terms of the known values at the n-th time-level and the unknown values at the $n+\frac{1}{2}$ time-level could be solved easily by an elimination method. If the procedure were to be repeated for the next half time-step such that the derivatives previously approximated at the n-th time-level were now approximated at the n+1 time-level and the other derivatives were approximated at the $n+\frac{1}{2}$ time level using the values obtained previously, the temperature and vorticity values could be obtained at the n+1 time-level. This is the method used in the present work.

In most cases the choice of derivatives which are approximated at the $n+\frac{1}{2}$ time-level is unimportant. This is not the case in the present problem because a significant amount of computing time can be saved by making the correct choice of the derivatives which are to be approximated at the $n+\frac{1}{2}$ time-level.

In section 2.6 it is stated that the sphere surface boundary condition for the vorticity is a funciton of time and must be approximated. However, the vorticity at the

axis of symmetry is constant and known; thus if the derivatives which involve the constant boundary conditions are approximated at the $n+\frac{1}{2}$ time-level, then iterations are only performed over the last half time-step. This means that in the vorticity transport equation the derivatives with respect to angle, θ, must be approximated at the $n+\frac{1}{2}$ time-level.

In the case of the energy equation, since the temperature at the axis of symmetry is a function of time and is constant at the sphere surface, a reverse procedure appears to be reasonable. That is, the temperature should be updated from the n-th time-level to the $n+\frac{1}{2}$ time-level in the j-direction and then be updated from the $n+\frac{1}{2}$ time-level to the n+1 time-level in the i-direction. This means that in the energy equation, the derivatives with respect to z, radial direction, must be approximated at the $n+\frac{1}{2}$ time-level.

However, numerical experiments revealed that for the present problem, a compatiable procedure for solving the vorticity transport and energy equations not only decreases the total time of computation but also increases the accuracy of the results.

Therefore, in the present work, in both the vorticity transport and energy equations, the derivatives with respect to angle are approximated at the first half time-step and the derivatives with respect to z, radial direction, are

approximated at the n+1 time-step.

3.3.3 Finite-Difference Representation of the Vorticity Transport Equation

The vorticity transport equation, equation (3.3.1), when written in finite-difference form for the time-step n to n+½ in the Θ-direction, is as follows:

$$e^{2z_i}\partial_n\left(G_{ij}^{n+1/4}\right) + \frac{1}{e^{z_i}\sin\Theta_j}\left\{\partial_i\left(\psi_{ij}^{n}\right)\left[\partial_j\left(G_{ij}^{n+\frac{1}{2}}\right) - 2\cot\Theta_j G_{ij}^{n+\frac{1}{2}}\right]\right.$$

$$\left. - \partial_j\left(\psi_{ij}^{n}\right)\left[\partial_i\left(G_{ij}^{n}\right) - 2\,G_{ij}^{n}\right]\right\}$$

$$= \partial_i^2\left(G_{ij}^{n}\right) - \partial_i\left(G_{ij}^{n}\right) + \partial_j^2\left(G_{ij}^{n+\frac{1}{2}}\right) - \cot\Theta_j\,\partial_j\left(G_{ij}^{n+\frac{1}{2}}\right)$$

$$+ e^{2z_i}\sin^2\Theta_j\,Gr\left[\cot\Theta_j\,\partial_j\left(T_{ij}^{n}\right) + \partial_i\left(T_{ij}^{n}\right)\right] \qquad (3.3.16)$$

For time-step n+½ to n+1, the finite-difference form of the vorticity transport equation, in the z-direction, is as follows:

$$e^{2z_i}\partial_n\left(G_{ij}^{n+\frac{3}{4}}\right) + \frac{1}{e^{z_i}\sin\Theta_j}\left\{\partial_i\left(\psi_{ij}^{n+\frac{1}{2}}\right)\left[\partial_j\left(G_{ij}^{n+\frac{1}{2}}\right) - 2\cot\Theta_j G_{ij}^{n+\frac{1}{2}}\right]\right.$$

$$\left. - \partial_j\left(\psi_{ij}^{n+\frac{1}{2}}\right)\left[\partial_i\left(G_{ij}^{n+1}\right) - 2G_{ij}^{n+1}\right]\right\}$$

$$= \partial_i^2\left(G_{ij}^{n+1}\right) - \partial_i\left(G_{ij}^{n+1}\right) + \partial_j^2\left(G_{ij}^{n+\frac{1}{2}}\right) - \cot\Theta_j\,\partial_j\left(G_{ij}^{n+\frac{1}{2}}\right)$$

$$+ e^{2z_i}\sin^2\Theta_j\,Gr\left[\cot\Theta_j\,\partial_j\left(T_{ij}^{n+\frac{1}{2}}\right) + \partial_i\left(T_{ij}^{n+\frac{1}{2}}\right)\right] \qquad (3.3.17)$$

Equation (3.3.16) can be expressed more clearly in the following manner:

$$\frac{2e^{2z_i}}{\Delta t} G_{ij}^{n+\frac{1}{2}} + \frac{\partial_i(\psi_{ij}^n)}{e^{z_i}\sin\Theta_j}\left[\partial_j(G_{ij}^{n+\frac{1}{2}}) - 2\cot\Theta_j G_{ij}^{n+\frac{1}{2}}\right]$$

$$-\partial_j^2(G_{ij}^{n+\frac{1}{2}}) + \cot\Theta_j\partial_j(G_{ij}^{n+\frac{1}{2}})$$

$$= \frac{2e^{z_i}}{\Delta t} G_{ij}^n + \frac{\partial_j(\psi_{ij}^n)}{e^{z_i}\sin\Theta_j}\left[\partial_i(G_{ij}^n) - 2G_{ij}^n\right]$$

$$+\partial_i^2(G_{ij}^n) - \partial_i(G_{ij}^n) + e^{2z_i}\sin^2\Theta_j Gr\left[\cot\Theta_j\partial_j(T_{ij}^n) + \partial_i(T_{ij}^n)\right] \qquad (3.3.18)$$

similarly, equation (3.3.17) becomes:

$$\frac{2e^{2z_i}}{\Delta t} G_{ij}^{n+1} - \frac{\partial_j(\psi_{ij}^{n+\frac{1}{2}})}{e^{z_i}\sin\Theta_j}\left[\partial_i(G_{ij}^{n+1}) - 2G_{ij}^{n+1}\right]$$

$$-\partial_i^2(G_{ij}^{n+1}) + \partial_i(G_{ij}^{n+1})$$

$$= \frac{2e^{2z_i}}{\Delta t} G_{ij}^{n+\frac{1}{2}} - \frac{\partial_i(\psi_{ij}^{n+\frac{1}{2}})}{e^{z_i}\sin\Theta_j}\left[\partial_j(G_{ij}^{n+\frac{1}{2}}) - 2\cot\Theta_j G_{ij}^{n+\frac{1}{2}}\right]$$

$$+\partial_j^2(G_{ij}^{n+\frac{1}{2}}) - \cot\Theta_j\partial_j(G_{ij}^{n+\frac{1}{2}})$$

$$+ e^{2z_i}\sin^2\Theta_j Gr\left[\cot\Theta_j\partial_j(T_{ij}^{n+\frac{1}{2}}) + \partial_i(T_{ij}^{n+\frac{1}{2}})\right] \qquad (3.3.19)$$

Equation (3.3.18) can be expanded into sets of simultaneous equations of the following form:

$$C_{1j}P^{n+\frac{1}{2}}_{i,j-1} + C_{2j}P^{n+\frac{1}{2}}_{i,j} + C_{3j}P^{n+\frac{1}{2}}_{i,j+1} = D^{n}_{j} \qquad (3.3.20)$$

where

$$D^{n}_{j} = C_{1i}P^{n}_{i-1,j} + C_{2i}P^{n}_{i,j} + C_{3i}P^{n}_{i+1,j} + C^{n}_{4ij} \qquad (3.3.21)$$

for i=2,3. . . . , in and j=2,3 . . . . ,jn, where in + 1 and jn + 1 are the total numbers of grid lines in the z and Θ directions, respectively, and P is a general working variable substituted in place of the values of G.

Similarly, equation (3.3.19) can be expanded into sets of simultaneous equations of the form:

$$C'_{1i}P^{n+1}_{i-1,j} + C'_{2i}P^{n+1}_{i,j} + C'_{3i}P^{n+1}_{i+1,j} = D^{n+\frac{1}{2}}_{i} \qquad (3.3.22)$$

where

$$D^{n+\frac{1}{2}}_{i} = C'_{1j}P^{n+\frac{1}{2}}_{i,j-1} + C'_{2j}P^{n+\frac{1}{2}}_{i,j} + C'_{3j}P^{n+\frac{1}{2}}_{i,j+1} + C^{n+\frac{1}{2}}_{4ij} \qquad (3.3.22)$$

As described before, since it does not appear to be possible to find a single system of finite-difference equations which possesses the transportive property over the entire space-time region of interest, four separate systems of equations corresponding to the signs of the two variable coefficients of the convective terms, must be used. This has been achieved by the use of weighting factors ω_z and ω_Θ in the first upwind differencing of the first order derivatives in the non-linear convective terms. According

to the signs of the variable coefficients, backward or forward difference equations would be used.

With the above remarks, the coefficients of equations (3.3.20) to (3.3.23) for backward , forward and central differences (in general $\omega=0$, $\omega=1$, and $\omega=0.5$, respectively) may be expressed as follows:

$$C_{1j} = -b_{4j} - KG_{ij}\,\Delta_i(\psi_{ij})\,(1-\omega_z) \tag{3.3.24}$$

$$C_{2j} = \frac{1}{X_i} + \frac{2}{ak^2} + KG_{ij}\Delta_i(\psi^n_{ij})(1-2\omega_z-2k\cot\Theta_j) \tag{3.3.25}$$

$$C_{3j} = -b_{3j} + KG_{ij}\Delta_i(\psi^n_{ij})\omega_z \tag{3.3.26}$$

$$C_{1i} = b_{2i} - KG_{ij}\Delta_j\,(\psi^n_{ij})\,(1-\omega_\Theta) \tag{3.3.27}$$

$$C_{2i} = \frac{1}{X_i} - \frac{2}{ah^2} + KG_{ij}\Delta_j\,(\psi^n_{ij})(1-2\omega_\Theta-2h) \tag{3.3.28}$$

$$C_{3i} = b_{1i} + KG_{ij}\Delta_j(\psi^n_{ij})\omega_\Theta \tag{3.3.29}$$

$$C'_{1j} = b_{4j} + KG_{ij}\Delta_i(\psi^{n+\frac{1}{2}}_{ij})\,(1-\omega_z) \tag{3.3.30}$$

$$C'_{2j} = \frac{1}{X_i} - \frac{2}{ak^2} - KG_{ij}\Delta_i\,(\psi^{n+\frac{1}{2}}_{ij})(1-2\omega_z-2k\cot\Theta_j) \tag{3.3.31}$$

$$C'_{3j} = b_{3j} - KG_{ij}\Delta_i(\psi^{n+\frac{1}{2}}_{ij})\omega_z \tag{3.3.32}$$

$$C'_{1i} = -b_{2i} + KG_{ij}\Delta_j(\psi^{n+\frac{1}{2}}_{ij})\,(1-\omega_\Theta) \tag{3.3.33}$$

$$C'_{2i} = \frac{1}{X_i} + \frac{2}{ah^2} - KG_{ij}\Delta_j\,(\psi^{n+\frac{1}{2}}_{ij})(1-2\omega_\Theta-2h) \tag{3.3.34}$$

$$C'_{3i} = -b_{1i} - KG_{ij}\Delta_j(\psi^{n+\frac{1}{2}}_{ij})\omega_\Theta \tag{3.3.35}$$

and,in general:

$$C_{4ij} = KT_{ij}\,Gr\,\cot\Theta_j h\,\Delta_j(T_{ij}) + k\Delta_i\,(T_{ij}) \tag{3.3.36}$$

In the calculation of the variable coefficients (3.3.24) to (3.3.36), the most up to date values of the relevant variables are used.

The other coefficients used in the finite-difference equations derived so far are defined as:

$$b_{1i} = \frac{1}{a} \left(\frac{1}{h^2} - \frac{1}{2h}\right) \tag{3.3.37}$$

$$b_{2i} = \frac{1}{a} \left(\frac{1}{h^2} + \frac{1}{2h}\right) \tag{3.3.38}$$

$$b_{3j} = \frac{1}{a} \left(\frac{1}{k^2} - \frac{1}{2k}\right) \tag{3.3.39}$$

$$b_{4j} = \frac{1}{a} \left(\frac{1}{k^2} + \frac{1}{2k}\right) \tag{3.3.40}$$

$$a = \frac{2}{h^2} + \frac{2}{k^2} \tag{3.3.41}$$

$$X_i = \frac{a\Delta t}{2\, e^{2z_i}} \tag{3.3.42}$$

$$KT_{ij} = C_R\, h_{3ij}\, h_{3ij} \tag{3.3.43}$$

$$KG_{ij} = \frac{C_R}{h_{3ij}} \tag{3.3.44}$$

where

$$C_R = \frac{1}{2ahk} \quad \text{and} \quad h_{3ij} = e^{z_i} \sin\Theta_j$$

It should be mentioned that the coefficients (3.3.37) to (3.3.41) are constants at each grid point and need to be computed only once. It will be seen in section 3.3.4 and 3.3.5, that the coefficients (3.3.37) to (3.3.44) are also used in finite-difference representation of the energy and stream function equations.

3.3.4 Finite-Difference Representation of the Energy Equation

As mentioned earlier in chapter 2, both the vorticity transport and the energy equations are partial differential equations that are elliptic with respect to the space variables and parabolic with respect to time. Therefore, the same method of solution can be used for both equations. Thus, Peaceman and Rachford's alternating direction implicit method is used to solve the energy equation.

The energy equation, equation (3.3.2), in finite-difference form for the time-step n to $n+\frac{1}{2}$ in the Θ-direction can be written as:

$$\mathrm{Pr}\, e^{2z_i} \partial_n (T_{ij}^{n+1/4}) + \frac{\mathrm{Pr}}{e^{z_i} \sin\Theta_j} \left[\partial_i (\psi_{ij}^n)\ \partial_j (T_{ij}^{n+\frac{1}{2}}) - \partial_j (\psi_{ij}^n)\ \partial_i (T_{ij}^n) \right]$$

$$= \partial_i^2 (T_{ij}^n) + \partial_i (T_{ij}^n) + \partial_j^2 (T_{ij}^{n+\frac{1}{2}}) + \cot\Theta_j \partial_j (T_{ij}^{n+\frac{1}{2}}) \quad (3.3.45)$$

and for time-step $n + \frac{1}{2}$ to $n+1$, in the z-direction, the energy equation becomes:

$$\mathrm{Pr}\, e^{2z_i} \partial_n (T_{ij}^{n+\frac{3}{4}}) + \frac{\mathrm{Pr}}{e^{z_i} \sin\Theta} \left[\partial_i (\psi_{ij}^{n+\frac{1}{2}}) \partial_j (T_{ij}^{n+\frac{1}{2}}) - \partial_j (\psi_{ij}^{n+\frac{1}{2}}) \partial_i (T_{ij}^{n+1}) \right]$$

$$= \partial_i^2 (T_{ij}^{n+1}) + \partial_i (T_{ij}^{n+1}) + \partial_j^2 (T_{ij}^{n+\frac{1}{2}}) + \cot\Theta_j \partial_j (T_{ij}^{n+\frac{1}{2}}) \quad (3.3.46)$$

Equation (3.3.45) can be expressed more clearly in the

following manner:

$$\frac{2Pr\, e^{2z_i}}{\Delta t} T_{ij}^{n+\frac{1}{2}} + \frac{Pr\, \partial_i(\psi_{ij}^n)}{z_i e^{z_i} \sin\Theta_j} \partial_j(T_{ij}^{n+\frac{1}{2}}) - \partial_j^2(T_{ij}^{n+\frac{1}{2}}) - \cot\Theta_j \partial_j(T_{ij}^{n+\frac{1}{2}})$$

$$= \frac{2Pr\, e^{2z_i}}{\Delta t} T_{ij}^{n} + \frac{Pr\, \partial_i(\psi_{ij}^n)}{z_i e^{z_i} \sin\Theta_j} \partial_i(T_{ij}^{n}) + \partial_i^2(T_{ij}^{n}) + \partial_i(T_{ij}^{n}) \quad (3.3.47)$$

Similarly, equation (3.3.46) becomes:

$$\frac{2Pr\, e^{2z_i}}{\Delta t} T_{ij}^{n+1} - \frac{Pr\, \partial_j(\psi_{ij}^{n+\frac{1}{2}})}{z_i e^{z_i} \sin\Theta_j} \partial_i(T_{ij}^{n+1}) - \partial_i^2(T_{ij}^{n+1}) - \partial_i(T_{ij}^{n+1})$$

$$= \frac{2Pr\, e^{2z_i}}{\Delta t} T_{ij}^{n+\frac{1}{2}} - \frac{Pr\, \partial_i(\psi_{ij}^{n+\frac{1}{2}})}{z_i e^{z_i} \sin\Theta_j} \partial_j(T_{ij}^{n+\frac{1}{2}}) + \partial_j^2(T_{ij}^{n+\frac{1}{2}})$$

$$+ \cot\Theta_j \partial_j(T_{ij}^{n+\frac{1}{2}}) \quad (3.3.48)$$

Equations (3.3.47) and (3.3.48) can be expanded into sets of simultaneous equations of the following form:

Equation (3.3.47) becomes:

$$F_{1j} P_{i,j-1}^{n+\frac{1}{2}} + F_{2j} P_{i,j}^{n+\frac{1}{2}} + F_{3j} P_{i,j+1}^{n+\frac{1}{2}} = R_j^n \quad (3.3.49)$$

where,

$$R_j^n = F_{1i} P_{i-1,j}^n + F_{2i} P_{i,j}^n + F_{3i} P_{i+1,j}^n \quad (3.3.50)$$

Equation (3.3.48) becomes:

$$F'_{1i} P_{i-1,j}^{n+1} + F'_{2i} P_{i,j}^{n+1} + F'_{3i} P_{i+1,j}^{n+1} = R_i^{n+\frac{1}{2}} \quad (3.3.51)$$

where,

$$R_i^{n+\frac{1}{2}} = F'_{1j} P_{i,j-1}^{n+\frac{1}{2}} + F'_{2j} P_{i,j}^{n+\frac{1}{2}} + F'_{3j} P_{i,j+1}^{n+\frac{1}{2}} \quad (3.3.52)$$

The variable P is a general working variable substituted for the T values or G values as with previous part.

The coefficients of equations (3.3.49) to (3.3.52) for the backward, forward, or central difference approximation may be expressed as follows:

$$F_{1j} = -b_{3j} - PrKG_{ij}\Delta_i(\psi^n_{ij})(1-\omega_z) \tag{3.3.53}$$

$$F_{2j} = \frac{Pr}{X_i} + \frac{2}{ak^2} + PrKG_{ij}\Delta_i(\psi^n_{ij})(1-2\omega_z) \tag{3.3.54}$$

$$F_{3j} = -b_{4j} + PrKG_{ij}\Delta_i(\psi^n_{ij})\omega_z \tag{3.3.55}$$

$$F_{1i} = b_{1i} - PrKG_{ij}\Delta_j(\psi^n_{ij})(1-\omega_\Theta) \tag{3.3.56}$$

$$F_{2i} = \frac{Pr}{X_i} - \frac{2}{ah^2} + PrKG_{ij}\Delta_j(\psi^n_{ij})(1-2\omega_\Theta) \tag{3.3.57}$$

$$F_{3i} = b_{2i} + PrKG_{ij}\Delta_j(\psi^n_{ij})\omega_\Theta \tag{3.3.58}$$

$$F'_{1j} = b_{3j} + PrKG_{ij}\Delta_i(\psi^{n+\frac{1}{2}}_{ij})(1-\omega_z) \tag{3.3.59}$$

$$F'_{2j} = \frac{Pr}{X_i} - \frac{2}{ak^2} - PrKG_{ij}\Delta_i(\psi^{n+\frac{1}{2}}_{ij})(1-2\omega_z) \tag{3.3.60}$$

$$F'_{3j} = b_{4j} - PrKG_{ij}\Delta_i(\psi^{n+\frac{1}{2}}_{ij})\omega_z \tag{3.3.61}$$

$$F'_{1i} = -b_{1i} + PrKG_{ij}\Delta_j(\psi^{n+\frac{1}{2}}_{ij})(1-\omega_z) \tag{3.3.62}$$

$$F'_{2i} = \frac{Pr}{X_i} + \frac{2}{ah^2} - PrKG_{ij}\Delta_j(\psi^{n+\frac{1}{2}}_{ij})(1-2\omega_\Theta) \tag{3.3.63}$$

$$F'_{3i} = -b_{2i} - PrKG_{ij}\Delta_j(\psi^{n+\frac{1}{2}}_{ij})\omega_\Theta \tag{3.3.64}$$

The other coefficients used in the above finite-difference equations are the same as derived in section 3.3.3.

3.3.5 Finite-Difference Representation of the Stream Function Equation

In the present work the stream function equation, equation (3.3.3), is solved at any time-step by successive over-relaxation. It should be recalled that time does not appear explicitly in the stream function equation.

The finite-difference form of the stream function equation is derived by first expressing equation (3.3.3) for the n-th time-step as follows:

$$\partial_i^2(\psi_{ij}^n) - \partial_i(\psi_{ij}^n) + \partial_j^2(\psi_{ij}^n) - \cot\Theta_j \partial_j(\psi_{ij}^n) = e^{2z_i} G_{ij}^n \tag{3.3.65}$$

By the use of the coefficients (3.3.37) to(3.3.41), equation (3.3.65) is expanded as follows:

$$\psi_{i,j}^n = b_{1i}\psi_{i+1,j}^n + b_{2i}\psi_{i-1,j}^n + b_{3j}\psi_{i,j+1}^n + b_{4j}\psi_{i,j-1}^n - c_i G_{i,j}^n \tag{3.3.66}$$

where

$$c_i = \frac{e^{2z_i}}{a} \tag{3.3.67}$$

A relaxation factor, ω_ψ, may be defined as follows:

$$\psi_{i,j}^{n,r+1} = \psi_{i,j}^{n,r} + \omega_\psi(\psi_{ij}^n - \psi_{i,j}^{n,r}) \tag{3.3.68}$$

where the contour r refers to the number of successive point iterations performed at the n-th time-step, and $\psi_{i,j}^{n,r+1}$ is the value of the stream function at the n-th time-step after r + 1 iterations. The stream function values, $\psi_{i,j}^{n,r+1}$, are resubstituted into equation (3.3.66) which is

then resolved with equaiton (3.3.68) until there is no significant difference between the stream function values $\psi_{i,j}^{n,r+1}$ and $\psi_{i,j}^{n,r}$.

3.3.6 Solution of the Systems of Algebraic Equations

The sets of simultaneous equations (3.3.20), (3.3.22), (3.3.49) and (3.3.51) are solved by Thomas'smethod as presented by Bruce et al (1953) and Lapidus (1962). As stated by Bruce et al (1953) "while the method is equivalent to plain Gaussian elimination, it avoids the error growth associated with the back solution of the elimination method, and also minimizes the storage problem in machine computation". The method may be summarized as follows.

Consider a system of n simultaneous equations with the following form:

$$
\begin{aligned}
C_{21}P_1 + C_{31}P_2 &= D_1 \\
C_{1r}P_{r-1} + C_{2r}P_r + C_{3r}P_{r+1} &= D_r \qquad r=2,3,\ldots,n-1 \\
C_{1n}P_{n-1} + C_{2n}P_n &= D_n
\end{aligned}
\tag{3.3.69}
$$

In the present work the coefficients C and D are known scalar quantities which are dependent on time as defined earlier in this section. In matrix notation, the set of equations (3.3.69) can be written as:

$$\underline{C}\ \underline{P} = \underline{D} \tag{3.3.70}$$

The matrix of coefficient $\underline{C}$, is a tridiagonal matrix. To solve equation (3.3.69), the variables, $P_1, \ldots P_{n-1}$ are eliminated from the first equation onward by putting,

$$W_1 = C_{21}$$

$$W_r = C_{2r} - C_{1r}q_r \qquad r=2,3, \ldots ,n$$

$$q_{r-1} = \frac{C_{3r-1}}{W_{r-1}} \qquad (3.3.71)$$

and

$$X_1 = \frac{D_1}{W_1}$$

$$X_r = \frac{D_r - C_{1r}X_{r-1}}{W_r} \qquad r=2,3, \ldots ,n \qquad (3.3.72)$$

By substitution, equations (3.3.71) and (3.3.72) transform the set of equations (3.3.69) to the following form:

$$P_n = X_n$$

$$P_r = X_r - q_r P_{r+1} \qquad r=1,2, \ldots n-1 \qquad (3.3.73)$$

If the quantities W,q, and X are calculated in order of increasing values of r, it follows that relation (3.3.73) can be used to calculate the variable P in order of decreasing r, that is $P_n, P_{n-1}, \ldots, P_2, P_1$.

3.4 FINITE-DIFFERENCE REPRESENTATION OF THE BOUNDARY AND INITIAL CONDITIONS

The boundary and initial conditions imposed on the system for the case of free convective heat transfer from a solid sphere are given in chapter 2. In this section the

boundary and initial conditions derived in section 2.6 are expressed in finite-difference form.

On consideration of figure 3.2.1 in which the index i varies from 1 at the surface of the sphere to IN1 at the outer boundary, and the index j varies from 1 at the upstream axis of symmetry, $\Theta = 0$, to JN1 at the downstream axis of symmetry, $\Theta = \pi$, then the boundary and initial conditions can be expressed in finite-difference form as follows:

3.4.1 Boundary Conditions

(a) Time-independent boundary conditions:

(i) Sphere surface:

The time-independent boundary conditions at the sphere surface are expressed by equations (2.6.1) and (2.6.3). The finite-difference forms of these conditions may be expressed as follows:

At z=0 (i=1):

$$\psi\Big|_{i=1,j} = 0 \; ; \; \frac{\partial\psi}{\partial z}\Big|_{i=1,j} = 0 \; ; \; \frac{\partial\psi}{\partial\Theta}\Big|_{i=1,j} = 0 \; ;$$

$$\frac{\partial^2\psi}{\partial\Theta^2}\Big|_{i=1,j} = 0 \; ; \qquad T\Big|_{i=1,j} = 1 \qquad (3.4.1)$$

(ii) Axis of symmetry:

The time-independent boundary conditions at the axis of symmetry, $\Theta = 0$ and $\Theta = \pi$, are expressed by equations (2.6.4), (2.6.7), and (2.6.9) . The finite-difference

forms of these conditions may be written as follows:

At $\Theta = 0$ $(j=1)$:

$$\psi\Big|_{i,j=1} = 0 \; ; \; \frac{\partial\psi}{\partial z}\Big|_{i,j=1} = 0 \; ; \; \frac{\partial^2\psi}{\partial z^2}\Big|_{i,j=1} = 0 \; ;$$

$$\frac{\partial\psi}{\partial\Theta}\Big|_{i,j=1} = 0 \; ; \; \zeta\Big|_{i,j=1} = 0 \; ; \; G\Big|_{i,j=1} = 0 \qquad (3.4.2)$$

At $\Theta = \pi$ $(j=JN1)$:

$$\psi\Big|_{i,j=JN1} = 0 \; ; \; \frac{\partial\psi}{\partial z}\Big|_{i,j=JN1} = 0 \; ; \; \frac{\partial^2\psi}{\partial z^2}\Big|_{i,j=JN1} = 0 \; ;$$

$$\frac{\partial\psi}{\partial\Theta}\Big|_{i,j=JN1} = 0 \; ; \; \zeta\Big|_{i,j=JN1} = 0 \; ; \; G\Big|_{i,j=JN1} = 0 \qquad (3.4.3)$$

(iii) Outer boundary:

The time-independent boundary conditions at the outer boundary for the dependent variables, ψ, ζ and T, are expressed by equations (2.6.11). The finite-difference forms of these conditions are as follows:

For $z = z_\infty$ $(i=IN1)$:

$$\psi\Big|_{i=IN1,j} = 0 \; ; \zeta\Big|_{i=IN1,j} = 0 \; ; \; G\Big|_{i=IN1,j} = 0 \; ; \; T\Big|_{i=IN1,j} = 0 \qquad (3.4.4)$$

(b) Time-dependent boundary conditions:

(i) Sphere surface:

The modified vorticity, G, at the sphere surface is given by equation (2.6.2) which is:

$$(e^{2z}G)\Big|_s = \frac{\partial^2\psi}{\partial z^2}\Big|_s \qquad (3.4.5)$$

Equation (3.4.5) in finite-difference form is as follows:

$$G^n_{i=1,j} = \left(\frac{\partial^2\psi}{\partial z^2}\right)^n_{i=1,j} \qquad (3.4.6)$$

where

$$G^n_{i=1,j} = \zeta^n_{i=1,j} \sin\theta_j$$

The surface vorticity is computed using a Taylor's series expansion of the stream function in the vicinity of the surface. For example; the values of the stream function at points (i=2,j,n), (i=3,j,n,) and (i=4,j,n) are:

$$\psi^n_{i=2,j} = \psi^n_{i=1,j} + \left\{h\frac{\partial}{\partial z} + \frac{h^2}{2!}\frac{\partial^2}{\partial z^2} + \frac{h^3}{3!}\frac{\partial^3}{\partial z^3} + \frac{h^4}{4!}\frac{\partial^4}{\partial z^4} + \cdots\right\}\psi^n \qquad (3.4.7)$$

$$\psi^n_{i=3,j} = \psi^n_{i=1,j} + \left\{2h\frac{\partial}{\partial z} + \frac{(2h)^2}{2!}\frac{\partial^2}{\partial z^2} + \frac{(2h)^3}{3!}\frac{\partial^3}{\partial z^3} + \frac{(2h)^4}{4!}\frac{\partial^4}{\partial z^4} + \cdots\right\}\psi^n \qquad (3.4.8)$$

$$\psi^n_{i=4,j} = \psi^n_{i=1,j} + \left\{3h\frac{\partial}{\partial z} + \frac{(3h)^2}{2!}\frac{\partial^2}{\partial z^2} + \frac{(3h)^3}{3!}\frac{\partial^3}{\partial z^3} + \frac{(3h)^4}{4!}\frac{\partial^4}{\partial z^4} + \cdots\right\}\psi^n \qquad (3.4.9)$$

All the derivatives in equations (3.4.7) to (3.4.9) are calculated at the surface, i=1. But from the boundary conditions given by equation (3.4.1) both ψ and $\frac{\partial\psi}{\partial z}$ are zero at the surface.

If third and higher order derivatives are neglected,

then from equation (3.4.7), one obtains:

$$\left(\frac{\partial^2\psi}{\partial z^2}\right)^n_{i=1,j} = \frac{2}{h^2}\ \psi^n_{2,j}$$

or

$$G^n_{i=1,j} = \frac{2}{h^2}\ \psi^n_{2,j} \qquad (3.4.10)$$

If third order derivatives are retained, then the following relationship is obtained from equations (3.4.7) and (3.4.8):

$$\left(\frac{\partial^2\psi}{\partial z^2}\right)^n_{i=1,j} = \frac{1}{2h^2}\ (8\psi^n_{i=2,j} - \psi^n_{i=3,j})$$

or

$$G^n_{i=1,j} = \frac{1}{2h^2}\ (8\psi^n_{i=2,j} - \psi^n_{i=3,j}) \qquad (3.4.11)$$

When the third and the fourth order derivatives are retained, equations (3.4.7) to (3.4.9) give the following expression:

$$\left(\frac{\partial^2\psi}{\partial z^2}\right)^n_{i=1,j} = \frac{1}{18h^2}\ (108\psi^n_{i=2,j} - 27\psi^n_{i=3,j} + 4\psi^n_{i=4,j})$$

or

$$G^n_{i=1,j} = \frac{1}{h^2}\ (6\psi^n_{i=2,j} - \frac{3}{2}\psi^n_{i=3,j} + \frac{2}{9}\psi^n_{i=4,j}) \qquad (3.4.12)$$

The first approximation (3.4.10) is the simplest but the least accurate. More accurate are the approximations (3.4.11) and (3.4.12). Al-Taha (1969) used approximation (3.4.11). Rafique (1971) used approximations (3.4.11) and (3.4.12). He found that for any Reynoldsnumber the differences between the final values of the surface vorticity using approximations (3.4.11) and (3.4.12), were very small. For example at a

Reynolds number of 500, the difference was only about 5%. Therefore, it is advantageous in terms of computing time, to use the approximation (3.4.11).

(ii) Axis of symmetry:

Along the axis of symmetry:

$$\left.\frac{\partial T}{\partial \Theta}\right|_{\Theta=0,\pi} = 0 \qquad (3.4.13)$$

The temperature along the axis of symmetry can then be computed using a Taylor's series expansion of the temperature in the angular direction, Θ, in the vicinity of the axis of symmetry. The procedure is the same as that used to approximate the surface vorticity.

Along the axis of symmetry $\Theta=0$, a forward difference scheme is used, while along the axis of symmetry $\Theta=\pi$, a backward difference scheme is used. The reason for using the different schemes can be explained with the help of figure 3.4.1 as follows:

For example, consider the temperature $T_{4,1}$ at grid point (4,1) along the axis of symmetry $\Theta=0$. The temperature $T_{4,1}$ at grid point (4,1) has to be approximated in terms of the temperatures at grid points (4,2), (4,3), ... (4,m): where m is the degree of the polynomial. Therefore:

$$T^n_{4,1} = F\ (T^n_{4,2}\ ,\ T^n_{4,3}\ ,\ .\ .\ .\ .\ ,\ T^n_{4,m}).$$

In order to do this a forward difference scheme has to be used.

However, the temperature $T_{4,JN1}$ at grid point (4,JN1) along the axis of symmetry $\Theta=\pi$, has to be approximated in terms of the temperatures at grid points (4,JN1-1), (4,JN1-2), . . . (4,JN1-m'), where (m'+1) is the degree of the polynomial. Therefore:

$$T^n_{4,JN1} = F(T^n_{4,JN1-1}, T^n_{4,JN1-2}, \cdots T^n_{4,JN1-m'})$$

Hence along the axis of symmetry $\Theta=\pi$, a backward difference scheme must be used.

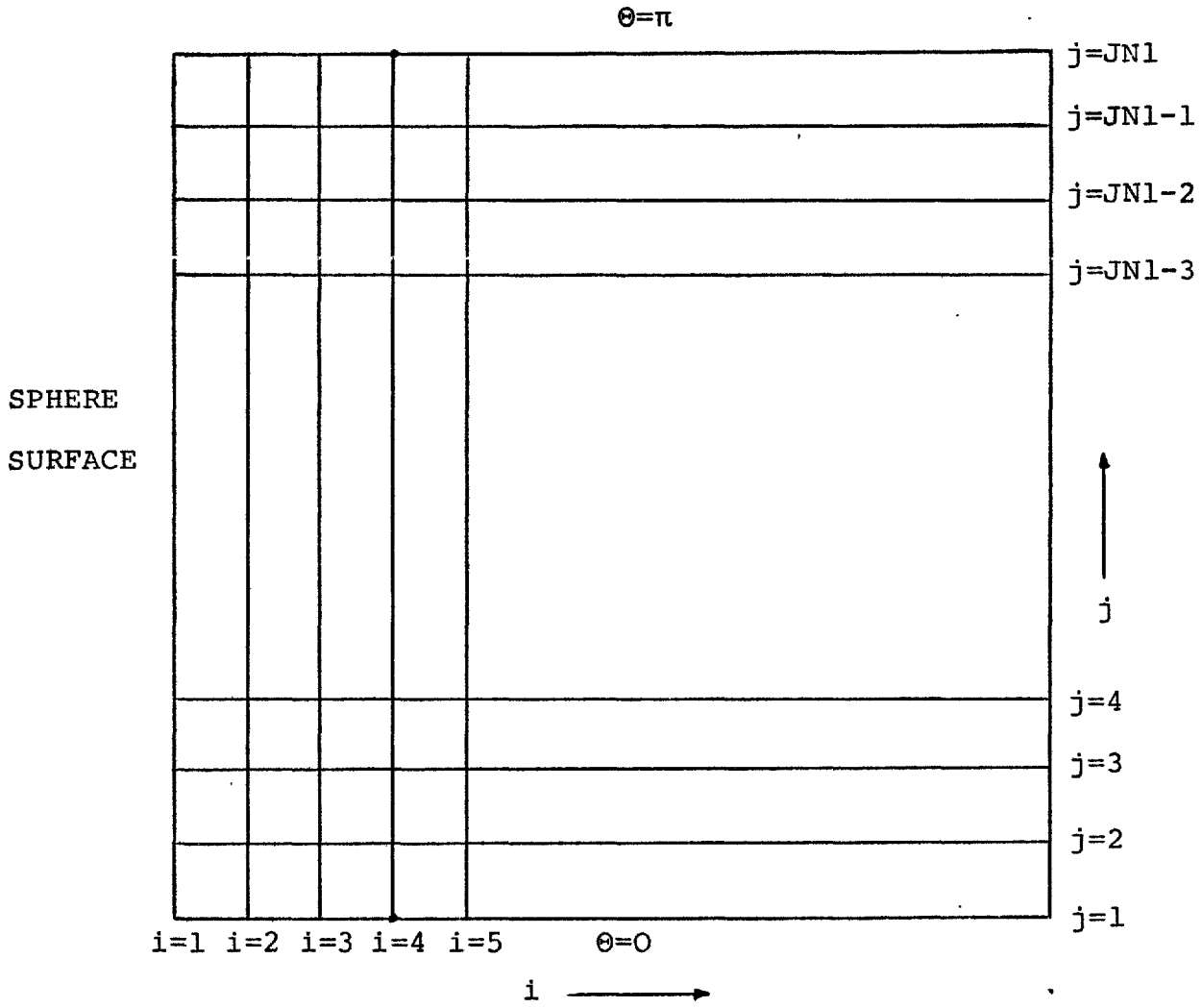

FIGURE 3.4.1 MESH STRUCTURE AROUND THE SPHERE

The temperature along the axis of symmetry $\Theta=0$, may be approximated as follows:

retaining third order derivatives:

$$T^n_{i,j=1} = \frac{1}{3}\,(T^n_{i,j=2} - T^n_{i,j=3}) \qquad (3.4.14)$$

retaining fourth order derivatives:

$$T^n_{i,j=1} = \frac{1}{11}\,(18T^n_{i,j=2} - 9T^n_{i,j=3} + 2T^n_{i,j=4}) \qquad (3.4.15)$$

retaining fifth order derivatives:

$$T^n_{i,j=1} = \frac{1}{25}\,(48T^n_{i,j=2} - 36T^n_{i,j=3} + 16T^n_{i,j=4} - 3T^n_{i,j=5}) \qquad (3.4.16)$$

Along the axis of symmetry $\Theta=\pi$, the temperature may be approximated as follows:

retaining third order derivates:

$$T^n_{i,j=JN1} = \frac{1}{3}\,(T^n_{i,j=JN1-1} - T^n_{i,j=JN1-2}) \qquad (3.4.17)$$

retaining fourth order derivatives:

$$T^n_{i,j=JN1} = \frac{1}{11}\,(18T^n_{i,j=JN1-1} - 9T^n_{i,j=JN1-2} + 2T^n_{i,j=JN1-3}) \qquad (3.4.18)$$

retaining fifth order derivatives:

$$T^n_{i,j=JN1} = \frac{1}{25}(48T^n_{i,JN1-1} - 36T^n_{i,j=JN1-2} + 16T^n_{i,j=JN1-3} - 3T^n_{i,j=JN1-4}) \qquad (3.4.19)$$

However, computational experiments showed that the final values of the late-time steady state average Nusselt numbers were only weakly dependent on the order of the approximations used for temperatures along the axis of symmetry, so that in all cases the use of equation (3.4.15) and (3.4.18) was considered to be satisfactory, both from a computational and an accuracy point of view.

3.4.2 Initial Conditions

The initial condition used for free convective heat transfer from a solid sphere, is expressed by equations (2.6.12) and (2.6.17) in Chapter 2. The finite-difference forms of equations (2.6.12) and (2.6.17) may be expressed as follows:

At t=0 (n=0)

$$\psi^{o}_{i,j} = 0 \; ; \; \zeta^{o}_{i,j} = 0 \; ; \; G^{o}_{i,j} = 0 \qquad (3.4.20)$$

$$T^{o}_{i,j} = \left(\frac{e^{z_{i=IN1}}}{e^{z_{i=IN1}}-1}\right) e^{-z_i} - \left(\frac{1}{e^{z_{i=IN1}}-1}\right) \qquad (3.4.21)$$

for all values of j.

Equations (3.3.20), (3.3.22), (3.3.49), (3.3.51), (3.3.66) and (3.3.68) together with the associated coefficients, boundary and initial conditions, are the set of finite-difference equations that are solved by the computer programme given in appendix F.

3.5 STABILITY AND CONVERGENCE

If $W(z,\Theta,t)$ is the exact solution of the initial value problem as described in chapter 2, and $w^n_{i,j}$ is the solution of the finite-difference equations derived in section 3.3, then the error of approximation $\varepsilon_{W^n_{i,j}}$ is given by:

$$\varepsilon_{W^n_{i,j}} = \left| w^n_{i,j} - W((i-1)h,(j-1)k, n\Delta t) \right| \qquad (3.5.1)$$

Now one may ask two questions (Richtmyer 1957):

1. What is the behaviour of $\varepsilon_{W^n_{i,j}}$ as $n \to \infty$ for fixed values of the mesh sizes, h,k and the time-step Δt?
2. What is the behaviour of $\varepsilon_{W^n_{i,j}}$ as h,k and $\Delta t \to 0$ for a fixed value of time?

The first question is one of numerical stability and, in general, the numerical method is considered to be stable if $\varepsilon_{W^n_{i,j}}$ remains bounded. The second question is one of convergence and the method is said to be convergent if $\varepsilon_{W^n_{i,j}}$ tends to zero.

The only convergence theorem that exists for partial differentail equations is for linear equations with constant coefficients; Lax's equivalence theorem which, as stated by Richtmyer (1957), says that a stable computation of the differential problem will yield results which converge to the solution of the consistent differential equation .

Richtmyer gives the development of the theory for a class of linear equations with constant coefficients, but points out that the theory is inadequate for complicated problems such as that studied in the present work.

Stability is a necessary condition for the solution of the difference problem to converge to the solution of the differential problem. Convergence is essential for the results to be meaningful in that the fundamental idea of an approximation is that the error can be made as small as one wishes. The importance of the concept of stability has been explained by many authors. As a general rule, a stability criterion involves a restriction on the time-step in terms of space increments , h and k, and the parameters of the system of equations. In the case of non-linear problems the stability criterion may also involve the dependent variable.

A useful method of stability analysis is based upon the use of difference equations in which all the coefficients are positive. In such cases the boundedness of the solution can be tested directly on the positivity of coefficients (Hellums 1960, Gosman 1969) and a sufficient condition for stability can often be established by inspection. This method may be described as follows.

By application of the upwind differencing technique described in section 3.2.1, the explicit finite- difference forms of the vorticity transport and energy equations can be written in the following general form:

$$W^{n+1}_{i,j} = a_{1i}W^{n}_{i+1,j} + a_{2i}W^{n}_{i-1,j} + a_{3j}W^{n}_{i,j+1} + a_{4j}W^{n}_{i,j-1} + a_{5ij}W^{n}_{i,j} + d^{n}_{i,j} \quad (3.5.2)$$

For equation (3.5.2) to be convergent, the following conditions must be satisfied:

(1) Each coefficient, a, must be positive

(2) The sum of the coefficients, a, must be less than or equal to unity at every grid node.

(3) The sum of the coefficients, a, must be less than unity at least at one grid node, and

(4) The variation of the coefficients, a, and d, from one cycle of iteration to another, must be sufficiently small.

As an example, the above conditions will be considered in relation to the energy equation.

The energy equation for a first order simple explicit scheme is given by equation (3.3.10). By the application of upwind differencing to the convective terms of equation (3.3.10) this equation can be written in explicit finite-difference form as follows:

$$T^{n+1}_{i,j} = a_{1i}T^{n}_{i+1,j} + a_{2i}T^{n}_{i-1,j} + a_{3j}T^{n}_{i,j+1} + a_{4j}T^{n}_{i,j-1} + a_{5ij}T^{n}_{i,j} \quad (3.5.3)$$

where:

$$a_{1i} = \frac{2X_i}{Pr}\left(Pr\ KG_{ij}\Delta_j(\psi^{n}_{ij})\ \omega_\Theta + b_{2i}\right) \quad (3.5.4)$$

$$a_{2i} = \frac{2X_i}{Pr}\left(-Pr\ KG_{ij}\Delta_j(\psi^{n}_{ij})(1-\omega_\Theta) + b_{1i}\right) \quad (3.5.5)$$

$$a_{3j} = \frac{2X_i}{Pr} (-Pr\ KG_{ij}\Delta_i(\psi^n_{ij})\ \omega_z + b_{4j}) \qquad (3.5.6)$$

$$a_{4j} = \frac{2X_i}{Pr} (Pr\ KG_{ij}\Delta_i(\psi^n_{ij})\ (1-\omega_z) + b_{3j}) \qquad (3.5.7)$$

$$a_{5ij} = 1+ \frac{2X_i}{Pr} (-Pr\ KG_{ij}\Delta_i(\psi^n_{ij})(1-2\omega_z)+Pr\ K\ G_{ij}\Delta_j(\psi^n_{ij})(1-2\omega_\Theta)-1) \qquad (3.5.8)$$

The other coefficients used in the above finite-difference equation are given by equations (3.3.37) to (3.3.44).

Now the difference equation for the case that both velocity components u_z and u_Θ, are positive, that is $(-\frac{\partial\psi}{\partial\Theta})^n_{i,j} > 0$ and $(\frac{\partial\psi}{\partial z})^n_{i,j} > 0$, is considered. Since the velocity components are positive, the terms in which the variable coefficients, $(-\frac{\partial\psi}{\partial\Theta})^n_{i,j}$ and $(\frac{\partial\psi}{\partial z})^n_{i,j}$, appear as coefficients, the convective terms, are approximated by backward differnces as described in section 3.2.1, i.e. $\omega_\Theta=\omega_z = 0$. Therefore, the coefficients of equation (3.5.3) become as follows:

$$a_{1i_+} = \frac{2X_i}{Pr}\ b_{2i} \qquad (3.5.9)$$

$$a_{2i_+} = \frac{2X_i}{Pr} (-Pr\ KG_{ij}\Delta_j(\psi^n_{ij}) + b_1) \qquad (3.5.10)$$

$$a_{3j_+} = \frac{2X_i}{Pr}\ b_{4j} \qquad (3.5.11)$$

$$a_{4j_+} = \frac{2X_i}{Pr} (Pr\ KG_{ij}\Delta_i(\psi^n_{ij}) + b_{3j}) \qquad (3.5.12)$$

$$a_{5ij_+} = 1+ \frac{2X_i}{Pr} (-Pr\ KG_{ij}\Delta_i(\psi^n_{ij})+PrKG_{ij}\Delta_j(\psi^n_{ij})-1) \qquad (3.5.13)$$

where the subscript + indicates that both variable coefficients $(-\frac{\partial\psi}{\partial\Theta})^n_{i,j}$ and $(\frac{\partial\psi}{\partial z})^n_{i,j}$ are positive.

The conditions (1) to (4) described above are now examined with reference to equation (3.5.3) whose coefficients are given by equations (3.5.9) to (3.5.13).

(i) Since both variable coefficients, $(-\frac{\partial\psi}{\partial\Theta})^n_{i,j}$ and $(\frac{\partial\psi}{\partial z})^n_{i,j}$, as well as the coefficients (3.3.37) to (3.3.44) given in section 3.3.3, are positive, therefore, all the coefficients of equation (3.5.3) are positive provided $a_{5ij_+} \geq 0$, or:

$$1+\frac{2X_i}{Pr}\left(-Pr\ KG_{ij}\Delta_i(\psi^n_{ij}) + PrKG_{ij}\Delta_j(\psi^n_{ij}) -1\right) \geq 0 \qquad (3.5.14)$$

By substitution of X_i and KG_{ij} given by equations (3.3.41) to (3.3.44), inequality (3.5.14) can be re-arranged to give:

$$\frac{1}{\Delta t_+} \geq -\frac{\Delta_j(\psi^n_{i,j})}{2ke^{2z_i}\sin\Theta_j}\frac{1}{he^{z_i}} + \frac{\Delta_i(\psi^n_{ij})}{2he^{2z_i}\sin\Theta_j}\frac{1}{ke^{z_i}} + \frac{2}{Pre^{2z_i}}\left(\frac{1}{h^2}+\frac{1}{k^2}\right) \qquad (3.5.15)$$

The relationships between the velocity components and the stream function are given by equations (2.5.3) and (2.5.4) as follows:

$$u_z = -\frac{1}{e^{2z}\sin\Theta}\frac{\partial\psi}{\partial\Theta}$$

$$u_\Theta = \frac{1}{e^{2z}\sin\Theta}\frac{\partial\psi}{\partial z}$$

The finite-difference approximations of relations (2.5.3) and (2.5.4) can be expressed as:

$$(u_z)^n_{ij} = -\frac{\Delta_j(\psi^n_{ij})}{2ke^{2z_i}\sin\Theta_j} \qquad (3.5.16)$$

$$(u_\theta)^n_{ij} = \frac{\Delta_i(\psi^n_{ij})}{2he^{z_i}\sin\theta_j} \qquad (3.5.17)$$

By substitution of equations (3.5.16) and (3.5.17) into inequality (3.5.15), the following restriction for the time-step, Δt, is obtained:

$$\frac{1}{\Delta t_+} \geq \frac{(u_z)^n_{ij}}{he^{z_i}} + \frac{(u_\theta)^n_{ij}}{ke^{z_i}} + \frac{2}{Pr\, e^{2z_i}}\left(\frac{1}{h^2} + \frac{1}{k^2}\right) \qquad (3.5.18)$$

(ii) It can be proved that the sum of the coefficients a_+ is always equal to unity except on the outer boundary.

From relations (3.6.11) to (3.6.15) one can write:

$$a_{1i_+} + a_{2i_+} + a_{3j_+} + a_{4j_+} + a_{5ij_+} = 1 + \frac{2x_i}{Pr}(b_{1i}+b_{2i}+b_{3j}+b_{4j}-1)$$

But from equations (3.3.37) to (3.3.41), it follows that:

$$b_{1i} + b_{2i} + b_{3j} + b_{4j} = 1$$

therefore:

$$a_{1i_+} + a_{2i_+} + a_{3j_+} + a_{4j_+} + a_{5ij_+} = 1$$

(iii) For the third condition, consider the outer boundary where:

$$T^n_{IN1,j} = 0$$

Thus, since the temperature values on the right hand side of equation (3.5.3) are positive, then in order for the boundary condition to be satisfied the coefficients must be equal to zero.

(iv) Finally, the condition (4) cannot be answered clearly since there is no way of defining mathematically what is meant by 'sufficiently small', instead, one must learn from experience; and experience has shown that this condition is usually fulfilled.

It can be shown that the restriction (3.5.18) holds irrespective of the sign of the velocity components, u_z and u_θ, (the variable coefficients, $(-\frac{\partial\psi}{\partial\theta})$ and $(\frac{\partial\psi}{\partial z})$), if absolute values are used in the inequality, and if the difference equation (3.5.3) are changed according to the sign of the varaible coefficients through weighting factors, ω_z and ω_θ, as prescribed in section 3.2.1. Therefore, the restriction on the time-step given by the inequality (3.5.18) can be generalized for all values of variable coefficients as follows:

$$\frac{1}{\Delta t} \geq \frac{\left|(u_z)^n_{ij}\right|}{he\,z_i} + \frac{\left|(u_\theta)^n_{ij}\right|}{ke\,z_i} + \frac{2}{Pre\,2z_i}\left(\frac{1}{h^2} + \frac{1}{k^2}\right) \qquad (3.5.19)$$

Restriction (3.5.19) is the stability criterion for the solution of the explicit finite-difference form of the energy equation. For Prandtl numbers, Pr, greater than unity, Pr in equation (3.5.19) should be replaced by unity (Hellums 1960).

It is clear that by appropriate use of the weighting factors, ω_z and ω_θ as prescribed in section 3.2.1, conditions (2), (3) and (4) are always satisfied.

In the most general problem the sign of the velocity

components u_z and u_θ may be expected to vary in the space-time grid. Hence for stability, different equations must be used in different parts of the space-time grid depending on the sign of the velocity components. This method of dealing with such first order partial derivatives is due to Lelevier according to Richtmyer and has been used for the convective terms of the present work.

In the present complex case of the solution of the equations which describe time-dependent free convective heat transfer form a solid sphere, a method of direct analysis of the stability of the vorticity transport equation does not exist. However, since the energy equation and the vorticity transport equation are interdependent, the time-step must be chosen such that both equations are satisfied.

None of the stability analyses are adequate for practical computational purposes. In fluid dynamics and heat transfer problems, the stability restrictions must be applied locally which is time consuming. In practice an unstable scheme of calculation usually yields meaningless numbers which overflow the accumulator of the computer after a relatively few time-steps. Therefore, a precise stability criterion is not essential.

For the study of non-linear equations, according to Roache (1972), Hicks (1969) suggests that the problems of stability criteria should be neglected and that attention should

be directed to problems of convergence. Fundamentally, it is required that the solution of the finite-difference equation should approach the solution of the partial differential equation so that stability considerations are of secondary interest. However, a great deal of numerical experimentation is often necessary in order to obtain a convergent solution.

3.6 COMPUTATIONAL PROCEDURE

The computational algorithm is based on the assumption that the entire numerical fields of the temperature, vorticity, and stream function are known at any given time, $n\Delta t$, and that it is required to determine the complete flow field at the next time-step, that is time $(n+1)\Delta t$.

The primary function of the main computational procedure for the first half time-step is to solve equation (3.3.49) for the temperature values at time $(n+\frac{1}{2})\Delta t$, to solve equation (3.3.20) for the vorticity values at time $(n+\frac{1}{2})\Delta t$, and to solve equation (3.3.68) for the stream function values at time $(n+\frac{1}{2})\Delta t$. For the second half time-step the procedure is to solve equation (3.3.51) for the temperature values at time $(n+1)\Delta t$, to solve equation (3.3.22) for the vorticity values at time $(n+1)\Delta t$, and to solve equation (3.3.68) for the stream function values at time $(n+1)\Delta t$. The solution procedure, starting from the initial condition, t=0 or n=0, will now be described as follows:

(i) For a particular solution of the time-dependent

equations for free convective heat transfer from a solid sphere, the Grashof number, Gr; the Prandtl number, Pr; the mesh sizes, h and k; The time-step, Δt; the radius of the outer boundary, r_∞ (z_∞); the relaxation factor and convergence criterion for the stream function, ω_ψ and ε_ψ; the relaxation factor and convergence criterion for the surface vorticity, ω_G and ε_G; and the relaxation factor and convergence criterion for the temperature along the axis of symmetry, ω_T and ε_T, are specified. The time-independent boundary conditions are also specified.

(ii) The initial values of the stream function and vorticity are set to zero throughout the flow field, according to equation (3.4.20). The initial value of temperature is obtained from equation (3.4.21).

(iii) Having determined the initial stream function values, the initial vorticity values, and the initial temperature values throughout the flow field, the temperature and vorticity values are updated by one-half of a time-step. In general the temperature values $T^n_{i,j}$ and the vorticity values $G^n_{i,j}$ are updated from the n-th time-step to the $(n+\frac{1}{2})$ time-step to give the values of $T^{n+\frac{1}{2}}_{i,j}$ and $G^{n+\frac{1}{2}}_{i,j}$. The updating is done by solving the set of simultaneous equations, equation (3.3.49) to give the temperature values and the set of simultaneous equations, equation (3.3.20) to give the vorticity values. The velues of the stream function at the previous time-step, the n-th time-step, are used for this part of the procedure. However, the temperature values used in equation (3.3.20) to obtain vorticity values $G^{n+\frac{1}{2}}_{i,j}$ are the newly calculated

values obtained from equation (3.3.49).

(iv) The stream funciton values at the $(n+\frac{1}{2})$ time-step are determined using successive over-relaxation in order to solve equations (3.3.66) and (3.3.68). The iterations are continued until the velues throughout the flow field satisfy the following convergence criterion:

$$\left|\psi_{i,j}^{r+1} - \psi_{i,j}^{r}\right| \leqslant \varepsilon_{\psi} \qquad (3.6.1)$$

where r is defined in section 3.

(v) Having determined the temperature values and the stream function values throughout the domain at the $(n+\frac{1}{2})$ time-step, the temperatures along the axis of symmetry are calculated using equations (3.4.15) and (3.4.18), respectively. The surface vorticity values are determined using equation (3.4.11).

(vi) In order to calculate the temperature values and the vorticity values at the new (n+1) time-step, the temperature values along the axis of symmetry and surface vorticity values at the (n+1) time-step are required, since they are unknown, a first approximation is made by assuming that the temperature values along the axis of symmetry and the surface vorticity values are the same at the two time levels $(n+\frac{1}{2})$ and (n+1). Therefore, the temperature values along the axis of symmetry and surface vorticity values at the $(n+\frac{1}{2})$ time-step are used as initial estimates of time-level (n+1). The temperature values and the vorticity values at the (n+1) time-

step are then obtained using the sets of simultaneous equations, given by equations (3.3.51) and (3.3.22), respectively. For this stage of calculation, the stream funciton values available from the $(n+\frac{1}{2})$ time-step are used wherever required.

However, for solution of equation (3.3.22) for the vorticity values, the most up to date values of temperature $T_{i,j}^{n+1}$, are used wherever required.

(vii) Having determined the vorticity values at the (n+1) time-step, the stream function values at the (n+1) time-step are obtained using successive over-relaxation, SOR, sweeps using equations (3.3.66) and (3.3.68) until criterion (3.6.1) is satisfied. The stream function values at the $(n+\frac{1}{2})$ time-step are used as a first approximation in the application of the successive over-relaxation method.

(viii) Having determined the temperature values and the stream function values at the (n+1) time-step, the temperature values along the axis of symmetry and the surface vorticity values at the (n+1) time-step, are redetermined using equations (3.4.15), (3.4.18) and (3.4.11) respectively.

(ix) The newly calculated temperatures along the axis of symmetry, and the surface vorticity values are compared with the corresponding values assumed previously during stages (vi) and (vii). If the differences are unacceptable, the procedure is repeated from stage (vi), until the following convergence criteria are satisfied:

$$\left| T_{i,j}^{n+1,r+1} - T_{i,j}^{n+1,r} \right| \leqslant \varepsilon_T \qquad (3.6.2)$$

at all points along the axis of symmetry, (j=1 and j=JN1),and:

$$\left| G^{n+1,r+1}_{i=1,j} - G^{n+1,r}_{i=1,j} \right| \leqslant \varepsilon_G \qquad (3.6.3)$$

In repeating the procedure from stage (vi) the latest available values of the stream function, $\psi^{n+1}_{i,j}$, and the temperatures along the axis of symmetry, $T^{n+1}_{i,j=1}$ and $T^{n+1}_{i,j=JN1}$, and the surface vorticity values, $G^{n+1}_{i=1,j}$ are used.

In order to prevent the solution from diverging and to minimize the number of iterations required for the convergence of the temperatures along the axis of symmetry and the convergence of surface vorticity values, the changes in the values of temperature along the axis of symmetry and the changes in the surface vorticity from one iteration cycle to the next are limited by means of the following relaxation factors:

$$T^{n+1,r+1}_{i,j} = T^{n+1,r}_{i,j} + \omega_T \left(T^{n+1}_{i,j} - T^{n+1,r}_{i,j} \right) \qquad (3.6.4)$$

for j=1 and j=JN1, and:

$$G^{n+1,r+1}_{i=1,j} = G^{n+1,r}_{i=1,j} + \omega_G \left(G^{n+1}_{i=1,j} - G^{n+1,r}_{i=1,j} \right) \qquad (3.6.5)$$

where $T^{n+1}_{i,j=1}$, $T^{n+1}_{i,j=JN1}$, and $G^{n+1}_{i=1,j}$ are the latest available values of the temperature along the axis of symmetry, $\Theta = 0$ and $\Theta = \pi$, and of the surface vorticity values obtained from equations (3.4.15), (3.4.18) and (3.4.11), respectively. For the next iteration, the values of $T^{n+1,r+1}_{i,j=1}$, $T^{n+1,r+1}_{i,j=JN1}$, and $G^{n+1,r+1}_{i=1,j}$ are used as the values of $T^{n+1,r}_{i,j=1}$, $T^{n+1,r}_{i,j=JN1}$, and $G^{n+1,r}_{i=1,j}$, respectively.

(x) The newly calculated values of the temperature, $T_{i,j}^{n+1}$, the vorticity, $G_{i,j}^{n+1}$, and the stream function, $\psi_{i,j}^{n+1}$, over the entire flow field now replace the 'old' values, i.e. the (n+1) time-level becomes the new n-th time-level and the entire procedure is repeated form stage (iii) for the next time-step.

(xi) At certain time intervals, the isotherms and the stream function and vorticity contours around the solid sphere are plotted and the surface pressure; frictional, formed, and total drag coefficients are calculated using the equations derived in appendices B and C. The local and average Nusselt numbers are calculated using the equations derived in appendix D.

(xii) As there is no simple way of establishing from one time-level to another whether or not the simulation is proceeding satisfactorily and also to gain greater insight into the numerical technique used, a high degree of user participation is necessary. This is achieved by transferring the flow field at the end of a certain number of time-steps on to a magnetic tape. The values of the temperature, vorticity and stream function are printed-out at this stage in order to check the results obtained and to consider whether any changes in the programme are necessary for the next run. At the start of the next run the data are read-in and manipulated according to decisions of the user.

(xiii) A constant time-step, t, is used over any one

run. The whole algorithm provides freedom to change the time-step, Δt, whenever desirable, i.e. either to minimize computing time for a complete solution over the entire time domain or to follow rapid changes in the flow field.

(xiv) This procedure is repeated for several computer runs until only small changes occur in the values of the local Nusselt number calculated from one time-step to the next. At this stage the solution is assummed to have reached the late-time steady state condition.

CHAPTER 4

RESULTS AND DISCUSSION

4.1 INTRODUCTION

The set of differential equations, initial and boundary conditions describing time-dependent free convective heat transfer from a solid sphere to a stagnant Newtonian medium were derived in chapter 2. In chapter 3 the differential equations were replaced by finite-difference equations and a set of non-linear algebraic equations were also developed in chapter 3.

Based on these procedures, the computer programme listed in appendix F was developed so that the stream function, vorticity and temperature distributions could be generated for a wide range of Grashof and Prandtl numbers. From these distributions other quantities which characterize the problem are calculated. These quantities are the local and average Nusselt numbers, the dimensionless pressure distribution at the sphere surface and the drag coefficients.

In this chapter the computer results for Grashof numbers, Gr, of 0.05, 1, 10, 25, 50 and 125 and a Prandtl number of 0.72; for Grashof numbers of 1250 and 12500 and a Prandtl number of 10; and a Grashof number of 50 and a Prandtl number of 100 are presented and discussed.

Once the Grashof and Prandtl numbers have been specified there are nine arbitrary constants which must also be specified before a solution can be obtained. These constants are the mesh sizes, h and k; the time-step, Δt; the radius of

the outer boundary, r_∞; the convergence criterion and the relaxation factor for the stream function, ε_ψ and ω_ψ; the convergence criterion and the relaxation factor for surface vorticity, ε_G and ω_G; and, finally, the convergence criterion and the relaxation factor for the temperature along the axis of symmetry, ε_T and ω_T.

The relaxation factors and convergence criteria are chosen on the basis of computational experiments such that the computational time is minimized while retaining acceptable accuracy. The optimum values of the constants used are given in table 1.

4.2 FACTORS WHICH INFLUENCE THE ACCURACY OF THE SOLUTION

Once a numerical solution has been obtained the most important question is; what is its accuracy? This mainly depends on round-off errors, truncation errors, and errors introduced by approximation of the boundary conditions.

(i) Influence of round-off errors

Round-off errors refer to the errors resulted from the rounding or truncation of the results of individual arithmetic operations on a computing machine. They arise because of the finite word length of digital computers. Analysis of round-off errors present in the final results of a numerical computation, usually termed the accumulated round-off errors, is difficult, particularly when the

algorithm used is of some complexity. This is because round-off errors introduce aberrant results; for example floating point addition and multiplication give rise to commutative round-off errors which are neither associative nor distributive, as has been shown by Forsythe (1970).

In the present work numerical calculations were made using a CDC7600 computer which works with fourteen decimal places. In view of this, it is probable that round-off errors generated from the integration of the equations during the time-dependent period did not affect the results appreaciably since fourteen decimal places was well beyond the accuracy which was desired in this work. However, as it is explained later in this thesis, this is not the case once the solution has reached the late-time steady state condition. Although an awareness of round-off error is important, it is generally true that, for numerical solution of partial differential equations of multi-dimensional fluid dynamics problems, the mesh increments are necessarily coarse enough for truncation errors to be the dominant errors (Roache 1972).

(ii) Influence of truncation errors

Truncation errors refer to the errors incurred by not retaining all the terms in a Taylor's series expansion. The accuracy which can be obtained with any finite-difference method of solution is largely dependent on the

truncation errors.

A particular kind of truncation error exhibited by some finite-difference represenations of convective terms is called 'false viscosity' (Wolfshtein 1967 and Rafique 1971). This error has often been analysed in the past under various names, such as 'numerical, artificial, or psuedo viscosity', or 'numerical or artificial diffusion'. This error has the effect of introducing into the equations an additional 'false diffusion' of the dependent variables. This false diffusion is primarily associated with the one-sided difference schemes which are used to represent the convective terms in transport equations. The effect of false diffusion is not restricted to the present method. All methods in which one-sided difference schemes have been used may be expected to suffer from it.

The interpretation of the false diffusion in complex cases of multi-dimensional viscous non-linear problems is difficult. Arguments have been made to the effect that accurate solutions are not possible unless the false viscosity introduced is much less than the real viscosity of the fluid (Rafique 1971). But the practical situation is not so bad. The solutions obtained by other authors for their multi-dimensional problems indicate the success of one-sided difference schemes.

From a formal examination of Taylor's series expansion

it may be concluded that central difference scheme is more accurate than upwind one-sided difference schemes. On the other hand, upwind difference schemes have several advantages in comparison with central difference scheme. In particular, upwind difference schemes are inherently more stable. Also, one-sided difference schemes possess the transportive property as described in chapter 3. The transportive property is as important as physically significant as the conservative property. In this sense, at least upwind difference schemes are more accurate than schemes with spaced-centered derivatives of the convective terms.

The choice between central difference scheme and one-sided difference schemes is, therefore, a compromise between truncation errors and transportive errors. Although it is true that truncation errors dominate the other errors, it is also true that upwind difference schemes are usually used because they ensure stability and rapid convergence; with this in mind, the reduced accuracy may seem an acceptable penalty.

It appears then, that usable solutions are obtainable using one-side difference schemes (Gosman 1969 and Roache 1972), although the effects of pseudo viscosity must be considered when assessing the accuracy of the results.

Truncation errors tend to zero as the mesh intervals tend to zero. Generally, the finer the mesh size; the

smaller will be the truncation errors and the faster will be the convergence of the numerical solutions. However, the reduction of mesh size will increase the number of grid points and, hence, the number of simultaneous equations to be solved. This in turn, will result in an increase in the amount of computer storage and computing time required to solve the finite-difference equations. Therefore, optimum values of the mesh sizes in space and time have to be used such that the truncation errors, and the errors which can be related to truncation errors, can be made acceptably small.

(iii) Influence of boundary conditions

Inaccuracies may be introduced through the choice of boundary condition to be satisfied. In particular; as mentioned earlier, equation (3.4.10) is less accurate than equation (3.4.11) for the calculation of the vorticity at the sphere surface.

The radius of the outer boundary affects the accuracy of the solutions obtained. For instance; if the outer boundary is taken to be too close to the sphere surface it affects the vorticity gradients around the sphere which in turn, change the values of the drag coefficients.

4.3 FACTORS WHICH INFLUENCE THE ECONOMY OF THE CALCULATION PROCEDURE

Accuracy is not the only factor which must be considered

in the evaluation and design of a numerical method. The total cost of obtaining solutions must be also considered. The factors which influence the economy of the present problem were found to be: the choice of time-step, the choice of convergence criteria for the stream function, voriticity and temperature, the choice of relaxation factors associated with these convergence criteria and, finally, the total number of mesh points (i, j).

In the present work values for all of the above factors were found on the basis of numerical experiments, and values were selected in order to achieve a balance between accuracy and economy.

(i) Choice of time-step

The time-step was chosen such that it would provide convergence of the numerical solution with acceptable accuracy and keep the total computing time within reasonable limits. Values of the time-step used to obtain solutions for different Grashof and Prandtl numbers are given in table 1.

(ii) Choice of convergence criterion

The computation time required at every time-step is proportional to the number of iterations which must be performed before the solution is said to have converged at that time-step; that is, when the effective change in the vorticity, stream function, or temperature values between

one iteration cycle and the next is acceptably small. What is acceptable is of course related to the accuracy desired. If higher accuracy is required, more iterations have to be performed, so that computing time becomes excessive. Therefore, once again, a balance must be made between the accuracy required and computing time used. There is little point in using excessive computing time when little is gained in the accuracy of the solution.

In the present work, the following convergence criterion was used:

$$\left| W_{i,j}^{n,r+1} - W_{i,j}^{n,r} \right| \ll \varepsilon_W$$

where the function W, can either be the stream function, the surface vorticity, or the temperature along the axis of symmetry, and r represents the number of iterations performed. Values of the convergence criteria used for different Grashof and Prandtl numbers solutions are given in table 1.

(iii) Choice of relaxation factor

The rate of convergence of an iterative solution procedure can sometimes be improved by over-relaxation since, the variation in the W's from one iteration cycle to the next can be forced to be greater than that which would be obtained in the normal iteration process. For this reason, where possible, over-relaxation was used. In the present

work, the following relaxation scheme was used:

$$W_{i,j}^{n,r+1} = W_{i,j}^{n,r} + \omega_W (W_{i,j}^{n} - W_{i,j}^{n,r})$$

where ω_W is a relaxation factor.

On the basis of numerical experiments, it was found that for the stream function, the optimum value of the relaxation factor varied between 1.5 to 2, while for the surface votticity, a relaxation factor of less than 1 had to be used in order to avoid divergence of solution. For the temperature along the axis of symmetry, the optimum value of the relaxation factor was found to be in the region of 1.1 to 1.5. The values used for the relaxation factors are given in table 1.

(iv) Choice of mesh size

As mentioned earlier, a reduction of the mesh size reduces the truncation errors but increases the number of grid points (i, j) at which the stream function, vorticity and temperature have to be calculated. This means that the number of simultaneous equations to be solved increases as does the computing time required for each iteration cycle. Therefore, once again, a compromise must be made between the accuracy required and the amount of computing time used.

In the following sections of this chapter, numerical solutions of the equations which describe free convective heat transfer from a solid sphere are presented. Solutions

are given for Grashof numbers (based on the radius of the sphere) of 0.05, 1, 10, 25, 50, 125 and a Prandtl number of 0.72. Solutions are also given for a Grashof number of 1250 and a Prandtl number of 10; for a Grashof number of 50 and a Prandtl number of 100; and for a Grashof number of 12500 and a Prandtl number of 10. It will be seen later in this chapter that the late-time steady state values obtained for the average Nusselt number, $\overline{Nu}$, were found to agree reasonably well with those obtained by other workers. However, there are no data available for comparison with other results obtained in the present work such as the distributions of the surface pressure, the total drag coefficients; form drag coefficient and viscous drag coefficient. Therefore, in the absence of a rigorous error analysis and lack of sufficient data, the question of how the solutions should be assessed was crucial.

To examine the accuracy and reliability of the late-time steady state values obtained in the present study of the numerical solutions for time-dependent free convective heat transfer from a solid sphere, the author obtained numerical solutions of the time-independent equations for a short range of Grashof numbers. The method of solution was a simple explicit method in which a central difference scheme was adopted for the diffusion terms of the equations and an upwind difference scheme for the convective terms. The result of this study are presented in table 2. As will

be seen later in this chapter, the late-time steady state results presented in table 1 and the steady state results presented in table 2 are in reasonable agreement.

Before presentation and discussion of the results obtained from the numerical solutions of the time-dependent equations, it is necessary to explain how a solution was assessed to have reached its late-time steady state condition.

A numerical simulation of a fluid dynamics or heat transfer problem is generally said to have reached its late-time steady state condition when the effective changes in the dependent variables from one time-level to the next become relatively small. Mathematically, the late-time steady state values of the dependent variables must remain unchanged as the integration proceed further with time.

On the basis of numerical experiments in the present work, however, it was found that once a numerical simulation had reached its late-time steady state condition, integration for a further period of time fluctuated values of the dependent variables. Eventually the values become physically unrealistic. This was mainly a result of the accumulation of round-off errors.

As explained earlier in this chapter, the magnitude of the round-off errors associated with any numerical algorithm depends upon the computing machine used, the particular

sequence of machine operations used, and the values of the various numbers involved in these machine operations. Integration of the equations during the time-dependent period gives rise to round-off errors which are random in behaviour since the time-dependent variables are changing with time, and as explained in section 4.2 it is unlikely that round-off errors during this period can appreciably affect the solution. However, further integration of the equations, once the solution has reached late-time steady state condition gives rise to round-off errors which are regular in behaviour since the dependent variables are no longer changing with time, thus, all the necessary arithmetic operations for carrying out the integration from one time-level to the next are performed on round-off errors which are propagated and accumulated throughout this part of the computation in a regular manner. As a result, the late-time steady state values obtained earlier for the dependent variables will be affected by the round-off errors if simulation is continued.

To avoid the undue accumulation of round-off errors in the present work, whenever the effective changes in the values of the dependent variables became relatively small, it was assumed that the simulation had reached the late-time steady state condition. The late-time variations with time of the flow characteristics are presented in tables 7 to 13.

The numerical results which will be presented in the following sections of this chapter and in tables 1 to 13 are in terms of the dimensionless variables defined in chapter 2; and in all the contour drawings the direction of flow along the axis of symmetry is from right to left.

4.4 NUMERICAL SOLUTION FOR A GRASHOF NUMBER OF 0.05 AND A PRANDTL NUMBER OF 0.72

The development with time of the streamlines starting from a motionless flow field around a heated solid sphere in conditions of free convective heat transfer at a Grashof number, Gr, of 0.05 and a Prandtl number, Pr, of 0.72 is shown in figures 4.4.1a to 4.4.1d. As mentioned earlier, the solid sphere was assumed to be enclosed in another spherical shell, namely the outer boundary. It was also assumed that the temperatures of the solid sphere and the spherical shell are uniform and unchanging with time but at two different levels. The temperature distribution within the fluid changes with time and the fluid near the hotter boundary, the sphere surface, tends to rise and that near the colder boundary, the outer boundary, tends to move downwards. The rising and descending currents generate a circulatory flow pattern as shown by the streamlines plotted in figures 4.4.1a to 4.4.1d. From the stream function contours, it can be observed that the fluid velocity increases from zero to its late-time steady state value.

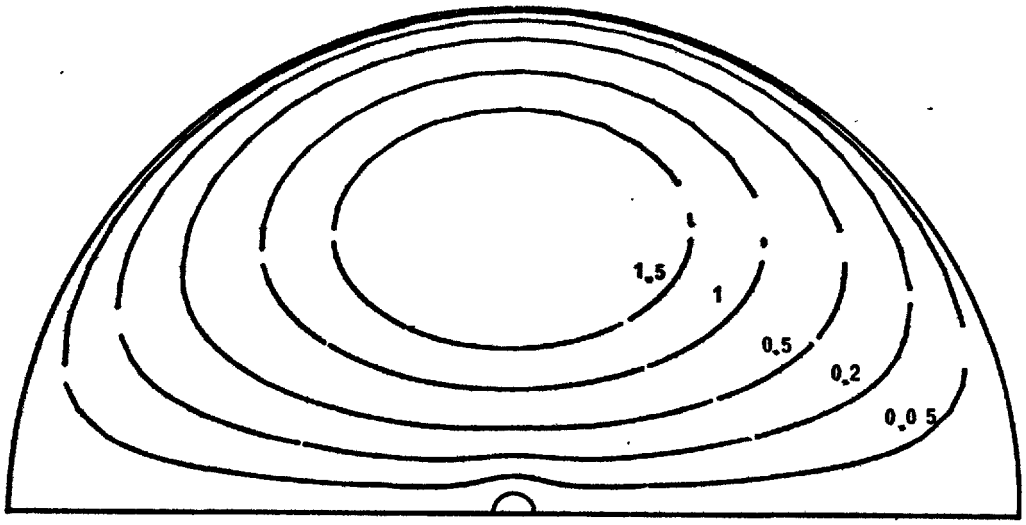

FIGURE 4.4.1b STREAMLINES AROUND THE SPHERE AT GRASHOF NUMBER OF 0.05 AND PRANDTL NUMBER OF 0.72 DIMENSIONLESS TIME . t = 20

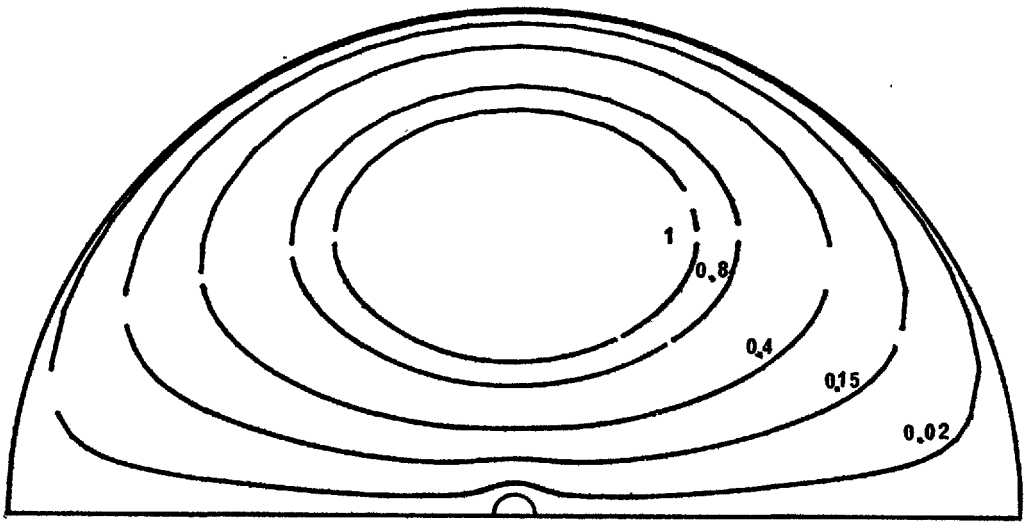

FIGURE 4.4.1a STREAMLINES AROUND THE SPHERE AT GRASHOF NUMBER OF 0.05 AND PRANDTL NUMBER OF 0.72 DIMENSIONLESS TIME . t = 12

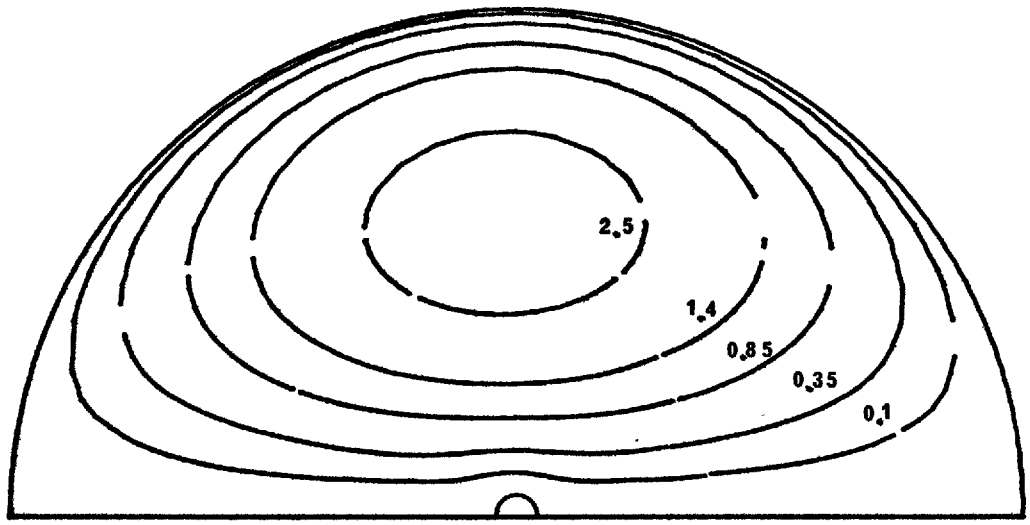

FIGURE 4.4.1d STREAMLINES AROUND THE SPHERE AT GRASHOF NUMBER OF 0.05 AND PRANDTL NUMBER OF 0.72 DIMENSIONLESS TIME , t =36

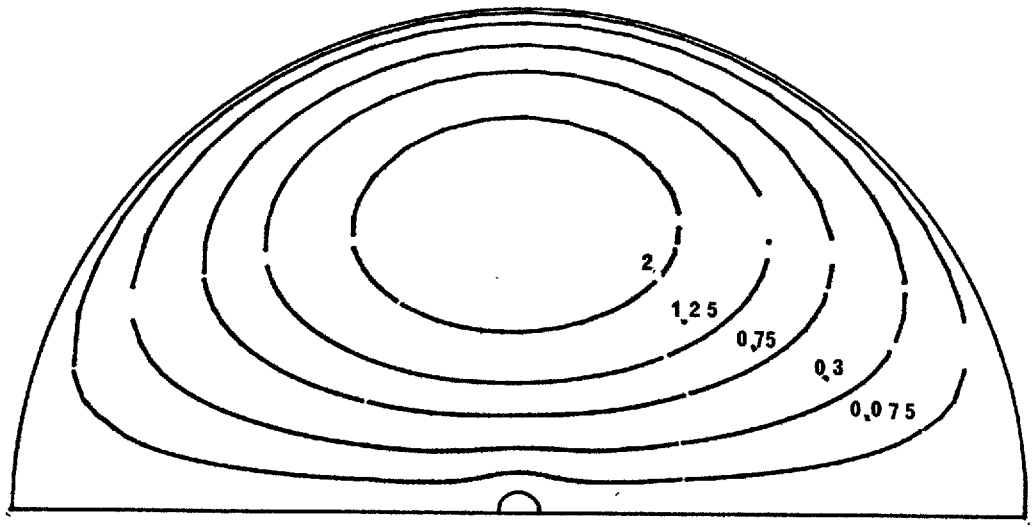

FIGURE 4.4.1c STREAMLINES AROUND THE SPHERE AT GRASHOF NUMBER OF 0.05 AND PRANDTL NUMBER OF 0.72 DIMENSIONLESS TIME , t =28

Late-time values of the local Nusselt number, the surface vorticity, and the surface pressure are presented in table 7. From this table one can observe that the above variables become almost independent of time during the dimensionless time period of 28 to 36.

Figures 4.4.2a to 4.4.2d show the development with time of the isotherms around the solid sphere. The time-dependent energy equation was solved using the radial steady state conduction solution as an initial condition. In the limiting case of a fluid at rest then in the absence of convective effects, the influence of the heated sphere extends uniformly in all directions. However, even at as small a Grashof number as 0.05, a comparison of the temperatures at distances far away from the solid sphere with the initial values reveals that there is weak convective process far away from the sphere surface. As a result, the temperatures in the upstream region of the solid sphere are less than those predicted by the pure conduction solution. Figure 4.4.2d shows the late-time steady state temperature distribution at a dimensionless time of 36.

The generation and diffusion of vorticity into the fluid around a solid sphere in conditions of free convective heat transfer can be seen in figures 4.4.3a to 4.4.3d which show the vorticity distribution as a function of time. From these figures one observes that the vorticity values are relatively small and that they are distributed almost

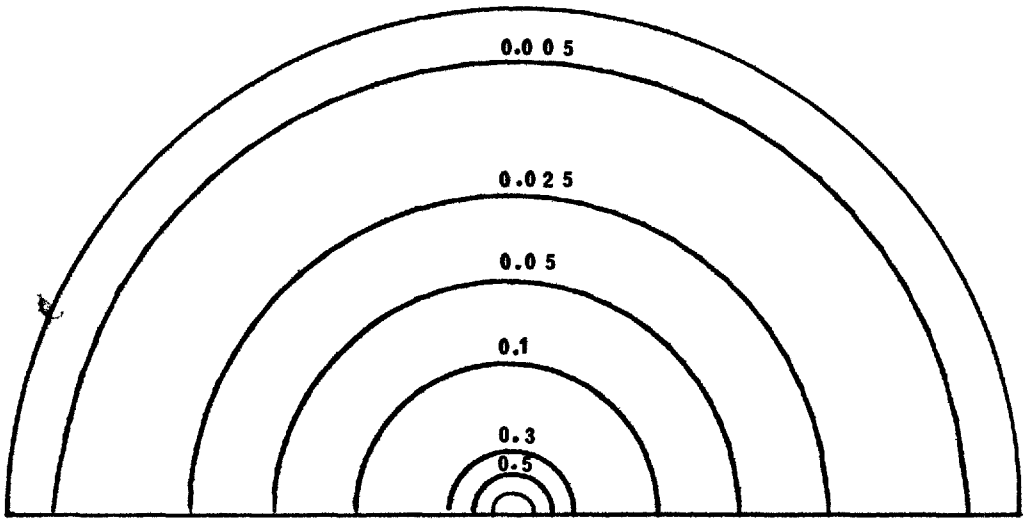

FIGURE 4.4.2b ISOTHERMS AROUND THE SPHERE AT GRASHOF NUMBER OF 0.05 AND PRANDTL NUMBER OF 0.72 DIMENSIONLESS TIME , t =20

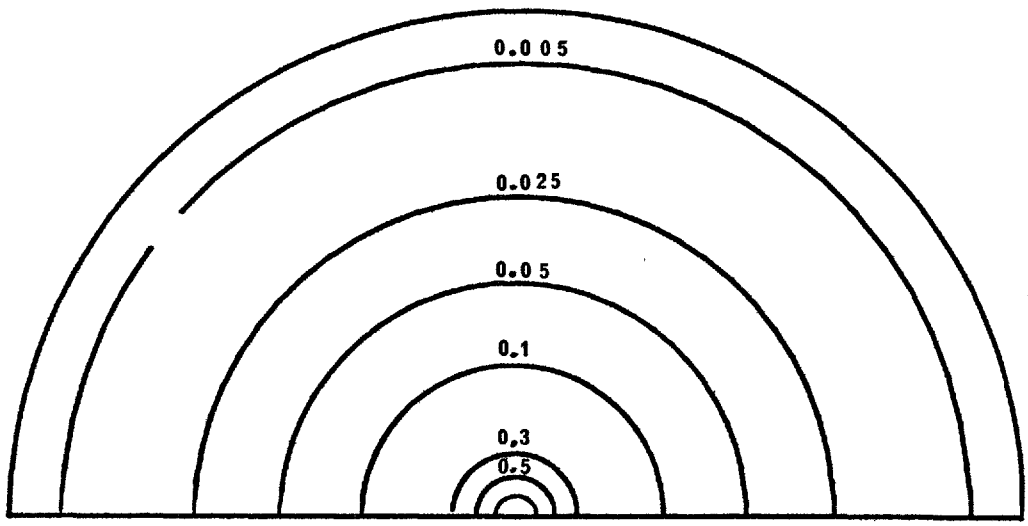

FIGURE 4.4.2a ISOTHERMS AROUND THE SPHERE AT GRASHOF NUMBER OF 0.05 AND PRANDTL NUMBER OF 0.72 DIMENSIONLESS TIME , t =12

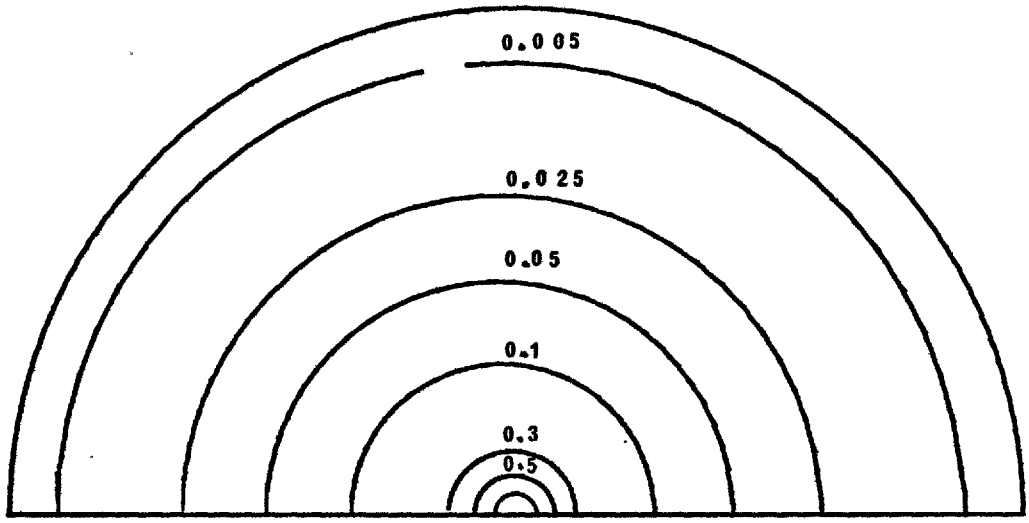

FIGURE 4.4.2d ISOTHERMS AROUND THE SPHERE AT GRASHOF NUMBER OF 0.05 AND PRANDTL NUMBER OF 0.72 DIMENSIONLESS TIME , t =36

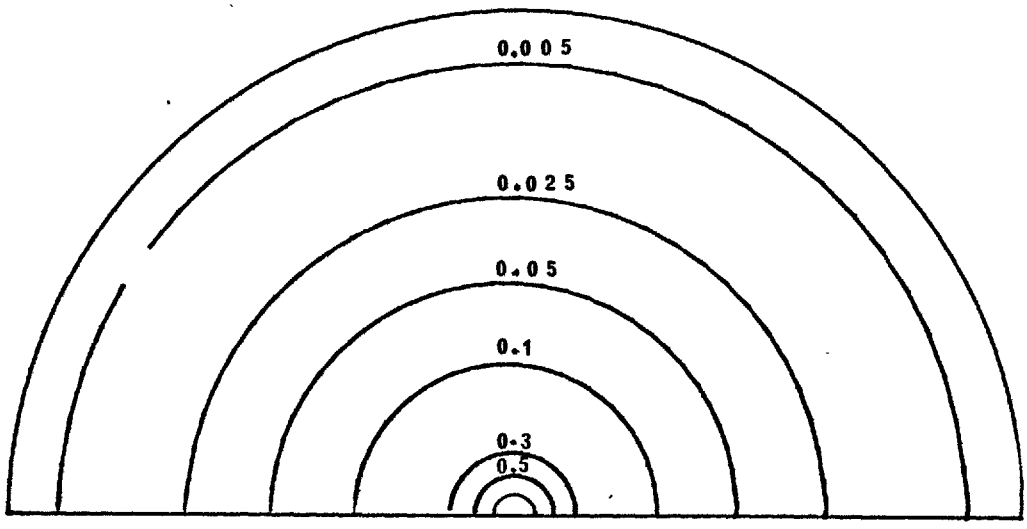

FIGURE 4.4.2c ISOTHERMS AROUND THE SPHERE AT GRASHOF NUMBER OF 0.05 AND PRANDTL NUMBER OF 0.72 DIMENSIONLESS TIME , t =28

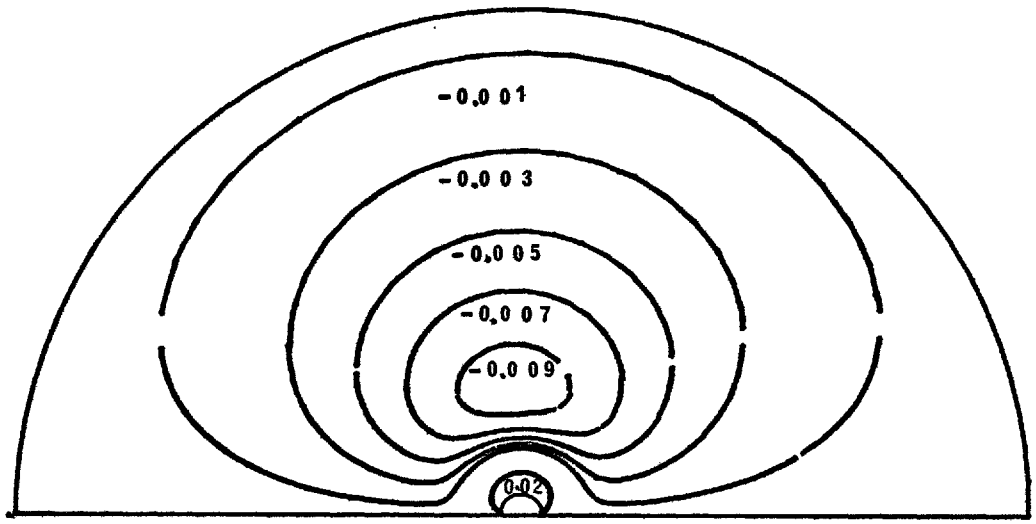

FIGURE 4.4.3b VORTICITY DISTRIBUTION AROUND THE SPHERE AT GRASHOF NUMBER OF 0.05 AND PRANDTL NUMBER OF 0.72 DIMENSIONLESS TIME . t =20

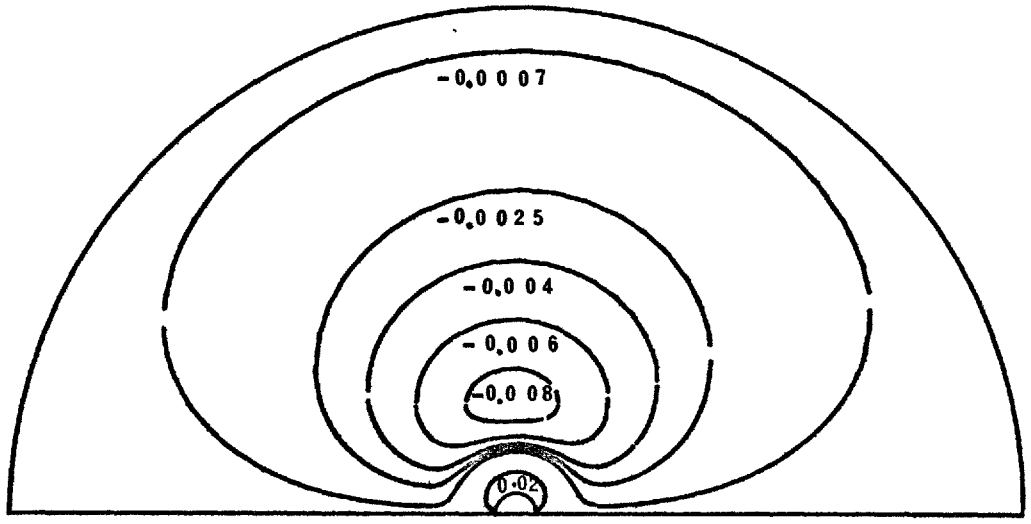

FIGURE 4.4.3a VORTICITY DISTRIBUTION AROUND THE SPHERE AT GRASHOF NUMBER OF 0.05 AND PRANDTL NUMBER OF 0.72 DIMENSIONLESS TIME . t =12

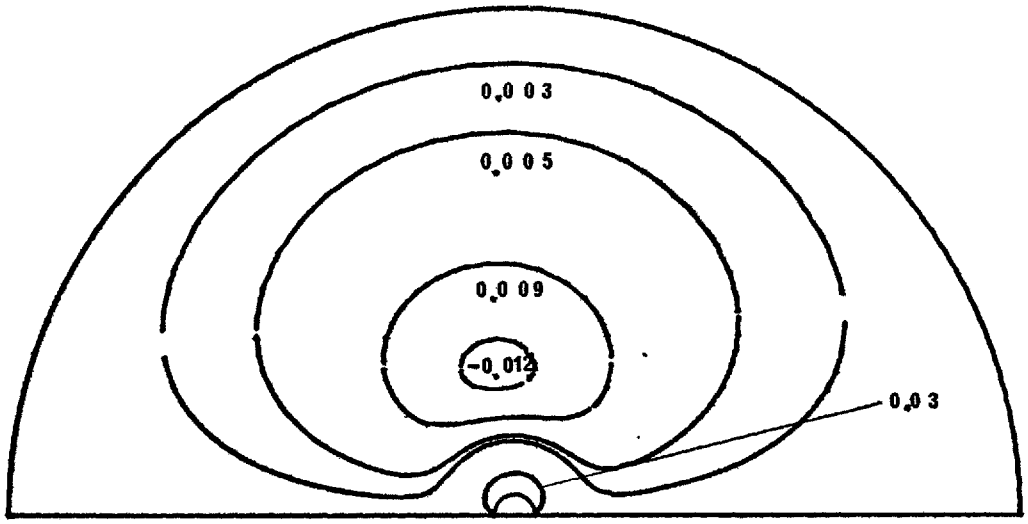

FIGURE 4.4.3d VORTICITY DISTRIBUTION AROUND THE SPHERE AT GRASHOF NUMBER OF 0.05 AND PRANDTL NUMBER OF 0.72 DIMENSIONLESS TIME , t =36

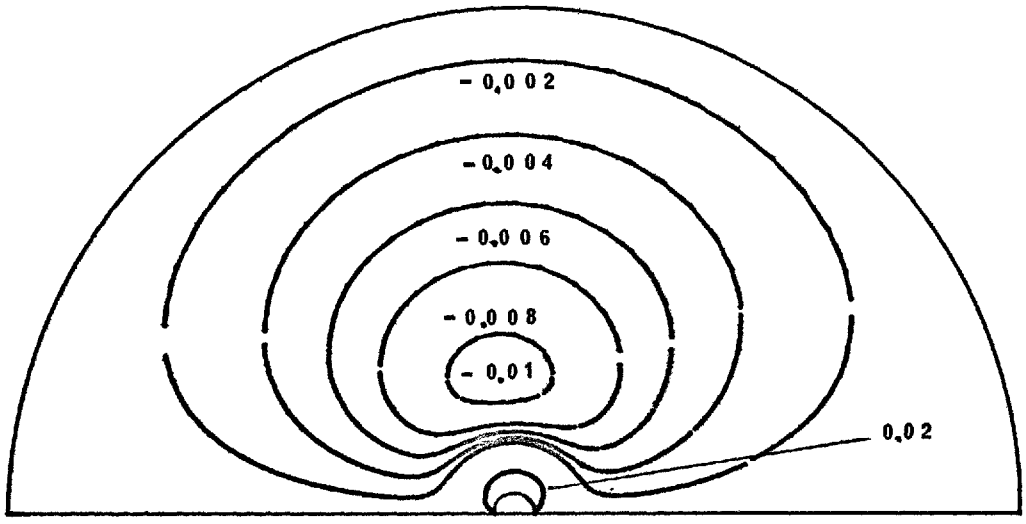

FIGURE 4.4.3c VORTICITY DISTRIBUTION AROUND THE SPHERE AT GRASHOF NUMBER OF 0.05 AND PRANDTL NUMBER OF 0.72 DIMENSIONLESS TIME , t =28

symmetrically about an imaginary plane normal to the axis of symmetry of flow and passing through the equator of the sphere. This may be explained as follows. At a Grashof number of 0.05 and a Prandtl number of 0.72, the fluid velocity is small and therefore, the convection of vorticity is small. The late-time steady state vorticity distribution at a dimensionless time of 36 is shown by figure 4.4.3d.

The temperature gradients normal to the sphere surface are evaluated from the temperature distributions. The temperature gradients are then used to calculate the local Nusselt number, Nu_θ, and the average or overall Nusselt number, $\overline{Nu}$, as described in appendix D. Figure 4.4.5 shows the variation of the local Nusselt number with dimensionless time, t. During the early stages of simulation, the difference between local Nusselt numbers at the front and rear stagnation points of the sphere is relatively small showing the weakness of the effects of convection. However, as simulation continues, the convective effects increase very slightly and the difference between the local Nusselt numbers at the front and rear stagnation points of the solid sphere increases.

Figure 4.4.8 shows the variation of the average Nusselt number with time. Since the steady state conduction, in a finite space (equation 2.6.17), is used as an initial dimensionless fluid temperature, the average Nusselt number starts from a value of 2.085 and increases continuously

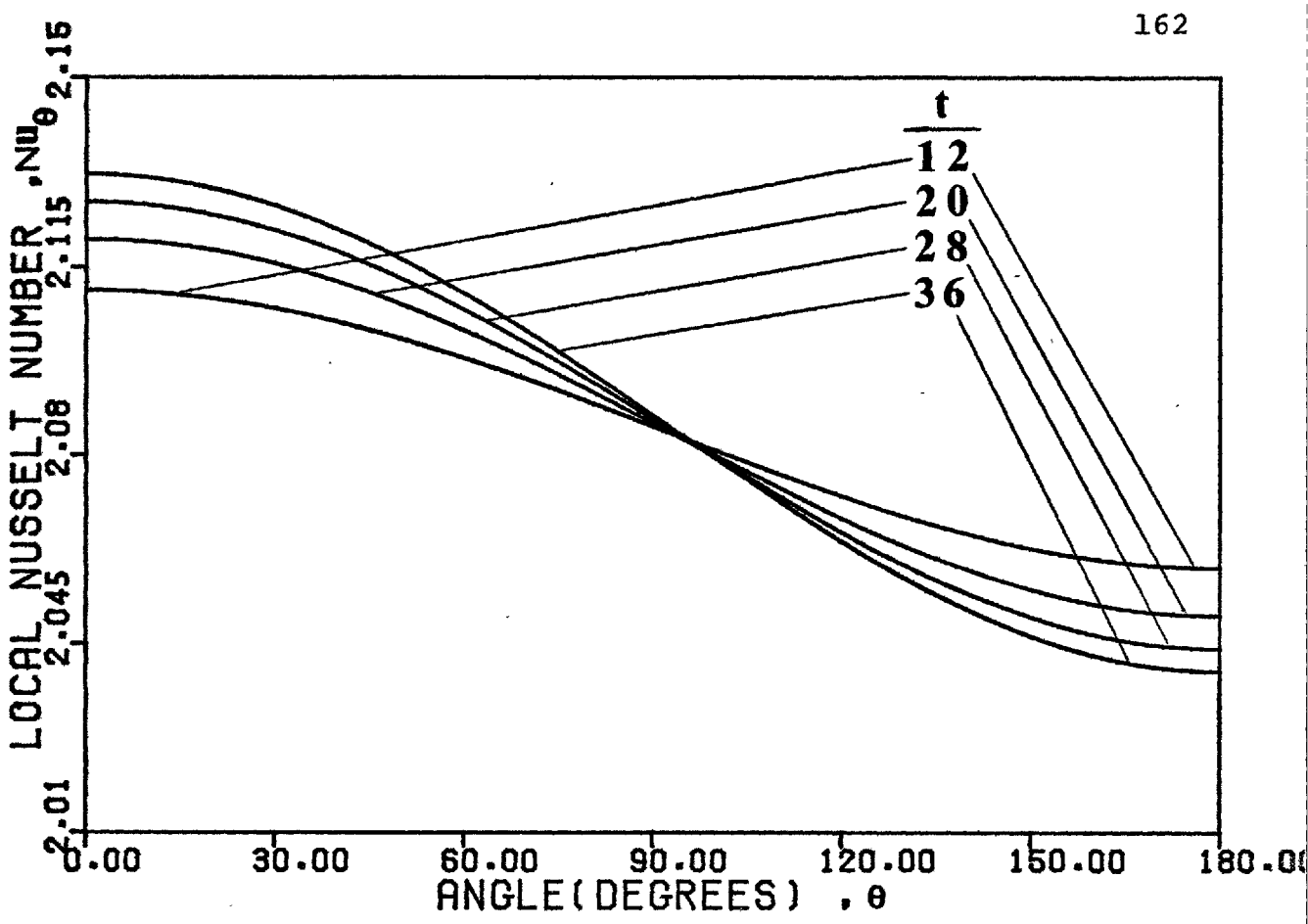

FIGURE 4.4.5 LOCAL NUSSELT NUMBER VERSUS TIME AT GRASHOF NUMBER OF 0.05 AND PRANDTL NUMBER OF 0.72

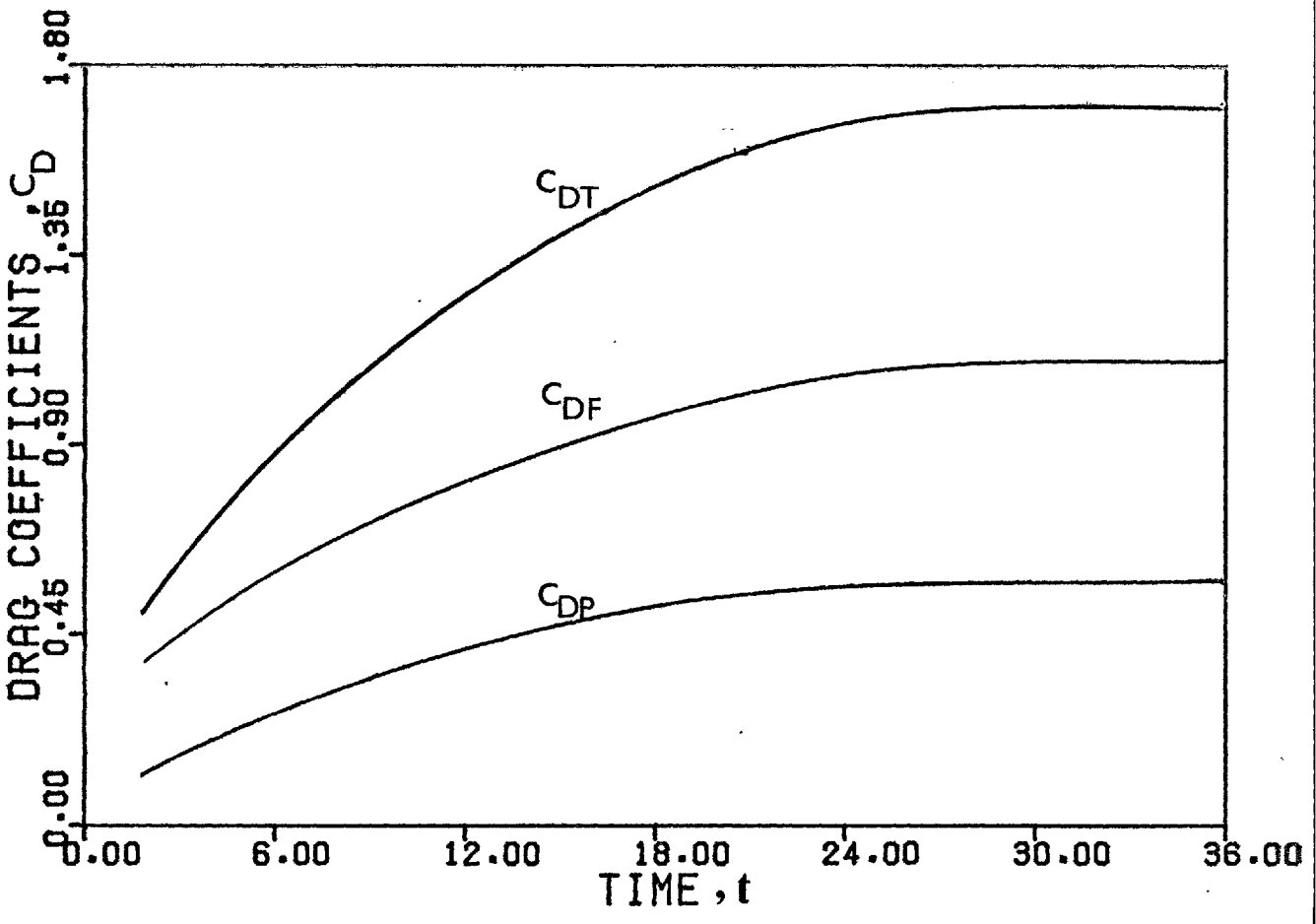

FIGURE 4.4.4 DRAG COEFFICIENTS VERSUS TIME AT GRASHOF NUMBER OF 0.05 AND PRANDTL NUMBER OF 0.72

towards its late-time steady state value. Table 3 shows a comparison of the late-time steady state values of the average Nusselt number obtained in the present study with the results obtained by other workers from their analytical and experimental studies. It is seen that the late-time steady state average Nusselt number calculated in this work for a Grashof number of 0.05 and a Prandtl number of 0.72 is slightly greater than the value obtained by Hossain (1966) from his analytical solution. The value of the average Nusselt number is, however, slightly underpredicted in comparison with experimental measurements.

The variation of surface vorticity, ζ_s, with time is plotted in figure 4.4.7. From this figure one observes that the surface vorticity is fairly symmetrically distributed about an imaginary plane placed between the upstream and downstream regions of the flow field. This is because the dominant mode of transfer close to the surface is diffusion as explained earlier. From figure 4.4.7 and table 7 it can also be seen that as simulation continues the surface vorticity increases until its late-time steady state value is attained.

From the stream function, vorticity and temperature distributions the dimensionless surface pressure is evaluated as described in appendix B. The variation with time of dimensionless surface pressure, K_θ, is shown in figure 4.4.6. From figure 4.4.6, it can be seen that as time increases,

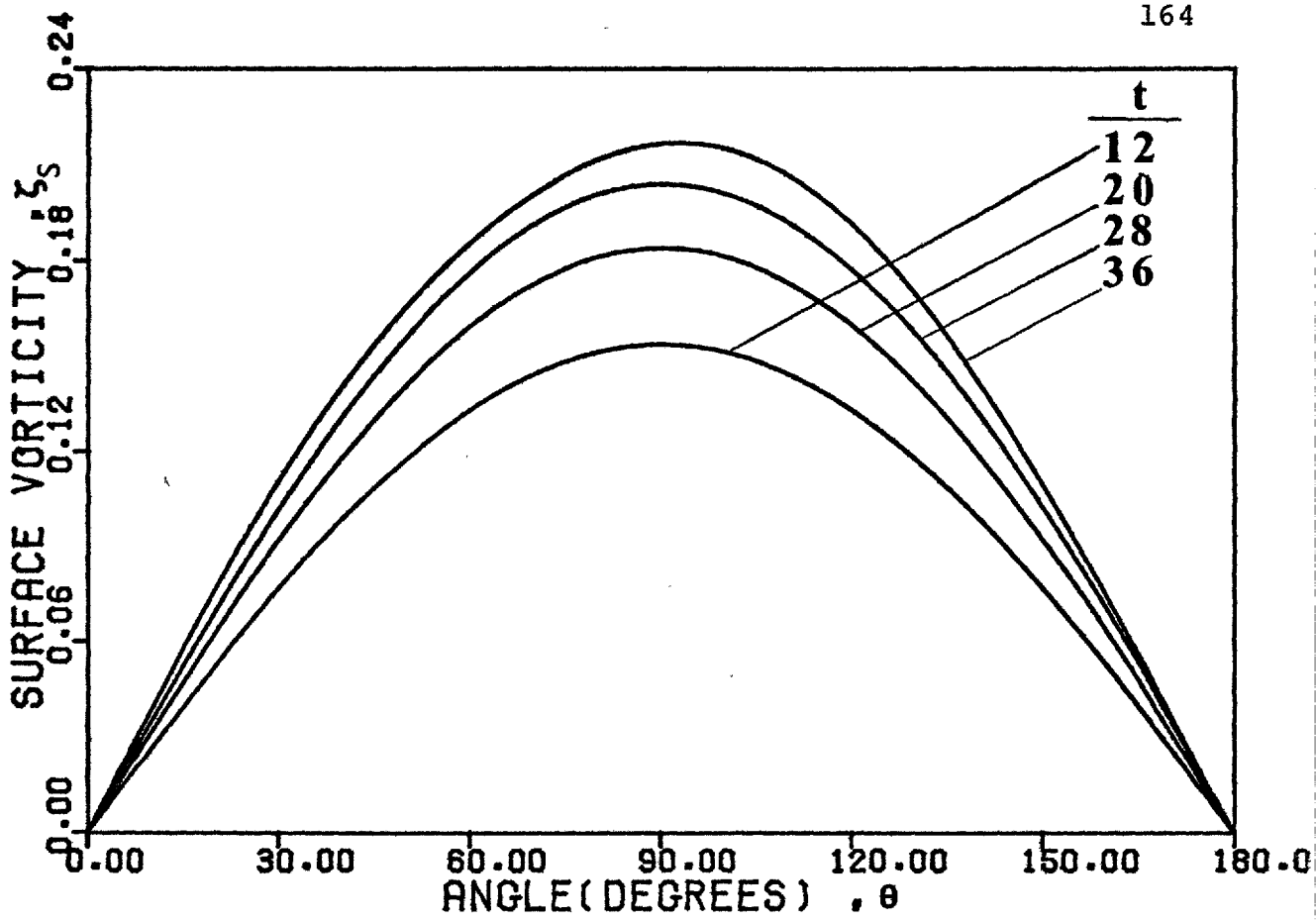

FIGURE 4.4.7 SURFACE VORTICITY VERSUS TIME AT GRASHOF NUMBER OF 0.05 AND PRANDTL NUMBER OF 0.72

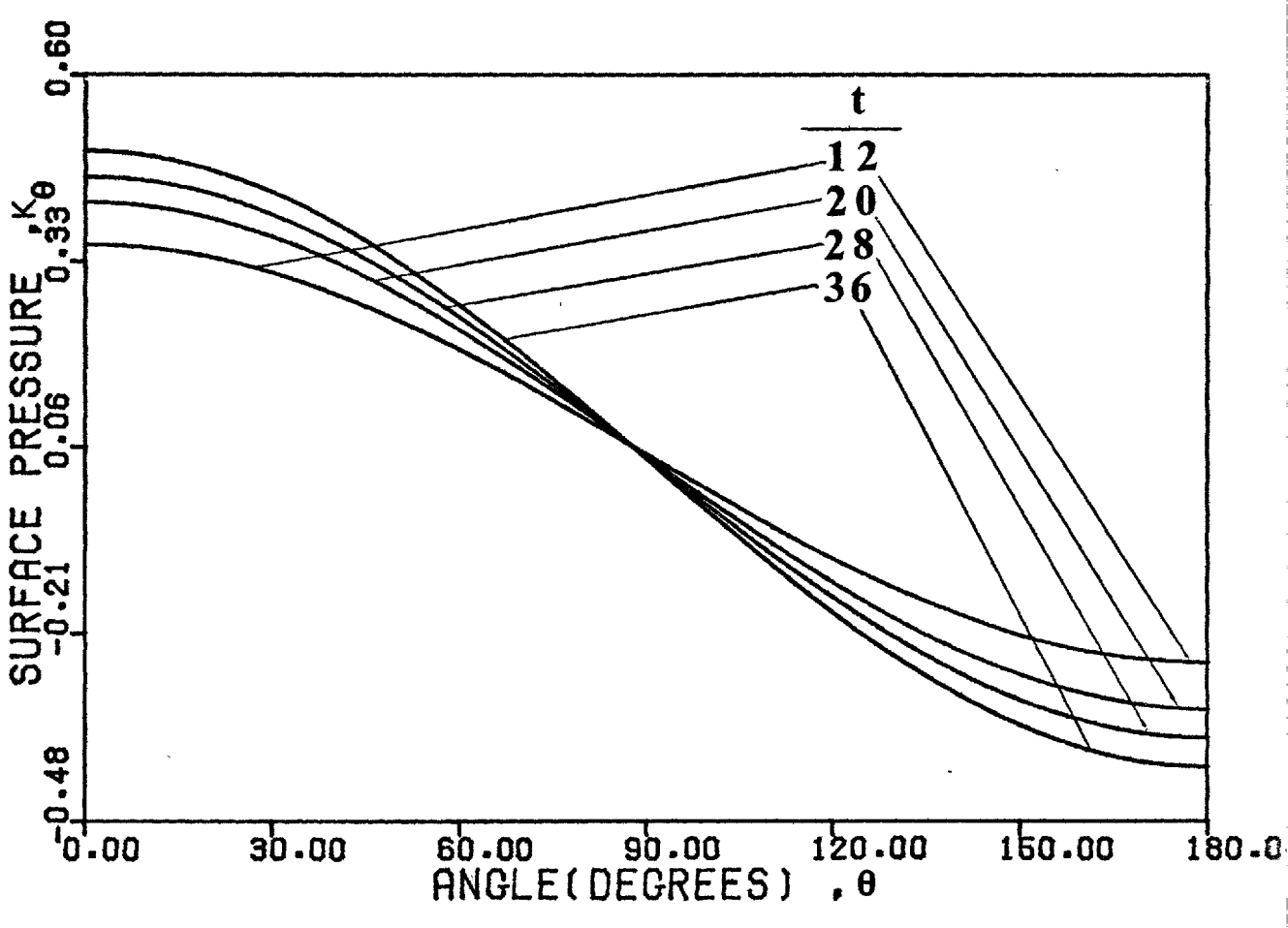

FIGURE 4.4.6 SURFACE PRESSURE VERSUS TIME AT GRASHOF NUMBER OF 0.05 AND PRANDTL NUMBER OF 0.72

the dimensionless surface pressure increases over the upstream region of the sphere and decreases over the downstream region of the sphere.

The behaviour of the drag coefficients with time is shown in figure 4.4.4. Both the pressure or form drag coefficient, C_{DP}, and the viscous or frictional drag coefficient, C_{DF}, show a smooth increase with dimensionless time, t. The reason why the drag coefficients increase with time may be explained as follows.

Consider equations (C.2.5) and (C.3.5) which are derived in appendix C and are as follows:

$$C_{DP} = \int_0^{\pi} K_{\Theta} \sin 2\Theta \, d\Theta \qquad \text{(C.2.5)}$$

$$C_{DF} = 4\int_0^{\pi} \zeta_S \sin^2\Theta \, d\Theta \qquad \text{(C.3.5)}$$

As the dimensionless time increases, the dimensionless surface pressure increases over the upstream region of the sphere and decreases over the downstream region of the sphere. The surface vorticity also increases with time. Therefore, both the form drag coefficient and the viscous drag coefficient increases with time.

The main results obtained from the numerical solution of the time-dependent problem are presented in table 1. Table 2 shows the main results of the time-independent problem. A comparison between tables 1 and 2 for a Grashof number of 0.05 and a Prandtl number of 0.72 shows the results

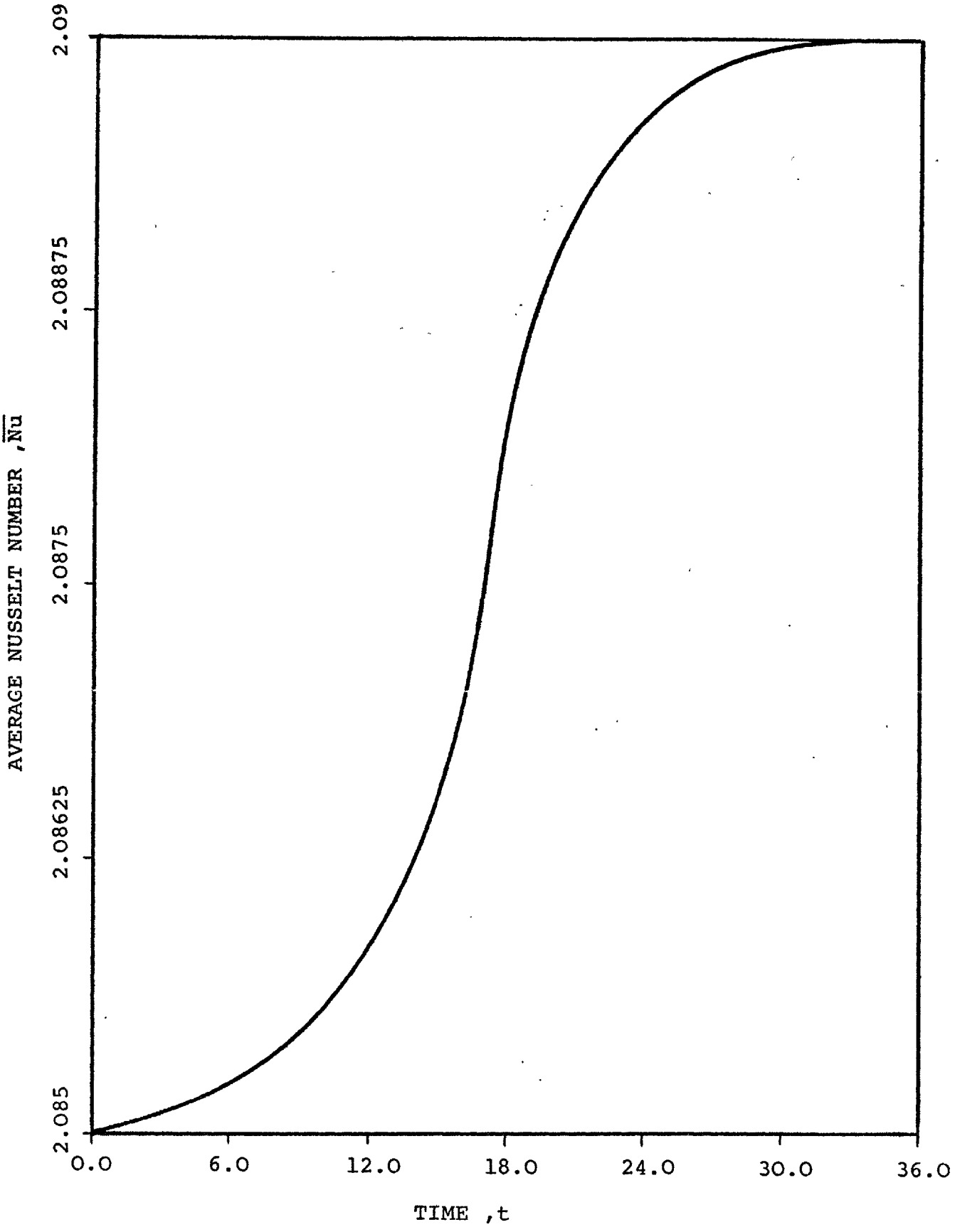

FIGURE 4.4.8 AVERAGE NUSSELT NUMBER VERSUS TIME AT GRASHOF NUMBER OF 0.05 AND PRANDTL NUMBER OF 0.72

obtained from the time-dependent and time-independent solutions are in good agreement.

4.5 NUMERICAL SOLUTION FOR A GRASHOF NUMBER OF 1 AND A PRANDTL NUMBER OF 0.72

Figures 4.5.1a to 4.5.1d and figures 4.5.2a to 4.5.2d show the streamlines and isotherms respectively, as a function of time around a solid sphere in conditions of free convection. Figures 4.5.1d and 4.5.2d show the stream function and temperature contours at the late-time steady state condition obtained at a dimensionless time, t, of 15.

As can be seen from figures 4.5.2a to 4.5.2d, during the early stages of simulation heat diffuses radially into the surrounding fluid, but as the transfer of heat continues the heated region extends downstream. As the dimensionless time approaches to its late-time steady state value, the thickness of the heated layer over the upstream region of the solid sphere decreases, while over the downstream region of the solid sphere, it increases. At the late-time steady state condition, the thickness of the heated layer increases with the angle, Θ, measured from the front stagnation point.

Figures 4.5.3a to 4.5.3d show the vorticity distribution as a function of time around the solid sphere. As can be seen from figure 4.5.3a, during the early stages of integration, the vorticity distribution around the solid sphere is

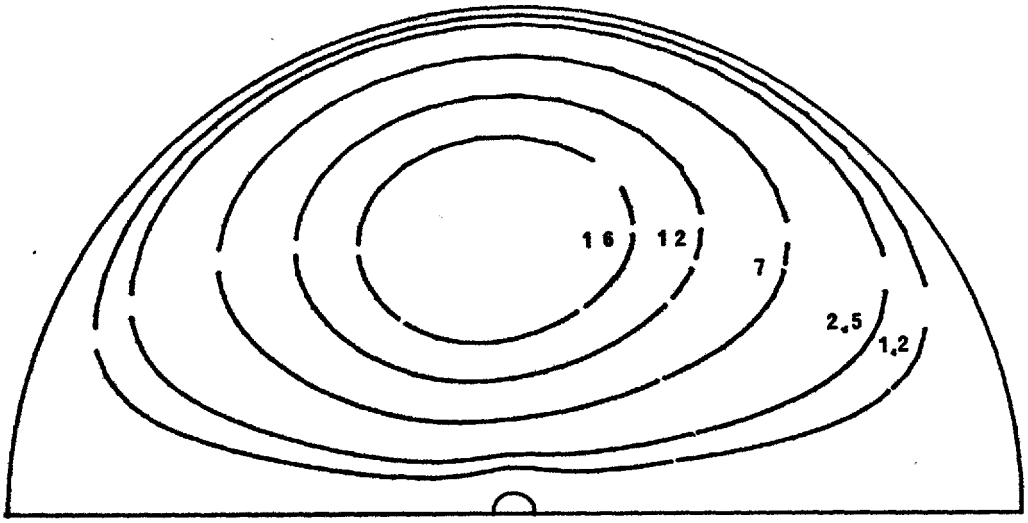

FIGURE 4.5.1b STREAMLINES AROUND THE SPHERE AT GRASHOF NUMBER OF 1 AND PRANDTL NUMBER OF 0.72 DIMENSIONLESS TIME , $t = 7$

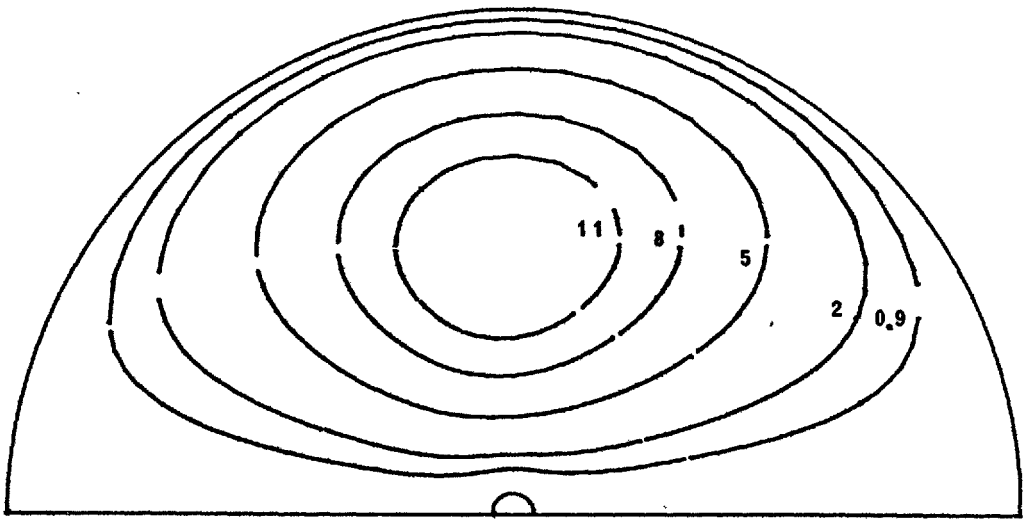

FIGURE 4.5.1a STREAMLINES AROUND THE SPHERE AT GRASHOF NUMBER OF 1 AND PRANDTL NUMBER OF 0.72 DIMENSIONLESS TIME , $t = 4$

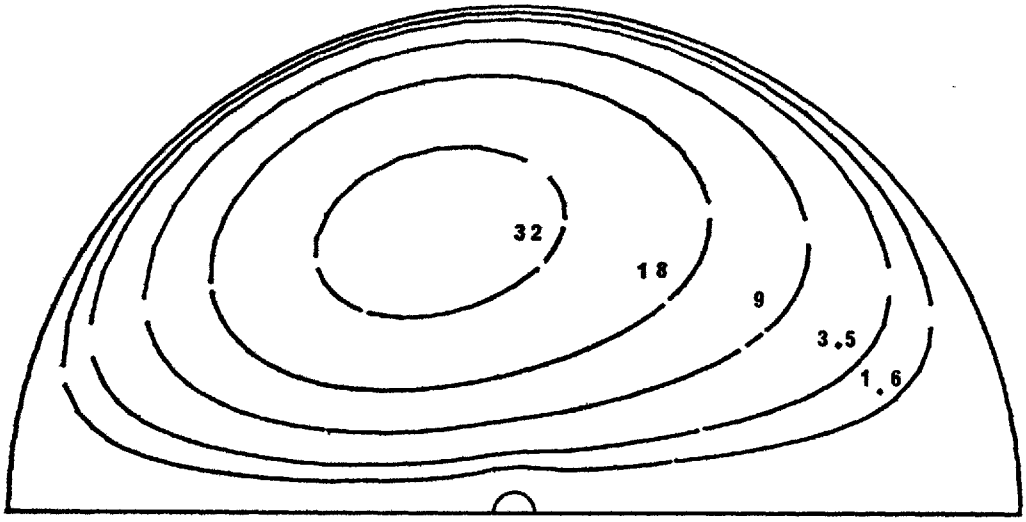

FIGURE 4.5.1d STREAMLINES AROUND THE SPHERE AT GRASHOF NUMBER OF 1 AND PRANDTL NUMBER OF 0.72 DIMENSIONLESS TIME , $t = 15$

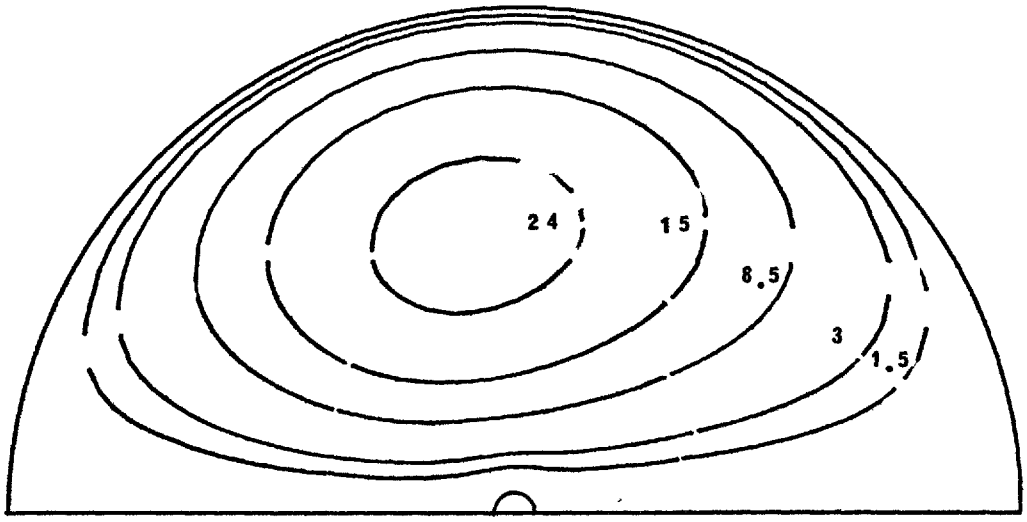

FIGURE 4.5.1c STREAMLINES AROUND THE SPHERE AT GRASHOF NUMBER OF 1 AND PRANDTL NUMBER OF 0.72 DIMENSIONLESS TIME , $t = 11$

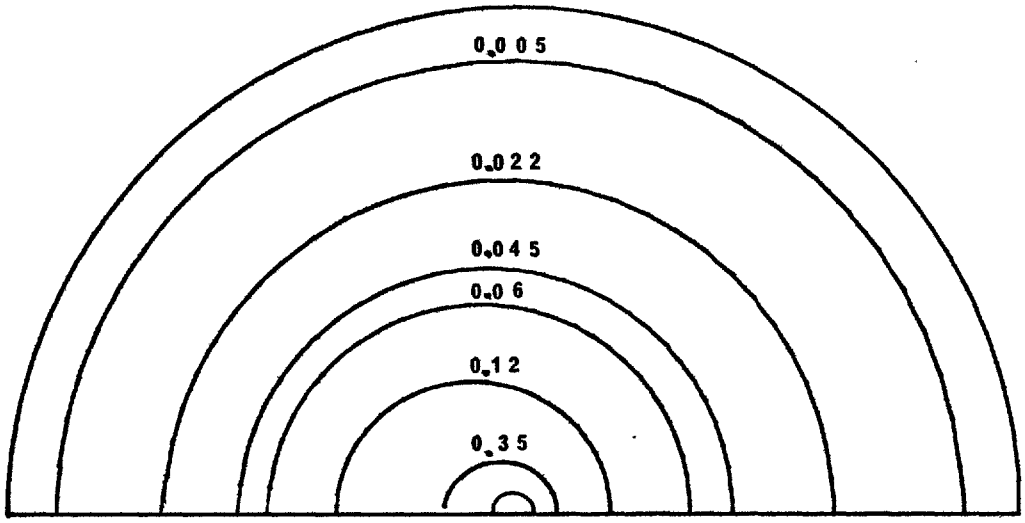

FIGURE 4.5.2b ISOTHERMS AROUND THE SPHERE AT GRASHOF NUMBER OF 1 AND PRANDTL NUMBER OF 0.72 DIMENSIONLESS TIME , t = 7

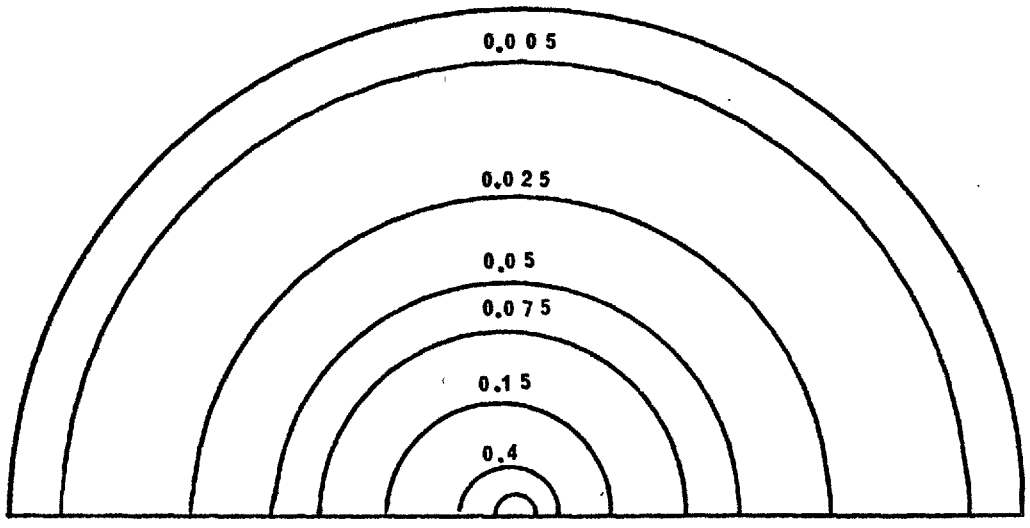

FIGURE 4.5.2a ISOTHERMS AROUND THE SPHERE AT GRASHOF NUMBER OF 1 AND PRANDTL NUMBER OF 0.72 DIMENSIONLESS TIME , t = 4

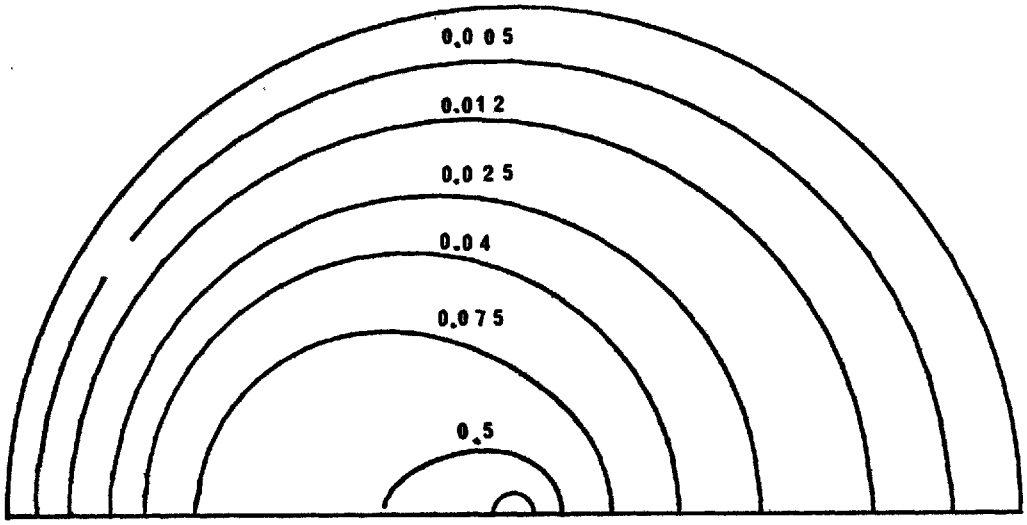

FIGURE 4.5.2d ISOTHERMS AROUND THE SPHERE AT GRASHOF NUMBER OF 1 AND PRANDTL NUMBER OF 0.72 DIMENSIONLESS TIME , $t = 15$

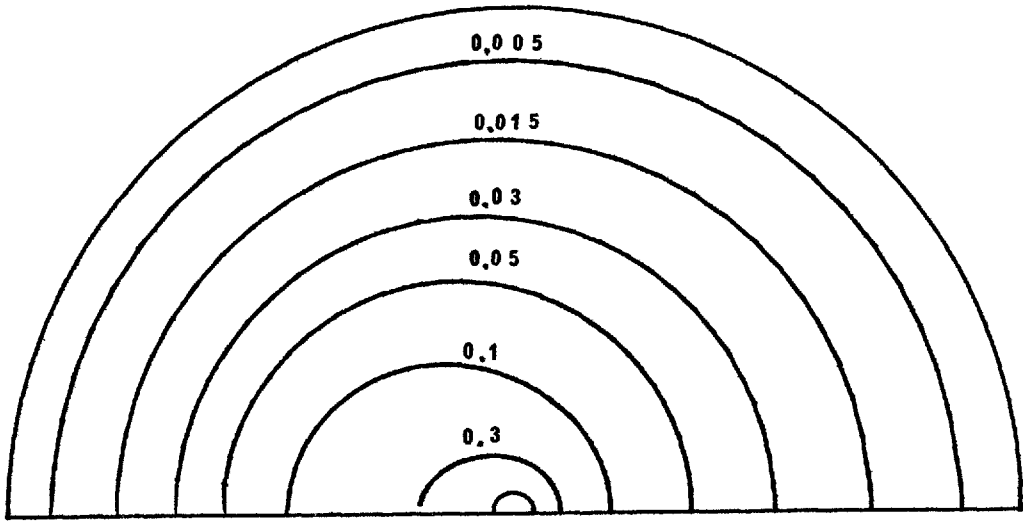

FIGURE 4.5.2c ISOTHERMS AROUND THE SPHERE AT GRASHOF NUMBER OF 1 AND PRANDTL NUMBER OF 0.72 DIMENSIONLESS TIME , $t = 11$

almost symmetrical about an imaginary plane placed between the upstream and downstream regions of the flow field. This is because during the early stages of simulation, the fluid velocity is small so that the effects of convection are small. However, as simulation continues the effects of convection increases and vorticity is convected more and more downstream. Figure 4.5.3d shows the vorticity contours at the late-time steady state condition.

Figure 4.5.5 shows the variation of the local Nusselt number with time for a Grashof number of 1 and a Prandtl number of 0.72 when steady state conduction is used as an initial dimensionless fluid temperature. During the initial stages of heat transfer, the local Nusselt number at the front stagnation point does not differ much from the local Nusselt number at the rear stagnation point. This is because intially, the velocity is small and heat transfer takes place mainly by unsteady state conduction. However, as time increases, the convective effects increase and the variation in the local Nusselt number becomes more pronounced. Generally, the local Nusselt numbers around the upstream region of the sphere increase steadily towards their late-time steady state values while those around the rear part of the sphere decrease at first and then increase as the late-time steady state condition is approached. This behaviour can be seen from figure 4.5.5 for a Prandtl number of 0.72.

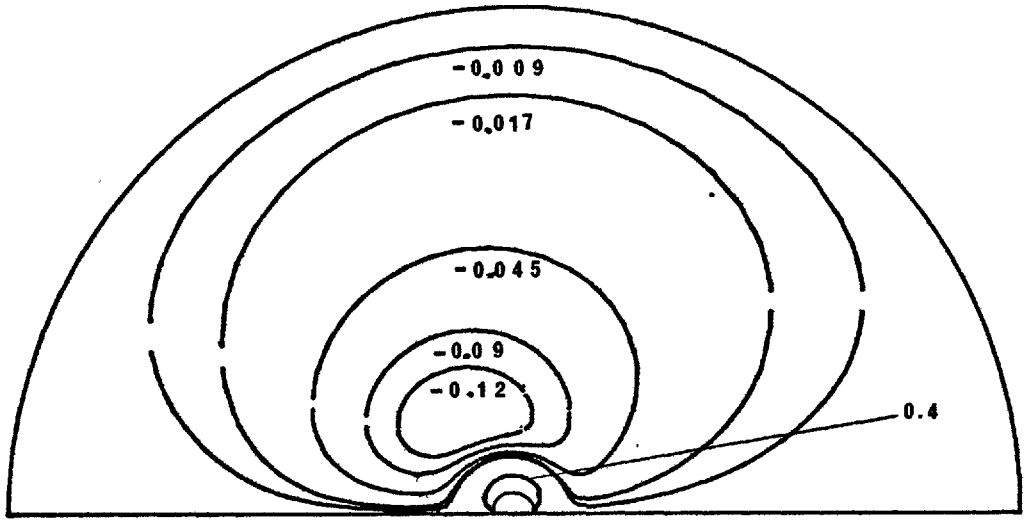

FIGURE 4.5.3b VORTICITY DISTRIBUTION AROUND THE SPHERE AT GRASHOF NUMBER OF 1 AND PRANDTL NUMBER OF 0.72 DIMENSIONLESS TIME , $t = 7$

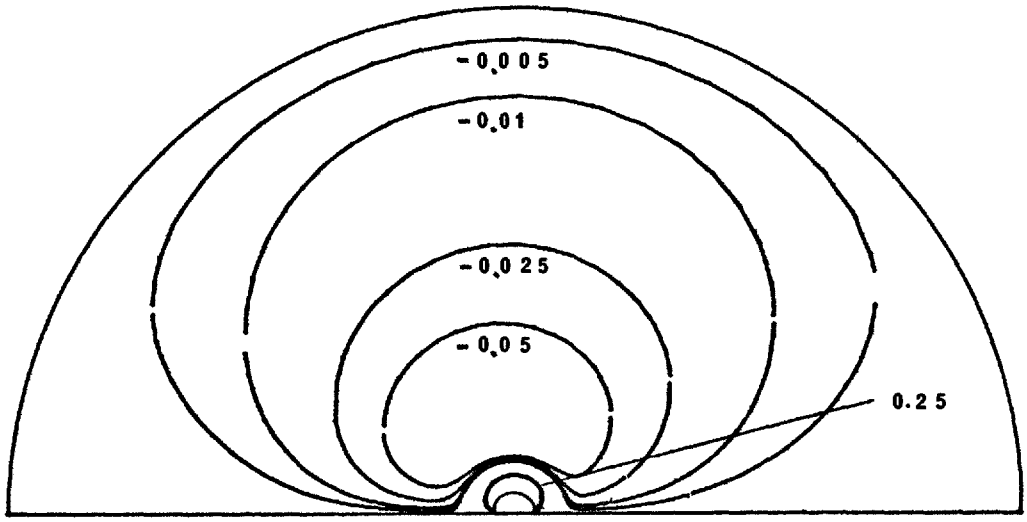

FIGURE 4.5.3a VORTICITY DISTRIBUTION AROUND THE SPHERE AT GRASHOF NUMBER OF 1 AND PRANDTL NUMBER OF 0.72 DIMENSIONLESS TIME , $t = 4$

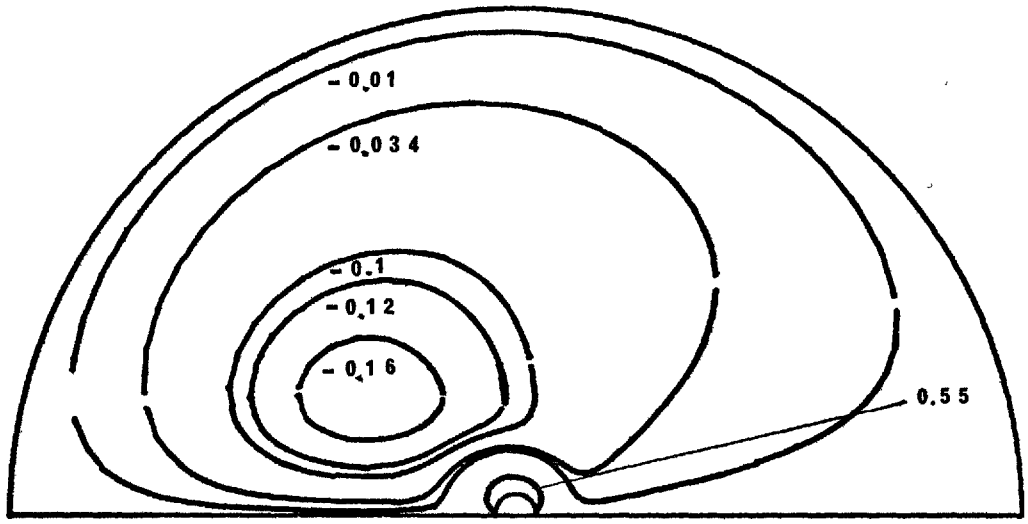

FIGURE 4.5.3d VORTICITY DISTRIBUTION AROUND THE SPHERE AT GRASHOF NUMBER OF 1 AND PRANDTL NUMBER OF 0.72 DIMENSIONLESS TIME , $t = 15$

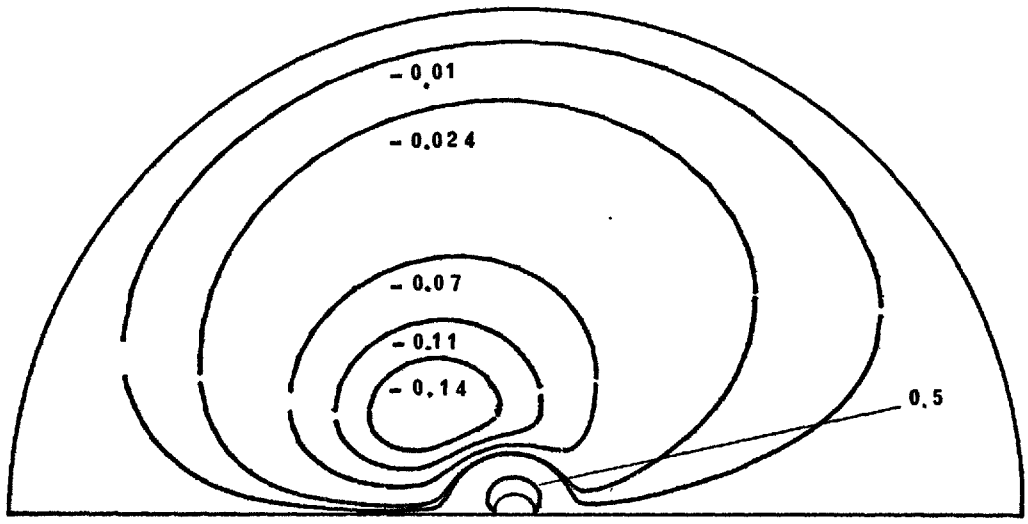

FIGURE 4.5.3c VORTICITY DISTRIBUTION AROUND THE SPHERE AT GRASHOF NUMBER OF 1 AND PRANDTL NUMBER OF 0.72 DIMENSIONLESS TIME , $t = 11$

The behaviour of the drag coefficients with time is shown by figure 4.5.4. The variation with time of the form drag coefficient, C_{DP}, the viscous drag coefficient, C_{DF}, and total drag coefficient, C_{DT}, follows a similar pattern to that shown by the Grashof number of 0.05 solution. Both the form drag and the viscous drag coefficients show a smooth increase with time.

The variation with time of the surface vorticity is shown in figure 4.5.7. From this figure one observes that the surface vorticity, for all times is almost symmetrically distributed about an imaginary plane situated between the upstream and the downstream regions of the flow. This shows that although convective effects are noticeable away from the sphere surface (figure 4.5.3d) the dominant mode of vorticity transport near to the surface is diffusion.

Figure 4.5.6 shows the variation of surface pressure with time. The behaviour with time of the surface pressure follows a similar pattern to that shown by the solution obtained for a Grashof number of 0.05. From figure 4.5.6 one observes that as time increases, the dimensionless surface pressure increases over the upstream region of the sphere and decreases over the downstream region.

The main results obtained from the numerical solution of the time-dependent problem for a Grashof number of 1 and a Prandtl number of 0.72 are presented in table 1.

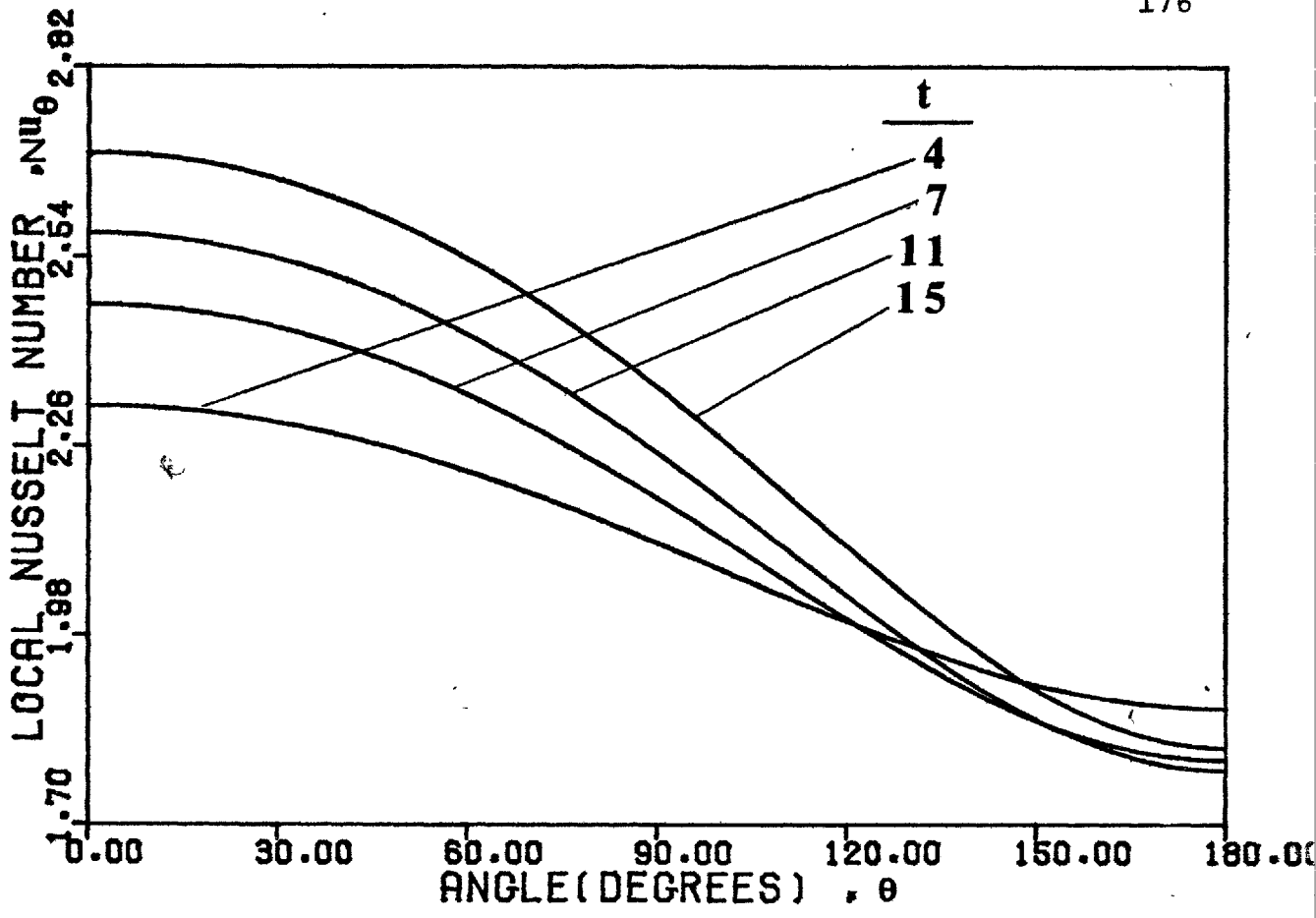

FIGURE 4.5.5 LOCAL NUSSELT NUMBER VERSUS TIME AT GRASHOF NUMBER OF 1 AND PRANDTL NUMBER OF 0.72

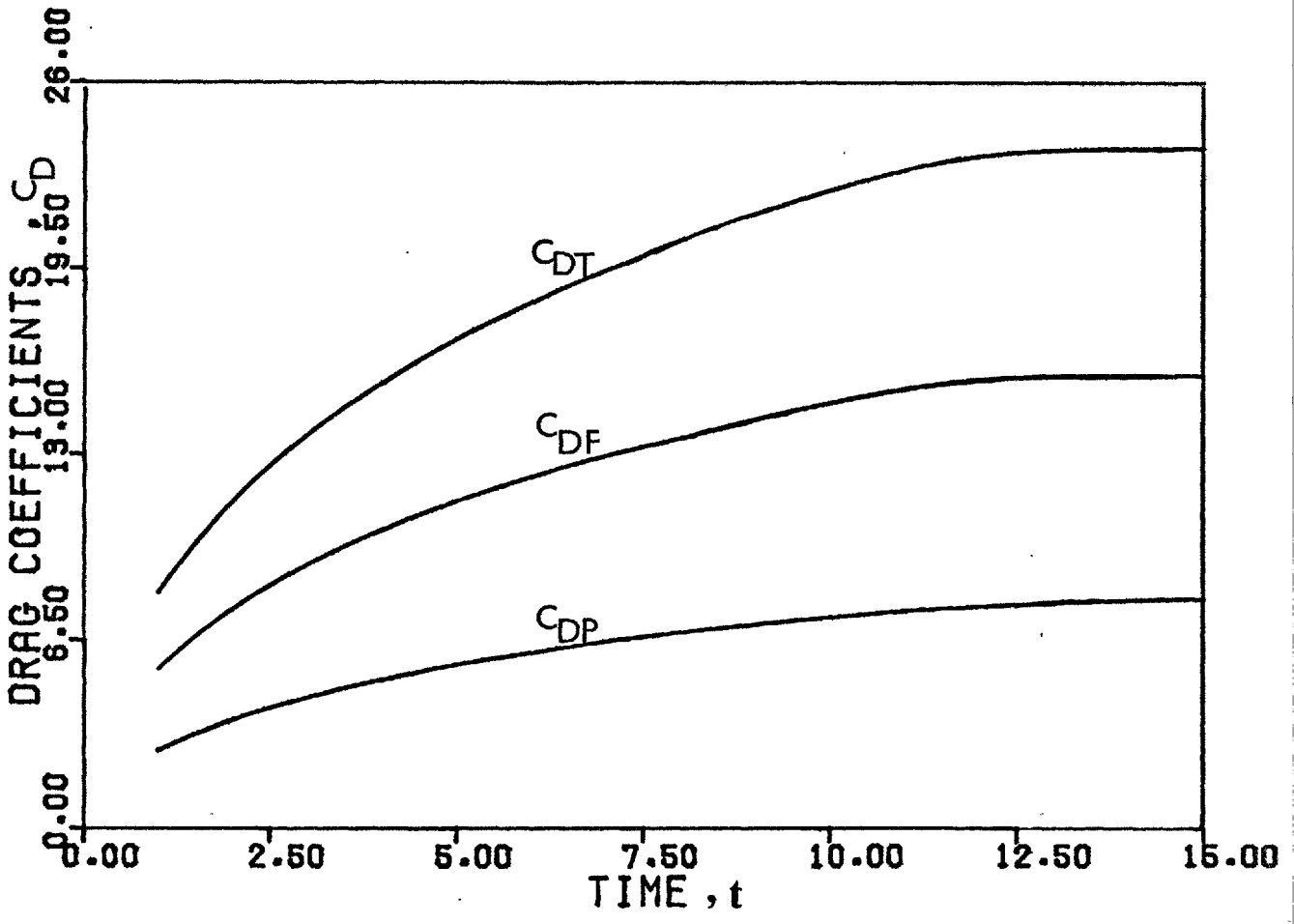

FIGURE 4.5.4 DRAG COEFFICIENTS VERSUS TIME AT GRASHOF NUMBER OF 1 AND PRANDTL NUMBER OF 0.72

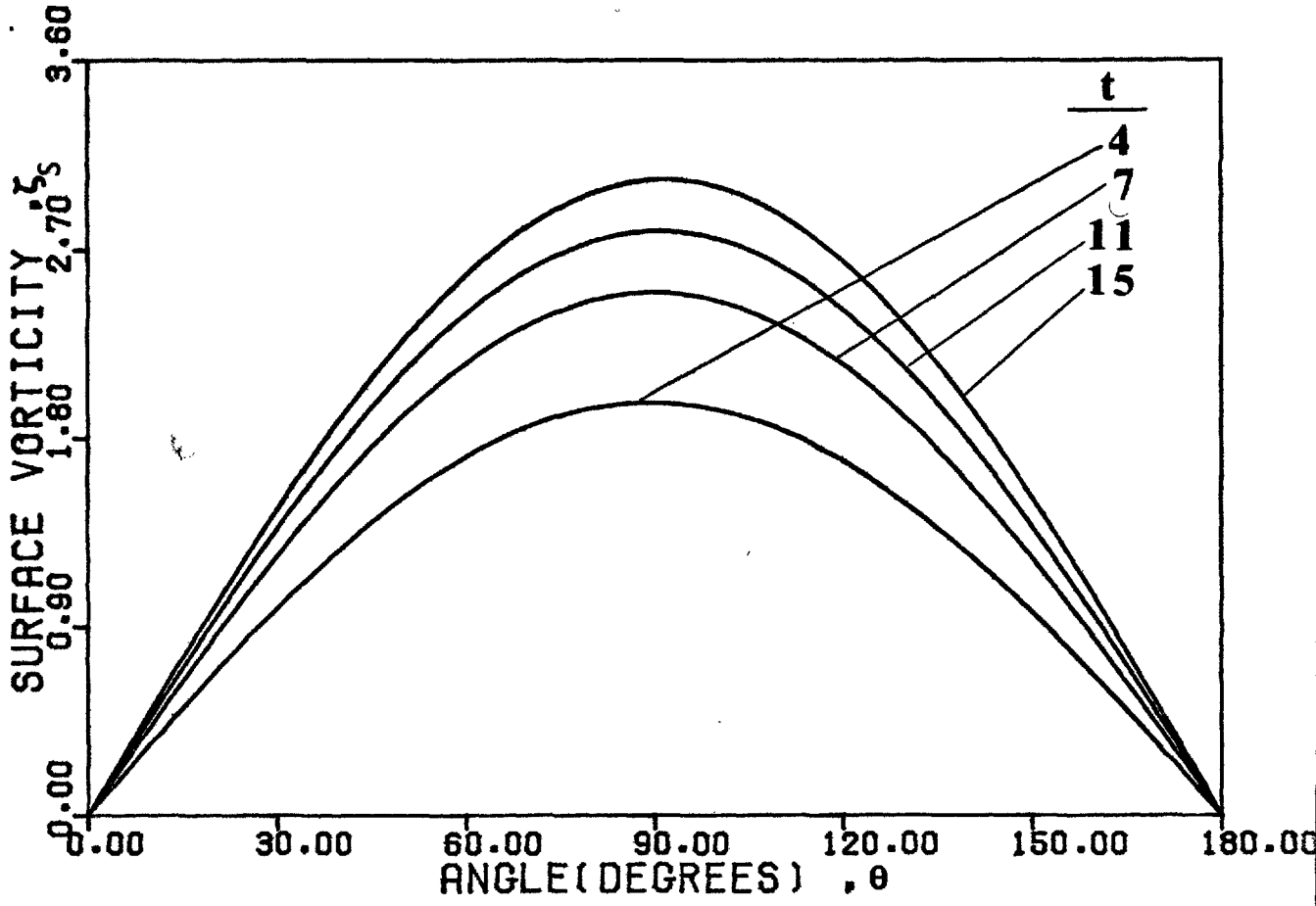

FIGURE 4.5.7 SURFACE VORTICITY VERSUS TIME AT GRASHOF NUMBER OF 1 AND PRANDTL NUMBER OF 0.72

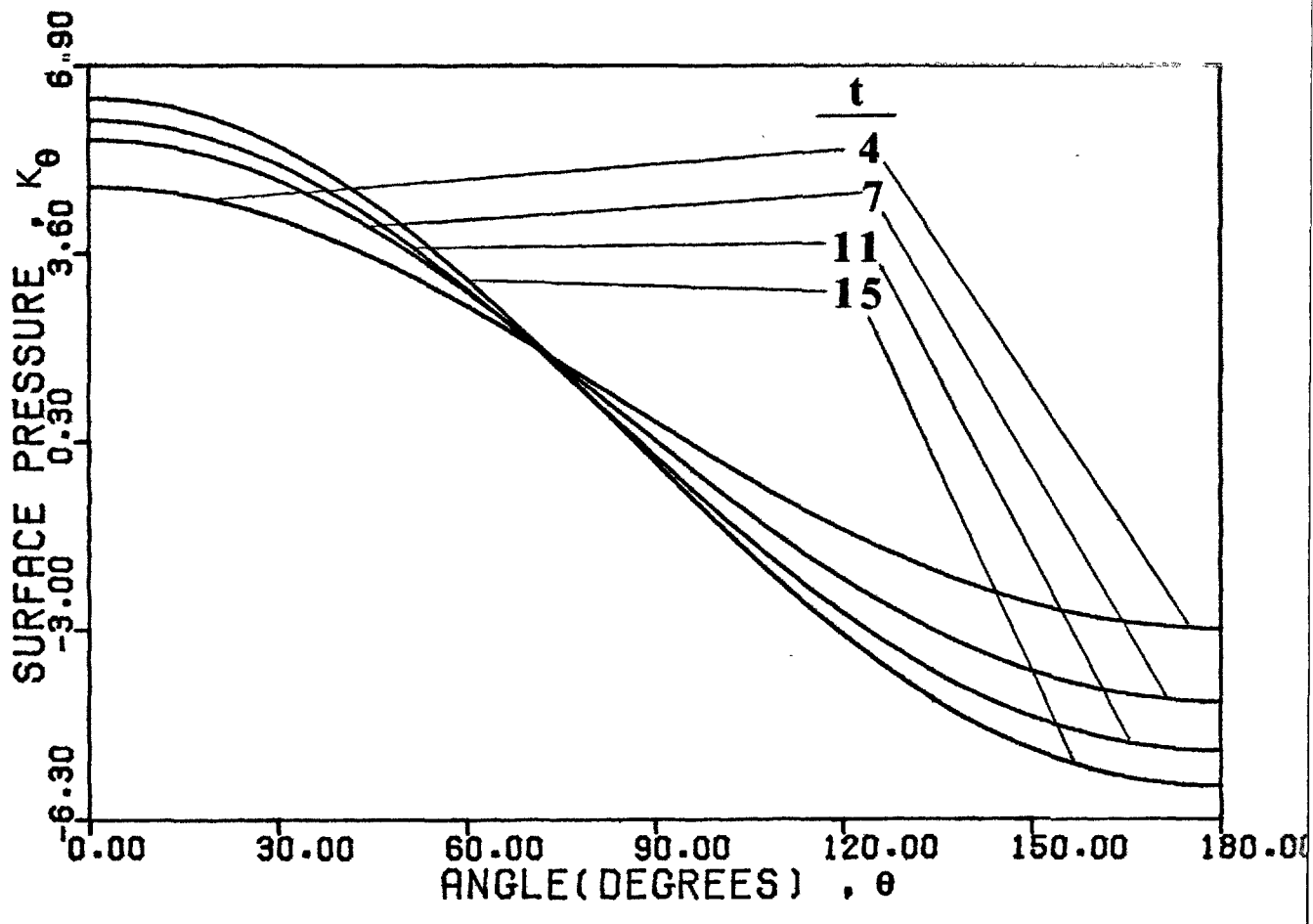

FIGURE 4.5.6 SURFACE PRESSURE VERSUS TIME AT GRASHOF NUMBER OF 1 AND PRANDTL NUMBER OF 0.72

From a comparison of the solutions obtained for Grashof number of 0.05 and 1, both for a Prandtl number of 0.72, one observes that the total dimensionless time, t, taken before late-time steady state conditions are reached is shorter in the case of a Grashof number of 1 than for a Grashof number of 0.05. This may be explained as follows:

The Grashof number represents the ratio of the buoyancy forces to the viscous forces. Therefore, an increase in the Grashof number represents an increase in the buoyancy forces relative to the viscous forces thus increasing the fluid velocity so that the effects of convection are increased. The increased convection currents lead to an increase in the rate of heat transfer from the sphere to the medium and will shorten the total dimensionless time taken to reach late-time steady state condition.

Table 8 represents the late-time values of the local Nusselt number, the surface vorticity, and the surface pressure as the simulation approaches the late-time condition . From this table it can be seen that the relative changes in the above variables during the dimensionless time period of 12 to 15 become relatively small indicating that the simulation has almost reached steady state condition .

The variation of the average Nusselt number with time is shown in figure 4.5.8. The average Nusselt number starts from a value of 2.085 and increases continuously towards its

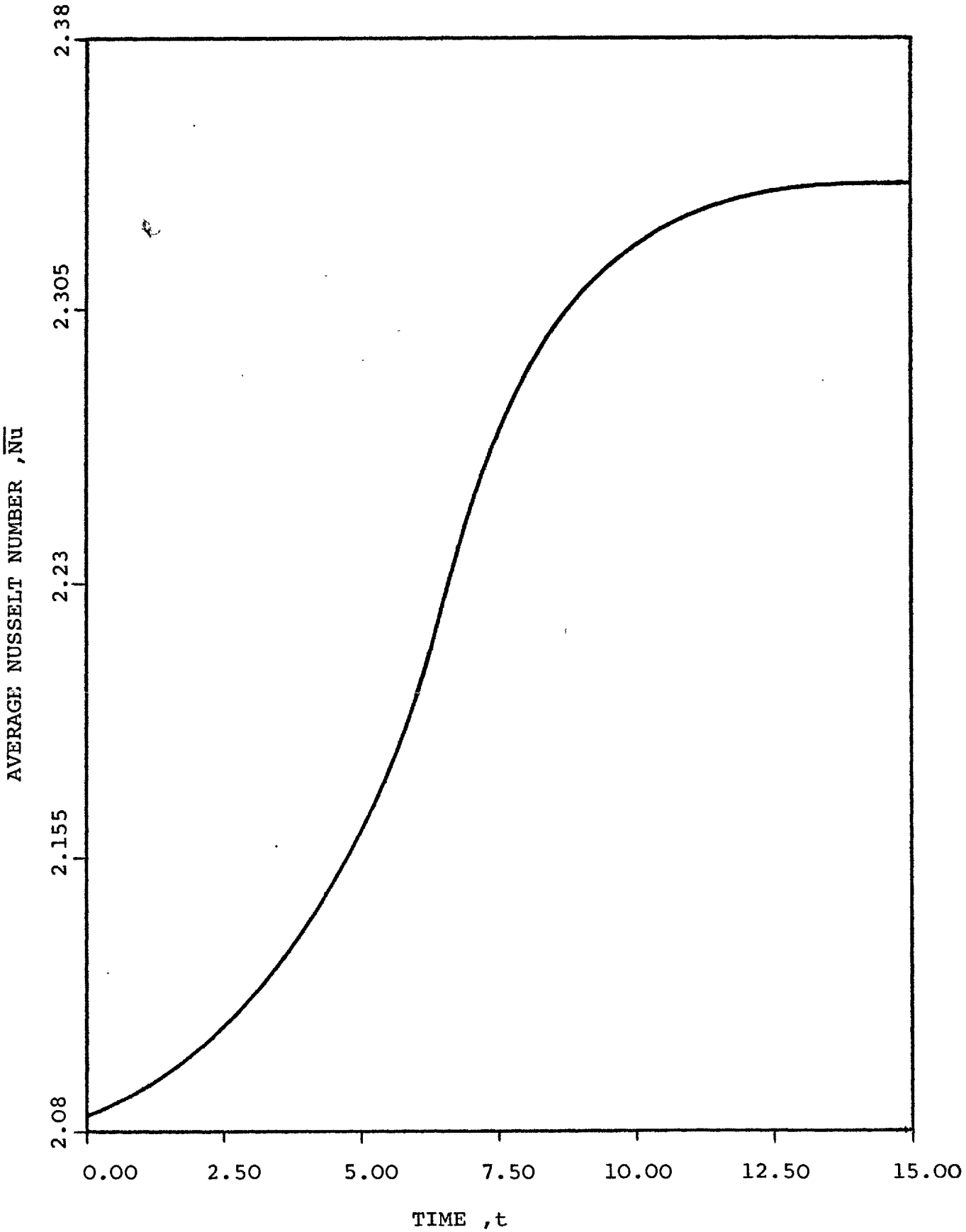

FIGURE 4.5.8 AVERAGE NUSSELT NUMBER VERSUS TIME AT GRASHOF NUMBER OF 1 AND PRANDTL NUMBER OF 0.72

late-time steady state value which calculated to be 2.34.

As can be seen from table 3, the late-time steady state average Nusselt number obtained in the present study for a Grashof number of 1 is in reasonable agreement with the available experimental measurements. Table 2 shows the main results obtained from the numerical solution of time-independent problem. As can be seen from tables 1 and 2, the results obtained from the solutions of the time-dependent and the time-independent equations for a Grashof number of 1 and a Prandtl number of 0.72 are also in reasonable agreement.

4.6 NUMERICAL SOLUTION FOR A GRASHOF NUMBER OF 10 AND A PRANDTL NUMBER OF 0.72

The development with time of circulatory flow at a Grashof number of 10 and a Prandtl number of 0.72 can be seen in figures 4.6.1a to 4.6.1d which show the streamlines around the solid sphere as a function of time. As can be observed from figures 4.6.1a and 4.6.1d during the early stages of simulation the streamlines follow a similar pattern to those shown by the solutions obtained for lower Grashof numbers. However, as simulation continues, the stream function contours are slightly moved downstream. This is because the Grashof number in this case is larger than in the previous cases so that the ratio of the buoyancy forces to the viscous forces is larger than in the previous cases thus increasing

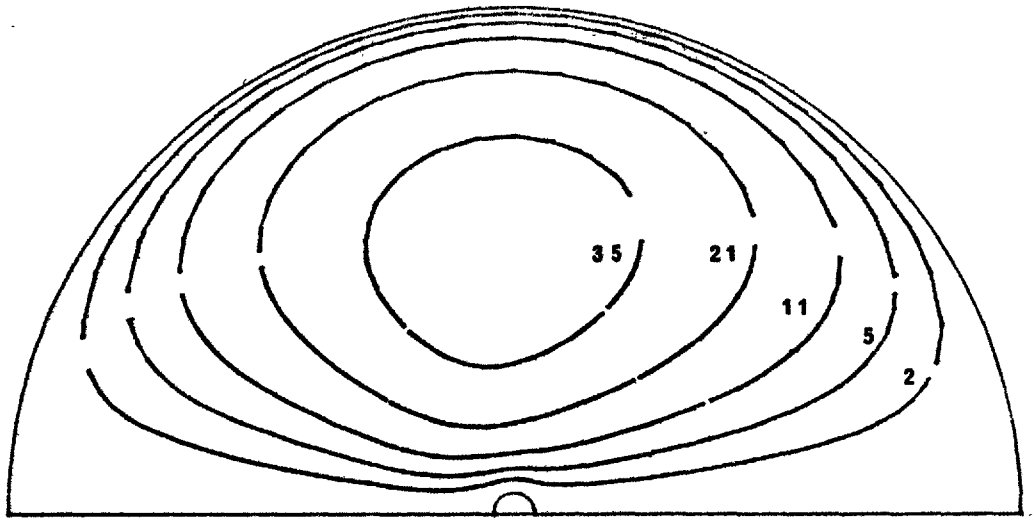

FIGURE 4.6.1b STREAMLINES AROUND THE SPHERE AT GRASHOF NUMBER OF 10 AND PRANDTL NUMBER OF 0.72 DIMENSIONLESS TIME . $t = 1.5$

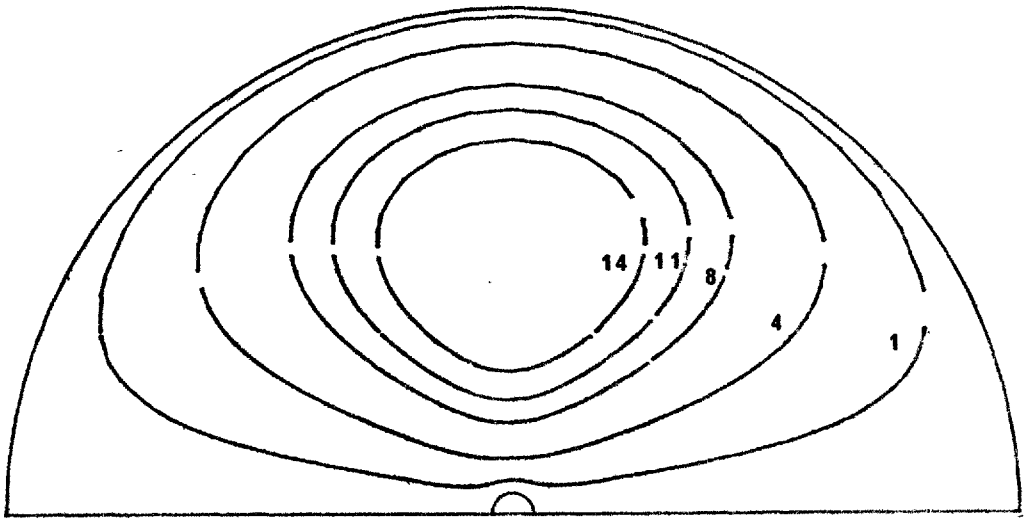

FIGURE 4.6.1a STREAMLINES AROUND THE SPHERE AT GRASHOF NUMBER OF 10 AND PRANDTL NUMBER OF 0.72 DIMENSIONLESS TIME . $t = 0.5$

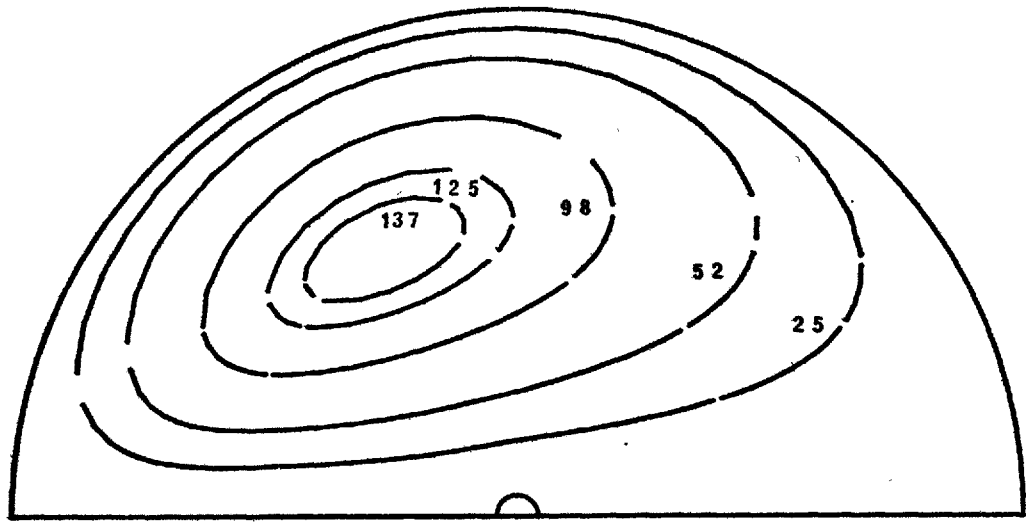

FIGURE 4.6.1d STREAMLINES AROUND THE SPHERE AT GRASHOF NUMBER OF 10 AND PRANDTL NUMBER OF 0.72 DIMENSIONLESS TIME , $t = 6$

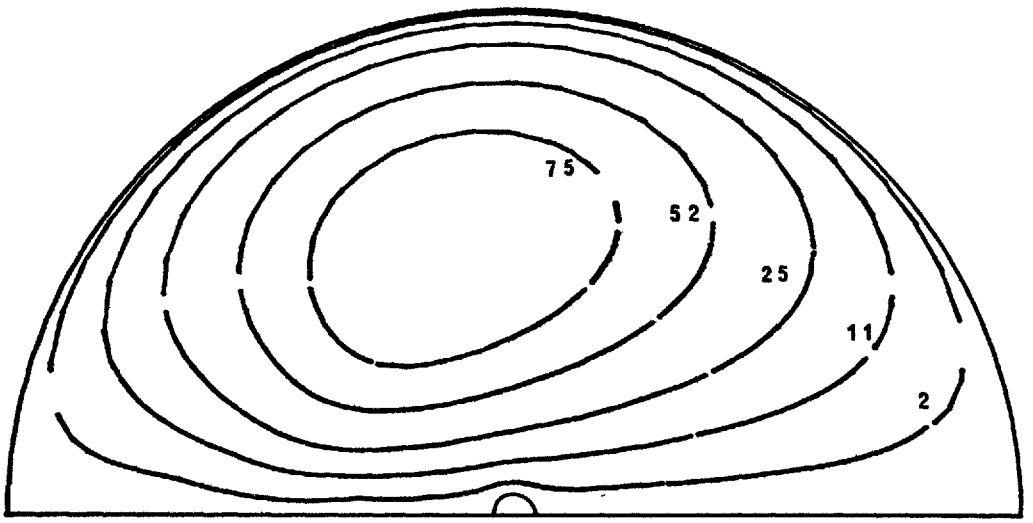

FIGURE 4.6.1c STREAMLINES AROUND THE SPHERE AT GRASHOF NUMBER OF 10 AND PRANDTL NUMBER OF 0.72 DIMENSIONLESS TIME , $t = 3.5$

effects of convection and the rate of heat transfer. As a result, the thickness of the heated layer adjacent to the upstream surface of the sphere is reduced. The increased velocity of the fluid passing the sphere causes the fluid in the immediate vicinity of the heated layer to be draged downstream so that the streamlines are shifted slightly from the upstream region to the downstream region of the flow field. This is shown in figure 4.6.1d.

Figures 4.6.2a to 4.6.2d show the development of the isotherms around the solid sphere. The steady state conduction solution was used as an initial condition for the time-dependent energy equation. During the early stages of simulation, the dominant mode of heat transfer is conduction and therefore, the influence of the heated body extends uniformly in all directions. This is shown by figure 4.6.2a. However, as integration proceeds with time, the isotherms begin to become closer to the surface of the sphere in the upstream region and to extend further from the sphere in the downstream region. The temperature distribution at the late-time steady state condition, is shown by figure 4.6.2d.

Figures 4.6.3a to 4.6.3d show the vorticity contours as a function of time around the solid sphere. The effects of convection in the solution can be seen in the vorticity distributic plots. As with the solution obtained for a Grashof number of 1, initially diffusion is the dominant

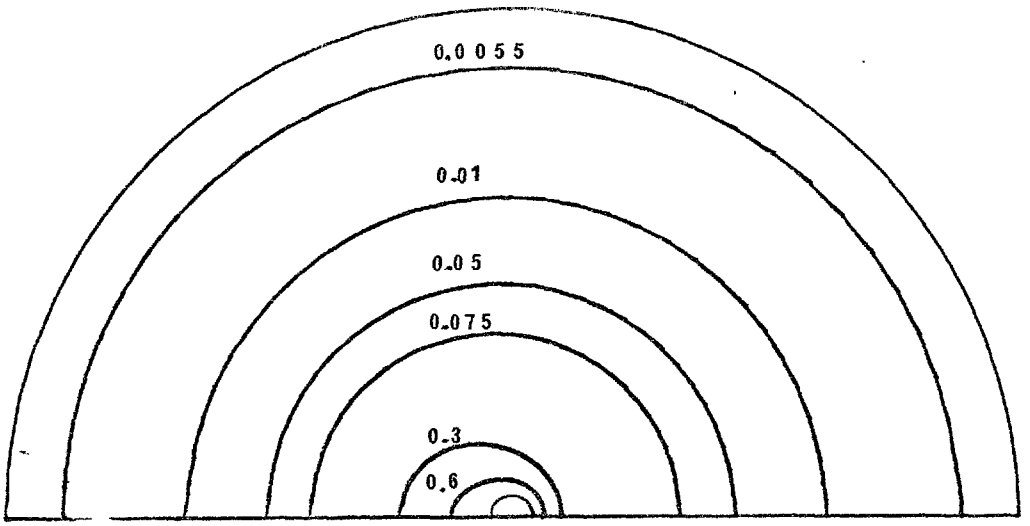

FIGURE 4.6.2b ISOTHERMS AROUND THE SPHERE AT GRASHOF NUMBER OF 10 AND PRANDTL NUMBER OF 0.72 DIMENSIONLESS TIME , $t = 1.5$

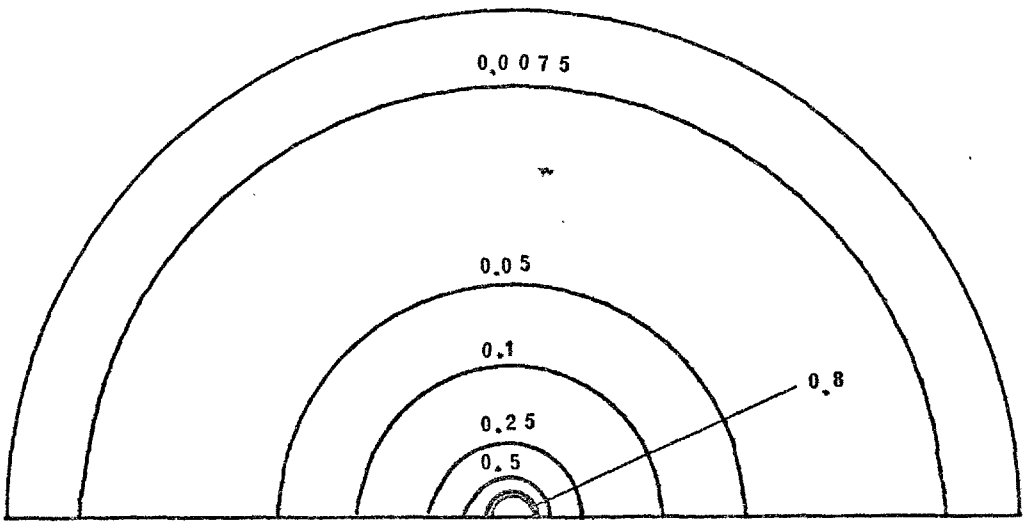

FIGURE 4.6.2a ISOTHERMS AROUND THE SPHERE AT GRASHOF NUMBER OF 10 AND PRANDTL NUMBER OF 0.72 DIMENSIONLESS TIME , $t = 0.5$

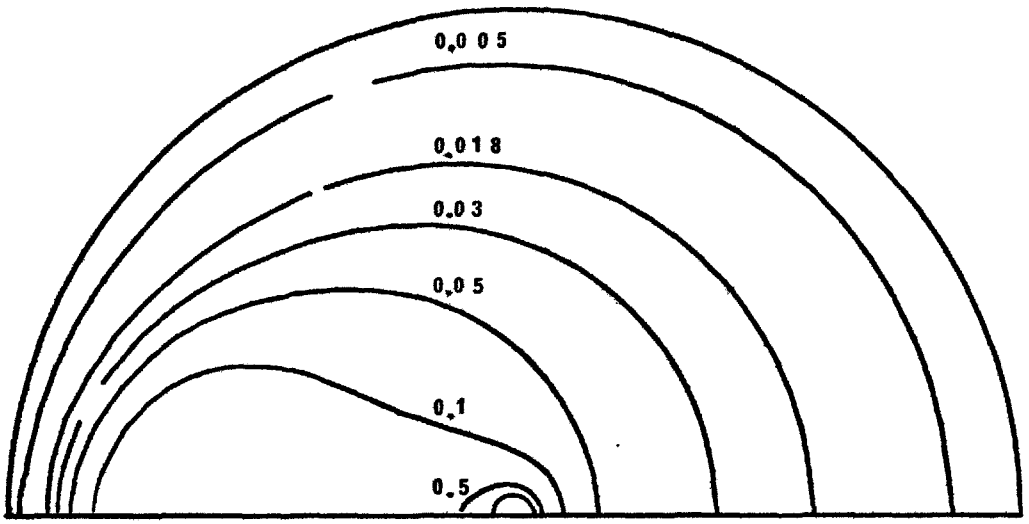

FIGURE 4.6.2d ISOTHERMS AROUND THE SPHERE AT GRASHOF NUMBER OF 10 AND PRANDTL NUMBER OF 0.72 DIMENSIONLESS TIME . t = 6

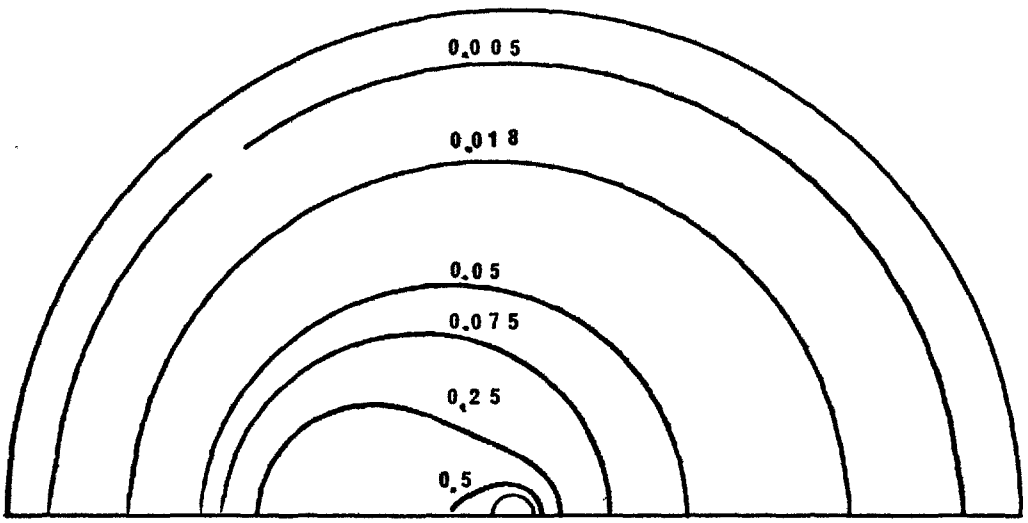

FIGURE 4.6.2c ISOTHERMS AROUND THE SPHERE AT GRASHOF NUMBER OF 10 AND PRANDTL NUMBER OF 0.72 DIMENSIONLESS TIME . t =3.5

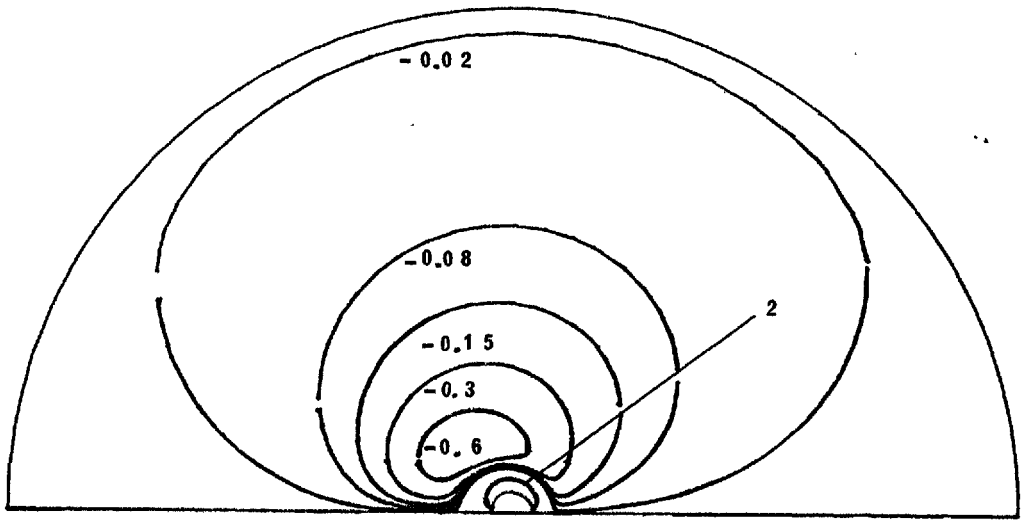

FIGURE 4.6.3b VORTICITY DISTRIBUTION AROUND THE SPHERE AT GRASHOF NUMBER OF 10 AND PRANDTL NUMBER OF 0.72 DIMENSIONLESS TIME , $t = 1.5$

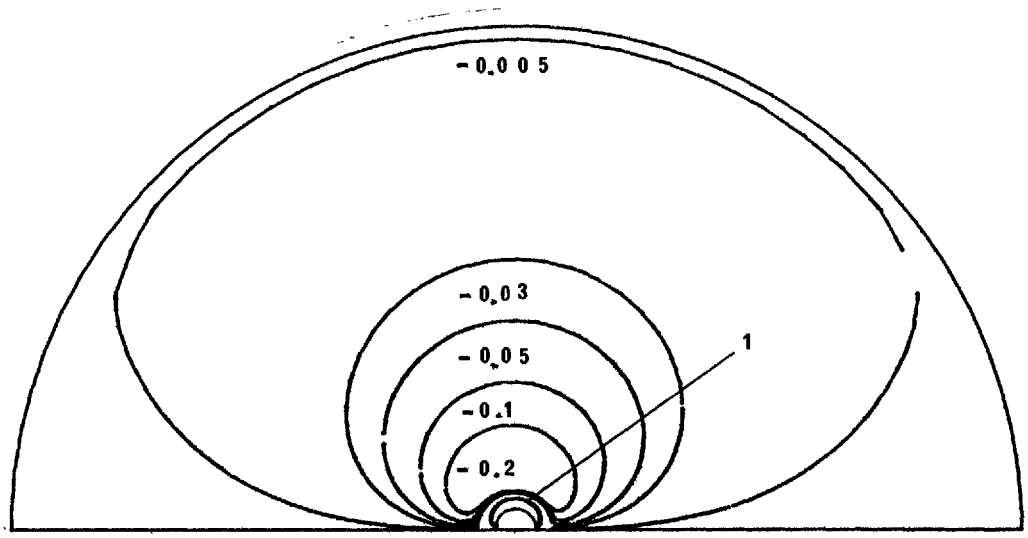

FIGURE 4.6.3a VORTICITY DISTRIBUTION AROUND THE SPHERE AT GRASHOF NUMBER OF 10 AND PRANDTL NUMBER OF 0.72 DIMENSIONLESS TIME , $t = 0.5$

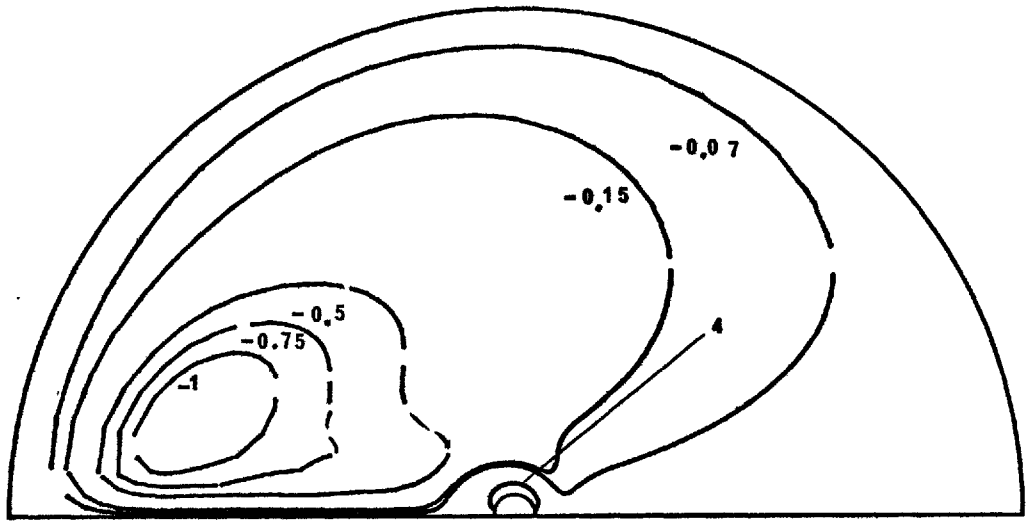

FIGURE 4.6.3d VORTICITY DISTRIBUTION AROUND THE SPHERE AT GRASHOF NUMBER OF 10 AND PRANDTL NUMBER OF 0.72 DIMENSIONLESS TIME , $t = 6$

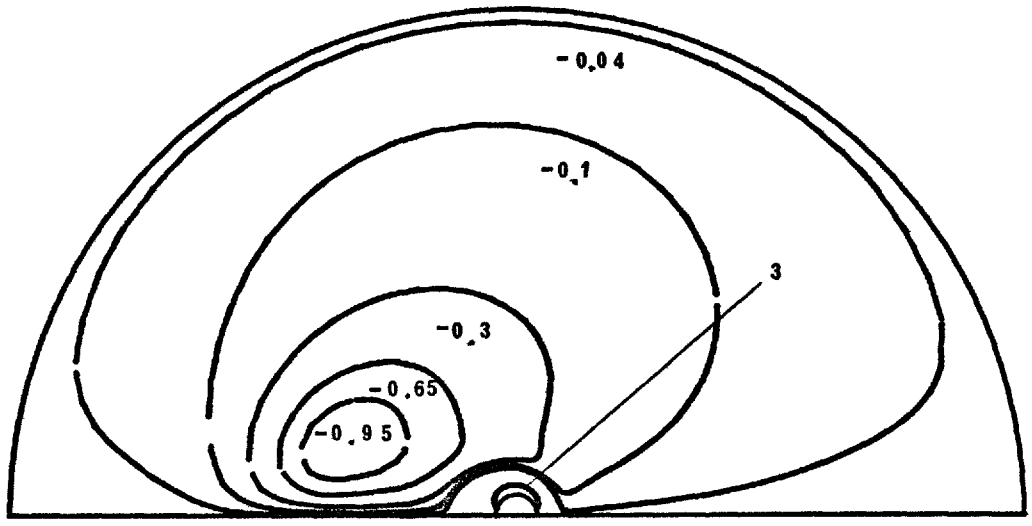

FIGURE 4.6.3c VORTICITY DISTRIBUTION AROUND THE SPHERE AT GRASHOF NUMBER OF 10 AND PRANDTL NUMBER OF 0.72 DIMENSIONLESS TIME , $t = 3.5$

mode of vorticity transport, as shown by figure 4.6.3a. However, after a dimensionless time, t, of about unity the effects of convection begin to distort the contours, as shown by figures 4.6.3b and 4.6.3c. The late-time steady state vorticity distribution obtained at a dimensionless time, t, of 6 is shown in figure 4.6.3d. As expected, the figure shows that the effects of convection on the vorticity contours are more pronounced than those shown by the solution obtained for a Grashof number of 1.

Figure 4.6.5 shows the variation of the local Nusselt number with time. The local Nusselt number around the solid sphere remains fairly constant during the early stages of heat transfer. However, as the convective effects increase in magnitude the local Nusselt numbers around the upstream region of the solid sphere increase until their late-time steady state values are attained. During the same period, the local Nusselt numbers around the downstream region of the sphere decrease at first but then increase as the late-time steady state condition is approached.

The behaviour of the drag coefficients with dimensionless time, t, is shown in figure 4.6.4. Initially, both the form drag coefficient, C_{DP}, and the viscous drag coefficient, C_{DF}, show the same behaviour as those discussed for Grashof numbers of 0.05 and 1. But, in the present case, the drag coefficients reach their late-time steady state values at a dimensionless time of 4. However, as can be seen from

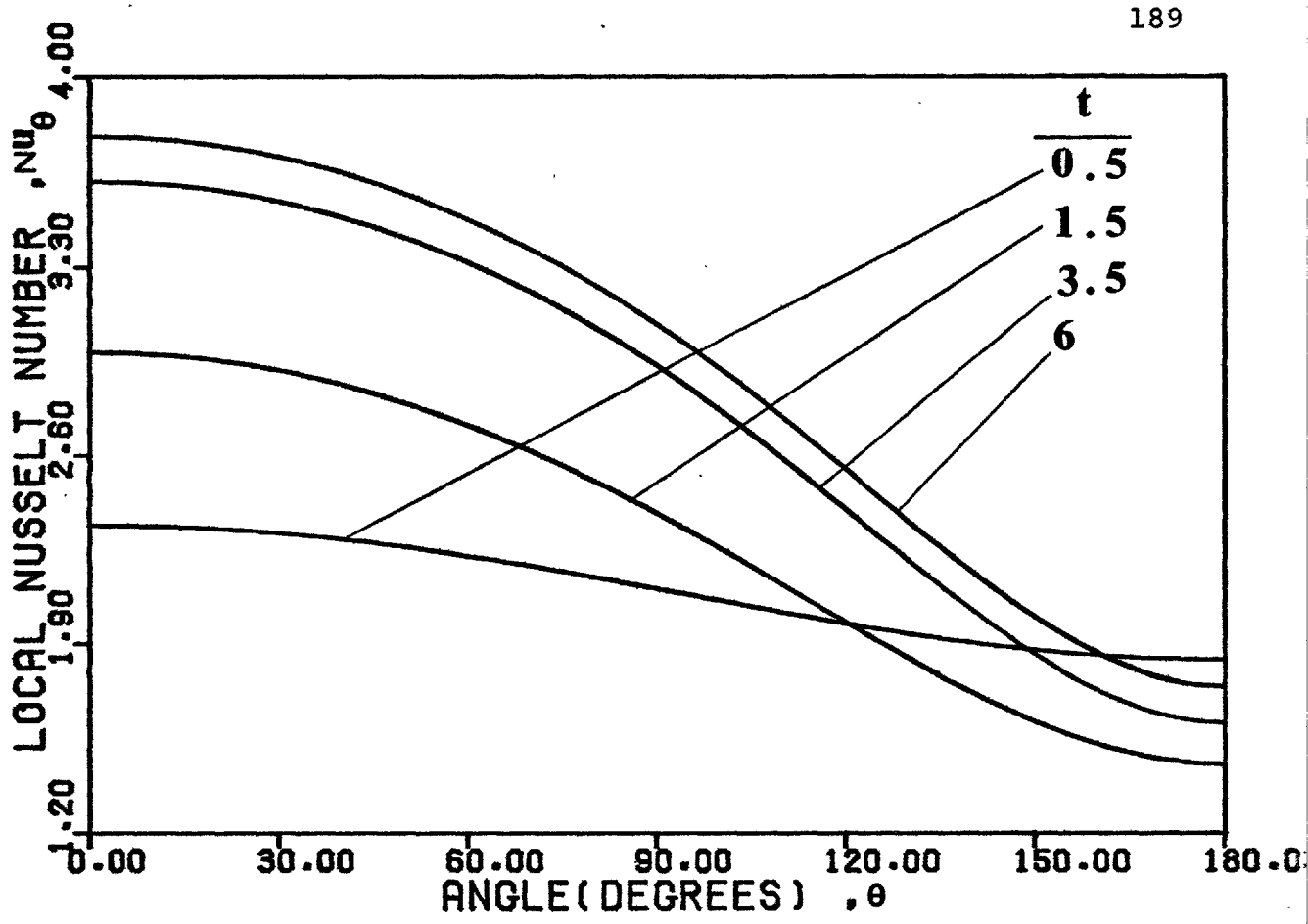

FIGURE 4.6.5 LOCAL NUSSELT NUMBER VERSUS TIME AT GRASHOF NUMBER OF 10 AND PRANDTL NUMBER OF 0.72

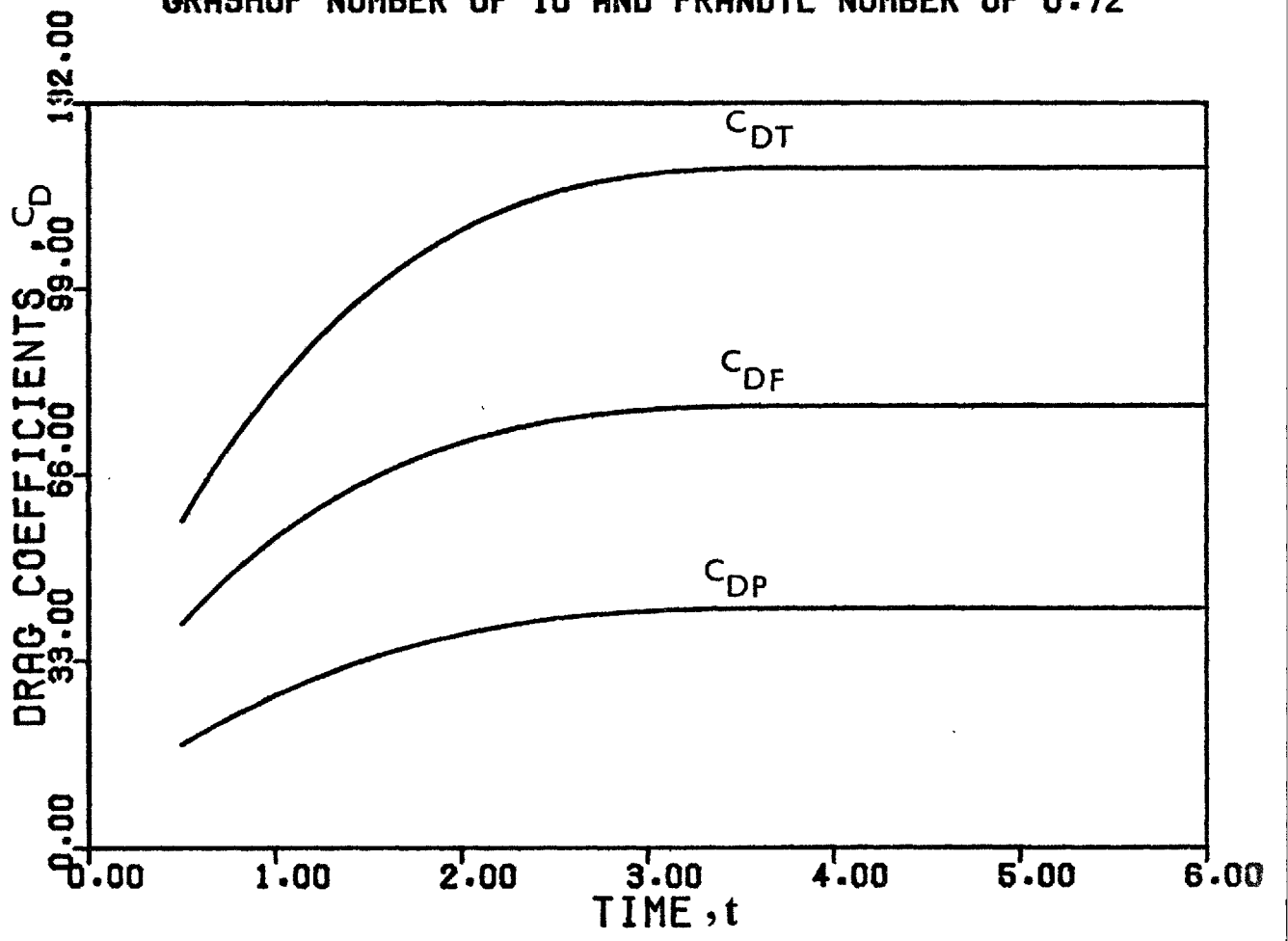

FIGURE 4.6.4 DRAG COEFFICIENTS VERSUS TIME AT GRASHOF NUMBER OF 10 AND PRANDTL NUMBER OF 0.72

table 9, the simulation had to be continued to a longer time since small changes in the local Nusselt number, the surface vorticity, and the surface pressure still continued to occur during the dimensionless time period of 4 to 6.

Figure 4.6.7 shows the behaviour of the surface vorticity with time. The variation of the surface vorticity with time follows a similar pattern to that shown by the solution obtained for a Grashof number of 1 in that the surface vorticity for all time, t, is almost symmetrically distributed about an imaginary plane placed between the upstream and downstream regions of the flow field. This shows that at a Grashof number of 10, the dominant mode of vorticity transport close to the surface is diffusion.

The variation with time of the surface pressure is shown in figure 4.6.6. From this figure one observes that as simulation continues, the dimensionless surface pressure over the upstream region of the sphere increases slowly towards its late-time steady state value. While the dimensionless surface pressure over the downstream region of the sphere continues to decrease until the late-time steady state condition is reached.

The average Nusselt number starts from a value of 2.085 because of the conduction initial condition used and increases continuously towards its late-time steady state value which is found to be 2.92. This can be seen from figure 4.6.8.

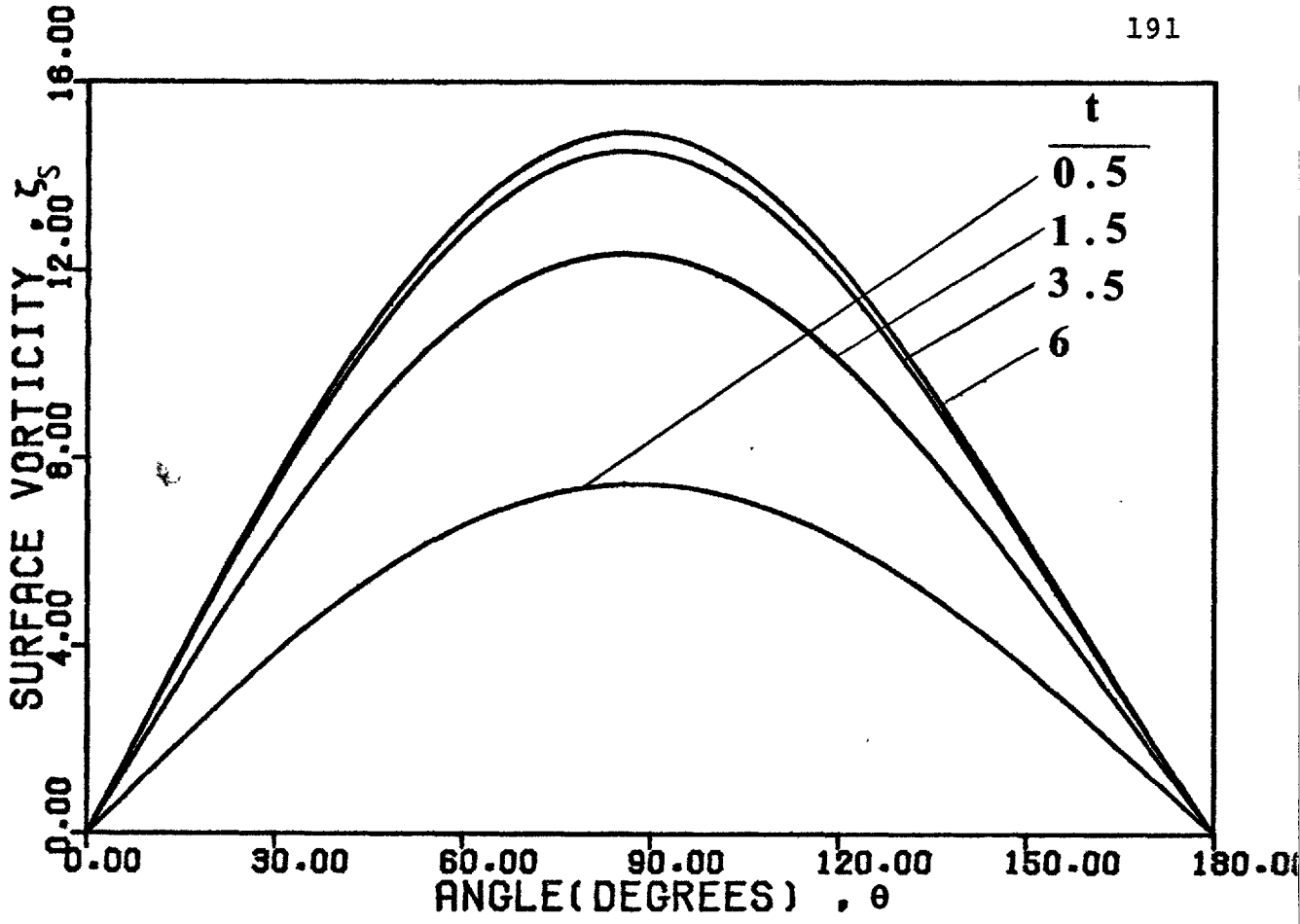

FIGURE 4.6.7 SURFACE VORTICITY VERSUS TIME AT GRASHOF NUMBER OF 10 AND PRANDTL NUMBER OF 0.72

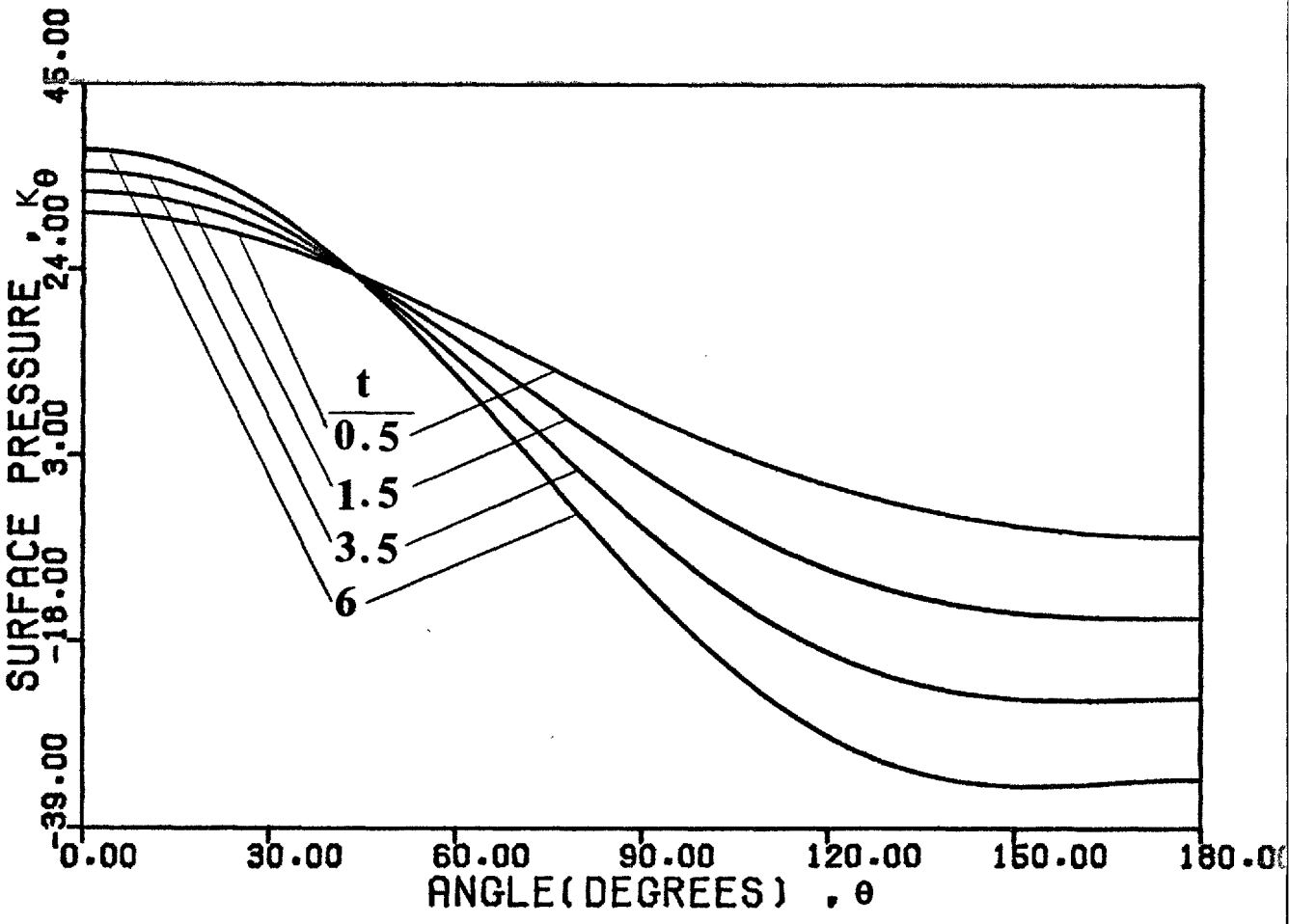

FIGURE 4.6.6 SURFACE PRESSURE VERSUS TIME AT GRASHOF NUMBER OF 10 AND PRANDTL NUMBER OF 0.72

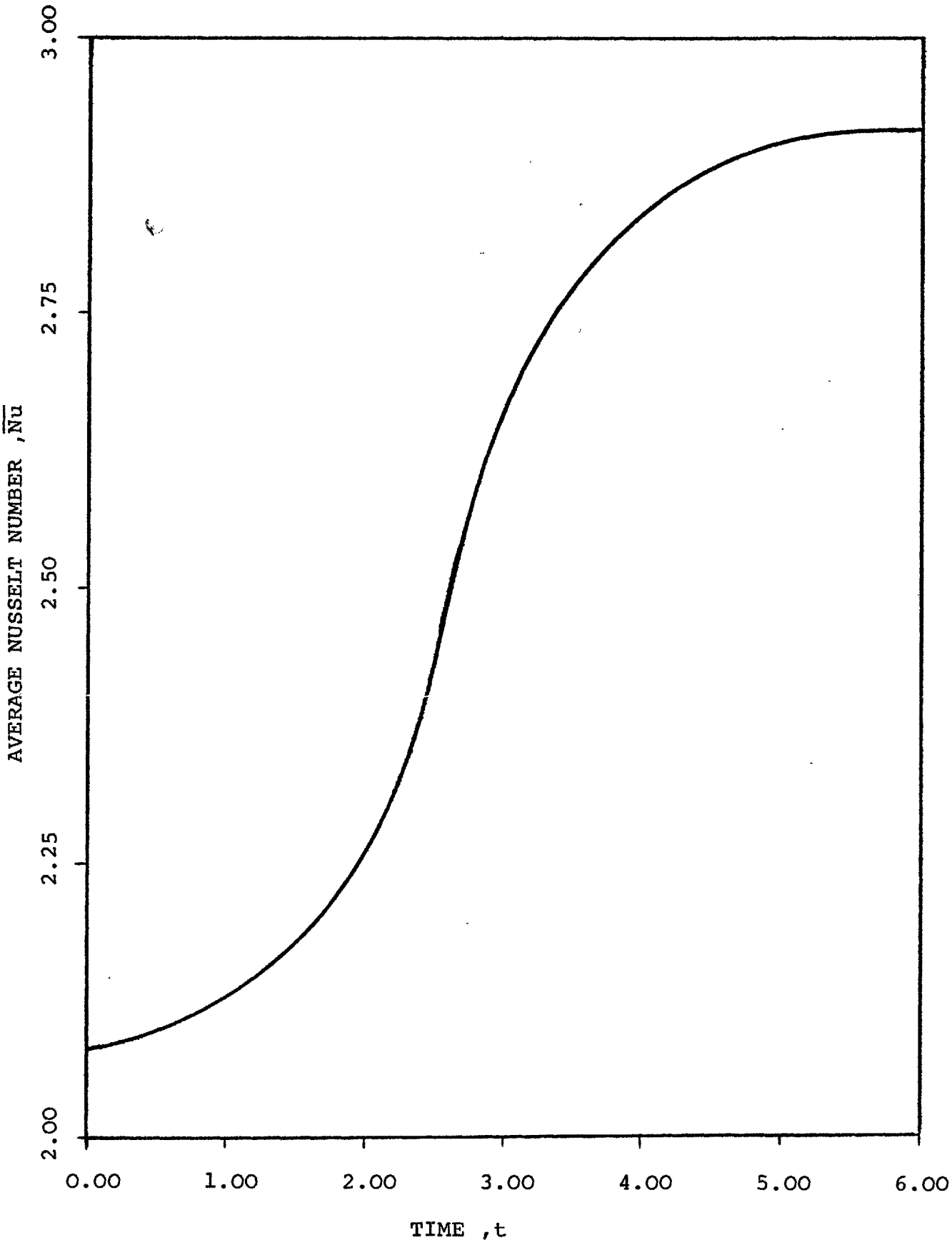

FIGURE 4.6.8 AVERAGE NUSSELT NUMBER VERSUS TIME AT GRASHOF NUMBER OF 10 AND PRANDTL NUMBER OF 0.72

Table 3 shows a comparison of the late-time steady state average Nusselt numbers obtained in the present work with the experimental measurements of the other workers. As can be seen the maximum discrepancy between the value of the average Nusselt number for the present case and other results for a Grashof number of 10 is about 12%. Table 2 shows the main results obtained from the numerical solutions of the time-independent equations. It is seen from tables 1 and 2 that the results calculated from the time-dependent and the time-independent solutions, for the present case, are in reasonable agreement.

It was decided to study the influence of mesh sizes and location of the outer boundary on the results. However, since these kinds of numerical experiments are expensive from a computational point of view, the simulation was carried out until the flow field was developed sufficiently for comparison purposes but not until late-time steady state condition was reached. The influence of the location of the outer boundary and mesh sizes on the results can be judged from table 4. It was generally observed that for a Grashof number of 10 and a Prandtl number of 0.72; for a specified location of the outer boundary, the use of coarser mesh sizes gives rise to smaller values of the flow characteristics than when fine meshes are used. Also, coarser mesh sizes were found to cause vorticity fluctuation close to the outer boundary. A reduction in the radius of the outer boundary,

was found to lead to the prediction of slightly smaller values for the flow characteristics such as the average Nusselt number, front stagnation pressure and drag coefficients.

The final choice of mesh sizes and location of the outer boundary, presented in table 1, was a compromise between computing economy and accuracy of results.

4.7 NUMERICAL SOLUTION FOR A GRASHOF NUMBER OF 25 AND A PRANDTL NUMBER OF 0.72

The simulation of the flow field starting from a motionless flow field around a solid sphere in conditions of free convection at a Grashof number of 25 and a Prandtl number of 0.72 can be seen in figures 4.7.1a to 4.7.1d which show the streamlines as a function of time. From these figures one observes that the stream function contours show a similar pattern to that discussed for a Grashof number of 10. Figure 4.6.1d shows that the streamlines at the late-time steady state conditions are displaced slightly in the downstream direction.

Table 10 represents the late-time values of the local Nusselt number, the surface vorticity, and the surface pressure. From this table one observes that these variables become relatively independent of time during the dimensionless time period of 1.5 to 2.16.

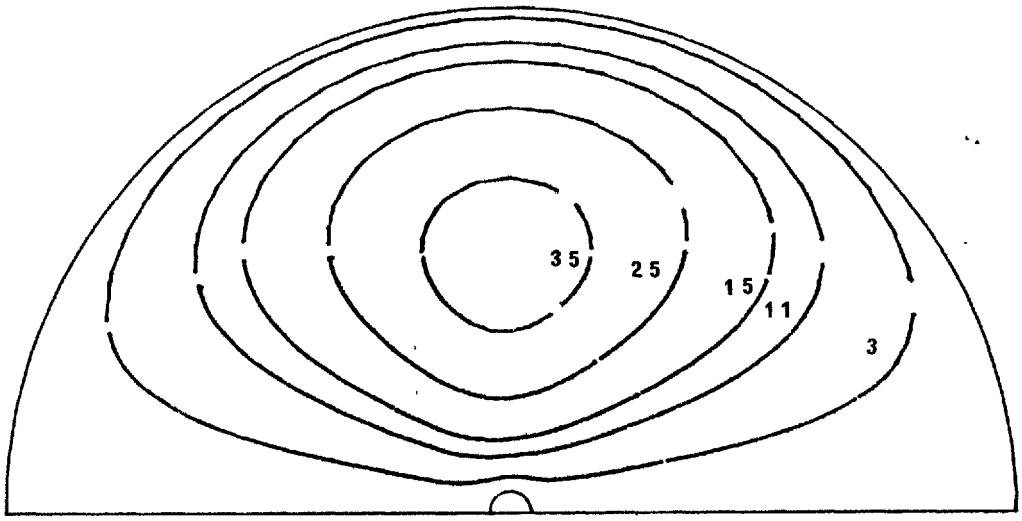

FIGURE 4.7.1b STREAMLINES AROUND THE SPHERE AT GRASHOF NUMBER OF 25 AND PRANDTL NUMBER OF 0.72 DIMENSIONLESS TIME , $t = 0.5$

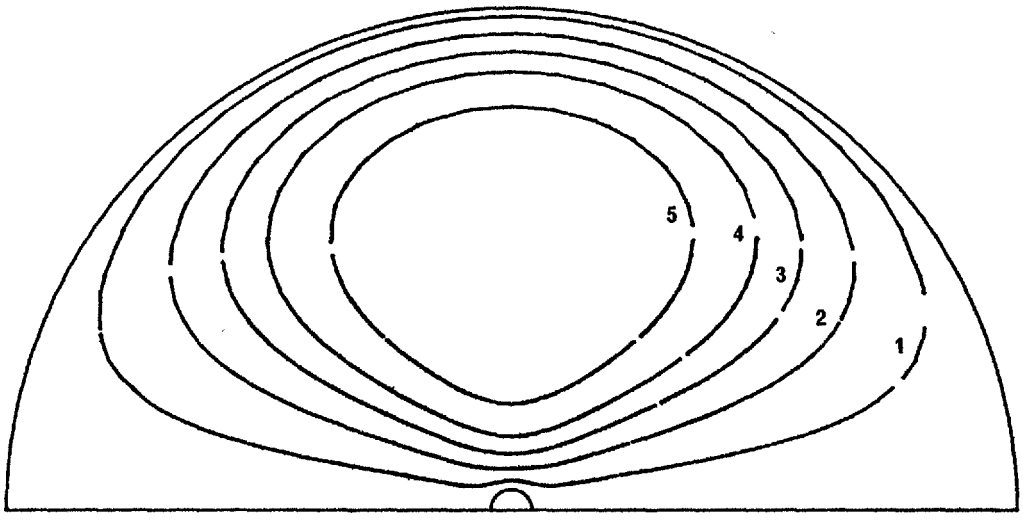

FIGURE 4.7.1a STREAMLINES AROUND THE SPHERE AT GRASHOF NUMBER OF 25 AND PRANDTL NUMBER OF 0.72 DIMENSIONLESS TIME , $t = 0.1$

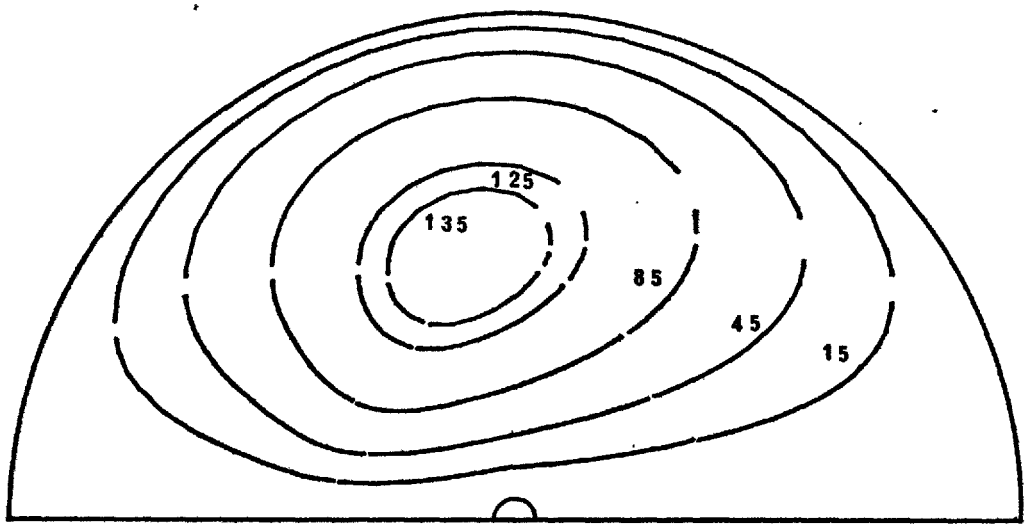

FIGURE 4.7.1d STREAMLINES AROUND THE SPHERE AT GRASHOF NUMBER OF 25 AND PRANDTL NUMBER OF 0.72 DIMENSIONLESS TIME , $t = 2.16$

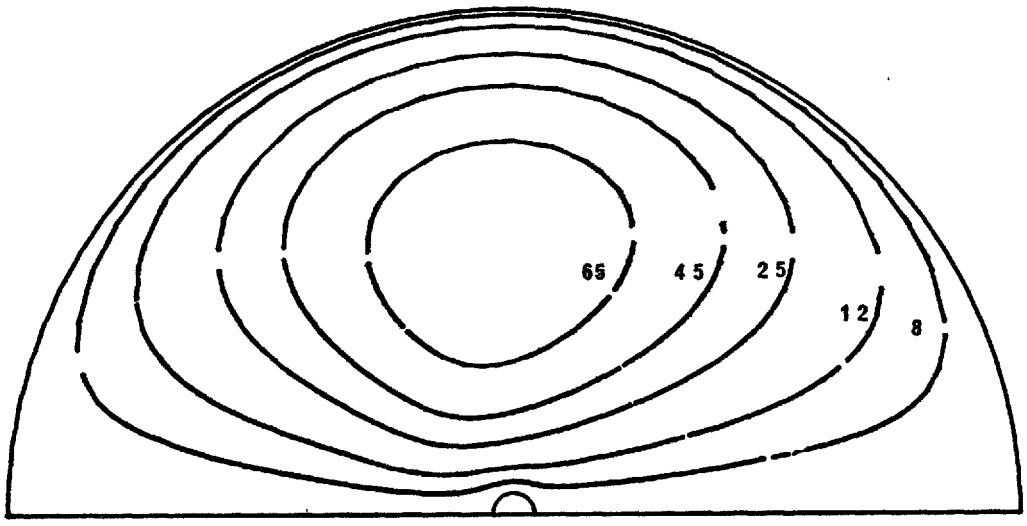

FIGURE 4.7.1c STREAMLINES AROUND THE SPHERE AT GRASHOF NUMBER OF 25 AND PRANDTL NUMBER OF 0.72 DIMENSIONLESS TIME , $t = 1$

The distributions of isotherms around the solid sphere for various dimensionless times, t, are shown in figures 4.7.1a to 4.7.1d. During the early stages of flow development, the thickness of the heated region around the solid sphere is almost uniform and heat transfer takes place mainly by unsteady state conduction. However, at a dimensionless time of approximately 0.5, the heated layer of the fluid in contact with the upstream region of the solid sphere starts to shrink while the heated layer over the downstream region continues to expand. Figure 4.7.2d shows the isotherms around the sphere at the late-time steady state condition.

The generation and development with time of vorticity around the solid sphere can be seen in figures 4.7.3a to 4.7.3d which show the vorticity distribution as a function of time. During the early stages of simulation, the vorticity contours, as shown in figure 4.7.3a, are almsot symmetrically distributed about an imaginary plane placed between the upstream and downstream of the flow field. However, as integration proceeds with time, the effects of convection on the distribution of vorticity become more important than the effects of diffusion. As the simulation continues, vorticity is convected more and more downstream. This can be seen in figures 4.7.3c and 4.7.3d.

The behaviour of the drag coefficients with time is shown in figure 4.7.4. Both the form drag coefficient and

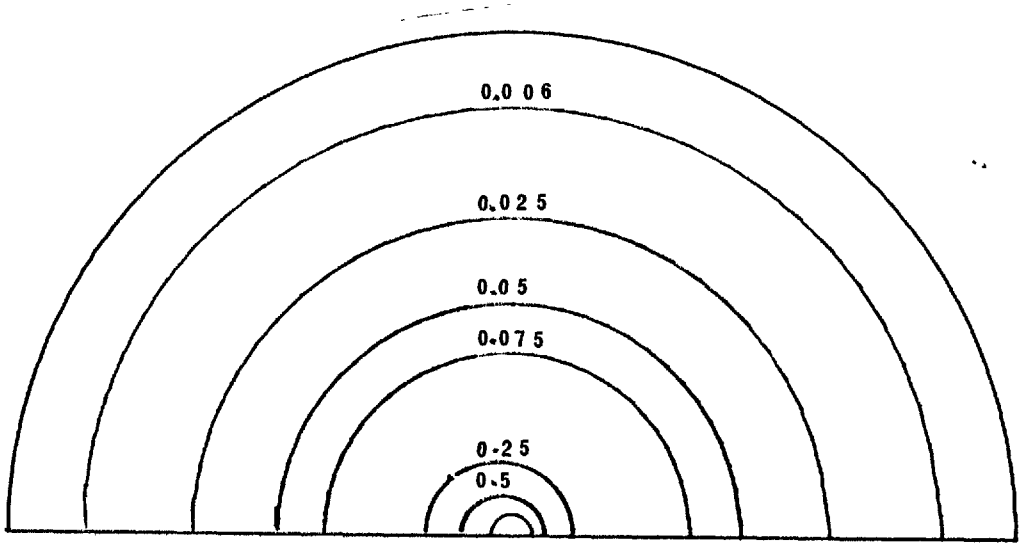

FIGURE 4.7.2b ISOTHERMS AROUND THE SPHERE AT GRASHOF NUMBER OF 25 AND PRANDTL NUMBER OF 0.72 DIMENSIONLESS TIME , $t = 0.5$

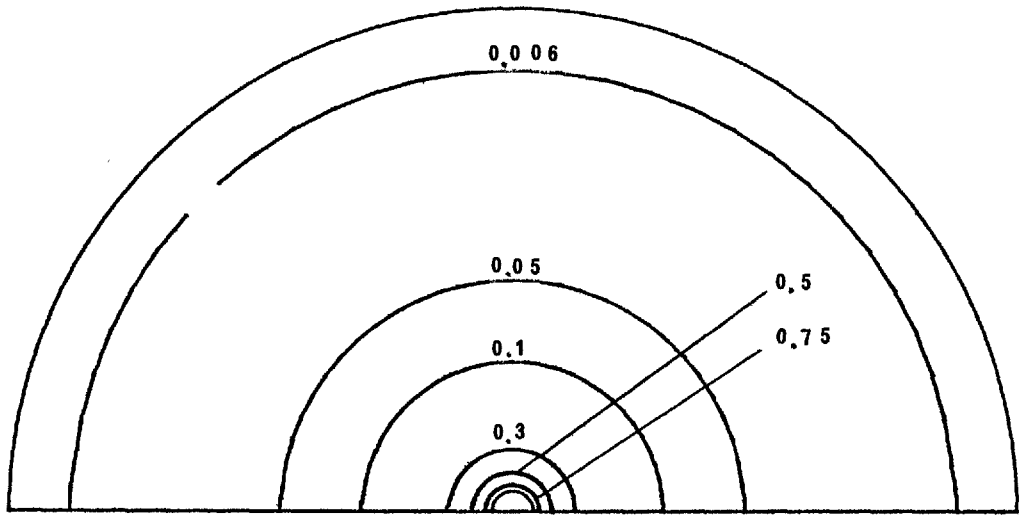

FIGURE 4.7.2a ISOTHERMS AROUND THE SPHERE AT GRASHOF NUMBER OF 25 AND PRANDTL NUMBER OF 0.72 DIMENSIONLESS TIME , $t = 0.1$

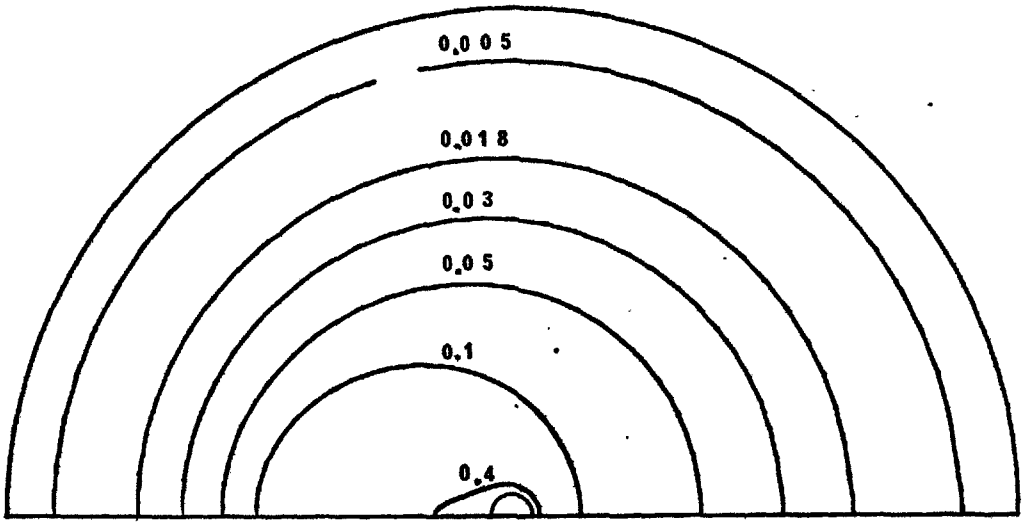

FIGURE 4.7.2d ISOTHERMS AROUND THE SPHERE AT GRASHOF NUMBER OF 25 AND PRANDTL NUMBER OF 0.72 DIMENSIONLESS TIME . t =2.16

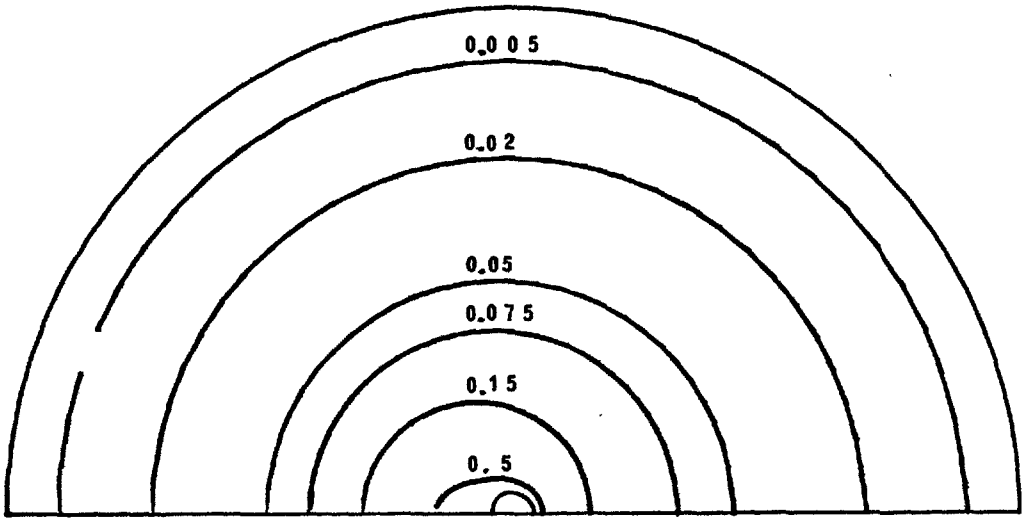

FIGURE 4.7.2c ISOTHERMS AROUND THE SPHERE AT GRASHOF NUMBER OF 25 AND PRANDTL NUMBER OF 0.72 DIMENSIONLESS TIME . t =1

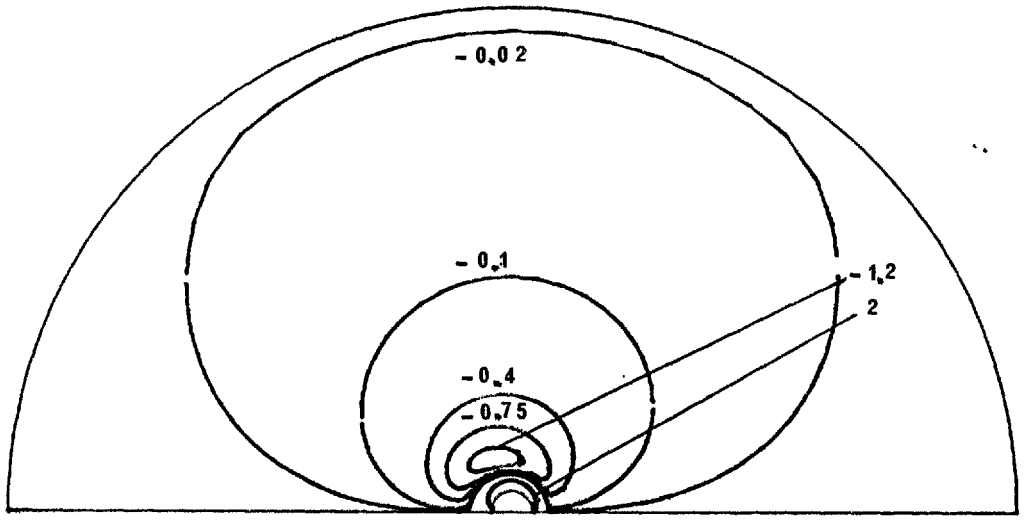

FIGURE 4 .7.3b VORTICITY DISTRIBUTION AROUND THE SPHERE AT GRASHOF NUMBER OF 25 AND PRANDTL NUMBER OF 0.72 DIMENSIONLESS TIME , $t = 0.5$

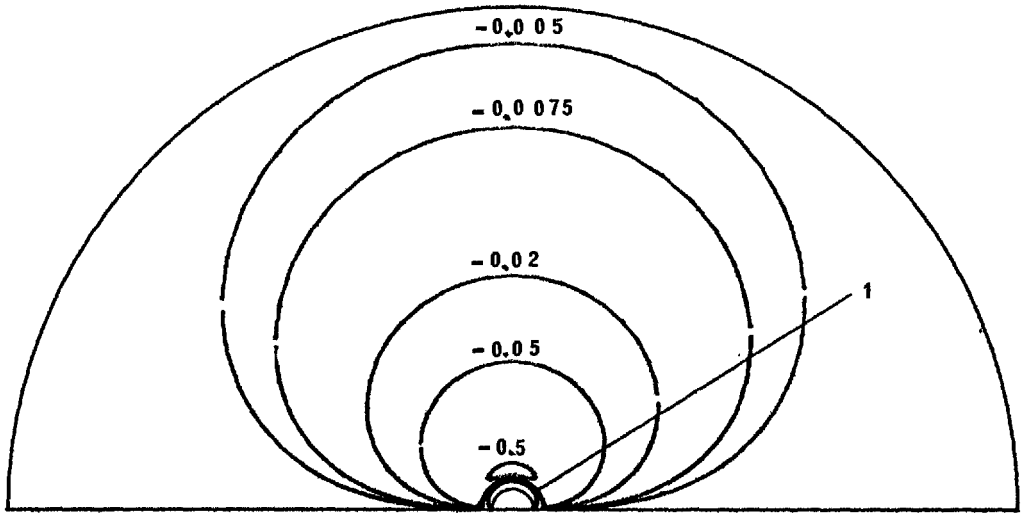

FIGURE 4 .7.3a VORTICITY DISTRIBUTION AROUND THE SPHERE AT GRASHOF NUMBER OF 25 AND PRANDTL NUMBER OF 0.72 DIMENSIONLESS TIME , $t = 0.1$

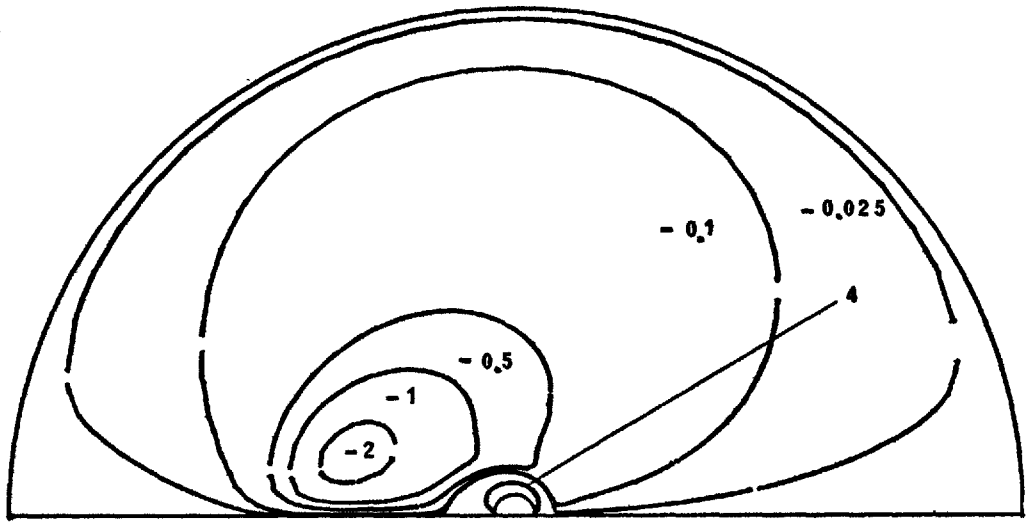

FIGURE 4.7.3d VORTICITY DISTRIBUTION AROUND THE SPHERE AT GRASHOF NUMBER OF 25 AND PRANDTL NUMBER OF 0.72 DIMENSIONLESS TIME , $t = 2.16$

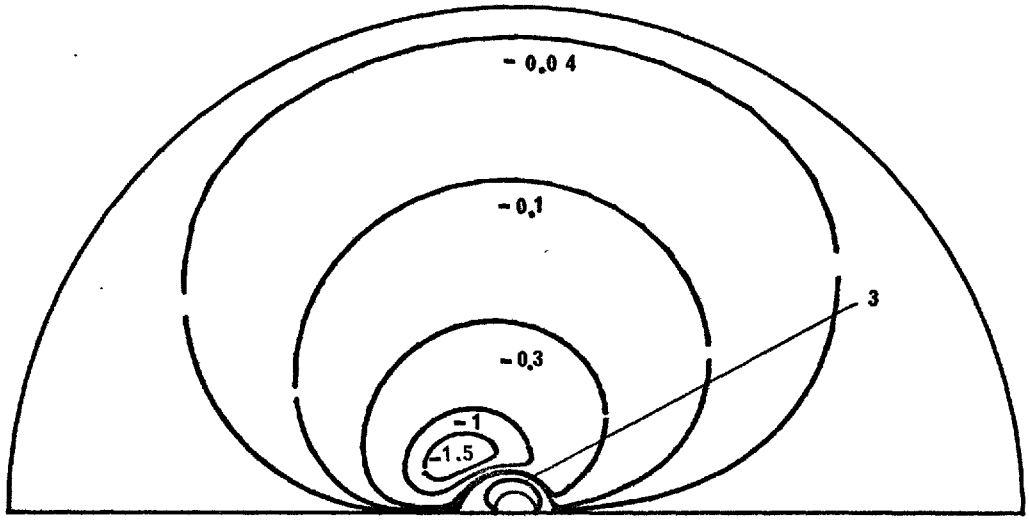

FIGURE 4.7.3c VORTICITY DISTRIBUTION AROUND THE SPHERE AT GRASHOF NUMBER OF 25 AND PRANDTL NUMBER OF 0.72 DIMENSIONLESS TIME , $t = 1$

the viscous drag coefficient follow the same pattern as shown previously by the solutions obtained at lower Grashof numbers. As can be seen from tables 1 and 2 the late-time steady state values of the drag coefficients obtained from the present study for a Grashof number of 25 and a Prandtl number of 0.72 are in reasonable agreement with the drag coefficients obtained from the numerical solution of the time-independent problem. The other quantities shown in these tables, for the present case, are also in reasonable agreement.

Figure 4.7.5 shows the variations of the local Nusselt number with time. Since steady state conduction is used as the initial condition, the local Nusselt number starts from a value of 2.085 which is constant around the solid sphere. However, as integration proceeds with time, the convective effects increase so that the local Nusselt numbers over the upstream region of the sphere increase continuously towards their late-time steady state values while the local Nusselt numbers over the rear part of the sphere first decrease and then increase towards their late-time steady state values.

The average Nusselt number starts from a value of 2.085 and increases continuously towards its late-time steady state value. This is shown in figure 4.7.8 which shows the variation of the average Nusselt number with dimensionless time.

The variation with time of the surface vorticity is shown in figure 4.7.7. From this figure it can be observed

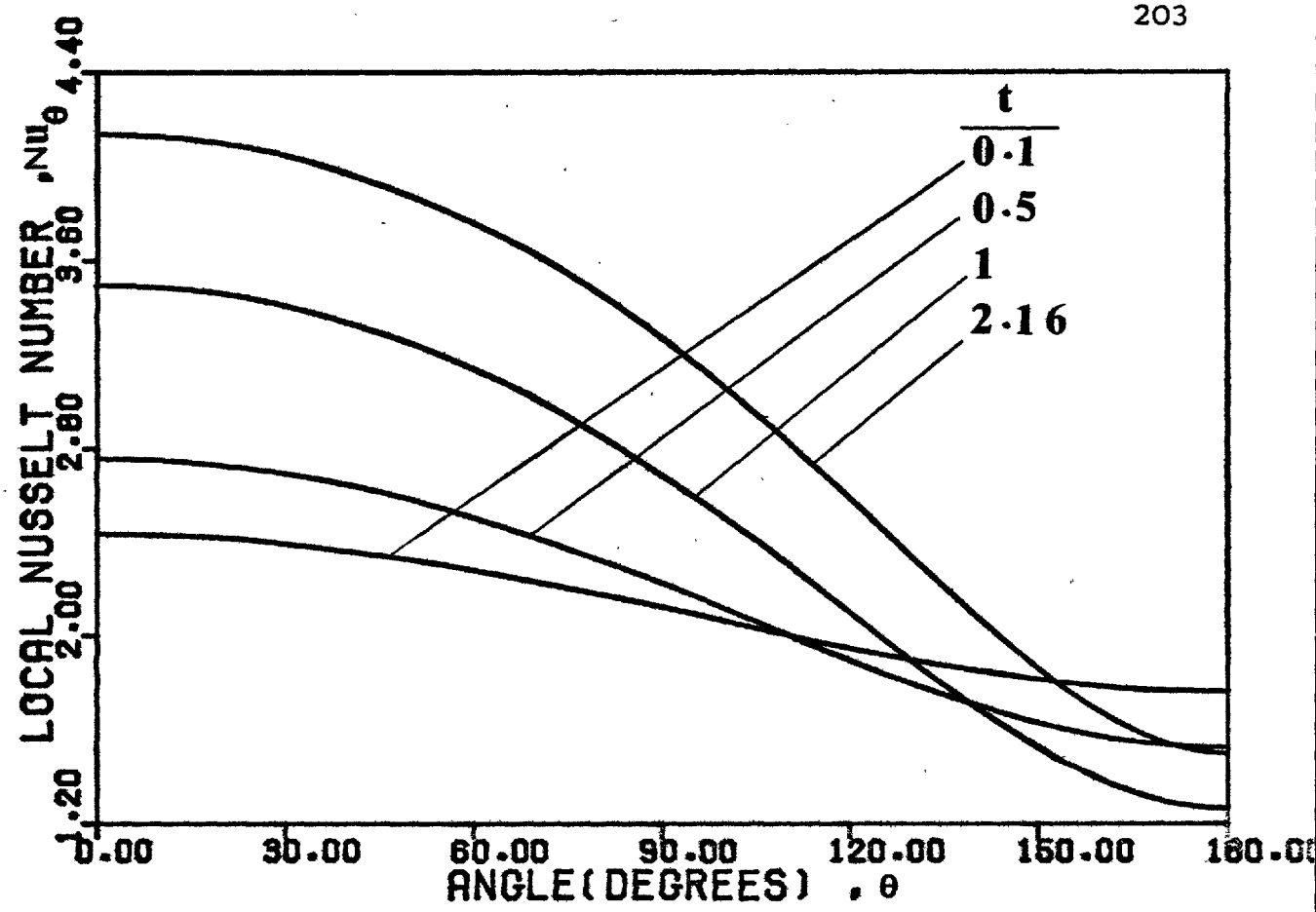

FIGURE 4.7.5 LOCAL NUSSELT NUMBER VERSUS TIME AT GRASHOF NUMBER OF 25 AND PRANDTL NUMBER OF 0.72

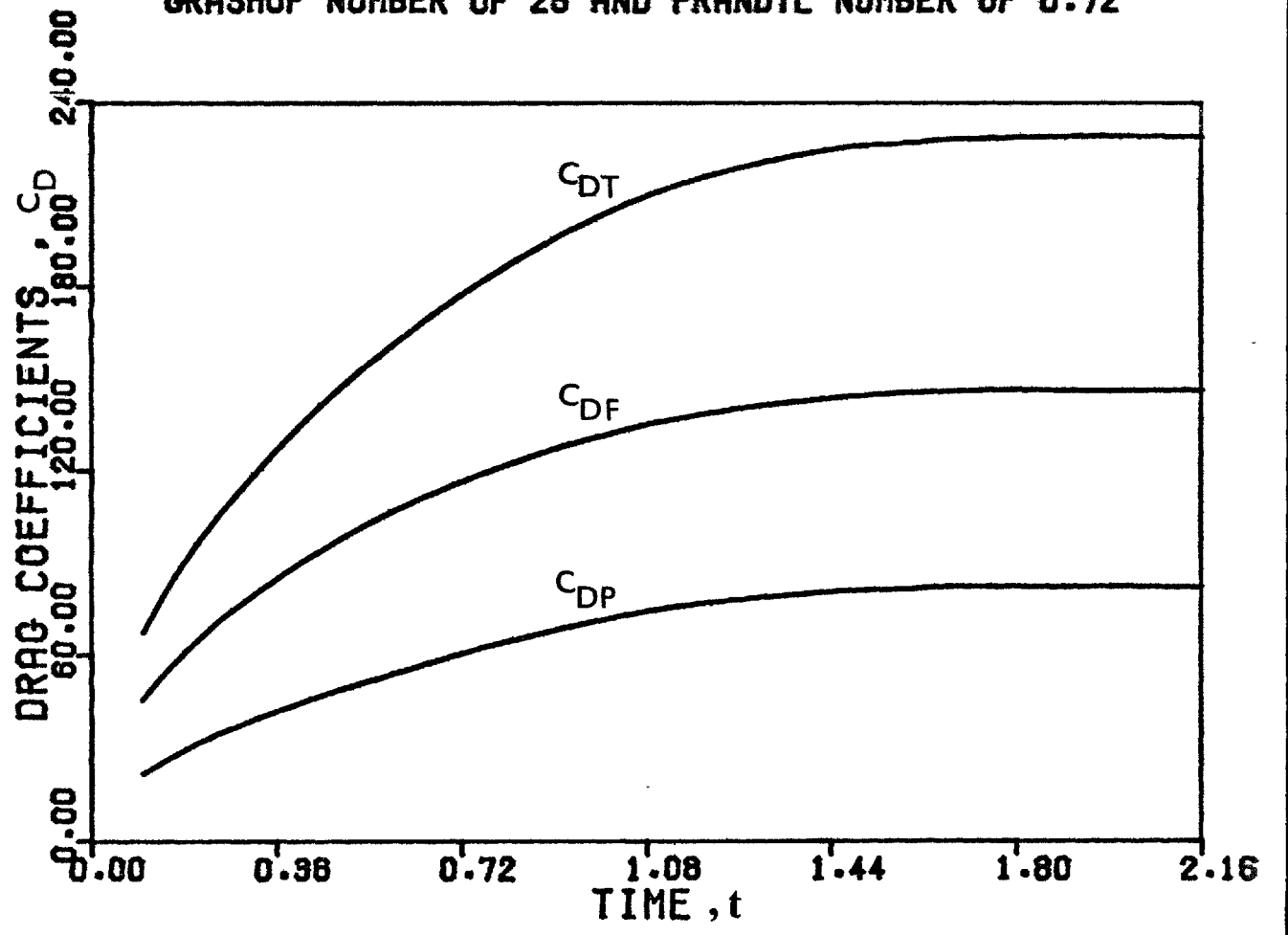

FIGURE 4.7.4 DRAG COEFFICIENTS VERSUS TIME AT GRASHOF NUMBER OF 25 AND PRANDTL NUMBER OF 0.72

that the surface vorticity values are initially small and almsot symmetrically distributed about an imaginary plane situated between the upstream and the downstream regions of the flow field. As simulation proceeds, the surface vorticity values increase but the symmetry of the distribution remains almost unchanged. This shows that at a Grashof number of 25 and a Prandtl number of 0.72, the dominant mode of vorticity transport very close to the surface is diffusion. However, as one moves away from the surface the dominant mode of vorticity transport changes from diffusion to convection.

The variation with time of the dimensionless surface pressure is shown in figure 4.7.6. Initially, the dimentionless surface pressure shows the same behaviour as that discussed for lower Grashof numbers in the previous sections. However, the late-time steady state surface pressure shows a shallow minimum at an angle of 145 degrees. The late-time surface pressure distributions obtained for lower Grashof numbers did not exhibit such a minimum.

The influence of the location of the outer boundary on the average Nusselt number, on the drag coefficients, and on the stagnation pressures can be judged from table 5. It can be seen that a reduction in the radius of the outer boundary from 24.53 to 20.08 sphere radii results in a reduction in the average Nusselt number of 6% and a reduction in the total drag coefficient of about 5%. Thus, as stated previously, the position of the outer boundary does affect

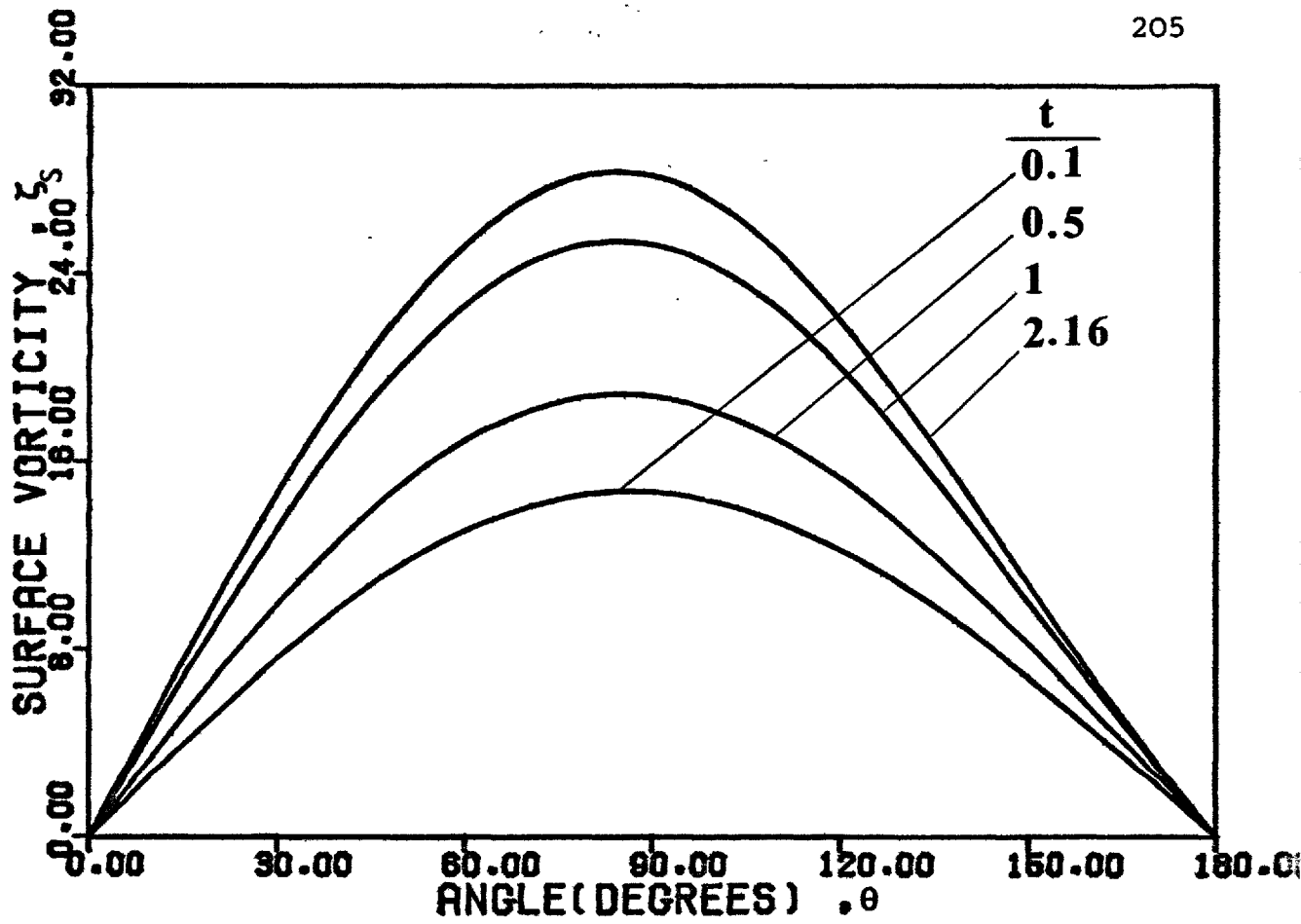

FIGURE 4.7.7 SURFACE VORTICITY VERSUS TIME AT GRASHOF NUMBER OF 25 AND PRANDTL NUMBER OF 0.72

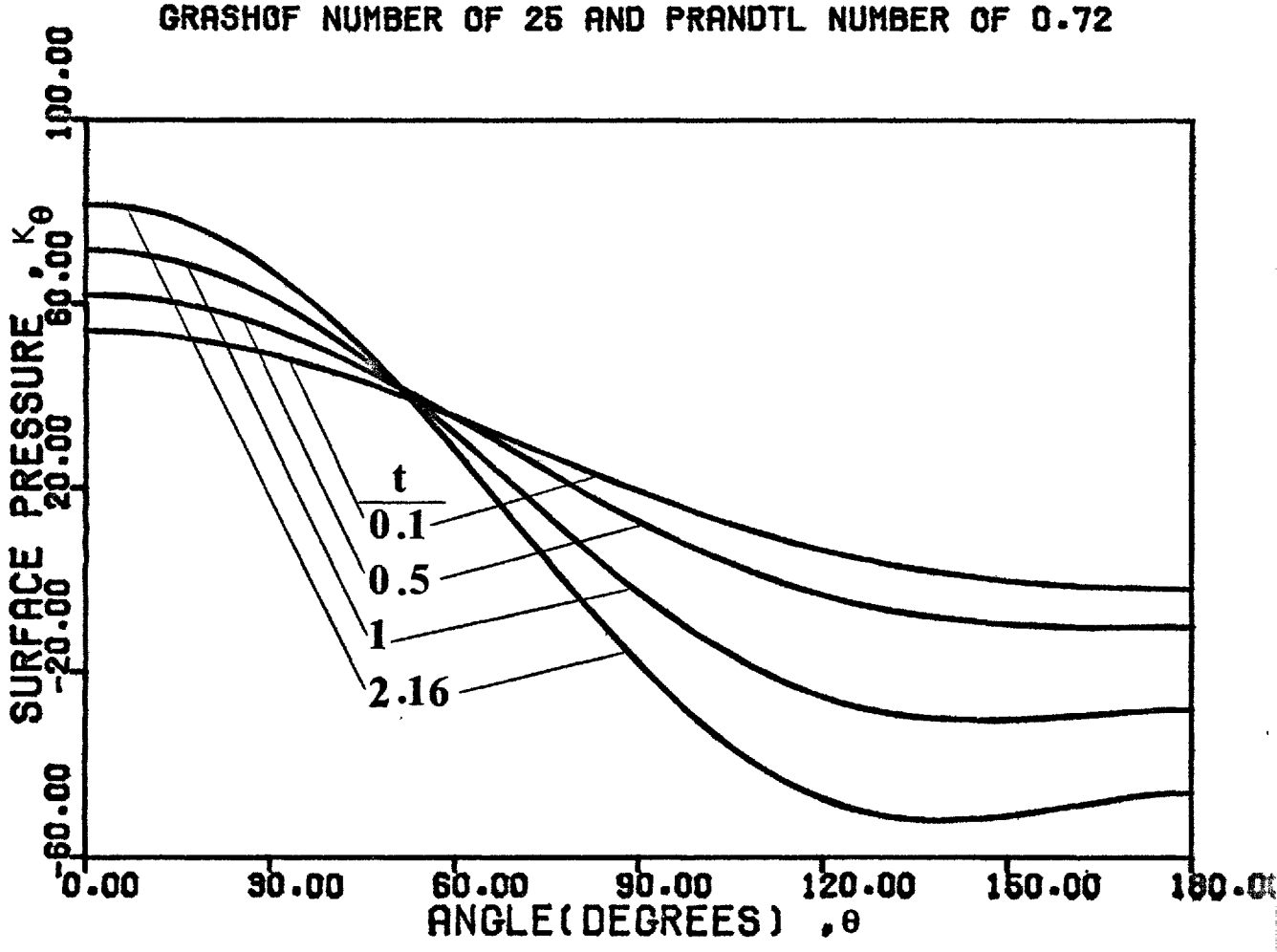

FIGURE 4.7.6 SURFACE PRESSURE VERSUS TIME AT GRASHOF NUMBER OF 25 AND PRANDTL NUMBER OF 0.72

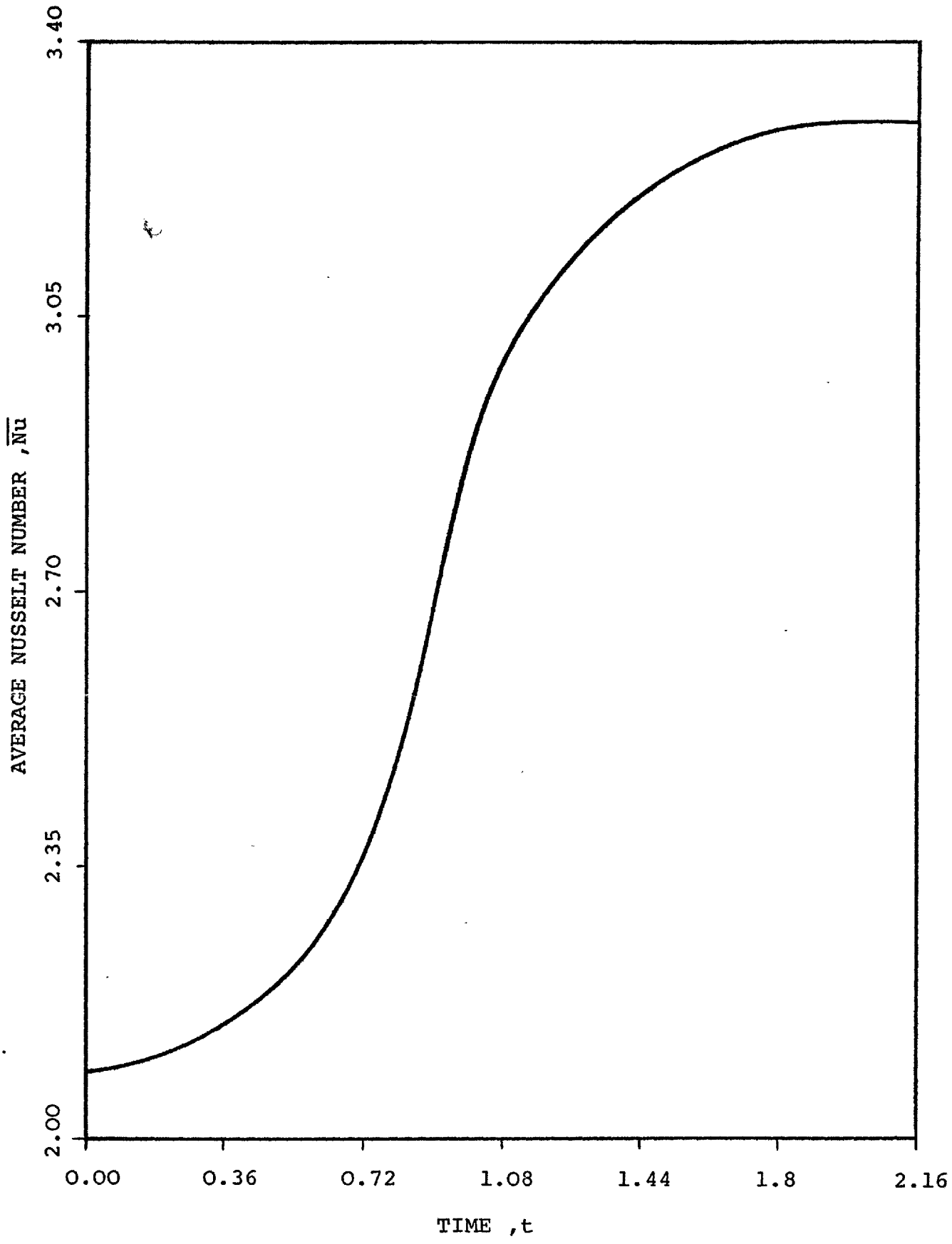

FIGURE 4.7.8 AVERAGE NUSSELT NUMBER VERSUS TIME AT GRASHOF NUMBER OF 25 AND PRANDTL NUMBER OF 0.72

the solution. However, computation storage limitations precluded the use of a larger flow field.

Table 3 presents a comparison of the late-time steady state values of the average Nusselt numbers obtained in the present study with experimental measurements. It is seen from this table that the average Nusselt number calculated in the present study for a Grashof number of 25 is in reasonable agreement with experimental measurements.

4.8 NUMERICAL SOLUTION FOR A GRASHOF NUMBER OF 50 AND A PRANDTL NUMER OF 0.72

The development with time of the flow pattern for free convective heat transfer from a solid sphere to a Newtonian fluid is shown in figures 4.8.1a to 4.8.1d. The development of the streamlines around the solid sphere is very similar to the cases described previously. Figure 4.8.1d shows that the stream function contours at the late-time steady state condition are displaced slightly downstream of the flow field. This is in accordance with the discussion given in previous sections.

Figures 4.8.2a to 4.8.2d show the development of the isotherms with time around the solid sphere. The time-dependent energy equation was solved using steady state radial conduction as the initial condition. The behaviour of the isotherms in figures 4.8.2a to 4.8.2d does not show

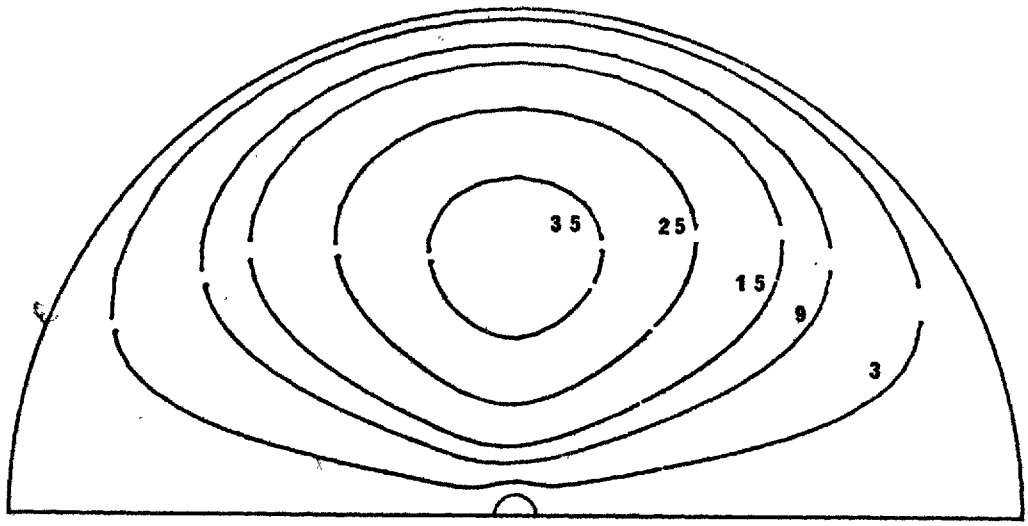

FIGURE 4.8.1b STREAMLINES AROUND THE SPHERE AT GRASHOF NUMBER OF 50 AND PRANDTL NUMBER OF 0.72 DIMENSIONLESS TIME , $t = 0.25$

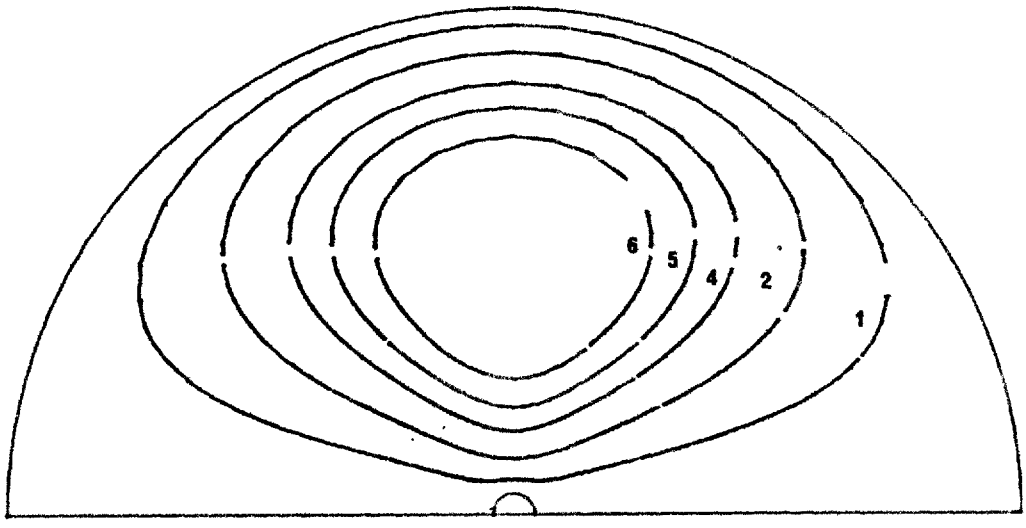

FIGURE 4.8.1a STREAMLINES AROUND THE SPHERE AT GRASHOF NUMBER OF 50 AND PRANDTL NUMBER OF 0.72 DIMENSIONLESS TIME , $t = 0.05$

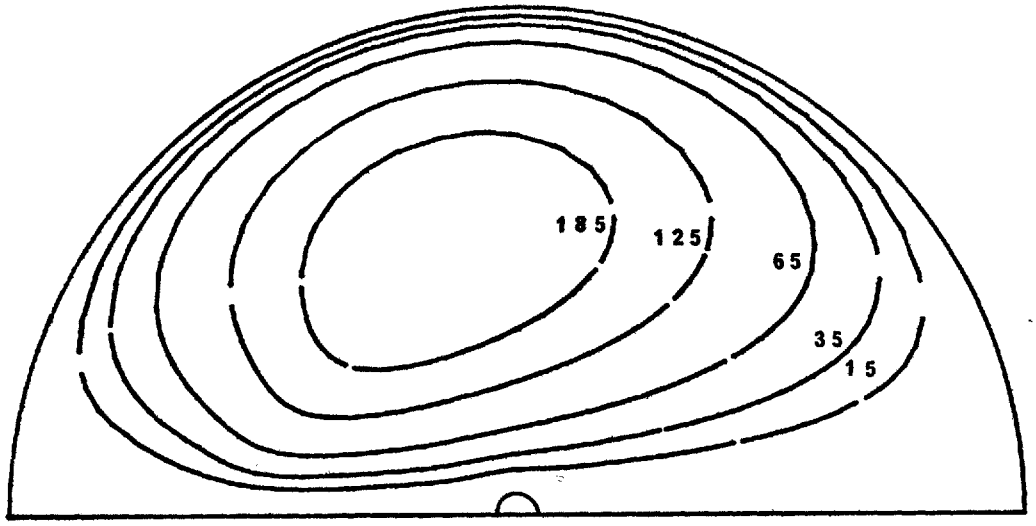

FIGURE 4.8.1d STREAMLINES AROUND THE SPHERE AT GRASHOF NUMBER OF 50 AND PRANDTL NUMBER OF 0.72 DIMENSIONLESS TIME . $t = 1.64$

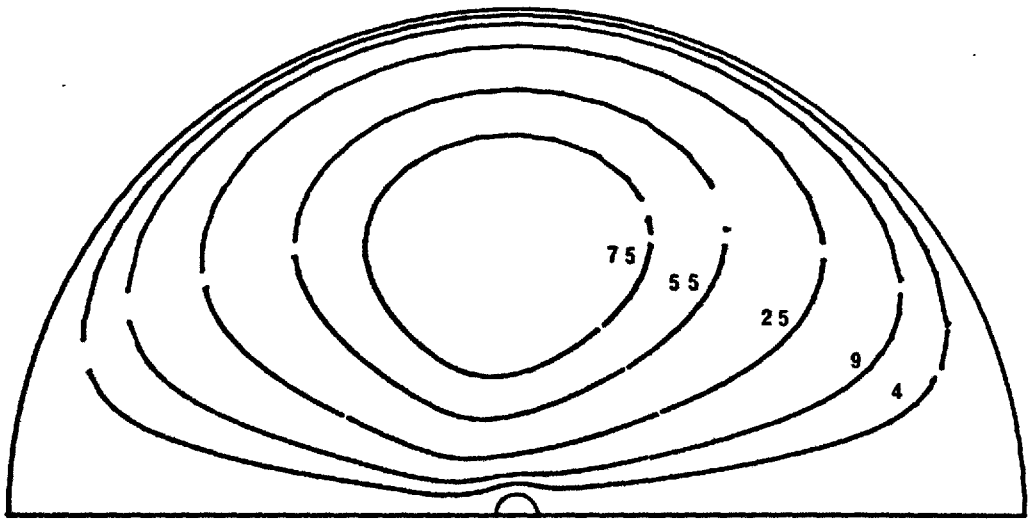

FIGURE 4.8.1c STREAMLINES AROUND THE SPHERE AT GRASHOF NUMBER OF 50 AND PRANDTL NUMBER OF 0.72 DIMENSIONLESS TIME . $t = 0.6$

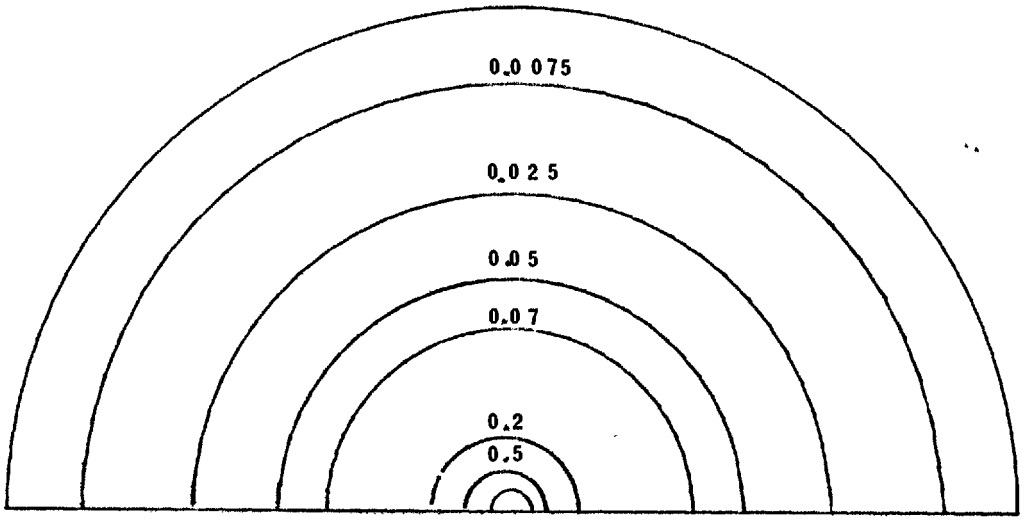

FIGURE 4.8.2b ISOTHERMS AROUND THE SPHERE AT GRASHOF NUMBER OF 50 AND PRANDTL NUMBER OF 0.72 DIMENSIONLESS TIME , t =0.25

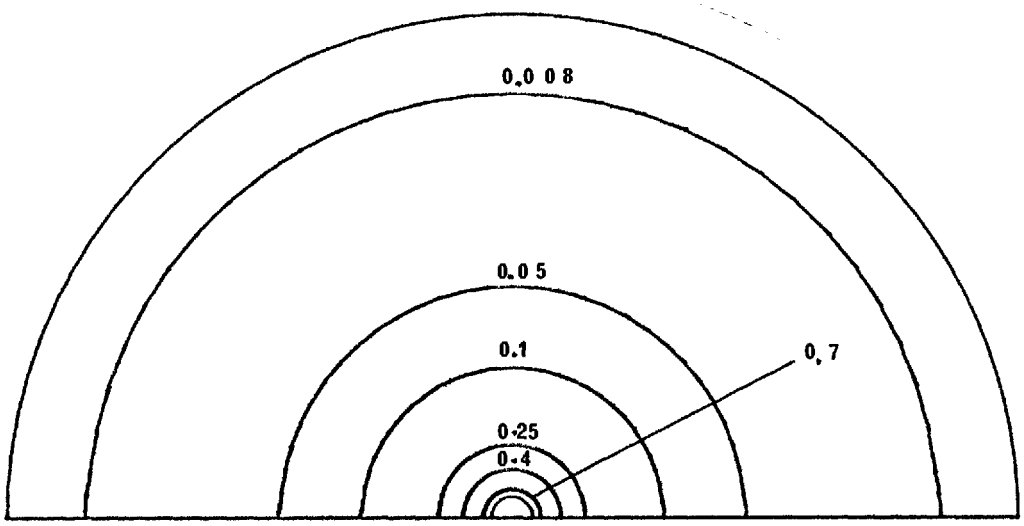

FIGURE 4.8.2a ISOTHERMS AROUND THE SPHERE AT GRASHOF NUMBER OF 50 AND PRANDTL NUMBER OF 0.72 DIMENSIONLESS TIME , t =0.05

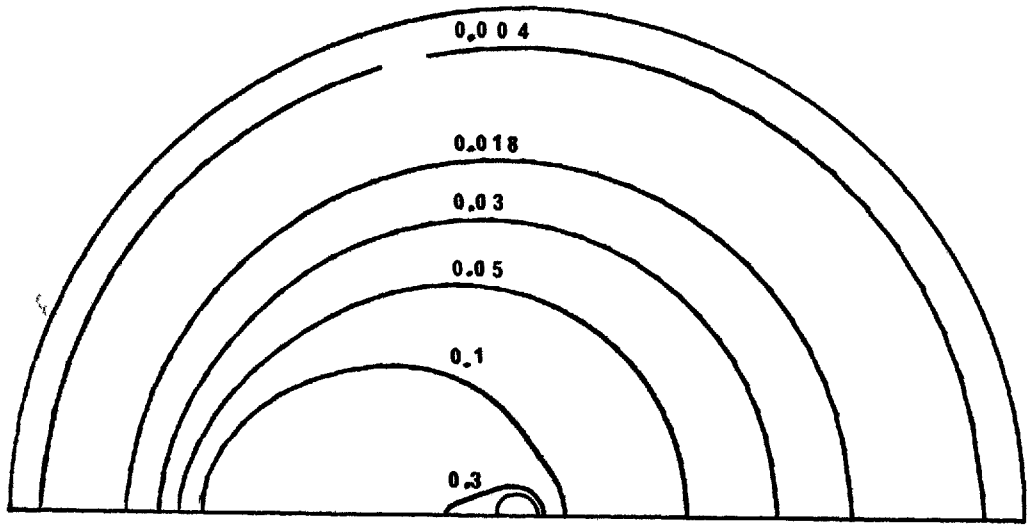

FIGURE 4.8.2d ISOTHERMS AROUND THE SPHERE AT GRASHOF NUMBER OF 50 AND PRANDTL NUMBER OF 0.72 DIMENSIONLESS TIME . $t = 1.64$

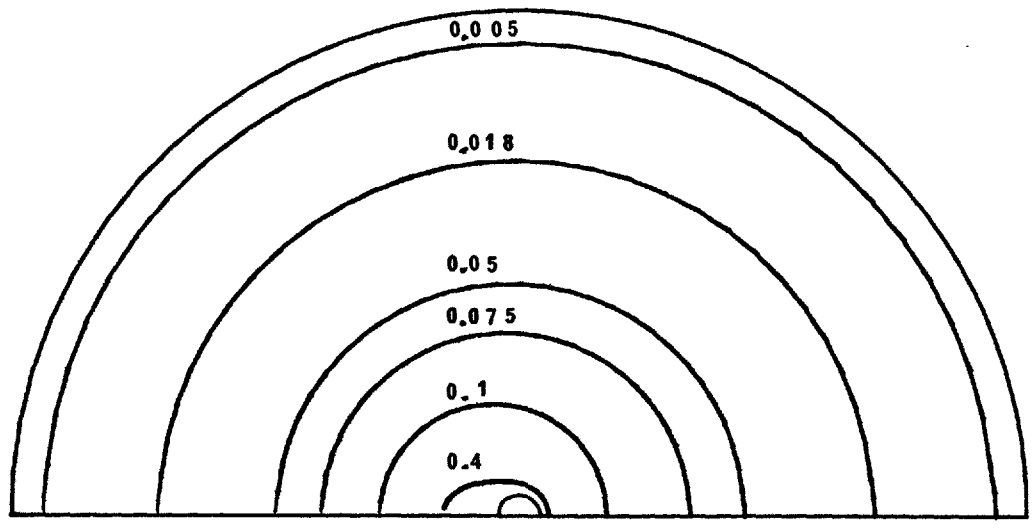

FIGURE 4.8.2c ISOTHERMS AROUND THE SPHERE AT GRASHOF NUMBER OF 50 AND PRANDTL NUMBER OF 0.72 DIMENSIONLESS TIME . $t = 0.6$

a marked difference from that for a Grashof number of 25 as shown in figures 4.7.2a to 4.7.2d. During the early stages of simulation, heat is transferred mainly by unsteady conduction in all directions. This is shown by figure 4.8.2a. However, as simulation proceeds, the convective effects increase in magnitude and the isotherms become closer to the surface of the sphere in the upstream region and extend further downstream at the rear of the sphere. The isotherms at the late-time steady state condition are shown by figure 4.8.2d.

The generation, diffusion and convection of vorticity from the sphere can be seen in figures 4.8.3a to 4.8.3d which show the vorticity distribution as a function of time. After an initial radial diffusion, shown by figure 4.8.3a, convection carries the vorticity to the downstream region of the sphere. The vorticity distribution at the late-time steady state condition is shown by figure 4.8.3d.

The behaviour of the drag coefficients with dimensionless time, t, is shown in figure 4.8.4. In common with all the other solutions obtained, both the form drag coefficient, C_{DP}, and the viscous drag coefficient, C_{DF}, show a continuous rise with time.

The variation with time of the local Nusselt number shown in figure 4.8.5, follows a similar pattern to those shown by the solutions for lower Grashof numbers. During

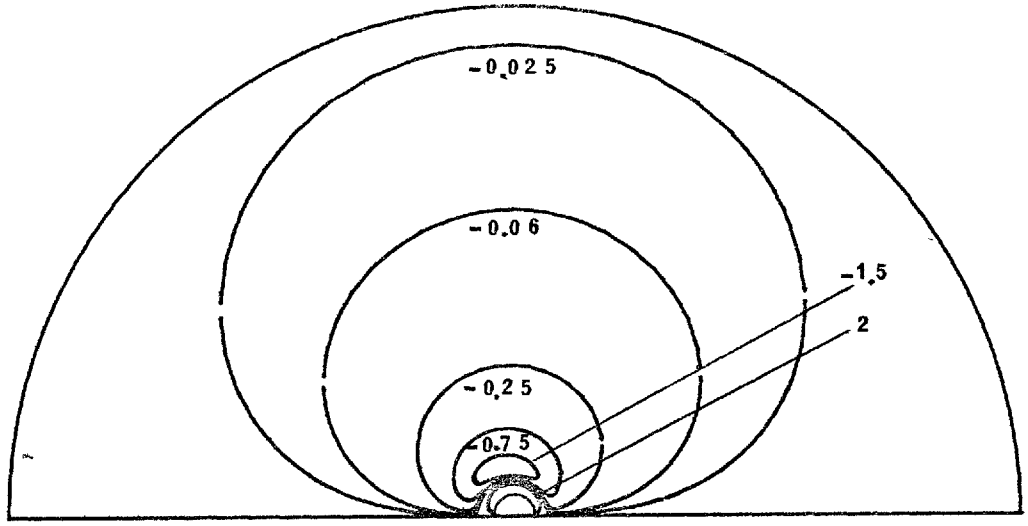

FIGURE 4.8.3b VORTICITY DISTRIBUTION AROUND THE SPHERE AT GRASHOF NUMBER OF 50 AND PRANDTL NUMBER OF 0.72 DIMENSIONLESS TIME , t =0.25

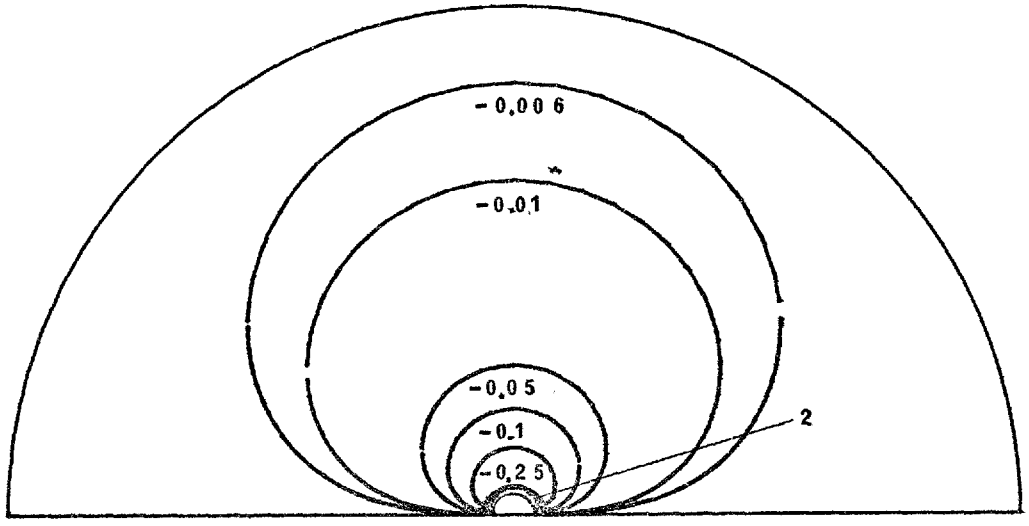

FIGURE 4.8.3a VORTICITY DISTRIBUTION AROUND THE SPHERE AT GRASHOF NUMBER OF 50 AND PRANDTL NUMBER OF 0.72 DIMENSIONLESS TIME , t =0.05

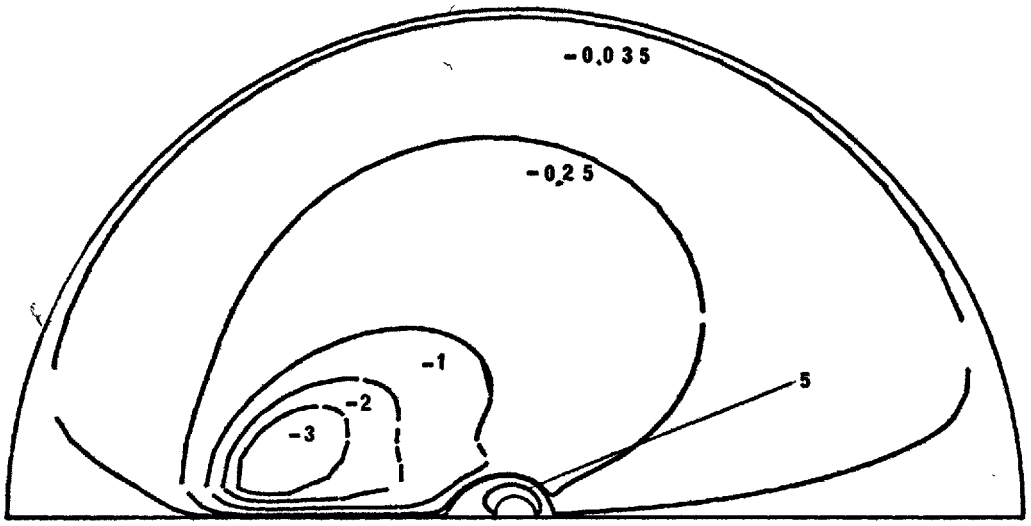

FIGURE 4 .8.3d VORTICITY DISTRIBUTION AROUND THE SPHERE AT GRASHOF NUMBER OF 50 AND PRANDTL NUMBER OF 0.72 DIMENSIONLESS TIME . $t = 1.64$

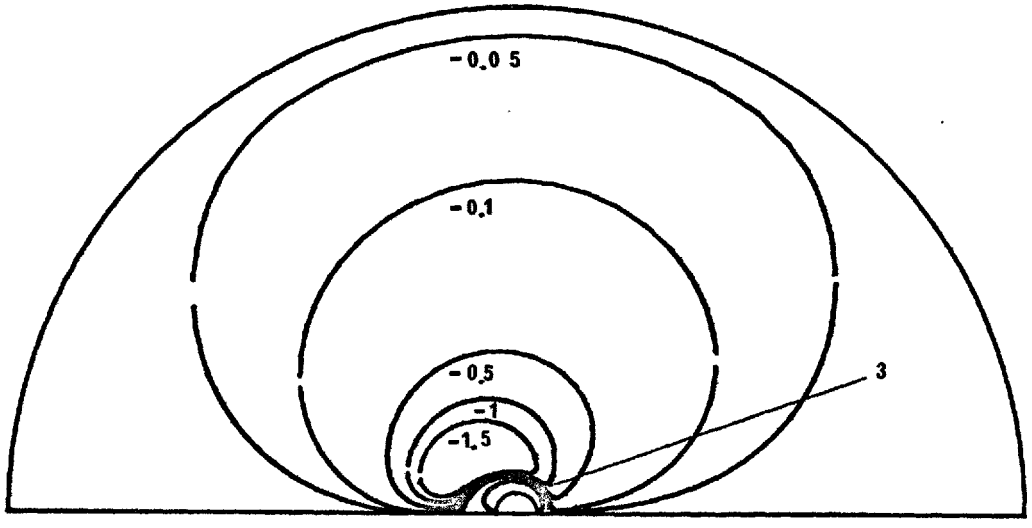

FIGURE 4 . 8 . 3c VORTICITY DISTRIBUTION AROUND THE SPHERE AT GRASHOF NUMBER OF 50 AND PRANDTL NUMBER OF 0.72 DIMENSIONLESS TIME . $t = 0.6$

the early stages of simulation, the local Nusselt number over the solid sphere remains fairly constant since heat transfer takes place mainly by unsteady conduction. However, as integration proceeds with time, convective effects increase and, as a result, the local Nusselt numbers over the upstream region of the solid sphere increase until their late-time steady state values are obtained. During the same period, the local Nusselt numbers over the downstream region of the sphere decrease at first but increase as the late-time steady state condition is approached.

Figure 4.8.7 shows the variation of the surface vorticity with time. This variation follows a similar pattern to those described in previous sections. The symmetrical distribution of surface vorticity about an imaginary plane placed between the upstream and downstream regions of the flow region confirms that at a Grashof number of 50, diffusion is the dominant mode of vorticity transport close to the sphere surface.

The variation with time of the surface pressure is shown in figure 4.8.6. It can be observed that as simulation proceeds with time , the surface pressure over the upstream region of the sphere increases slowly towards its late-time steady state value. The dimensionless surface pressure over the downstream region of the sphere decreases but as shown by figure 4.8.6, at a dimensionless

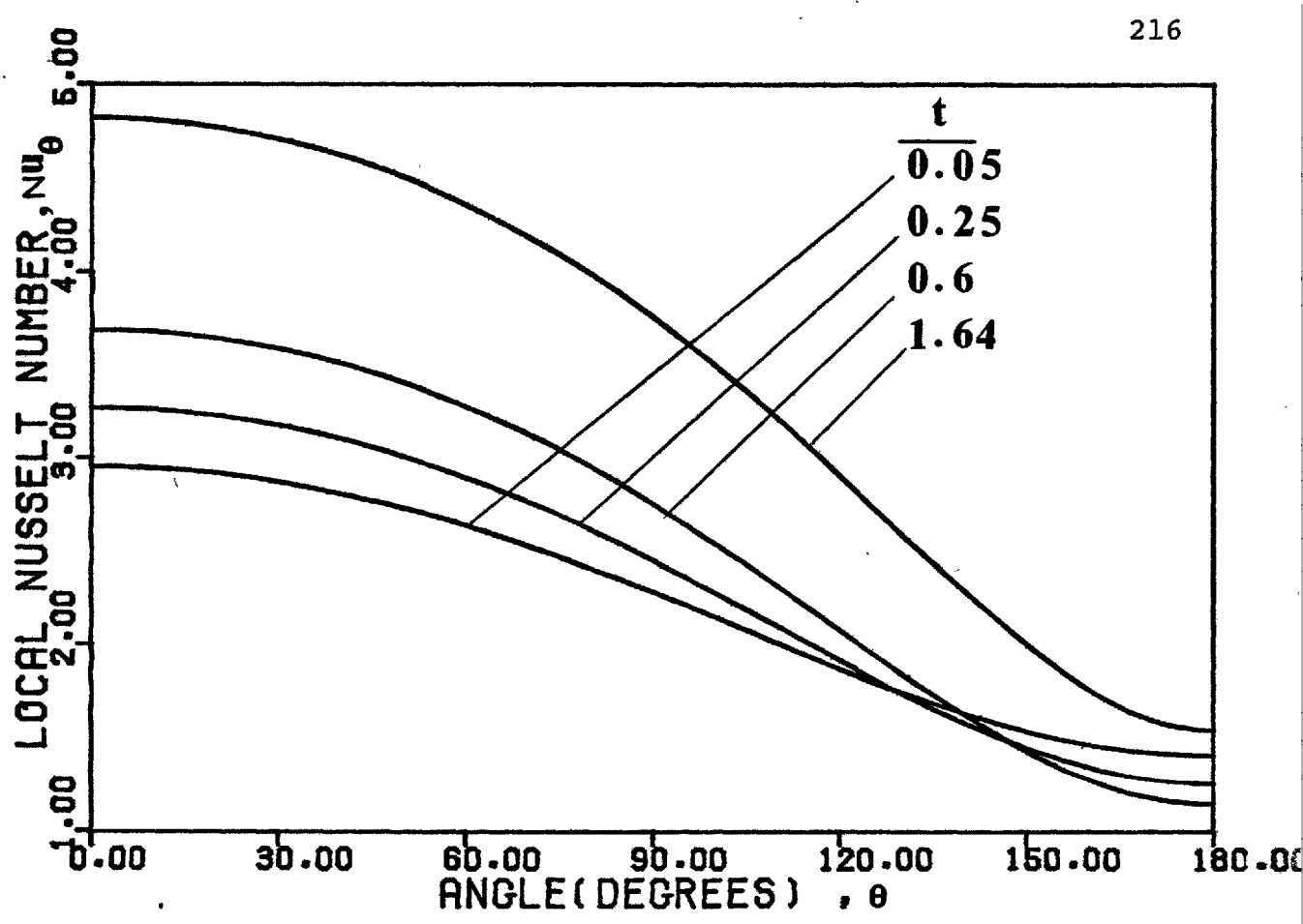

FIGURE 4.8.5 LOCAL NUSSELT NUMBER VERSUS TIME AT GRASHOF NUMBER OF 50 AND PRANDTL NUMBER OF 0.72

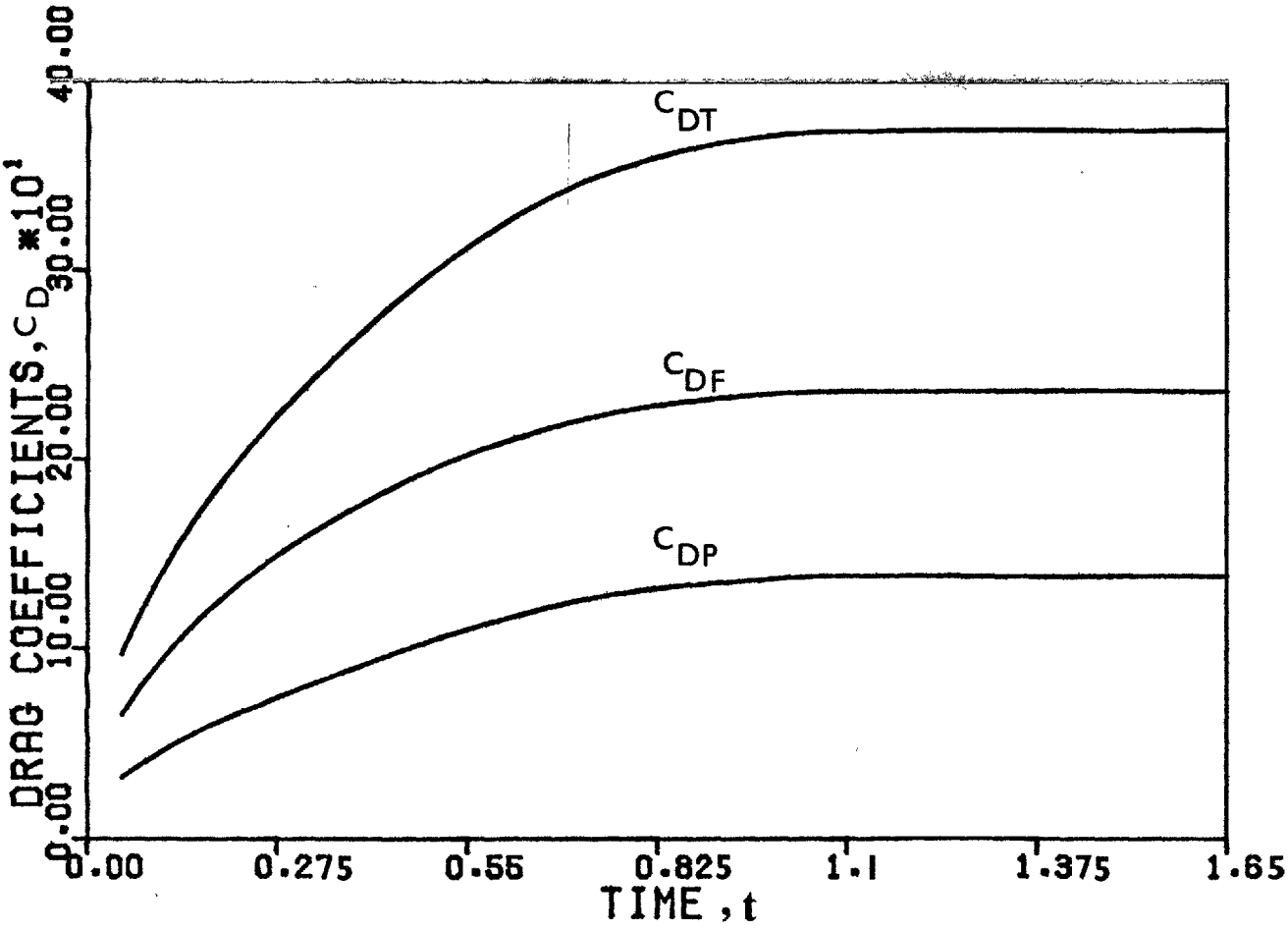

FIGURE 4.8.4 DRAG COEFFICIENTS VERSUS TIME AT GRASHOF NUMBER OF 50 AND PRANDTL NUMBER OF 0.72

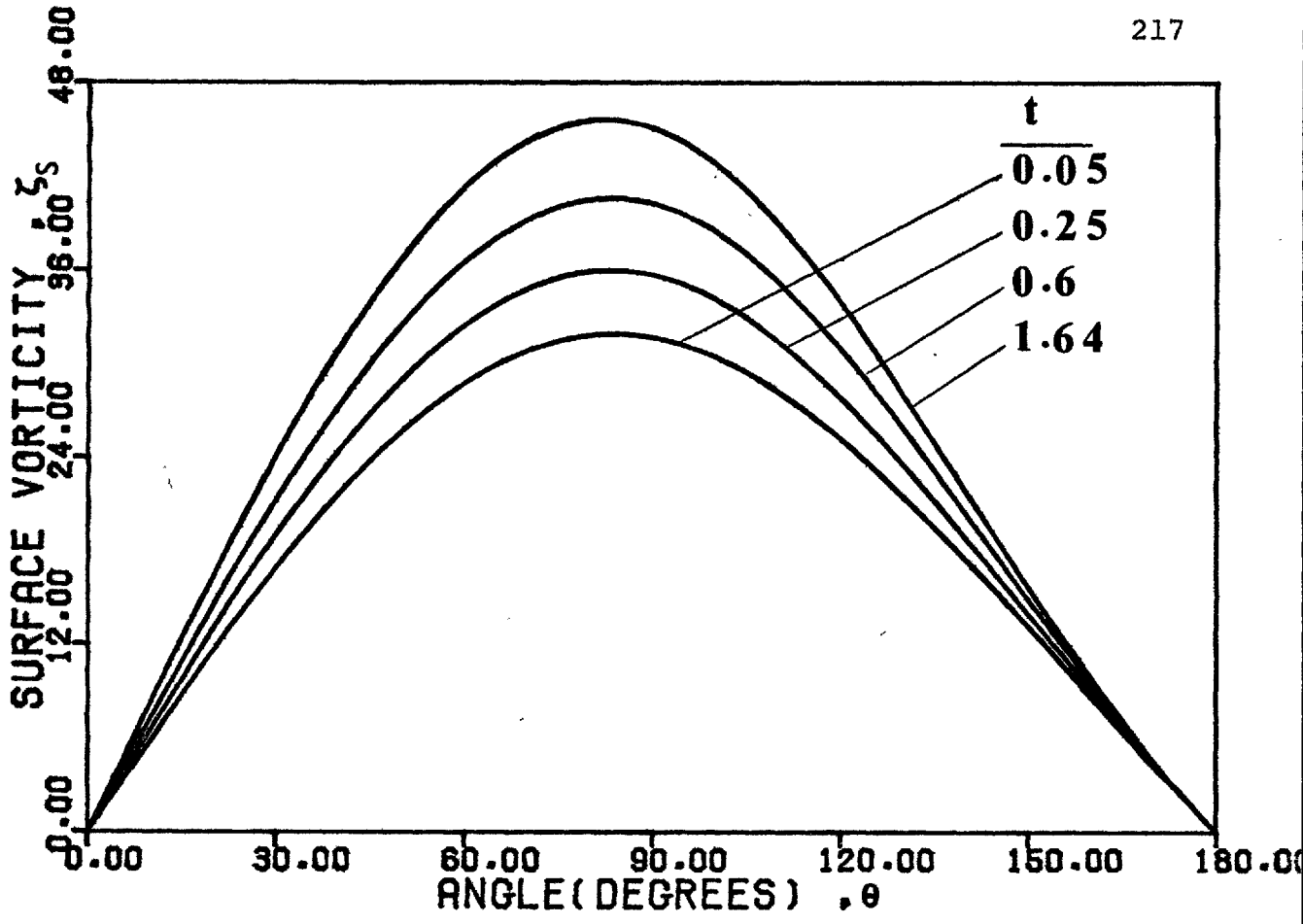

FIGURE 4.8.7 SURFACE VORTICITY VERSUS TIME AT GRASHOF NUMBER OF 50 AND PRANDTL NUMBER OF 0.72

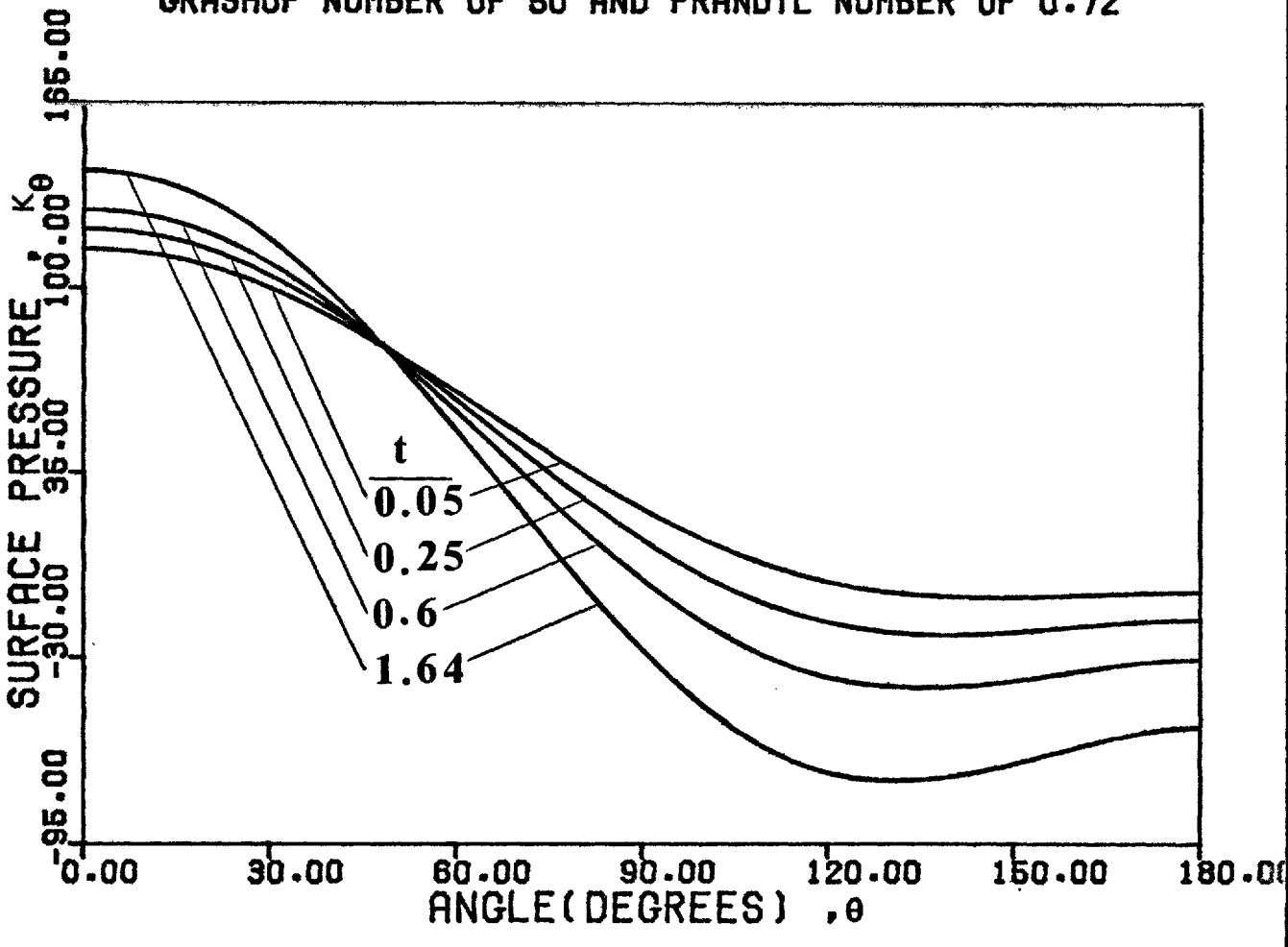

FIGURE 4.8.6 SURFACE PRESSURE VERSUS TIME AT GRASHOF NUMBER OF 50 AND PRANDTL NUMBER OF 0.72

time, t, of about 0.3 the dimensionless surface pressure starts to show a shallow minimum which develops with time.

The average Nusselt number, $\overline{Nu}$, as in the previous cases, starts from a steady state conduction value of 2.085 and increases continuously towards its late-time steady state value as shown by figure 4.8.8. The late-time steady state value of the average Nusselt number for a Grashof number of 50 and a Prandtl number of 0.72 is found to be 3.82 which according to table 3 is in reasonable agreement with experimental measurements.

The influence of the location of the outer boundary on the results obtained for a Grashof number of 50 and a Prandtl number of 0.72 can be judged from table 5. It can be observed that a reduction in the radius of the outer boundary from 24.53 to 16.44 sphere radii leads to the prediction of smaller values for the overall flow characteristics. The final choice of the location of outer boundary was a compromise between economy and accuracy of results.

Table 11 presents the values of the local Nusselt number, the surface vorticity, and the surface pressure as integration approaches the late-time condition. From this table it can be observed that the relative changes in the above variables during the dimensionless time period of 1.1 to 1.6 become small. This shows that at a dimensionless time of about 1.6 the simulation has reached steady state condition.

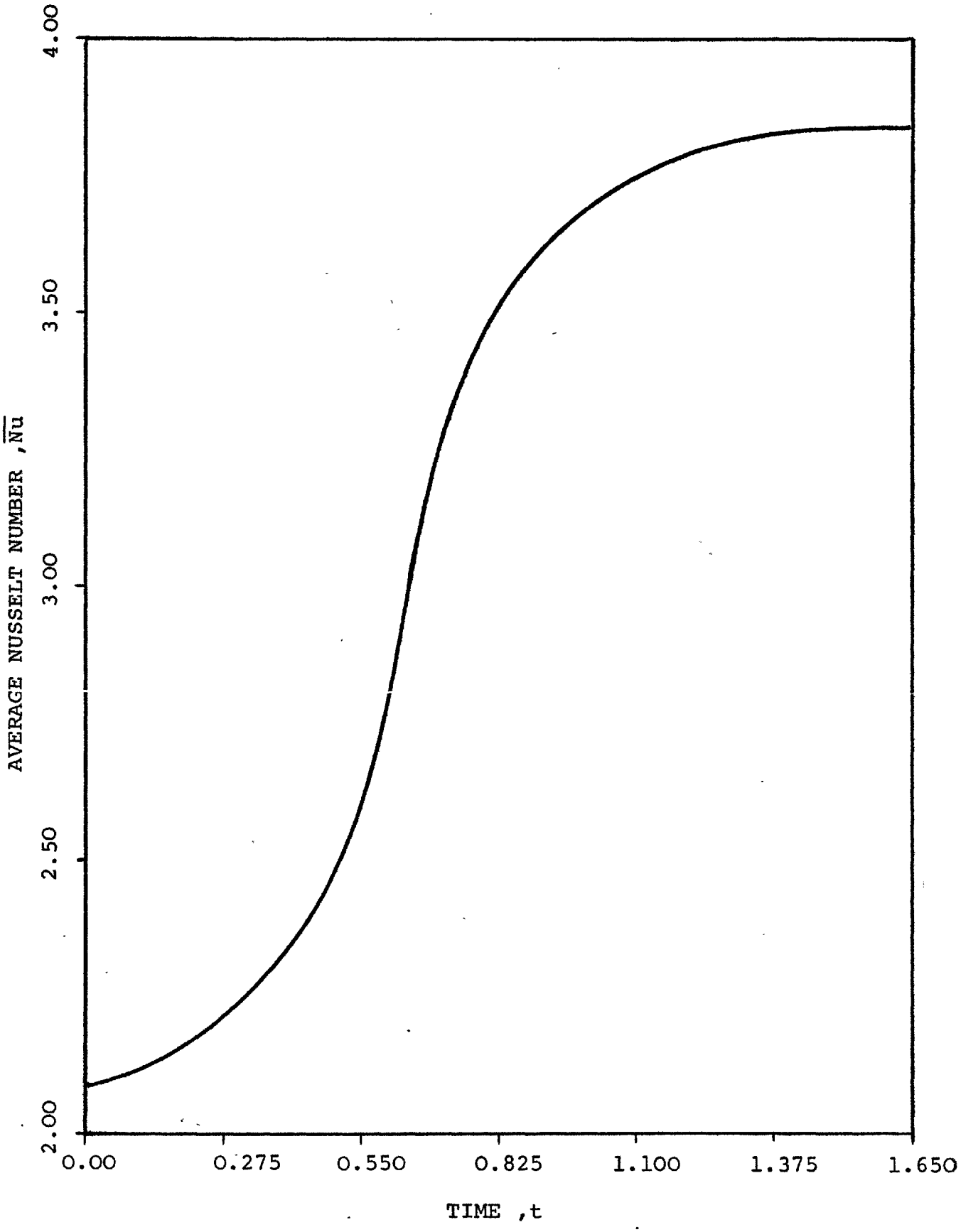

FIGURE 4.8.8 AVERAGE NUSSELT NUMBER VERSUS TIME AT GRASHOF NUMBER OF 50 AND PRANDTL NUMBER OF 0.72

4.9 NUMERICAL SOLUTION FOR A GRASHOF NUMBER OF 125 AND A PRANDTL NUMBER OF 0.72

The simulation of the flow field around a solid sphere in conditions of free convective heat transfer at a Grashof number of 125 and a Prandtl number of 0.72 can be seen in figures 4.9.1a to 4.9.1d which show the stream function contours as a function of time. The stream function contours in figures 4.9.1a and 4.9.1d are not significantly different from those obtained for a Grashof number of 50. However, as integration proceeds the heated layer adjacent to the upstream surface of the sphere becomes thiner and the fluid velocity increases throughout the flow field. The increased velocity of the fluid in the vicinity of the sphere causes the fluid close to the sphere surface to be draged downstream so that the streamlines are shifted slightly from the upstream region to the downstream region of the flow field. This is shown in figure 4.9.1d.

The development with time of the isotherms is shown by figures 4.9.2a to 4.9.2d. The development of the isotherms is similarto that described before for smaller Grashof numbers. Starting from an initial condition of pure radial conduction, the influence of the heated body extends uniformly in all directions. However, as simulation proceeds, it is clearly seen from figures 4.9.2b and 4.9.2c that in the region upstream of the solid sphere the isotherms move closer to the sphere surface whereas in the downstream

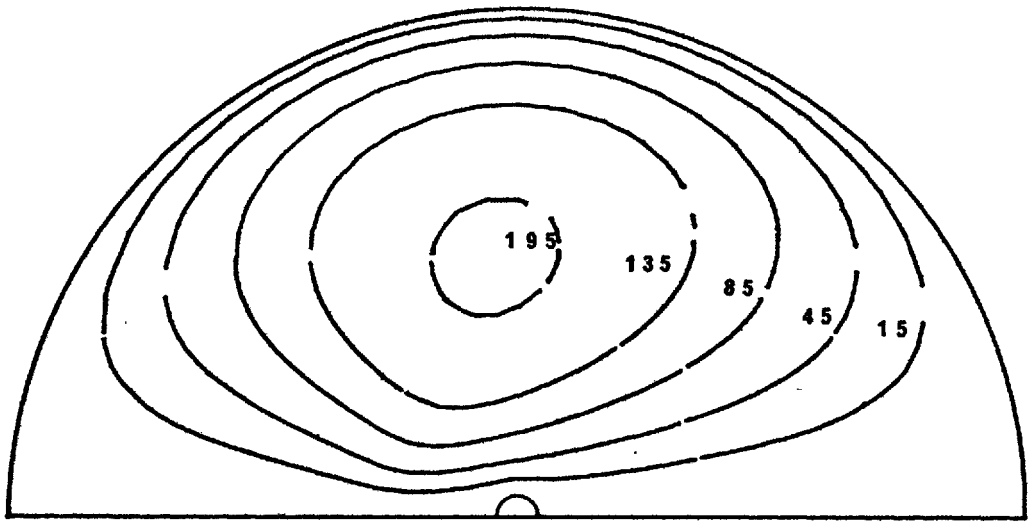

FIGURE 4.9.1b STREAMLINES AROUND THE SPHERE AT GRASHOF NUMBER OF 125 AND PRANDTL NUMBER OF 0.72 DIMENSIONLESS TIME . $t = 0.55$

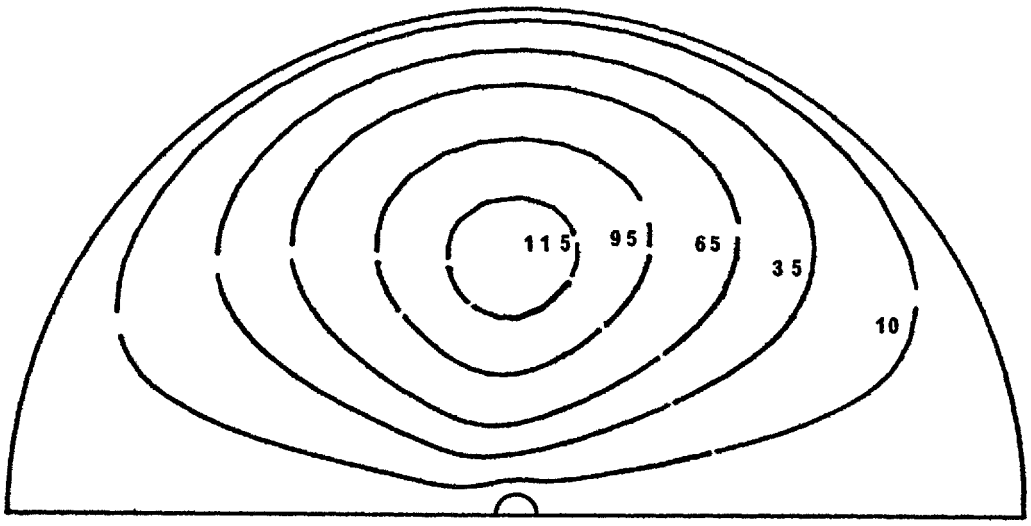

FIGURE 4.9.1a STREAMLINES AROUND THE SPHERE AT GRASHOF NUMBER OF 125 AND PRANDTL NUMBER OF 0.72 DIMENSIONLESS TIME . $t = 0.3$

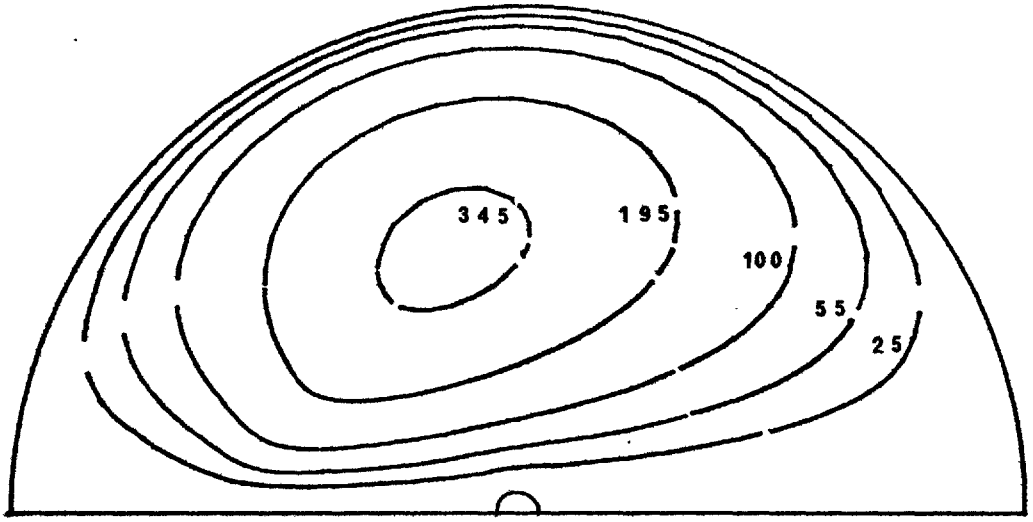

FIGURE 4.9.1d STREAMLINES AROUND THE SPHERE AT GRASHOF NUMBER OF 125 AND PRANDTL NUMBER OF 0.72 DIMENSIONLESS TIME , $t = 0.96$

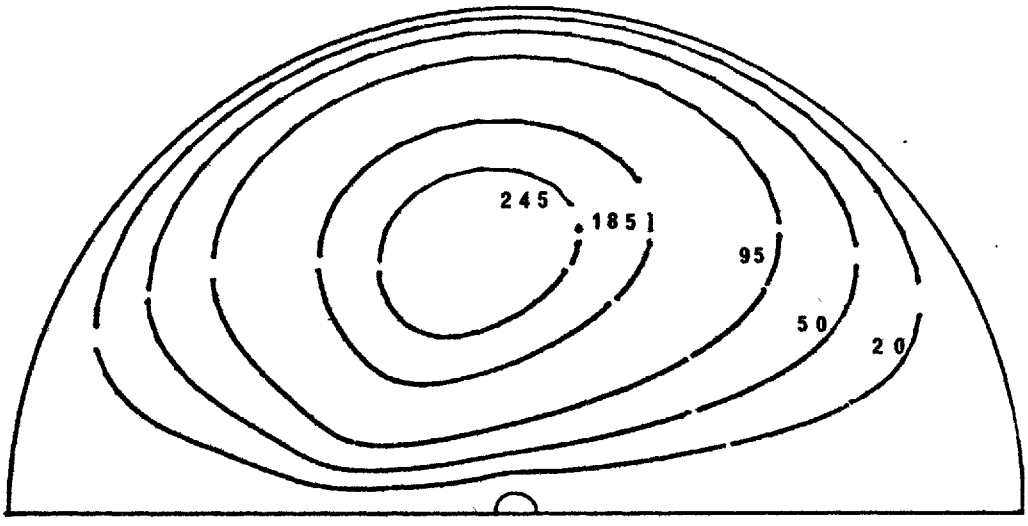

FIGURE 4.9.1c STREAMLINES AROUND THE SPHERE AT GRASHOF NUMBER OF 125 AND PRANDTL NUMBER OF 0.72 DIMENSIONLESS TIME , $t = 0.75$

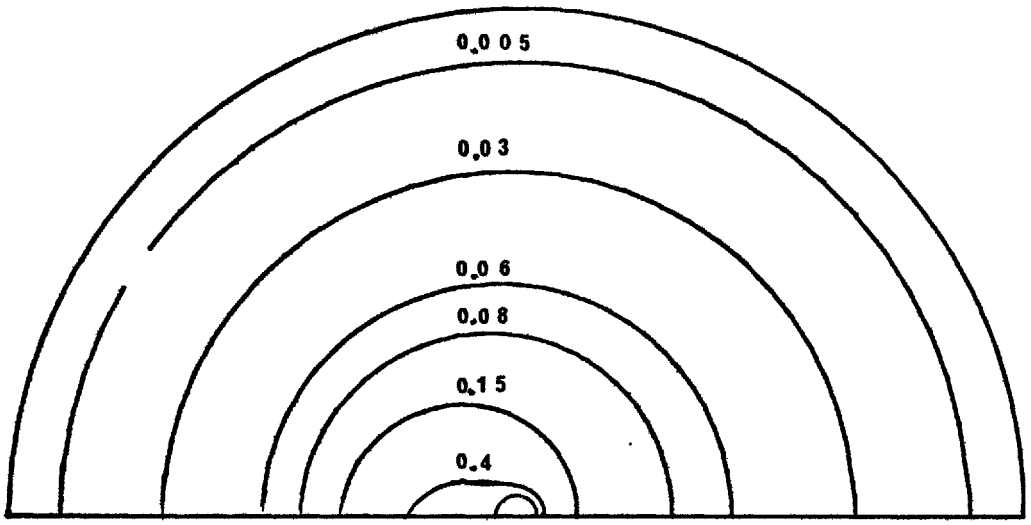

FIGURE 4.9.2b ISOTHERMS AROUND THE SPHERE AT GRASHOF NUMBER OF 125 AND PRANDTL NUMBER OF 0.72 DIMENSIONLESS TIME . t =0.55

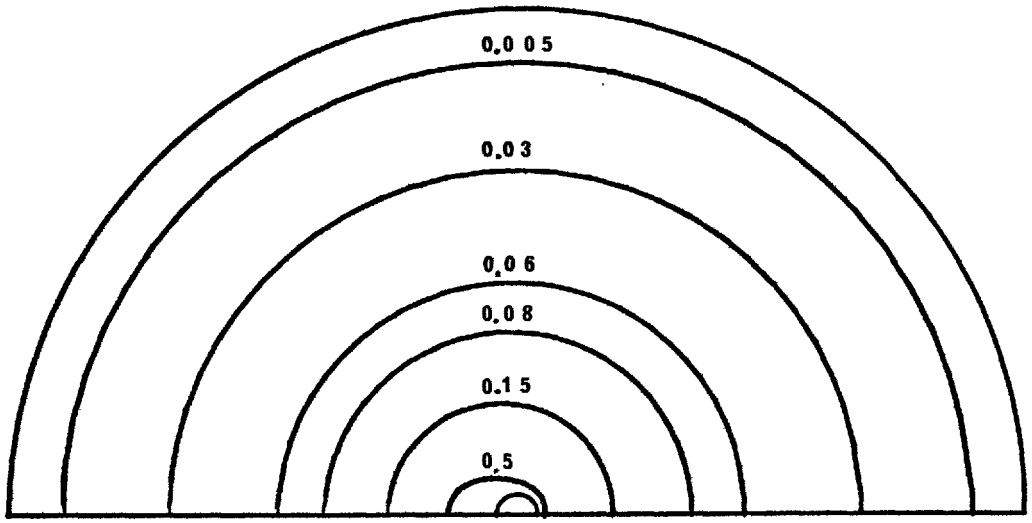

FIGURE 4.9.2a ISOTHERMS AROUND THE SPHERE AT GRASHOF NUMBER OF 125 AND PRANDTL NUMBER OF 0.72 DIMENSIONLESS TIME . t =0.3

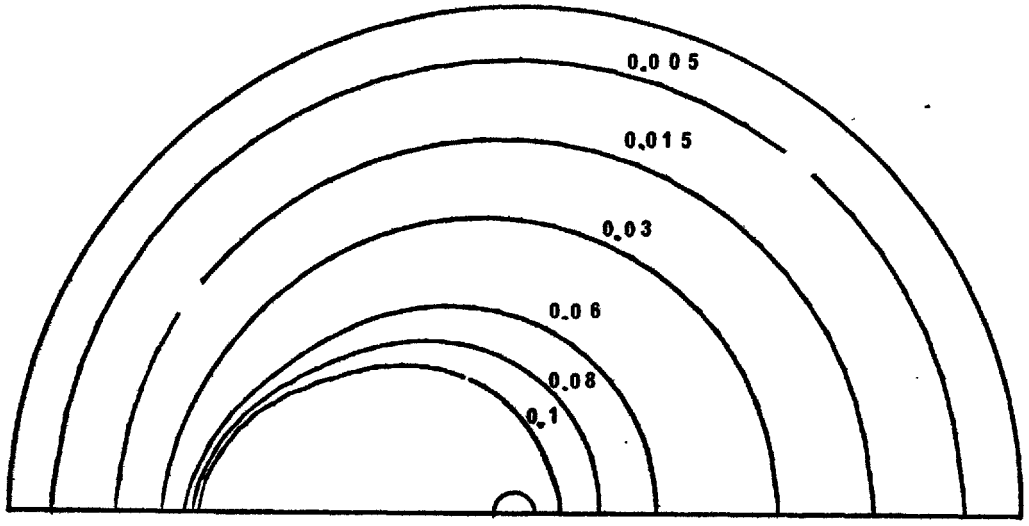

FIGURE 4.9.2d ISOTHERMS AROUND THE SPHERE AT GRASHOF NUMBER OF 125 AND PRANDTL NUMBER OF 0.72 DIMENSIONLESS TIME , $t = 0.96$

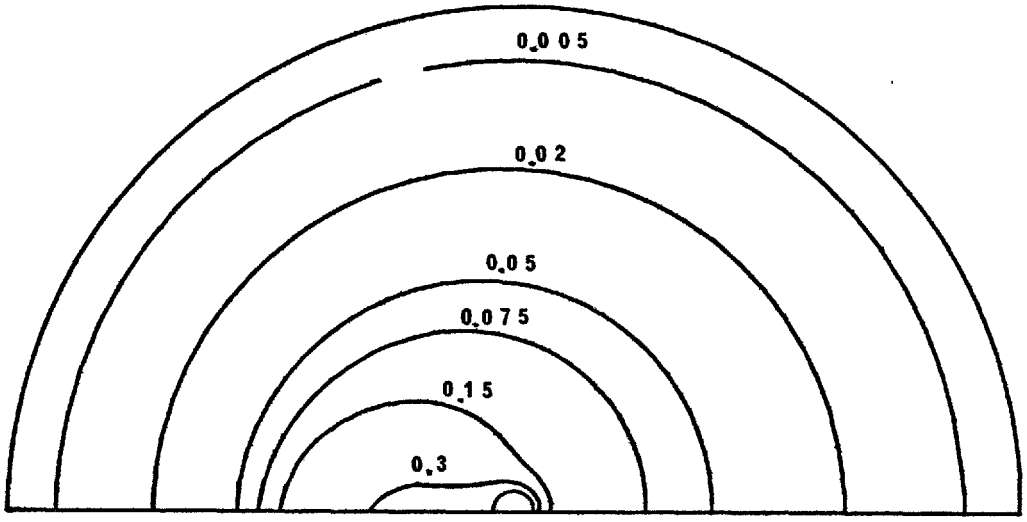

FIGURE 4.9.2c ISOTHERMS AROUND THE SPHERE AT GRASHOF NUMBER OF 125 AND PRANDTL NUMBER OF 0.72 DIMENSIONLESS TIME , $t = 0.75$

region the isotherms move further from the surface. Figure 4.9.3d shows the late-time steady state temperature contours around the solid sphere. In general as the Grashof number is increased, it is to be expected that the late-time thickness of the heated layer around the upstream region of the solid sphere will decrease and in the limiting case of very large Grashof numbers the so-called 'boundary layer problem' may be obtained.

The generation and development with time of vorticity around the solid sphere can be seen in figures 4.9.3a to 4.9.3d. Initially, since the fluid velocity is relatively small, the convective effects are small and the vorticity distribution around the sphere is almost symmetrical about an imaginary plane which separates the upstream and downstream regions of the flow region. However, as the velocity approaches its late-time steady state value, the vorticity is convected more and more downstream. Figure 4.9.3d shows the vorticity contours at the late-time steady state condition.

The variation with time of the drag coefficients, figure 4.9.4, follows the same pattern as those obtained for lower Grashof numbers. Both the form drag coefficient and the viscous drag coefficient increase rapidly with time and reach their late-time steady state values very quickly.

Table 12 shows the late-time values of the local Nusselt number, the surface vorticity, and the surface pressure.

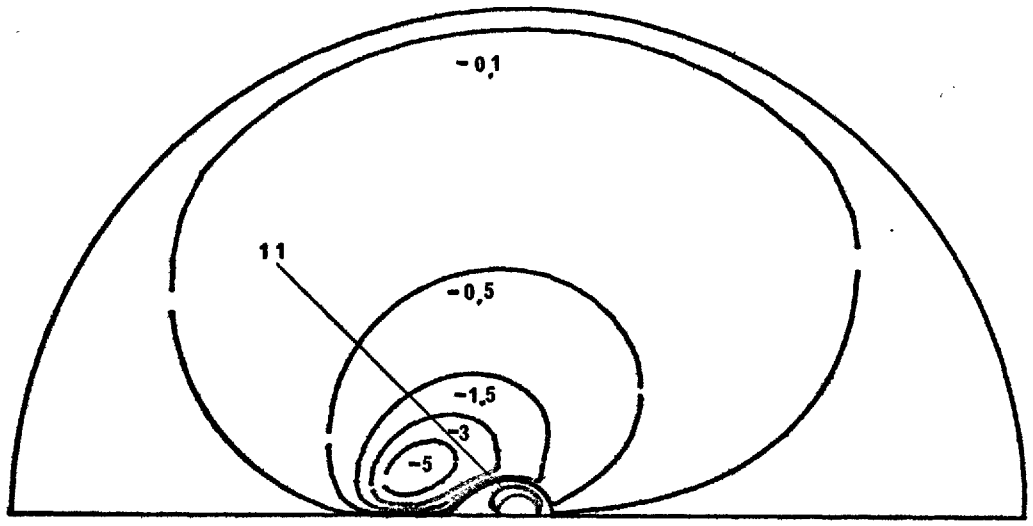

FIGURE 4 . 9 .3b VORTICITY DISTRIBUTION AROUND THE SPHERE AT GRASHOF NUMBER OF 125 AND PRANDTL NUMBER OF 0.72 DIMENSIONLESS TIME , $t = 0.55$

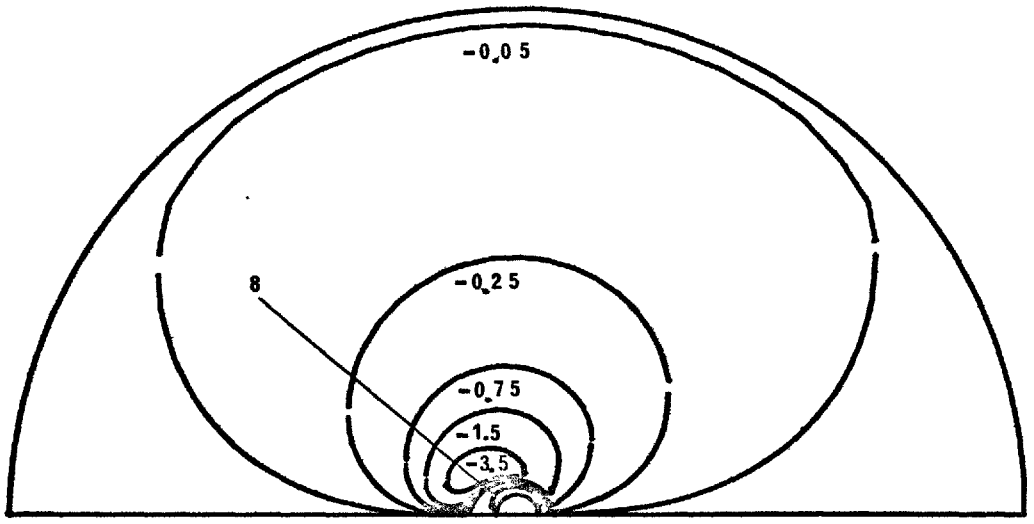

FIGURE 4 .9.3a VORTICITY DISTRIBUTION AROUND THE SPHERE AT GRASHOF NUMBER OF 125 AND PRANDTL NUMBER OF 0.72 DIMENSIONLESS TIME , $t = 0.3$

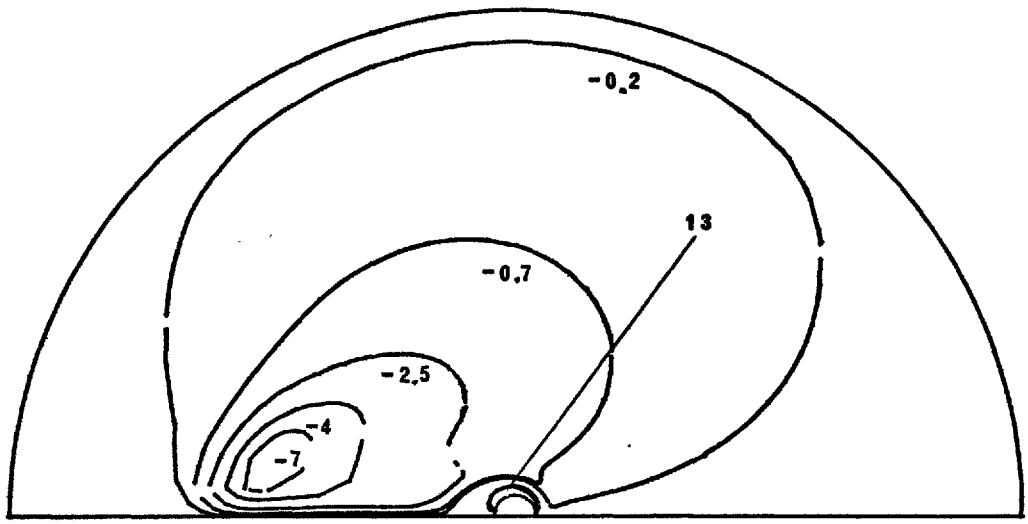

FIGURE 4.9.3d VORTICITY DISTRIBUTION AROUND THE SPHERE AT GRASHOF NUMBER OF 125 AND PRANDTL NUMBER OF 0.72 DIMENSIONLESS TIME , $t = 0.96$

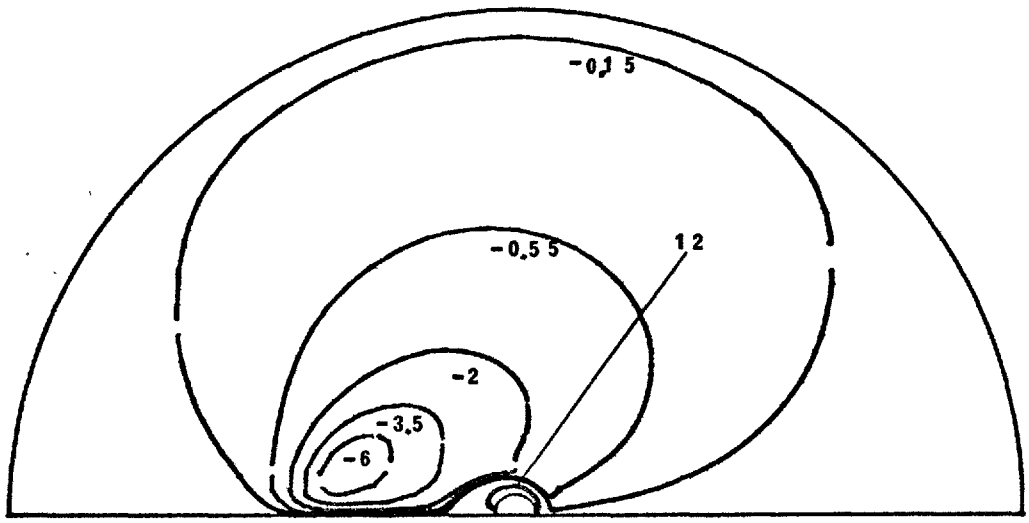

FIGURE 4.9.3c VORTICITY DISTRIBUTION AROUND THE SPHERE AT GRASHOF NUMBER OF 125 AND PRANDTL NUMBER OF 0.72 DIMENSIONLESS TIME , $t = 0.75$

From this tables it can be seen that the above variables become relatively independent of time during the dimensionless time period between 0.75 and 0.95.

Figure 4.9.5 shows the variation of the local Nusselt number with time. The local Nusselt number around the sphere remains fairly constant during the early stages of simulation. However, as simulation proceeds with time, the local Nusselt numbers over the upstream region of the sphere increase towards their late-time steady state values while the local Nusselt numbers over the rear part of the sphere first decrease rapidly and then increase slowly towards their late-time steady state values.

The variation with time of the average Nusselt number is shown in figure 4.9.8. The average Nusselt number starts from a value of 2.085 and increases continuously towards its late-time steady state value. Table 3 shows that the late-time steady state value obtained for the average Nusselt number is in reasonable agreement with available experimental measurements.

The variation with time of the surface pressure is shown in figure 4.9.6. From this figure one observes that as simulation continues the dimensionless surface pressure over the upstream region of the sphere increases very slowly towards its late-time steady state value. During the same period, the dimensionless surface pressure over the downstream region of the sphere decreases and shows a shallow

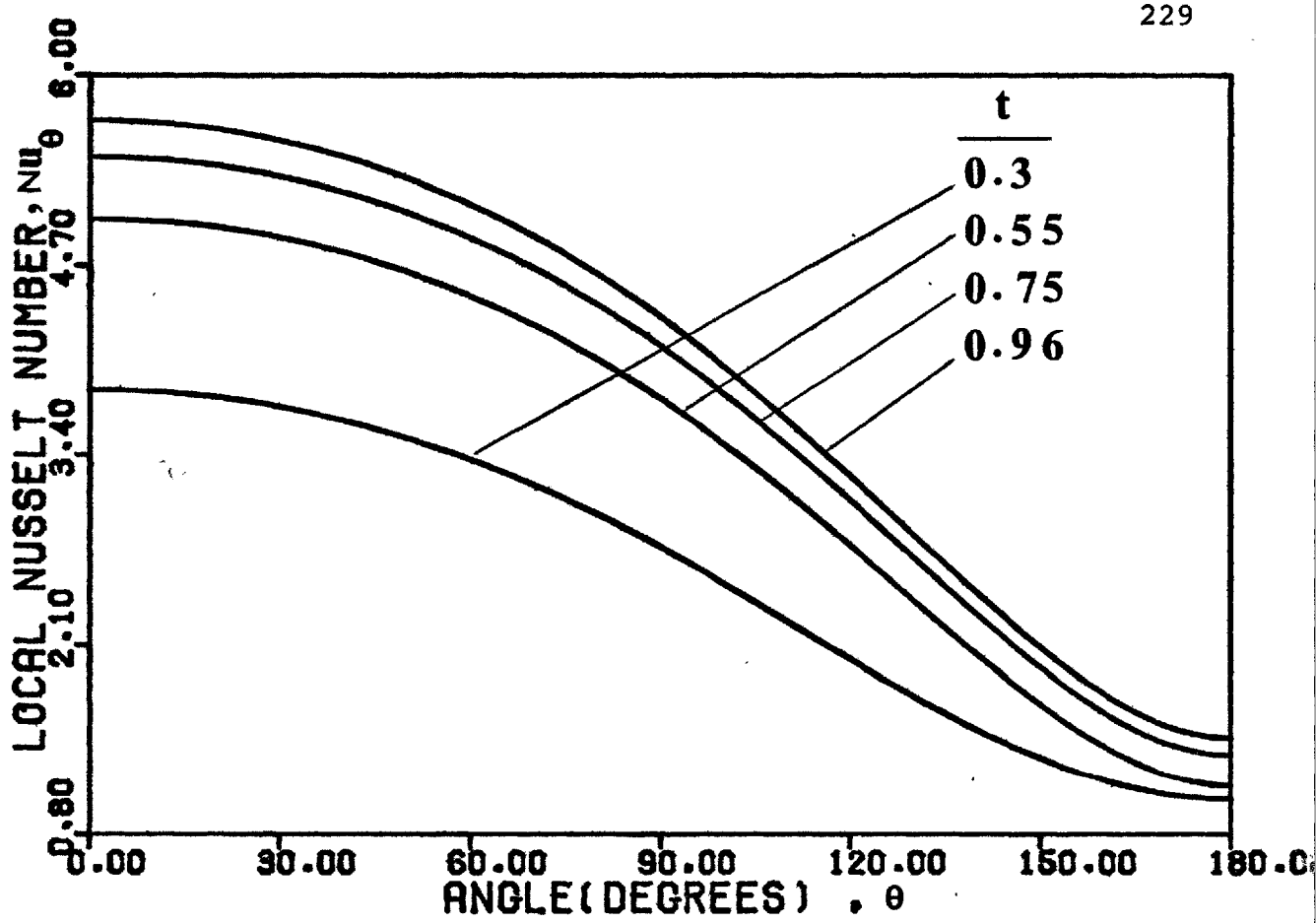

FIGURE 4.9.5 LOCAL NUSSELT NUMBER VERSUS TIME AT GRASHOF NUMBER OF 125 AND PRANDTL NUMBER OF 0.72

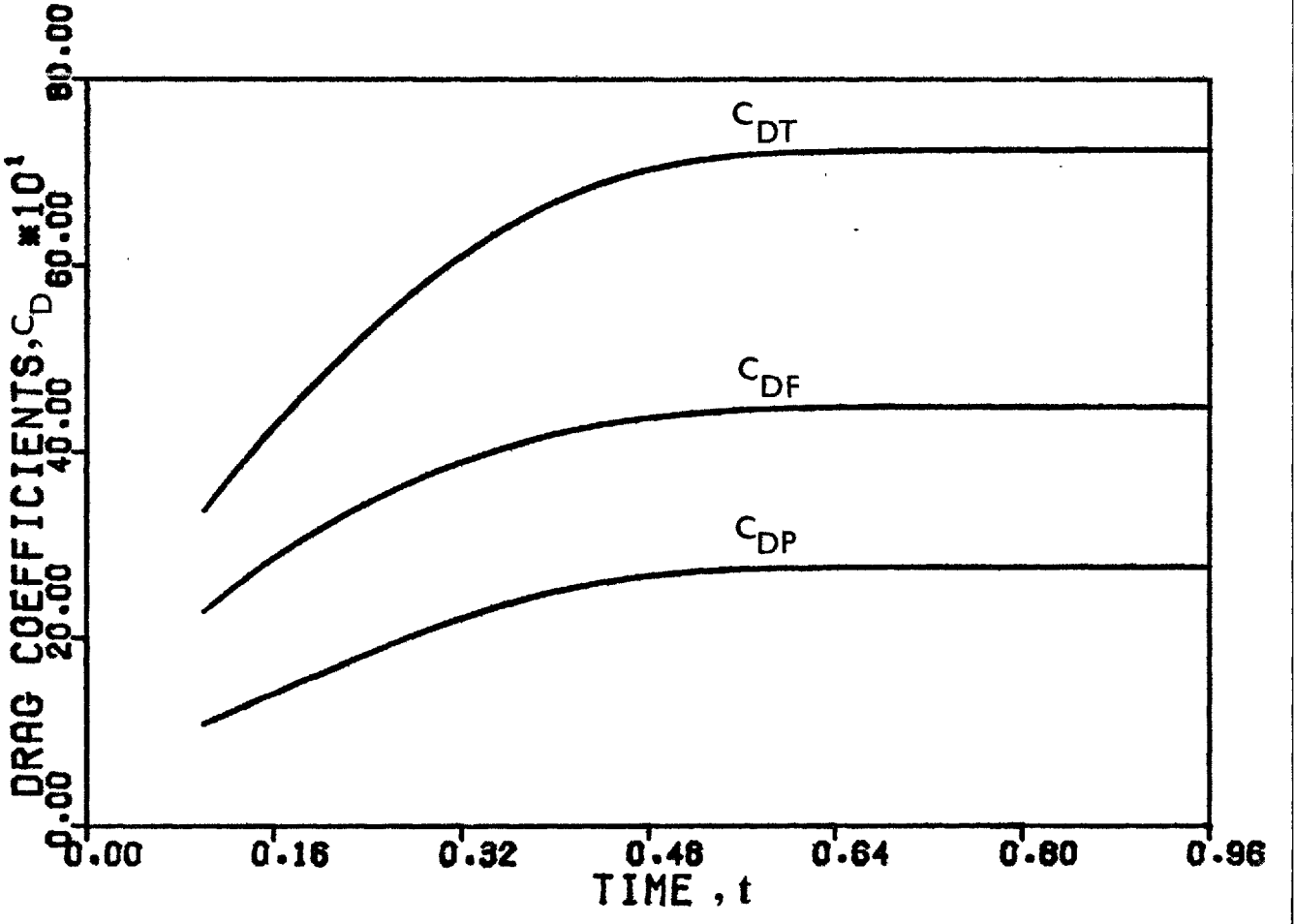

FIGURE 4.9.4 DRAG COEFFICIENTS VERSUS TIME AT GRASHOF NUMBER OF 125 AND PRANDTL NUMBER OF 0.72

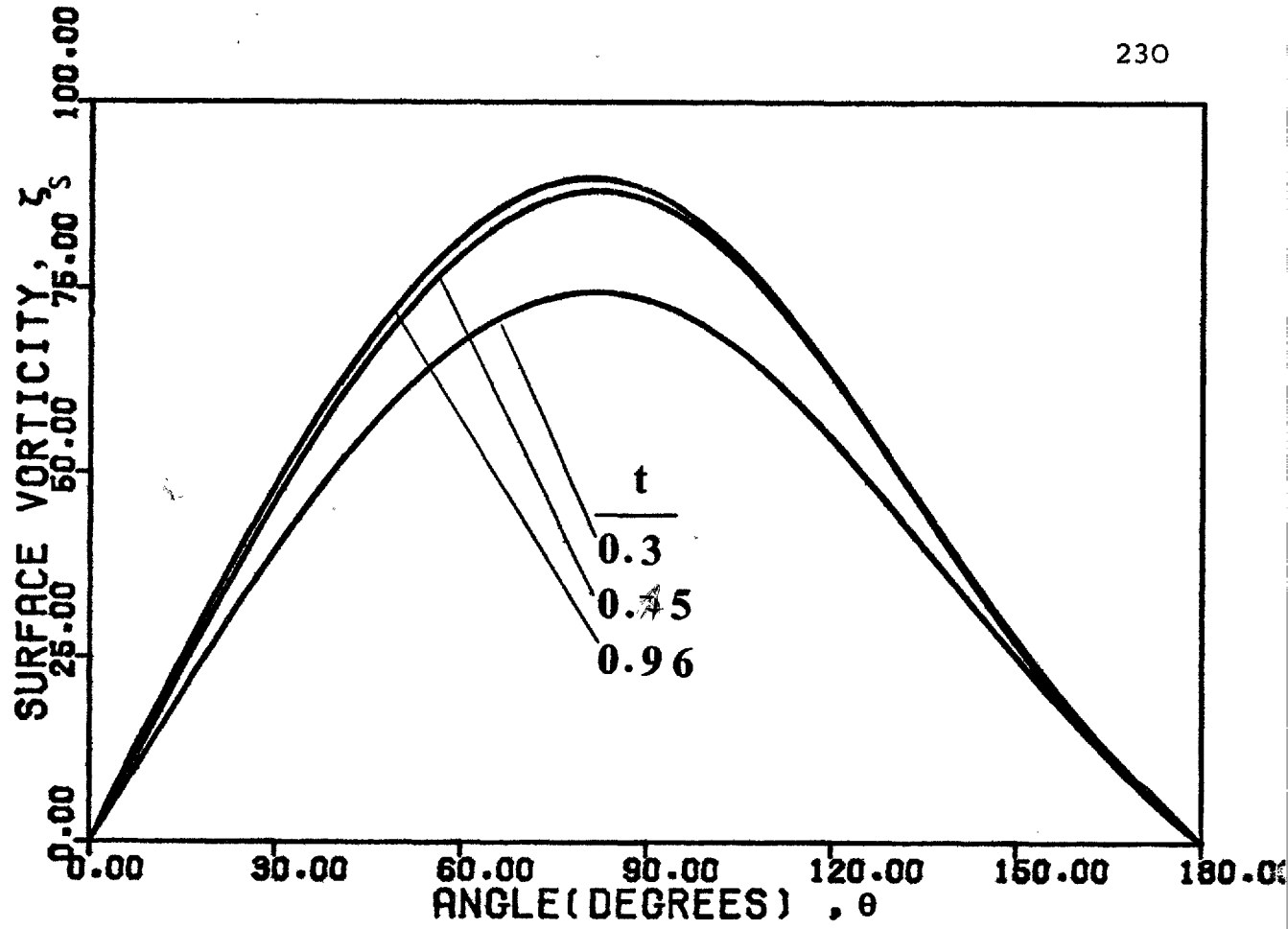

FIGURE 4.9.7 SURFACE VORTICITY VERSUS TIME AT GRASHOF NUMBER OF 125 AND PRANDTL NUMBER OF 0.72

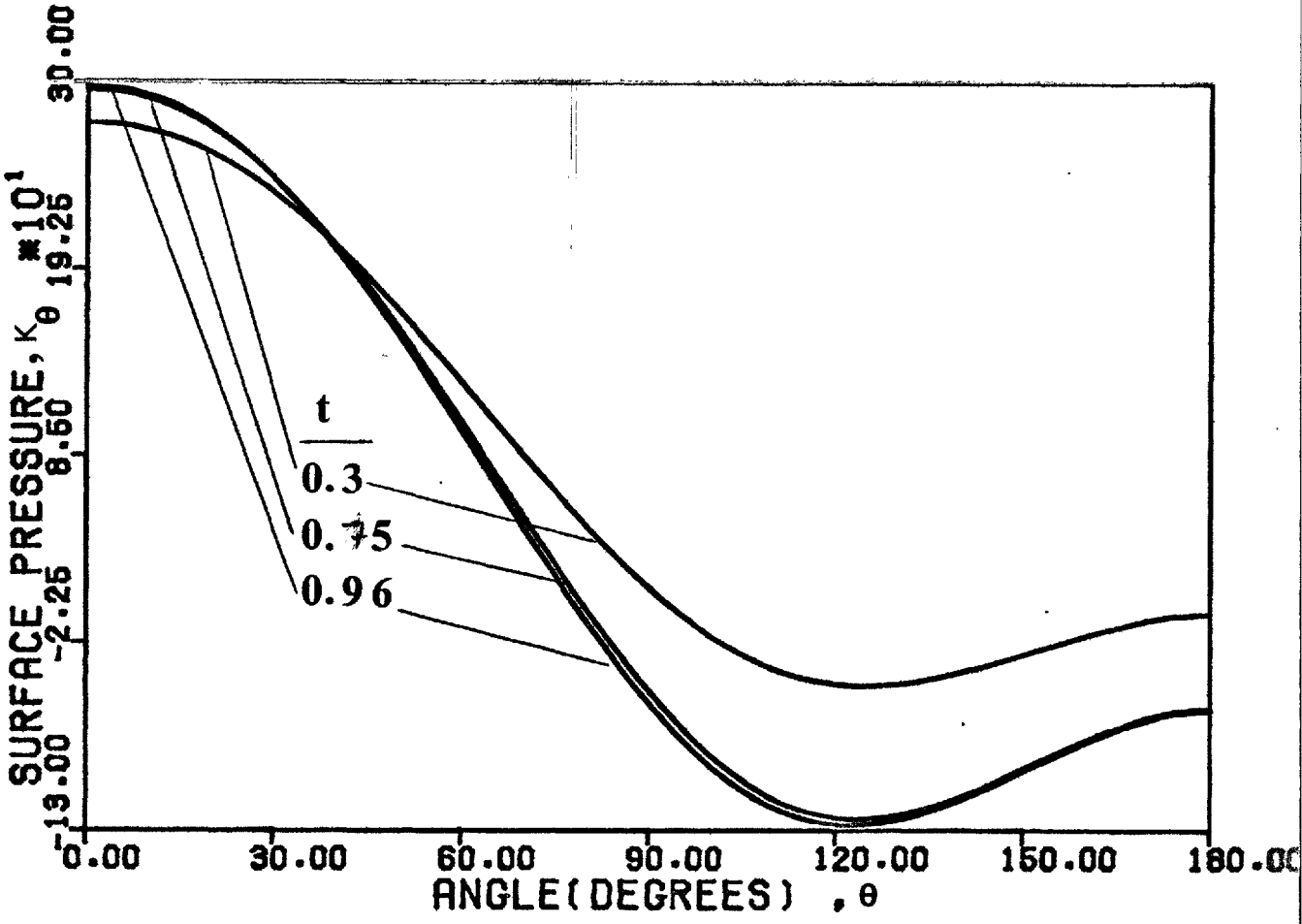

FIGURE 4.9.6 SURFACE PRESSURE VERSUS TIME AT GRASHOF NUMBER OF 125 AND PRANDTL NUMBER OF 0.72

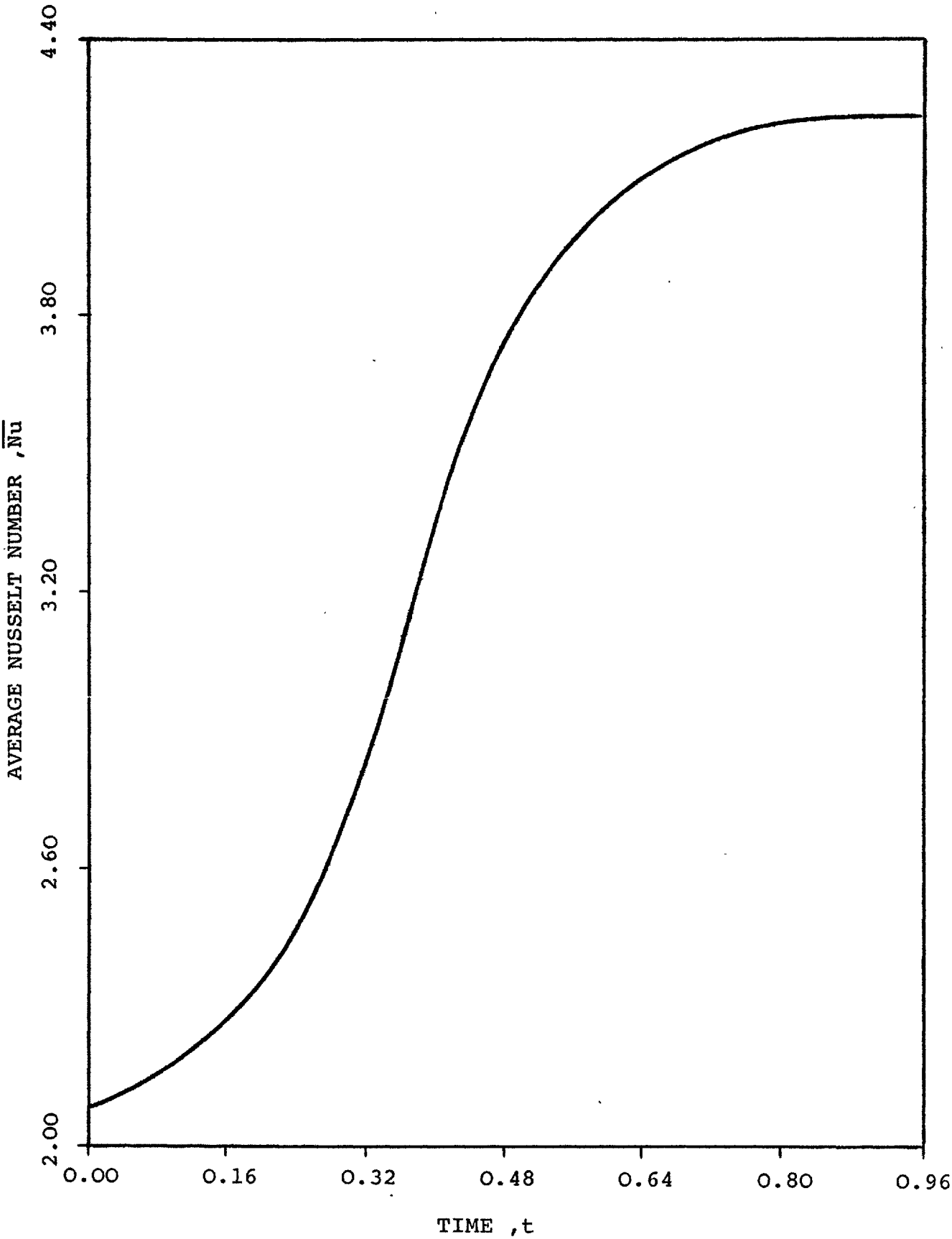

FIGURE 4.9.8 AVERAGE NUSSELT NUMBER VERSUS TIME AT GRASHOF NUMBER OF 125 AND PRANDTL NUMBER OF 0.72

minimum at an angle of 120 degrees.

Figure 4.9.7 shows the variation of surface vorticity with time. During the early stages of simulation, radial diffusion is the dominant mode of vorticity transport. The late-time steady state surface vorticity distribution shows a slight asymmetry between the upstream and downstream regions of the sphere.

It is clear that flow characteristics such as surface vorticity, surface pressure, drag coefficients, and local and average Nusselt numbers are dependent upon the velocity and temperature distributions. As velocity and temperature change with time, the flow characteristics also change with time. However, the solutions obtained for Grashof numbers greater than 1, show that the drag coefficients, the surface pressure, and the surface vorticity are relatively less sensitive to small variations in the velocity and temperature distributions than the local Nusselt number. In particular, tables 9 to 13 show that the relative difference in the local Nusselt numbers from one time-level to the next is greater than the relative differences exhibited by the other flow characteristics. Furthermore, the most important quantities in heat transfer problems are the local and the average Nusselt numbers. For the above reasons the approach to the late-time steady state condition in the present work, was best judged by observing the relative variation of the local Nusselt number with dimensionless time.

4.10 NUMERICAL SOLUTION FOR A GRASHOF NUMBER OF 1250 AND A PRANDTL NUMBER OF 10

The development with time of the streamlines around a solid sphere for free convection at a Grashof number of 1250 and a Prandtl number of 10 can be seen in figures 4.10.1a to 4.10.1d. The development with time of the flow patterns around the solid sphere is similar to those described in previous sections. As in the previous cases, the stream function contours at late-time steady state condition are displaced slightly to the downstream region of the flow field. This can be observed from figure 4.10.1d.

The development with time of the isotherms around the solid sphere starting from steady state radial conduction is shown in figures 4.10.2a to 4.10.2d. As expected, conduction is the dominant mode of transfer during the early stages of simulation and heat is mainly transferred by unsteady conduction in all directions. This is shown by figure 4.10.2a. However, as simulation continues, the thickness of heated layer adjacent to the upstream region of the sphere decreases with time whereas, the thickness of the heated layer of fluid adjacent to the downstream region of the solid sphere continues to increase and forms a region of heated fluid which extends downstream to the vicinity of the outer boundary.

The generation, diffusion, and convection of vorticity

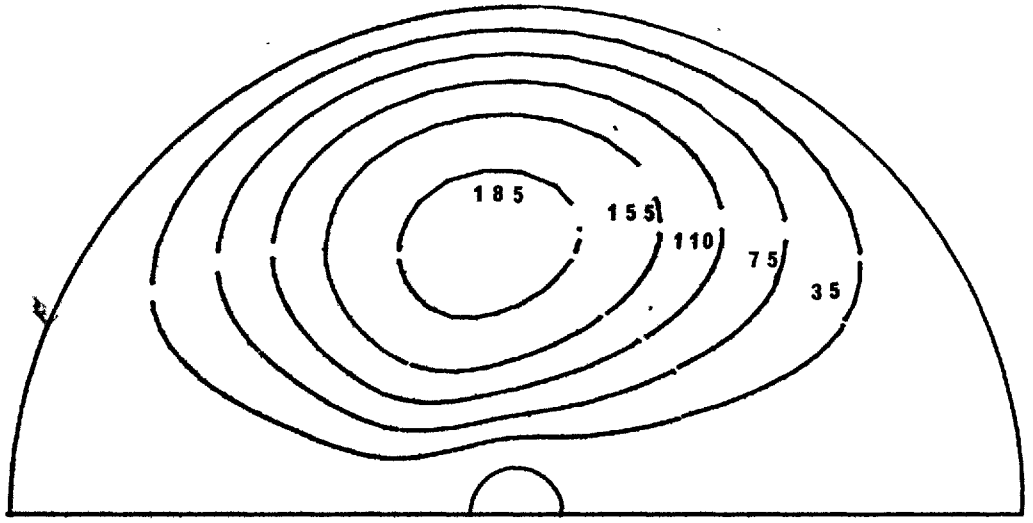

FIGURE 4.10.1b STREAMLINES AROUND THE SPHERE AT GRASHOF NUMBER OF 1250 AND PRANDTL NUMBER OF 10 DIMENSIONLESS TIME , $t = 0.1$

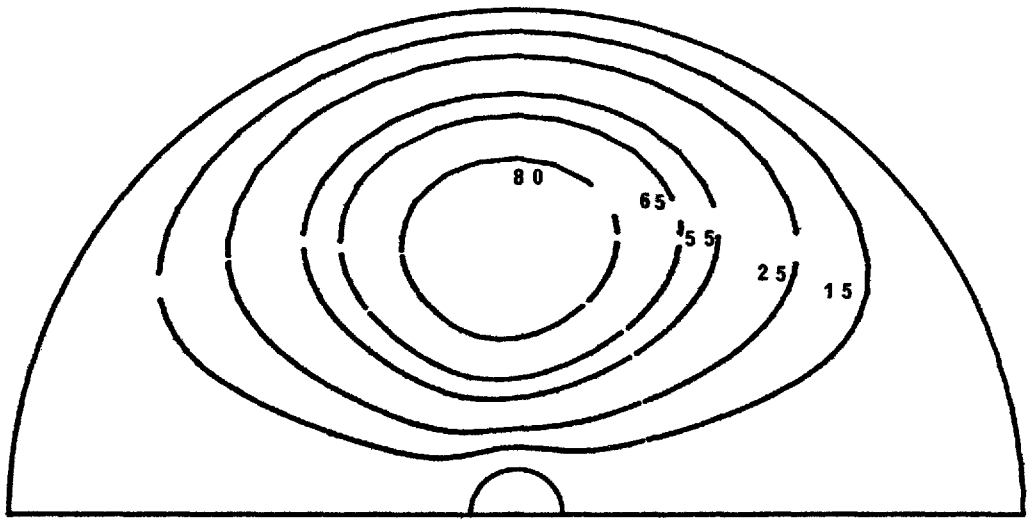

FIGURE 4.10.1a STREAMLINES AROUND THE SPHERE AT GRASHOF NUMBER OF 1250 AND PRANDTL NUMBER OF 10 DIMENSIONLESS TIME , $t = 0.05$

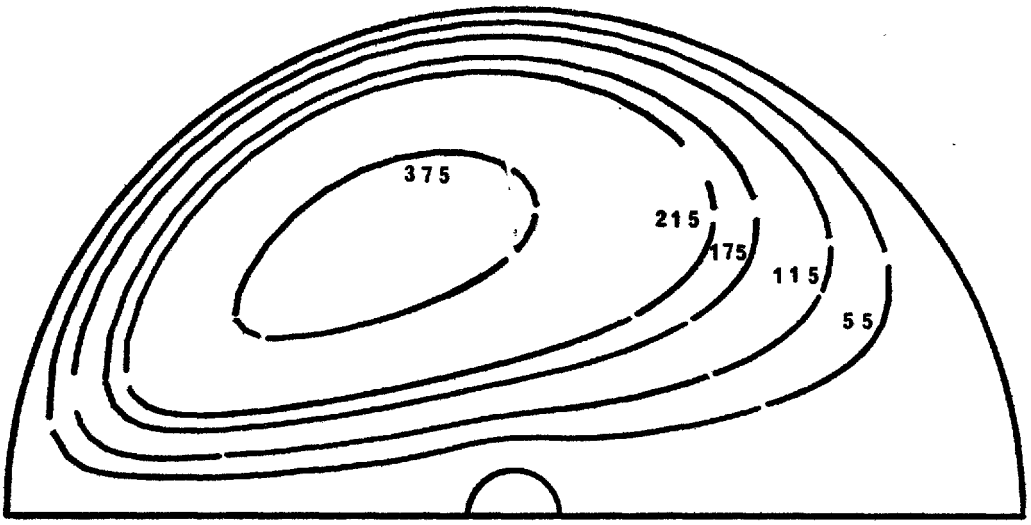

FIGURE 4.10.1d STREAMLINES AROUND THE SPHERE AT GRASHOF NUMBER OF 1250 AND PRANDTL NUMBER OF 10 DIMENSIONLESS TIME , $t = 0.24$

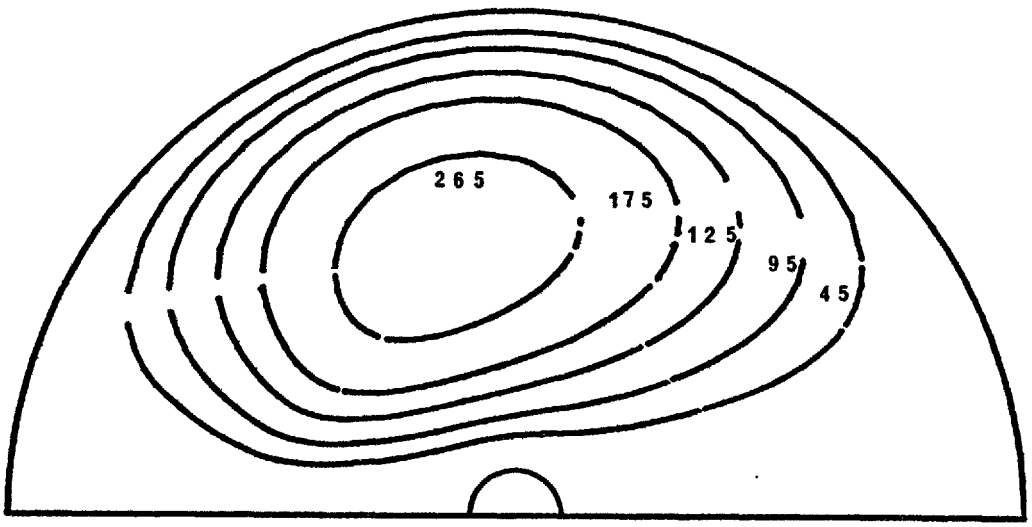

FIGURE 4.10.1c STREAMLINES AROUND THE SPHERE AT GRASHOF NUMBER OF 1250 AND PRANDTL NUMBER OF 10 DIMENSIONLESS TIME , $t = 0.15$

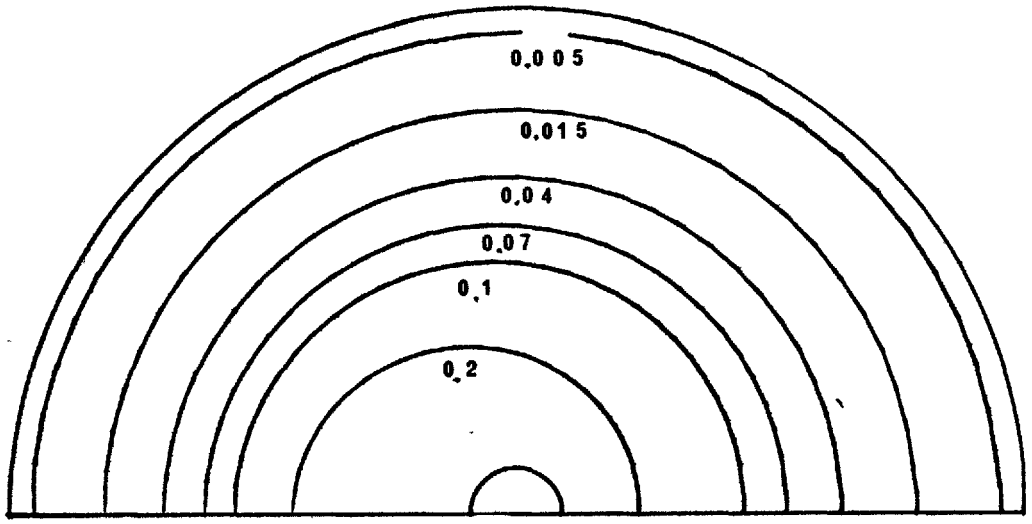

FIGURE 4.10.2b ISOTHERMS AROUND THE SPHERE AT GRASHOF NUMBER OF 1250 AND PRANDTL NUMBER OF 10 DIMENSIONLESS TIME . $t = 0.1$

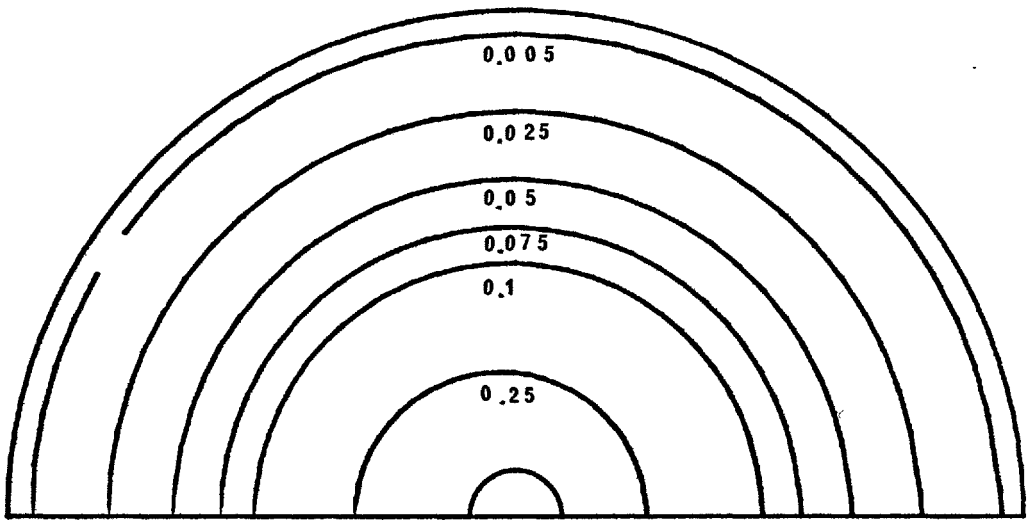

FIGURE 4.10.2a ISOTHERMS AROUND THE SPHERE AT GRASHOF NUMBER OF 1250 AND PRANDTL NUMBER OF 10 DIMENSIONLESS TIME . $t = 0.05$

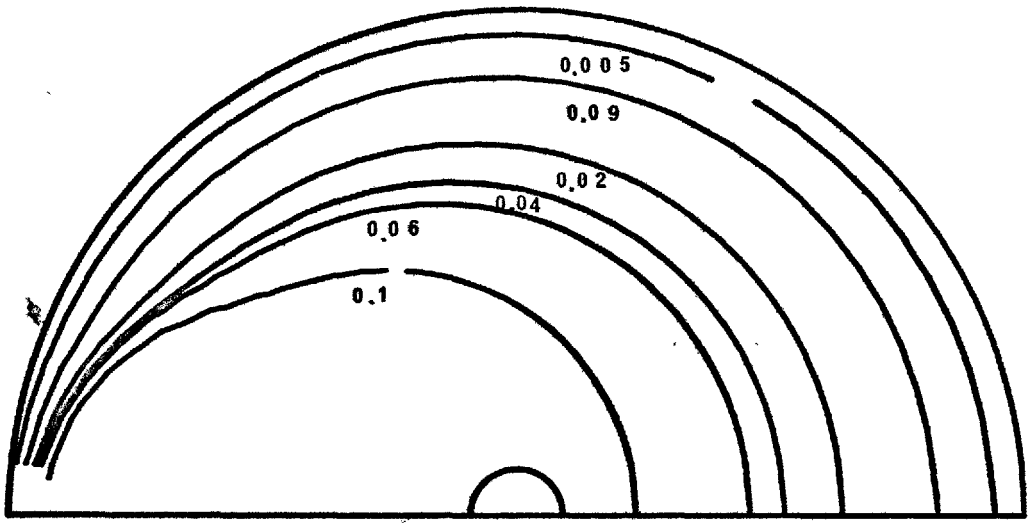

FIGURE 4.10.2d ISOTHERMS AROUND THE SPHERE AT GRASHOF NUMBER OF 1250 AND PRANDTL NUMBER OF 10 DIMENSIONLESS TIME , $t = 0.24$

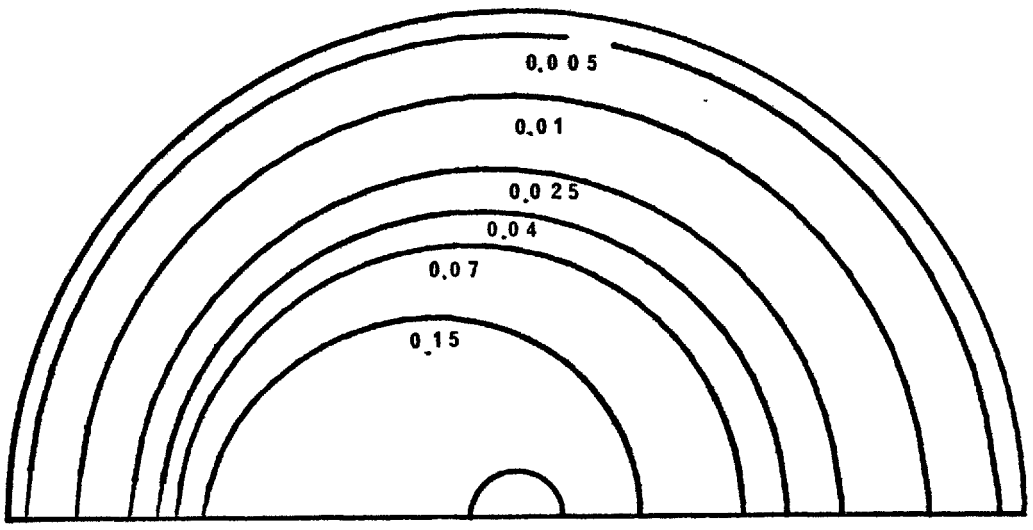

FIGURE 4.10.2c ISOTHERMS AROUND THE SPHERE AT GRASHOF NUMBER OF 1250 AND PRANDTL NUMBER OF 10 DIMENSIONLESS TIME , $t = 0.15$

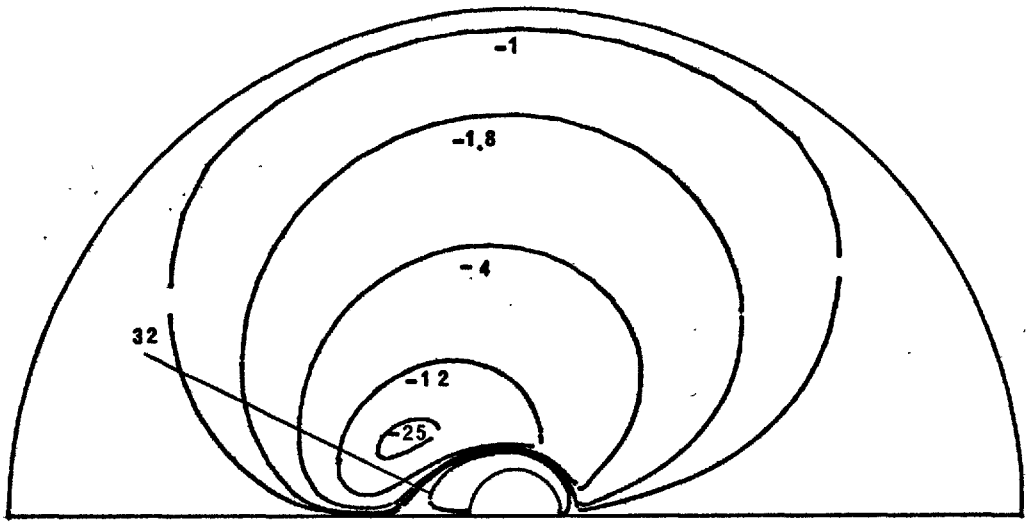

FIGURE 4.10.3b VORTICITY DISTRIBUTION AROUND THE SPHERE AT GRASHOF NUMBER OF 1250 AND PRANDTL NUMBER OF 10 DIMENSIONLESS TIME , $t = 0.1$

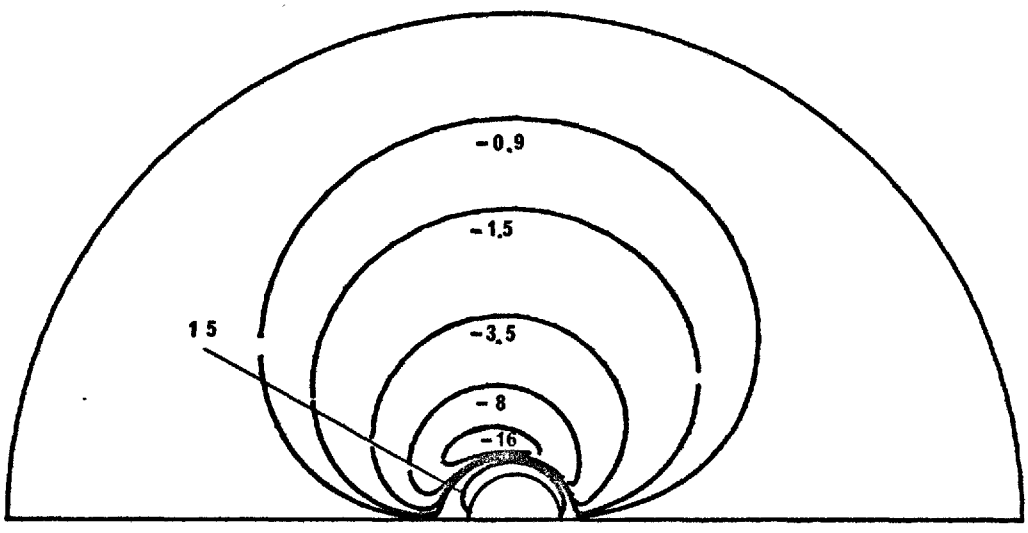

FIGURE 4.10.3a VORTICITY DISTRIBUTION AROUND THE SPHERE AT GRASHOF NUMBER OF 1250 AND PRANDTL NUMBER OF 10 DIMENSIONLESS TIME , $t = 0.05$

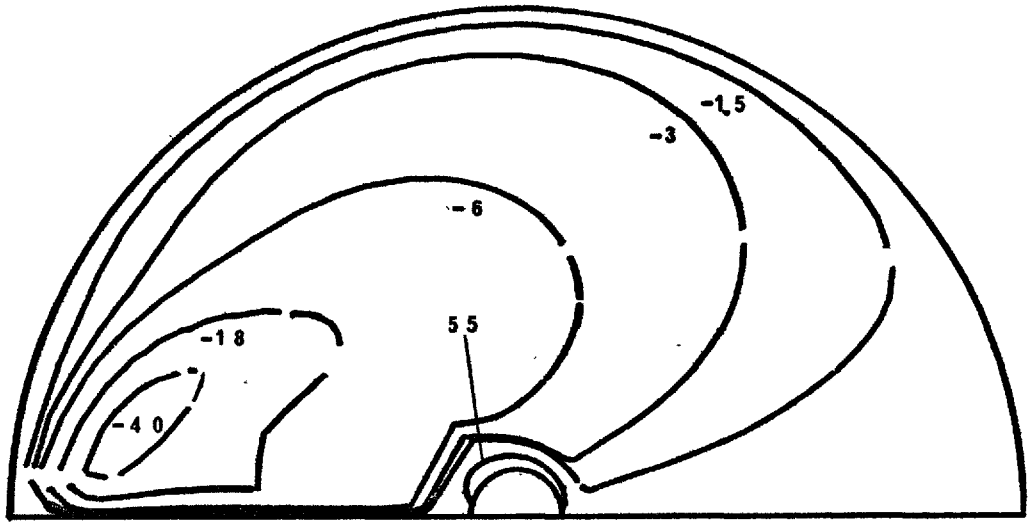

FIGURE 4.10.3d VORTICITY DISTRIBUTION AROUND THE SPHERE AT GRASHOF NUMBER OF 1250 AND PRANDTL NUMBER OF 10 DIMENSIONLESS TIME . $t = 0.24$

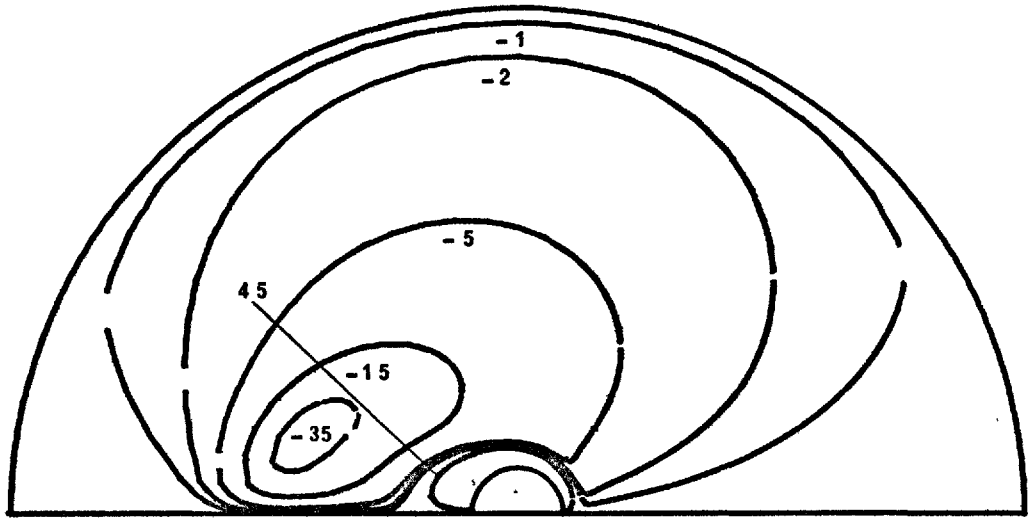

FIGURE 4.10.3c VORTICITY DISTRIBUTION AROUND THE SPHERE AT GRASHOF NUMBER OF 1250 AND PRANDTL NUMBER OF 10 DIMENSIONLESS TIME . $t = 0.15$

around the solid sphere can be seen in figures 4.10.3a to 4.10.3d which show the vorticity contours as a function of time. During the initial stages of simulation, the vorticity contours are regular and, since during this period the dominant mode of vorticity transport is diffusion, the vorticity contours are symmetrically distributed about an imaginary plane situated between the upstream and downstream regions of the flow field. However, as integration proceeds with time the effects of vorticity convection increase and the vorticity is convected more and more downstream. The late-time steady state vorticity distribution shown in figure 4.10.3d at a dimensionless time of 0.24 is more influenced by convection than the distributions obtained for smaller Grashof numbers.

The variation with time of the drag coefficients is shown in figure 4.10.4. Both the form drag and viscous drag coefficients increase rapidly towards their late-time steady state values which they reach at a dimensionless time of almost 0.14. However, simulation was continued to a much larger time since relative changes in the surface vorticity, the surface pressure, and, in particular, in the local Nusselt number still continued to occur during the dimensionless time period of 0.15 to 0.24. This can be observed from table 13 which represents the late-time values of the above variables during the time period of 0.15 to 0.24.

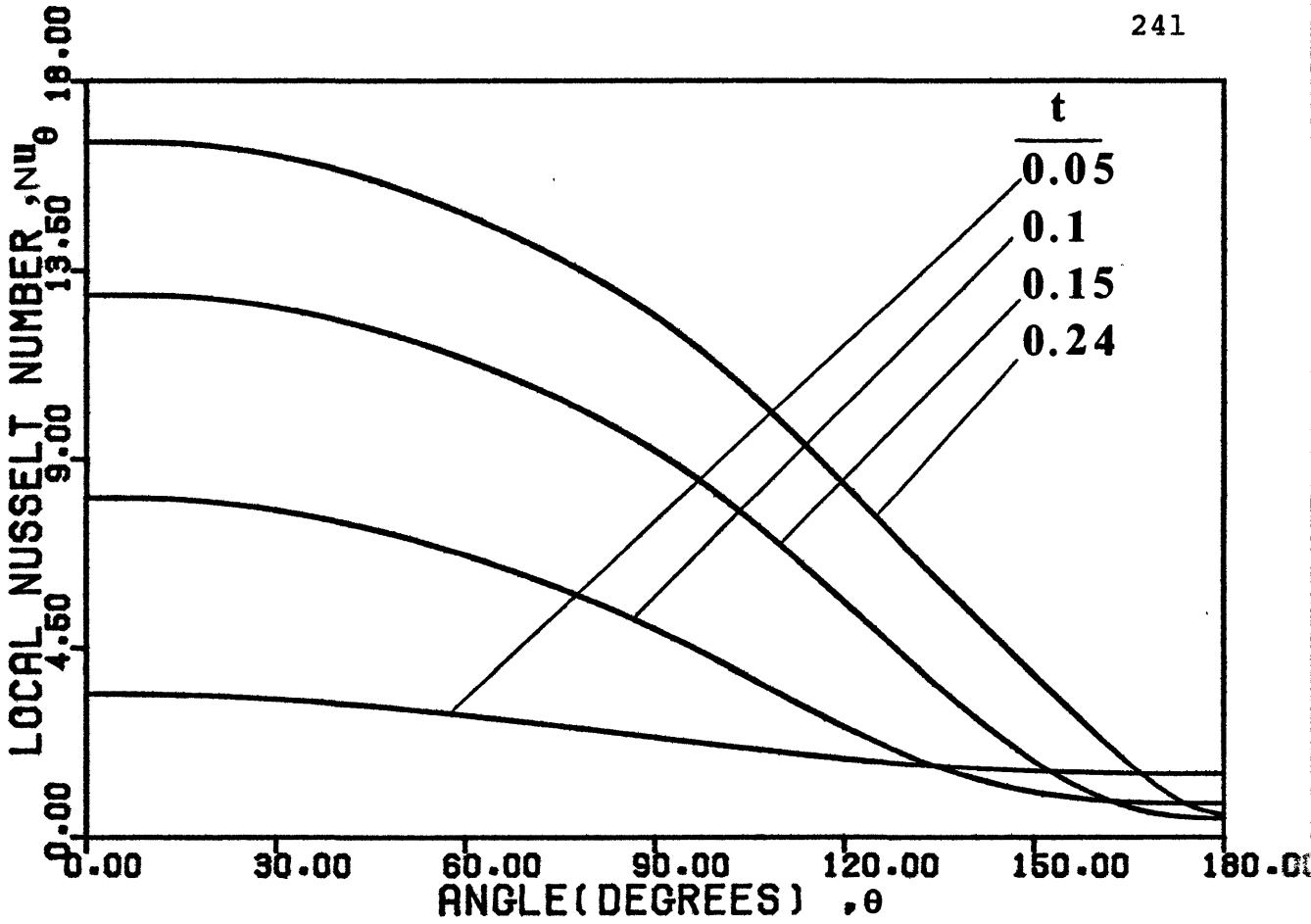

FIGURE 4.10.5 LOCAL NUSSELT NUMBER VERSUS TIME AT GRASHOF NUMBER OF 1250 AND PRANDTL NUMBER OF 10

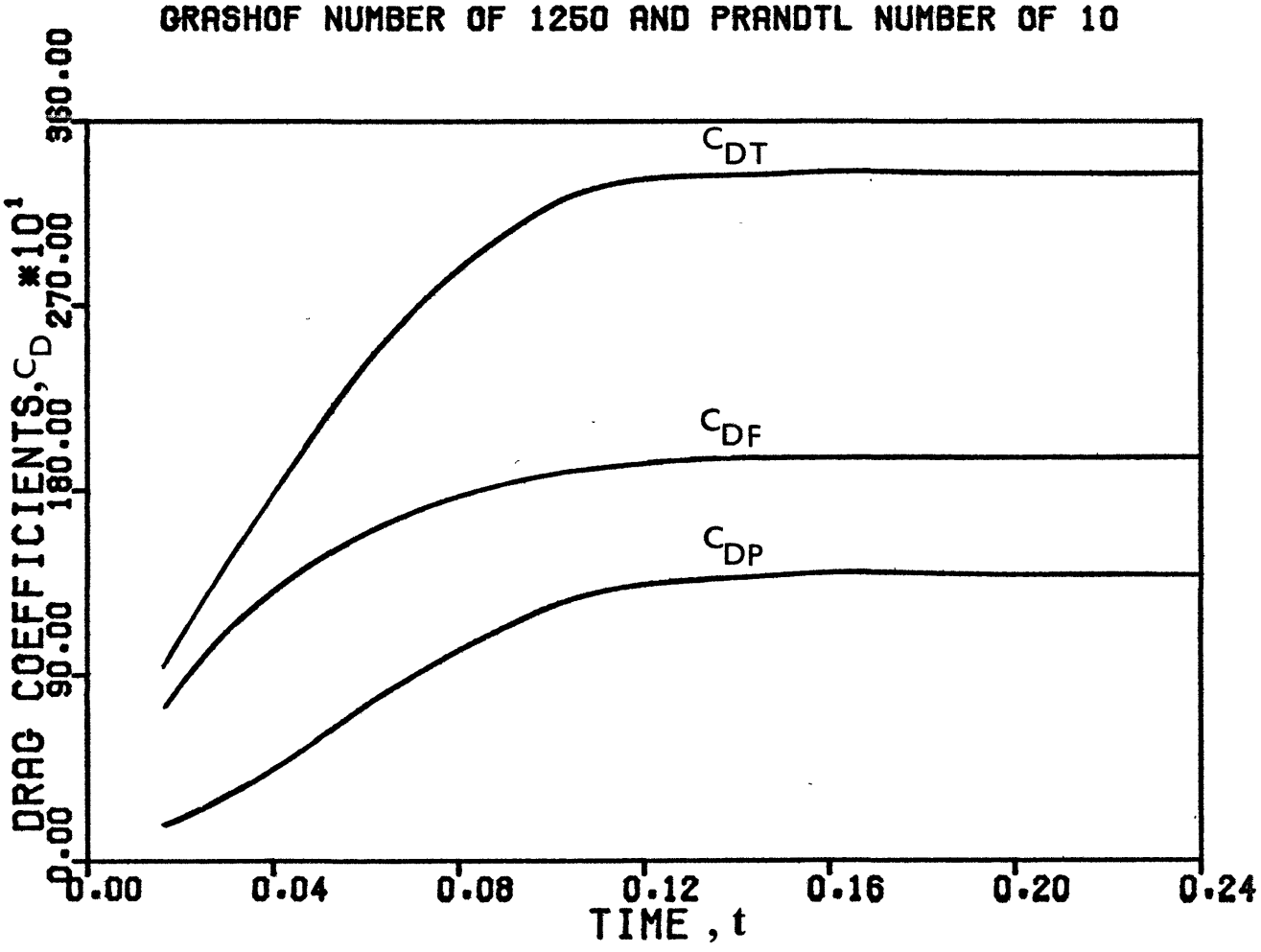

FIGURE 4.10.4 DRAG COEFFICIENTS VERSUS TIME AT GRASHOF NUMBER OF 1250 AND PRANDTL NUMBER OF 10

It is observed for a Grashof number of 1250 and a Prandtl number of 10 the total dimensionless time taken for the solution to reach its late-time steady state condition is much shorter than that for a Grashof number of 125 and a Prandtl number of 0.72. This is accordance with the reasoning given earlier which related the total dimensionless time taken before late-time steady state conditions are reached to the inverse of the Grashof number. The larger Grashof number gives rise to larger velocities which in turn, accelerate the simulation.

The variation with time of the local Nusselt number is shown in figure 4.10.5. During the early stages of simulation, heat transfer takes place mainly by unsteady state conduction. This can be seen by examination of the distribution of the local Nusselt number at dimensionless time of 0.05 shown in figure 4.10.5 which shows that the local Nusselt number is almost constant around the sphere surface. As integration proceeds with time, the local Nusselt number for the upstream region of the sphere increase until their late-time steady state values are reached. During the same period of time, the local Nusselt numbers, for the downstream region of the sphere decrease at first but increase as the late-time steady state condition is approached.

All the solutions obtained so far show that the local Nusselt number at late-time steady state condition decreases

as the angle Θ, measured from the front stagnation point, increases. This behaviour is conceivable from the following physical consideration. At lower values of Θ, relatively cooler fluid moves towards the sphere surface and this causes a higher rate of heat transfer. As the angle Θ, increases the fluid becomes warmer and this in turn, causes a lower rate of heat transfer. From the plots given for the variation of local Nusselt number as a function of time, it is also observed that the change in the local Nusselt number with the angle is much greater at higher values of the Grashof number than at lower values. This behaviour indicates that at relatively low Grashof numbers, heat transfer takes place partly by conduction and partly by convection. However, at higher Grashof number heat is transferred mainly by convection with relatively little contribution by conduction.

The behaviour of the average Nusselt number with time is shown in figure 4.10.8. The average Nusselt number starts from a value of 2.085 and increases with time to its late-time steady state value.

The variations with time of the surface pressure and surface vorticity are shown in figures 4.10.6 and 4.10.7, respectively. It is seen from figure 4.10.6 that as integration proceeds with time, the surface pressure increases in the upstream region and decreases in the downstream region. The distribution shows a shallow

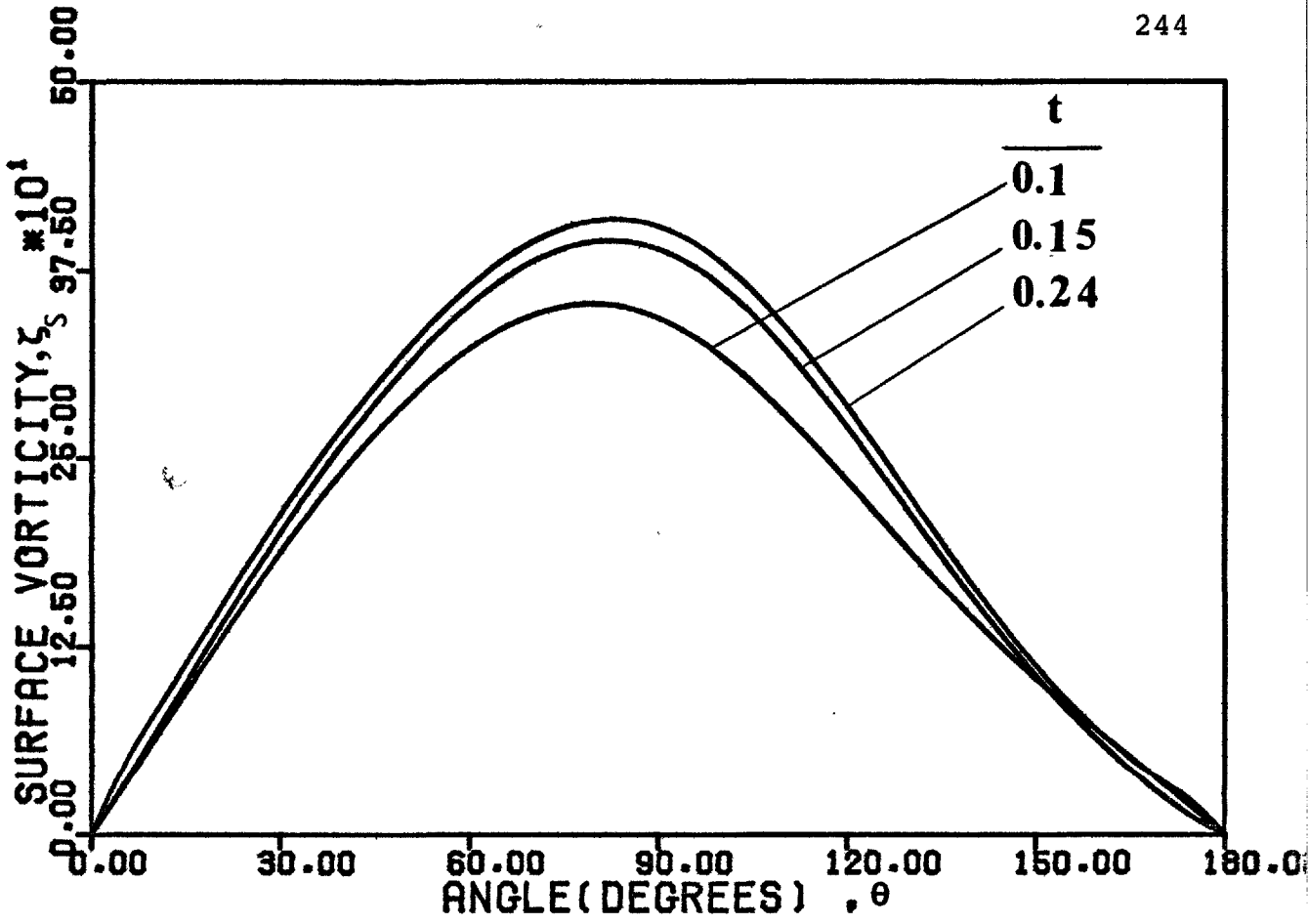

FIGURE 4.10.7 SURFACE VORTICITY VERSUS TIME AT GRASHOF NUMBER OF 1250 AND PRANDTL NUMBER OF 10

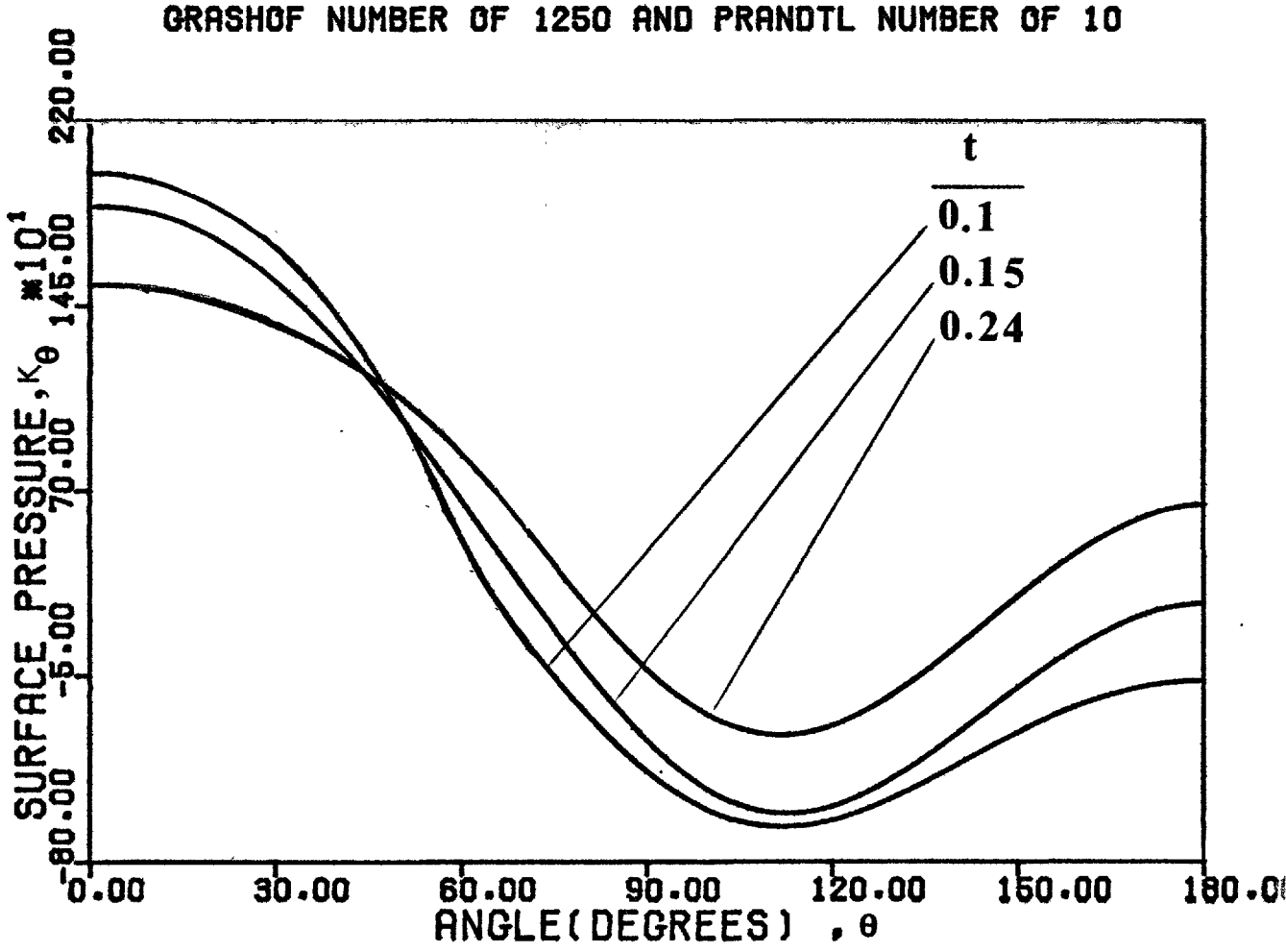

FIGURE 4.10.6 SURFACE PRESSURE VERSUS TIME AT GRASHOF NUMBER OF 1250 AND PRANDTL NUMBER OF 10

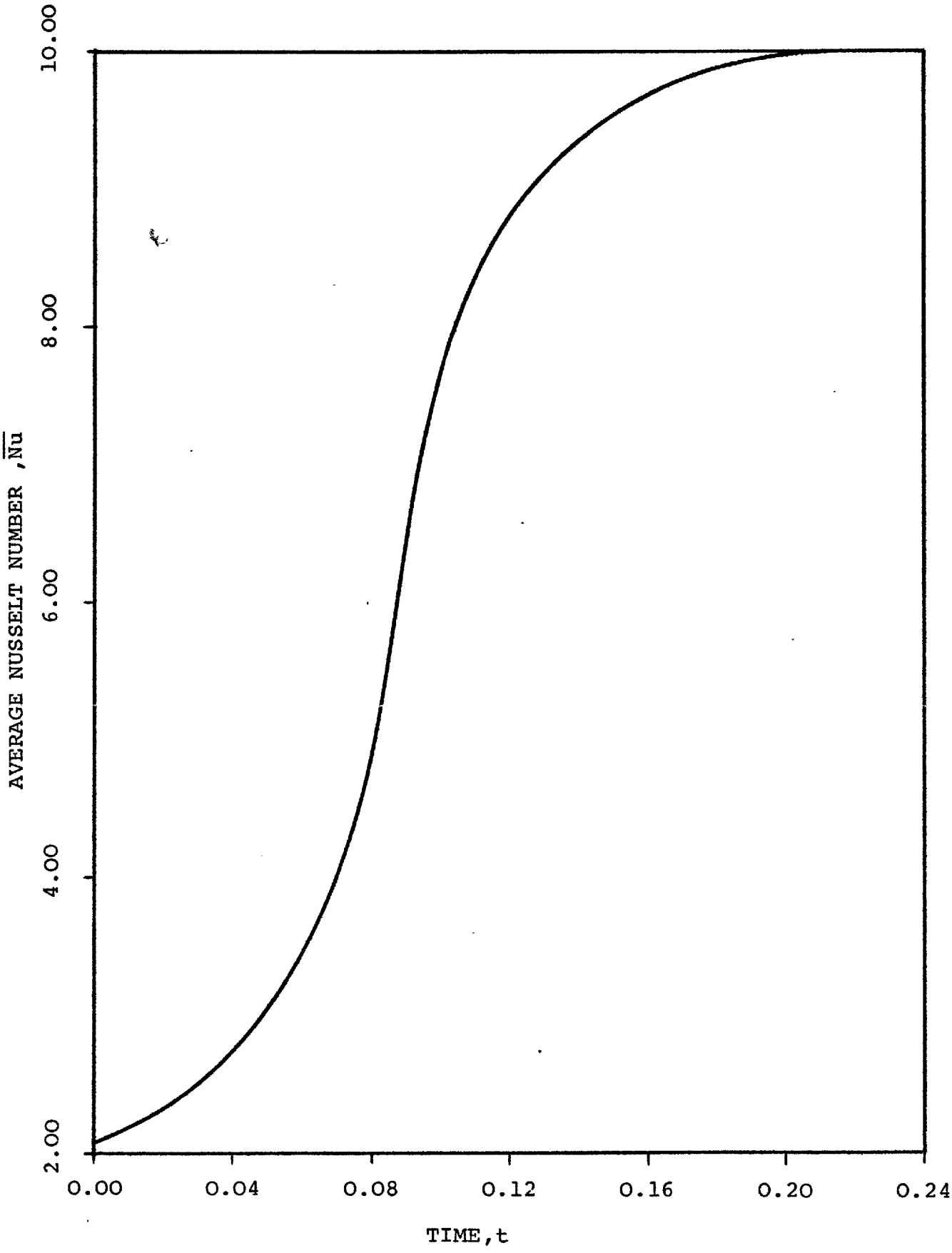

FIGURE 4.10.8 AVERAGE NUSSELT NUMBER VERSUS TIME AT GRASHOF NUMBER OF 1250 AND PRANDTL NUMBER OF 10

minimum at angle of 110^{o}.

Comparison of the late-time steady state surface vorticity distribution for a Grashof number of 125 and a Prandtl number of 0.72 with that for a Grashof number of 1250 and Prandtl number of 10 solution, figures 4.9.7 and 4.10.7, respectively, shows greater asymmetry between the upstream and the downstream flow regions in the case of a Grashof number of 1250 and a Prandtl number of 10.

4.11 ADDITIONAL SOLUTIONS

To examine the capability of the numerical technique used and the computer programme developed in this thesis, additional solutions for a relatively larger Grashof number of 12500 and a Prandtl number of 10 and a solution for a Grashof number of 50 and a relatively larger Prandtl number of 100 were obtained. These solution will now be discussed.

The development with time of the stream function, temperature, and vorticity around a heated solid sphere in conditions of free convection to a Newtonian medium starting from a motionless flow at a Grashof number of 12500 and a Prandtl number of 10 were similar to those described for a Grashof number of 1250 and a Prandtl number of 10. After an initial period in which radial conduction of heat and radial diffusion of vorticity

dominate the transport processes, convective effects become the dominant mode of transfer. At the late-time steady state condition, as was expected, the effects of convection were more pronounced than in previous cases in which the Grashof numbers were smaller. In particular, the surface vorticity showed greater asymmetry between the upstream and downstream regions in comparison with the previous cases. However, the variations of the surface pressure, the drag coefficients, the local and the average Nusselt numbers with time followed similar patterns to those obrained for a Grashof number of 1250 and a Prandtl number of 10. The total dimensionless time taken before the late-time steady state condition was reached was found to be 0.09 which was shorter than those for the cases already described. The main results obtained for the solution of a Grashof number of 12500 and a Prandtl number of 10 are presented in table 6.

The solution obtained for a Grashof number of 50 and a Prandtl number of 100 is slightly different from the solution obtained for a Grashof number of 50 and a Prandtl number of 0.72. During the early stages of the simulation, conduction was the dominant mode of heat transfer but as simulation continued, the fluid velocity and the convective effects increased and the thickness of the heated region upstream of the sphere in the immediate vicinity of the sphere surface decreased with time. However, the heated

region downstream of the sphere extended with time. As may be expected, it was observed that the thickness of heated layer adjacent to the upstream region of the solid sphere for a Grashof number of 50 and a Prandtl number of 100 was less than that for a Grashof number of 50 and a Prandtl number of 0.72. However, the reverse was the case in the downstream region.

The variation with time of the surface vorticity, the surface pressure, the drag coefficients, the local Nusselt number, and the average Nusselt number followed a similar pattern to those described for the Grashof number of 50 and Prandtl number of 0.72. The local Nusselt number around the solid sphere remained fairly constant during the early stages of heat transfer. However, as simulation continued, the local Nusselt numbers over the upstream region of the sphere increased until their late-time steady state values were attained. During the same period the local Nusselt numbers over the downstream region of the sphere decreased at first but increased as the late-time steady state condition was approached. Late-time steady state values of the local Nusselt numbers at the front and rear stagnation points were found to be 16.4 and 0.39, respectively. The main results obtained for a Grashof number of 50 and a Prandtl number of 100 are presented in table 6.

4.12 GENERAL DISCUSSION

In chapter 2, it was observed that experimental studies of free convective heat transfer from solid bodies have been directed primarily towards obtaining correlations which express the average rates of heat transfer in terms of dimensionless groups which specify the system. These dimensionless groups for free convection are the average Nusselt number, $\overline{Nu}$, the Grashof number, Gr, and the Prandtl number, Pr. The correlations usually take the following form:

$$\overline{Nu} = A + BGr^{n_1} Pr^{n_2} \qquad (4.12.1)$$

For generality and ease of use, it is desireable to present a relationship between the average Nusselt numbers obtained in this work, and the Grashof and the Prandtl numbers, in the form of expression (4.12.1).

The constant A in equation (4.12.1) may be considered to be the value of the average Nusselt number that would be obtained in the limiting case of zero Grashof number. This limiting case would thus be that of steady state conduction from a heated solid sphere to an infinite stagnant medium of lower temperature for which the average Nusselt number has a value of 2.

To determine the best values of the constant B and the exponents n_1 and n_2 of the equation (4.12.1), extensive computer experiments, based on the late-time steady state average Nusselt numbers obtained from the numerical solutions

of the time-dependent and time-independent equations were carried out. The computer experiments revealed that it was not possible to find a single relationship which fitted the data for the wide range of Grashof numbers used in this thesis. Two different relationships were used as follows:

$$\overline{Nu} = 2 + 0.39562(Ra)^{0.42} \qquad (4.12.2)$$

for:

$$0.035 \ll Ra \ll 36$$
$$0.05 \ll Gr \ll 50$$
$$0.7 \ll Pr \ll 100 \qquad (4.12.3)$$

and;

$$\overline{Nu} = 2 + 0.75159(Ra)^{0.25} \qquad (4.12.4)$$

for:

$$36 \ll Ra \ll 125000$$
$$50 \ll Gr \ll 12500$$
$$0.7 \ll Pr \ll 100 \qquad (4.12.5)$$

where: $Ra = Gr \times Pr$.

Figure 4.12.1 shows the variation of the late-time steady state average Nusselt number with Grashof number, for a Prandtl number of 0.72. The analytical solution of Hossain (1966), and experimental data of Mathers et al (1957), Tsubouchi and Sato (1960), and Yuge (1960) are also included in figure 4.12.1.

Figure 4.12.2 shows the variation of the late-time steady state average Nusselt number obtained in this work

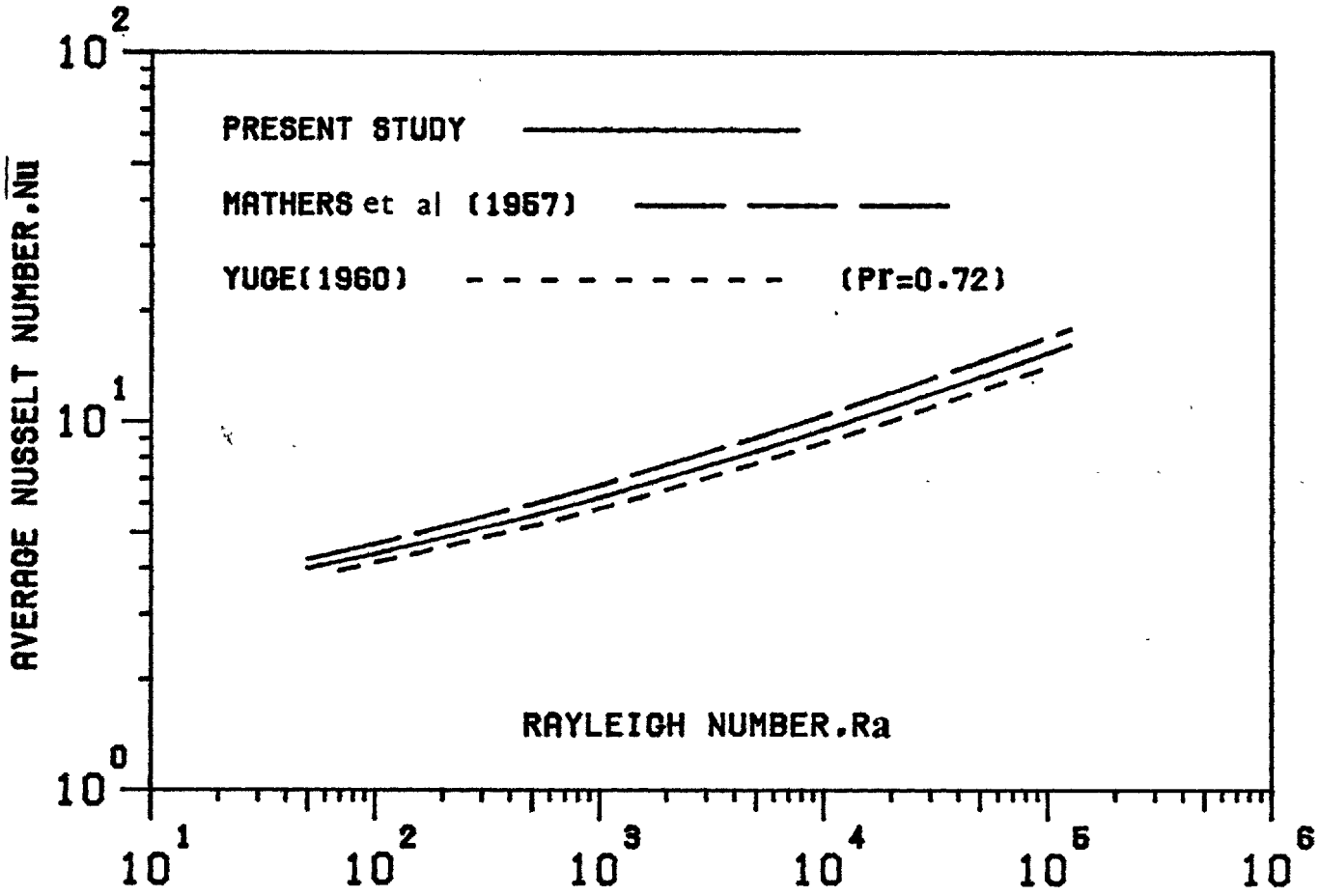

FIGURE 4.12.2 COMPARISON OF AVERAGE NUSSELT NUMBER

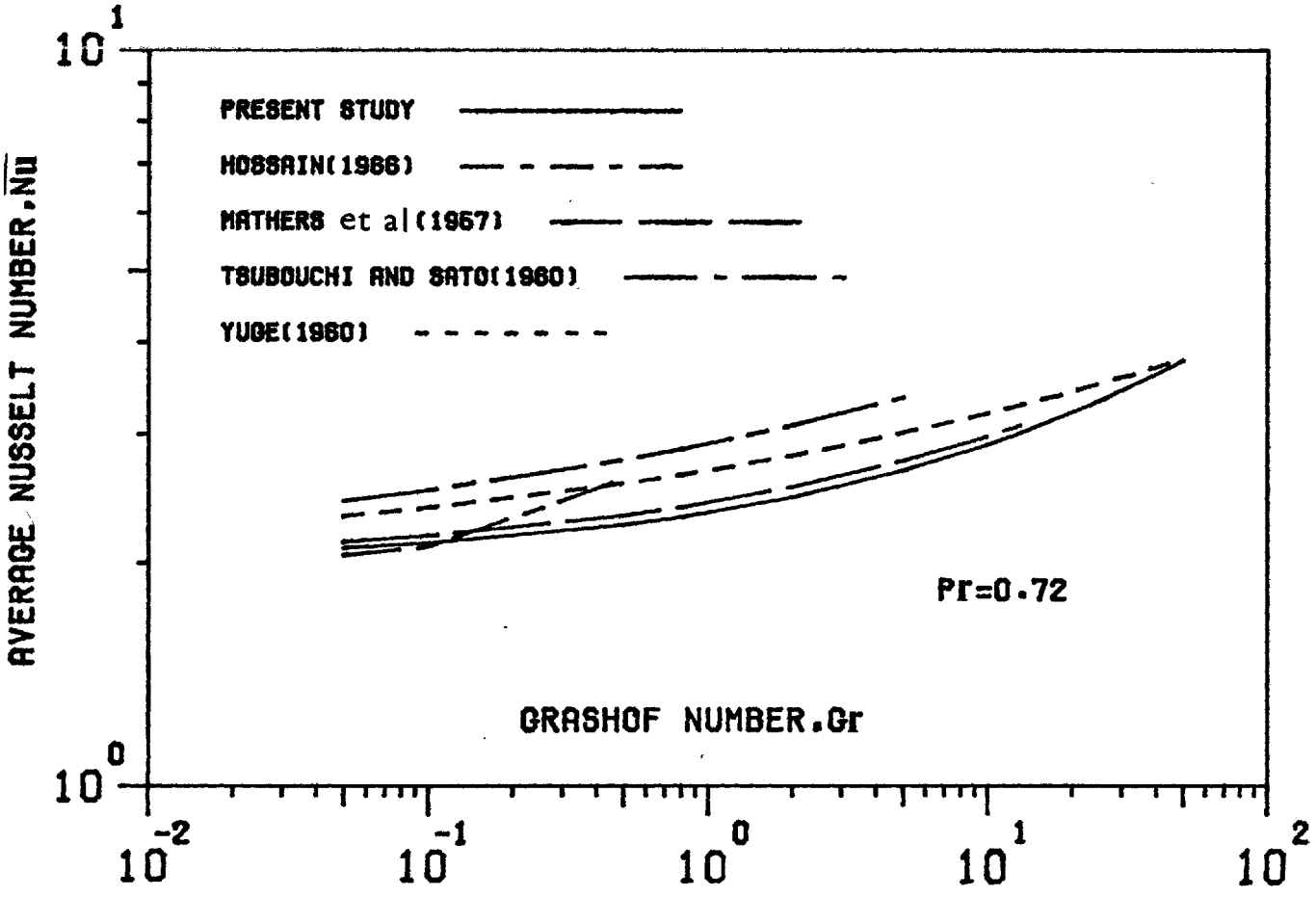

FIGURE 4.12.1 LOG($\overline{Nu}$) VERSUS LOG(Gr)

with Rayleigh number, Ra. In figure 4.12.2, experimental results of Yuge (1960), (for Pr=0.72) and Mathers et al (1957) are also plotted for comparison purposes. The present solutions predict lower values of the average Nusselt number than the experimental measurements shown in figure 4.12.1 and 4.12.2. The maximum difference, relative to the results of Mathers et al is about 11%; relative to the results of Tsubouchi and Sato and to the results of Ranz and Marshall it is about 20%.

It must be noted that most experimental measurements of free convective heat transfer rates are influenced by forced convection and suffer from losses due to conduction and radiaiton leading to overestimation of values of the average Nusselt number. It is possible that the lower experimental values of the Nusselt numbers shown in figures 4.12.1 and 4.12.2 are the most likely to be correct. Furthermore, the properties of the system, such as; fluid density, viscosity, and thermal conductivity are frequently not known accurately enough to give accurate evaluations of the average Nusselt number.

As a check on the accuracy of the numerical solutions a few numerical tests were conducted as follows:

Dimensionless surface pressures were computed using two different methods. In the first method the surface pressures were calculated from the vorticity values as

expressed by equation (B.3.8) in appendix B. In the second method the calculation was based on the stream function values as expressed by equation (B.3.14). The difference between the surface pressure values obtained using the two different methods was in the region of 1% to 15% based on the values obtained from equation (B.3.8). To determine the cause of the above discreponcy, numerous computational experiments were carried out from which the following conclusion was drawn.

The numerical solutions of the equations of free convective heat transfer from a solid sphere presented in this thesis give a good approximation of the local values of the temperature, the stream function, and the vorticity. Using these values, it is possible to obtain good approximations of the first order derivatives of the temperature, the stream function, and the vorticity. The second and higher order derivatives of these variables are less accurate and any integration which requires second order and, in particular, higher order derivatives, will yield inaccurate results.

In order to provide a further check on the accuracy of the numerical solutions the following first order derivatives were calculated from the solutions: the first order derivative of temperature with respect to angle, Θ, along the axis of symmetry; the first order derivatives

of the stream function along the surface of the sphere and on the axis of symmetry with respect to θ and z; and the first order derivative of vorticity with respect to θ along the axis of symmetry. For all the solutions, the values of the above derivatives were found to have a magnitude of 10^{-10} to 10^{-20} and to be relatively close to the required value of zero.

The average central processor time required to obtain a late-time steady state solution was found to be approximately three and half hours when using the University of London Computer Centre's CDC7600 digital computer.

4.13 TIME-INDEPENDENT SOLUTIONS

The numerical technique developed for the solution of the time-independent equations provided solutions which for Grashof numbers up to 25 were in reasonable agreement with the late-time solutions of the time-dependent equations. For Grashof numbers of 10 and 25, some vorticity fluctuations were noticed close to the outer boundary. This fluctuation behaviour has been recorded by other authors working on the numerical calculation of flow fields. It is generally known, however, that as long as the magnitude of the fluctuations is relatively small, it is unlikely that the solution, and, in particular, the derived flow characteristics close to sphere surface, will be affected. However, the surface vorticity and, as a consequence, the surface pressure, and

the drag coefficients were slightly affected by the fluctuations of the vorticity at the outer boundary, in the solution obtained for a Grashof number of 50 and a Prandtl number of 0.72. To avoid numerical divergence of the surface vorticity, it was necessary to use much smaller relaxation factors and to increase the values of the convergence criteria. Even so, for Grashof numbers greater than 50, time-independent solutions could not be obtained. The average central processor time required to obtain a solution for Grashof numbers of 0.05 to 1 was found to be about one hour, for Grashof numbers between 1 and 25 it was found to be about three hours and for Grashof numbers between 25 and 50 it was found to be about four hours when using the University of London Computer Centre's CDC7600 digital computer.

CHAPTER 5

CONCLUSIONS

CONCLUSIONS

The results of the present study may be summarised as follows:

1. A finite-difference method of solution of the Navier-Stokes and energy equations has been developed for axisymmetric time-dependent free convective heat transfer from a solid sphere.

2. The time-dependent Navier-Stokes equation was expressed in the form of a vorticity transport equation and a stream function equation. The energy equation was expressed in a form similar to the vorticity transport equation. These three equations were solved simultaneously. The vorticity transport and energy equations were solved using Peaceman and Rachford's alternating direction implicit, ADI, method. The stream functin equation was solved using a point interative successive over-relaxation, SOR, method.

3. In order to preserve the transportive property and to obtain convergence, an upwind differencing scheme was used for the finite-difference representation of the convective terms of the vorticity transport and energy equations.

4. A computer programme was developed to solve the finite-difference equations. Numerical solutions were obtained for Grashof numbers of 0.05, 1, 10, 25, 50, 125 for a Prandtl number of 0.72. Solutions were also obtained

for Grashof numbers of 1250 and 12500 for a Prandtl number of 10; and for a Grashof number of 50 and a Prandtl number of 100.

5. The solutions showed that for all the Grashof and Prandtl numbers used, the distributions of vorticity and temperature around the solid sphere remained almost symmetrical about an imaginary plane located between the upstream and downstream regions of the flow field during the early stages of simulation. However, as integration proceeded with time the effects of convection increased until the late-time steady state solutions were attained.

6. It was observed that at low Grashof numbers, the late-time steady state stream function, vorticity, and temperature distributions remained almost symmetrical about an imaginary plane placed between the upstream and downstream regions of the flow field. However, an examination of the temperature distribution revealed that even at a small Grashof number of 0.05 weak convection processes were present in the region close to the outer boundary. As the Grashof number was increased the convective effects became more and more pronounced and the vorticity and the heated fluid were convected more and more into the downstream region of the flow field. At the same time the thickness of the thermal layer around the upstream region of the sphere decreased and the streamlines were displaced in the downstream region

of the flow field.

7. It was observed that the total dimensionless time taken before late-time steady state conditions were reached became shorter as the Grashof number was increased.

8. The solutions were used to calculate other quantities which characterize the free convective flow such as;the local and average Nusselt numbers, the dimensionless surface pressure, the pressure drag coefficent, and the viscous drag coefficient. These quantities showed different sensitivities to small variations of velocity and temperature with time. In particular, the local Nusselt number appeared to be particularly sensitive and was used in order to judge the approach to the late-time steady state solutions.

9. During the early stages of simulation, the local Nusselt number was approximately constant around the solid sphere. However, as the simulation continued the local Nusselt numbers over the upstream region of the sphere increased towards their late-time steady state values while the local Nusselt numbers over the downstream region of the sphere decreased at first and then increased to their late-time steady state values. It was also observed that the average Nusselt numbers increased conitnuously from their initial values which corresponded to that of steady state conduction to their late-time steady state

values. The computed values of the late-time steady state average Nusselt number found to be slightly low in comparison with experimental data available in the literature.

10. It was observed that the surface vorticity distributions for small and moderate Grashof numbers, remained almost symmetrical about an imaginary plane situated between the upstream and downstream regions of the flow field.

11. Dimensionless pressure distributions at the surface of the sphere were computed from the vorticity values and also from the stream function values. The difference between the results obtained from the two different methods was in the region of 1% to 15% based on the values obtained from vorticity values. With the increasing Grashof number, the dimensionless surface pressure over the upstream region of the sphere increased while the dimensionless surface pressure over the downstream region of the sphere decreased and exhibited a shallow minimum which developed with time.

12. The viscous drag and pressure drag coefficients were found to increase quickly to their late-time steady state values which increased with Grashof number. The pressure drag coefficents were calculated from vorticity values as well as from values of the stream function. The difference between the results obtained from the two

different methods was in the region of 1% to 15% based on the values obtained from vorticity distribution.

13. The use of Peaceman and Rachford'd alternating direction implicit method yielded stable numerical solutions of the equations which describe time-dependent free convective heat transfer from a solid sphere. The solutions were quantitatively reliable as far as could be ascertained from a comparison of the predicted results with existing experimental data.

14. The solution procedure developed in this work has been used to obtain solutions for a restricted range of Grashof and Prandtl numbers and has also been applied to only one geometrical shape; the sphere. However, as procedure has been shown to provide reliable results it could probably be used to obtain solutions for problems involving different geometries and different values of the Grashof and Prandtl numbers.

APPENDICES

APPENDIX A

VECTOR RELATIONSHIP, ORTHOGONAL CURVILINEAR COORDINATE SYSTEM AND TRANSFORMATION OF THE POLAR COORDINATE SYSTEM TO RECTANGULAR SYSTEM

A.1 Vector Algebra

A vector quantity can be expressed as follows:

$$\bar{A} = A_1\bar{e}_1 + A_2\bar{e}_2 + A_3\bar{e}_3 \qquad \text{(A.1.1)}$$

where $\bar{e}_1$, $\bar{e}_2$ and $\bar{e}_3$ are the unit vectors in X_1, X_2 and X_3 directions, respectively, and A_1, A_2 and A_3 are the scalar components of the vector $\bar{A}$.

For orthogonal coordinate systems, the scalar and vector products of two vectors $\bar{A}$ and $\bar{B}$ become:

$$\bar{A}.\bar{B} = A_1B_2 + A_2B_2 + A_3B_3 \qquad \text{(scalar product)} \quad \text{(A.1.2)}$$

$$\bar{A}x\bar{B} = \begin{vmatrix} e_1 & e_2 & e_3 \\ A_1 & A_2 & A_3 \\ B_1 & B_2 & B_3 \end{vmatrix} \qquad \text{(vector product)} \quad \text{(A.1.3)}$$

A.2 Vector Operators in Orthogonal Curvilinear Coordinate System

It can be shown (Spiegel 1959) that the vector operator ∇ has the following form in orthogonal curvilinear coordinate system (X_1, X_2, X_3):

$$\nabla = \frac{\bar{e}_1}{h_1}\frac{\partial}{\partial X_1} + \frac{\bar{e}_2}{h_2}\frac{\partial}{\partial X_2} + \frac{\bar{e}_3}{h_3}\frac{\partial}{\partial X_3} \qquad \text{(A.2.1)}$$

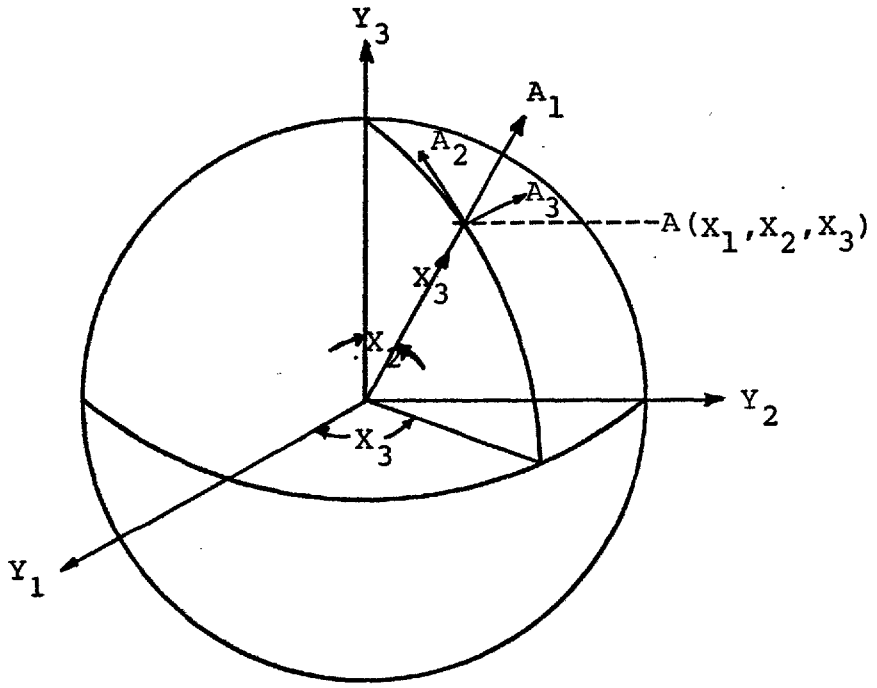

FIGURE A.2.1 ORTHOGONAL CURVILINEAR COORDINATE SYSTEM

where h_i (i = 1,2,3) are the scale factors.

Equation (A.2.1) is used to derive the expression for the gradient, divergence and curl operators in orthogonal curvilinear coordinates.

The gradient of a scalar quantity φ is given by:

$$\text{grad } \varphi = \nabla\varphi = \frac{\bar{e}_1}{h_1}\frac{\partial\varphi}{\partial X_1} + \frac{\bar{e}_2}{h_2}\frac{\partial\varphi}{\partial X_2} + \frac{\bar{e}_3}{h_3}\frac{\partial\varphi}{\partial X_3} \qquad \text{(A.2.2)}$$

If $\bar{A}$ is a vector quantity defined by equation (A.1.1), then the divergence and curl of $\bar{A}$ are given by:

$$\text{div } \bar{A} = \nabla \cdot \bar{A} = \frac{1}{h_1 h_2 h_3}\left[\frac{\partial}{\partial X_1}(h_2 h_3 A_1) + \frac{\partial}{\partial X_2}(h_1 h_3 A_2) + \frac{\partial}{\partial X_3}(h_1 h_2 A_3)\right] \qquad \text{(A.2.3)}$$

$$\text{curl } \bar{A} = \nabla \times \bar{A} = \frac{1}{h_1 h_2 h_3} \begin{vmatrix} h_1\bar{e}_1 & h_2\bar{e}_2 & h_3\bar{e}_3 \\ \frac{\partial}{\partial X_1} & \frac{\partial}{\partial X_2} & \frac{\partial}{\partial X_3} \\ h_1 A_1 & h_2 A_2 & h_3 A_3 \end{vmatrix} \qquad \text{(A.2.4)}$$

Equations (A.2.2) to (A.2.4) show clearly that div $\bar{A}$ is a scalar quantity, but that grad φ and curl $\bar{A}$ are both vector quantities.

The divergence of grad φ, $\nabla^2\varphi$, is an important quantity and can be expressed, using equations (A.2.2) and (A.2.3), as follows:

$$\begin{aligned} \nabla \cdot (\nabla\varphi) &= \nabla^2\varphi \\ &= \frac{1}{h_1 h_2 h_3} \left[\frac{\partial}{\partial X_1} \left(\frac{h_2 h_3}{h_1} \frac{\partial \varphi}{\partial X_1} \right) \right. \\ &\quad + \frac{\partial}{\partial X_2} \left(\frac{h_1 h_3}{h_2} \frac{\partial \varphi}{\partial X_2} \right) \\ &\quad \left. + \frac{\partial}{\partial X_3} \left(\frac{h_1 h_2}{h_3} \frac{\partial \varphi}{\partial X_3} \right) \right] \end{aligned} \qquad \text{(A.2.5)}$$

It can be shown (Spiegel 1959) that for spherical polar coordinates scale factors have the following forms:

$$X_1 = r \qquad X_2 = \Theta \qquad X_3 = \Phi$$
$$h_1 = 1 \qquad h_2 = r \qquad h_3 = r\sin\Theta$$

A.3 Vector Relationship

The following relationships between vector operators

can be found in standard texts such as Kreyszig (1967) and Spiegel (1959). They are used to express the vector operators in standard forms whose transformations to any orthogonal curvilinear coordinate system are immediate.

$$\nabla(\bar{A}.\bar{B}) = (\bar{A}.\nabla)\bar{B} + (\bar{B}.\nabla)\bar{A} + \bar{A} \times (\nabla \times \bar{B}) + \bar{B} \times (\nabla \times \bar{A}) \qquad (A.3.1)$$

$$\nabla \times (\bar{A} \times \bar{B}) = \bar{A}(\nabla . \bar{B}) - \bar{B}(\nabla . \bar{A}) - (\bar{A}.\nabla)\bar{B} + (\bar{B}.\nabla)\bar{A} \qquad (A.3.2)$$

$$\nabla^2 \bar{A} = \nabla(\nabla . \bar{A}) - \nabla \times (\nabla \times \bar{A}) \qquad (A.3.3)$$

$$(\bar{A}.\nabla)\,\varphi = \bar{A}.\nabla\varphi \qquad (A.3.4)$$

$$\text{curl grad } \varphi = \nabla \times (\nabla\varphi) = 0 \qquad (A.3.5)$$

$$\text{div curl } \bar{A} = \nabla . (\nabla \times \bar{A}) = 0 \qquad (A.3.6)$$

A.4 Transformation of Polar Coordinate System to Rectangular System

The spherical polar coordinate system, (r,Θ,Φ), has been arranged as shown in figure 2.2.1. As explained earlier, for the case of axisymmetric flow with no rotation past a stationary sphere, the component of velocity in the Φ - direction is zero everywhere, and all variables are independent of Φ. Thus, the coordinates in the meridian plane, (r,Θ), are the only coordinates required to describe the flow and the spherical polar coordinate system is reduced to the polar coordinate system, (r,Θ).

Consider the dimensionless polar coordinates (r,Θ) and Cartesian coordinates (Y_2, Y_3). In general, for any complex number W there corresponds a point P with Cartesian coordinates (Y_2, Y_3) or with polar coordinates (r,Θ) as follows (Kreysizig 1967):

$$W = Y_2 + iY_3 \qquad (A.4.1)$$

$$W = r\, e^{i\Theta} \qquad (A.4.2)$$

This is shown in figure A.4.1. Therefore, the polar coordinates (r,Θ) can be related to the Cartesian coordinates (Y_2, Y_3) as follows:

$$Y_2 + iY_3 = r\, e^{i\Theta} \qquad (A.4.3)$$

but according to Euler formula:

$$e^{i\Theta} = \cos\Theta + i\sin\Theta$$

hence;

$$Y_2 + iY_3 = r\,(\cos\Theta + i\sin\Theta) \qquad (A.4.4)$$

By equating the real and imaginary parts of relation (A.4.4), the following relations can be obtained:

$$Y_2 = r\cos\Theta \qquad (A.4.5)$$

$$Y_3 = r\sin\Theta \qquad (A.4.6)$$

By elimination of Θ between expressions (A.4.5) and (A.4.6), the following relationship can be obtained:

$$Y_2^2 + Y_3^2 = r^2 \qquad (A.4.7)$$

which, for different values of r, describes a family of concentric circles as shown in figure A.4.2.

By elimination of r between relations (A.4.5) and (A.4.6), the following relationship can be obtained:

$$Y_3 = (\tan\Theta)\ Y_2$$

which, for different values of Θ, describes a family of radiating straight lines as shown in figure A.4.2.

For the reasons given in chapter 2, it is desirable to transform the dimensionless polar coordinates (r,Θ) to a system of rectangular coordinates. This transformation may take place through an exponential function as follows:

$$F = e^{W} \qquad (A.4.8)$$

which defines a mapping which is conformal everywhere, because its derivative is different from zero at every point. Now if $F = e^{z+i\Theta}$, then from relations (A.4.1)

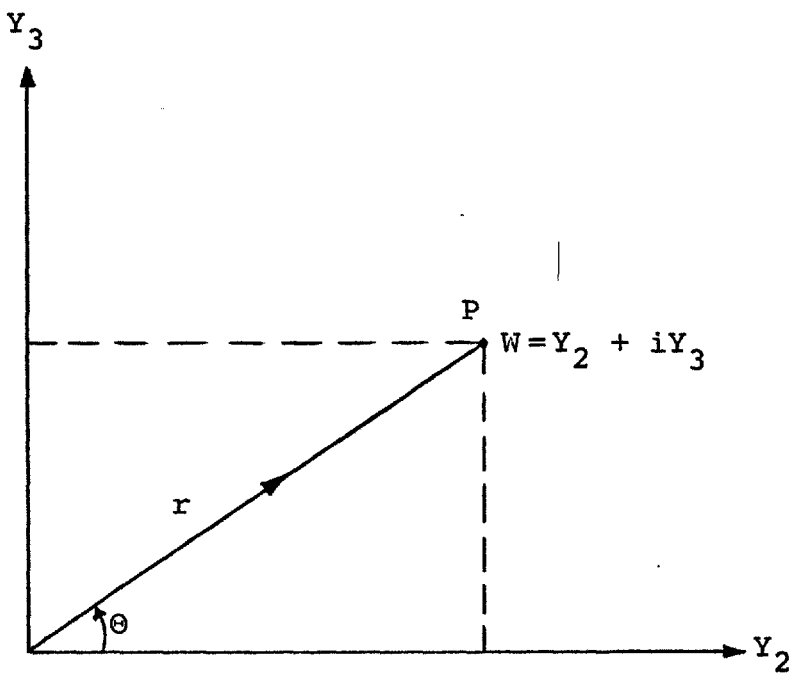

FIGURE A.4.1 GEOMETRICAL REPRESENTATION OF A COMPLEX NUMBER

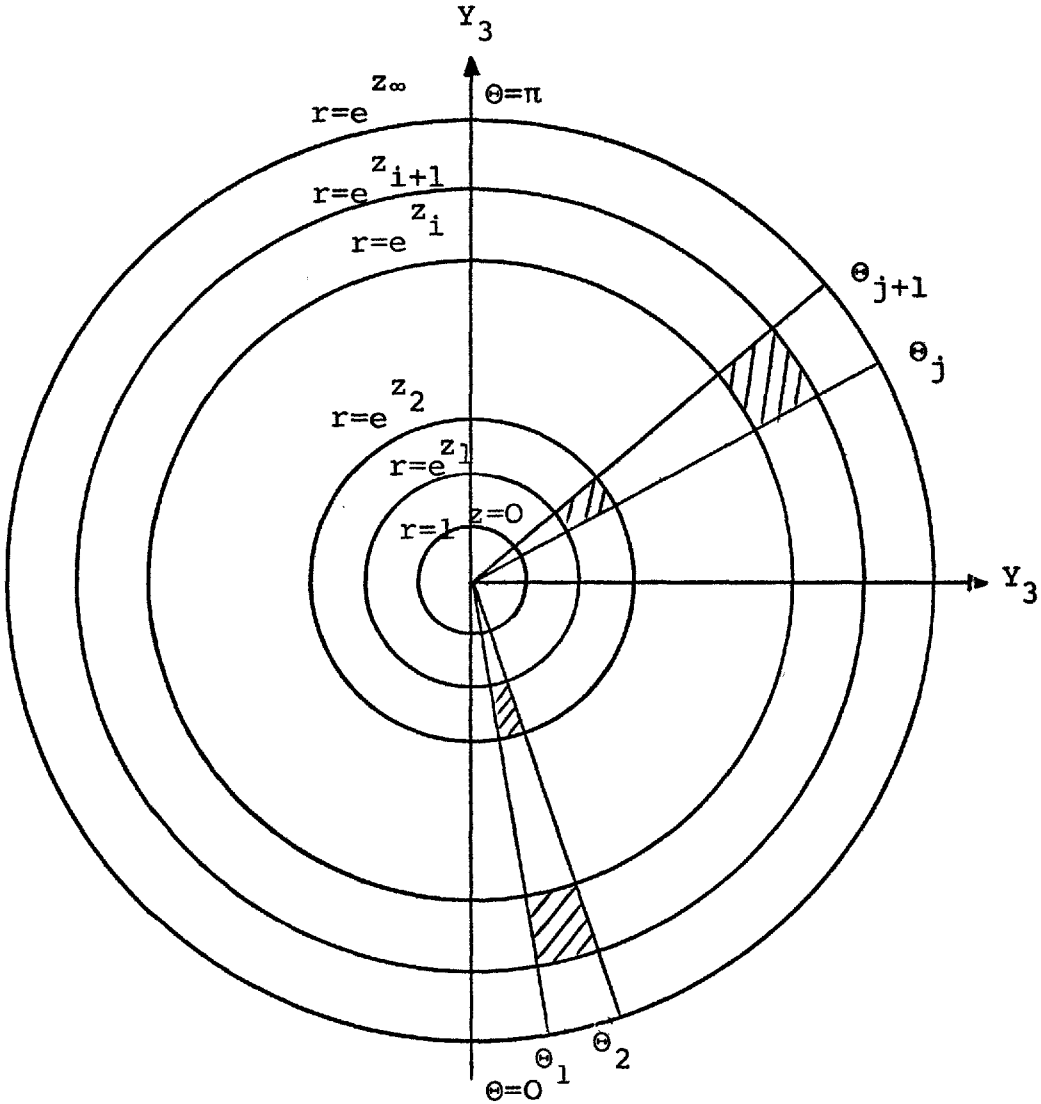

FIGURE A.4.2 POLAR COORDINATES (r,Θ) IN A MERIDIAN PLANE

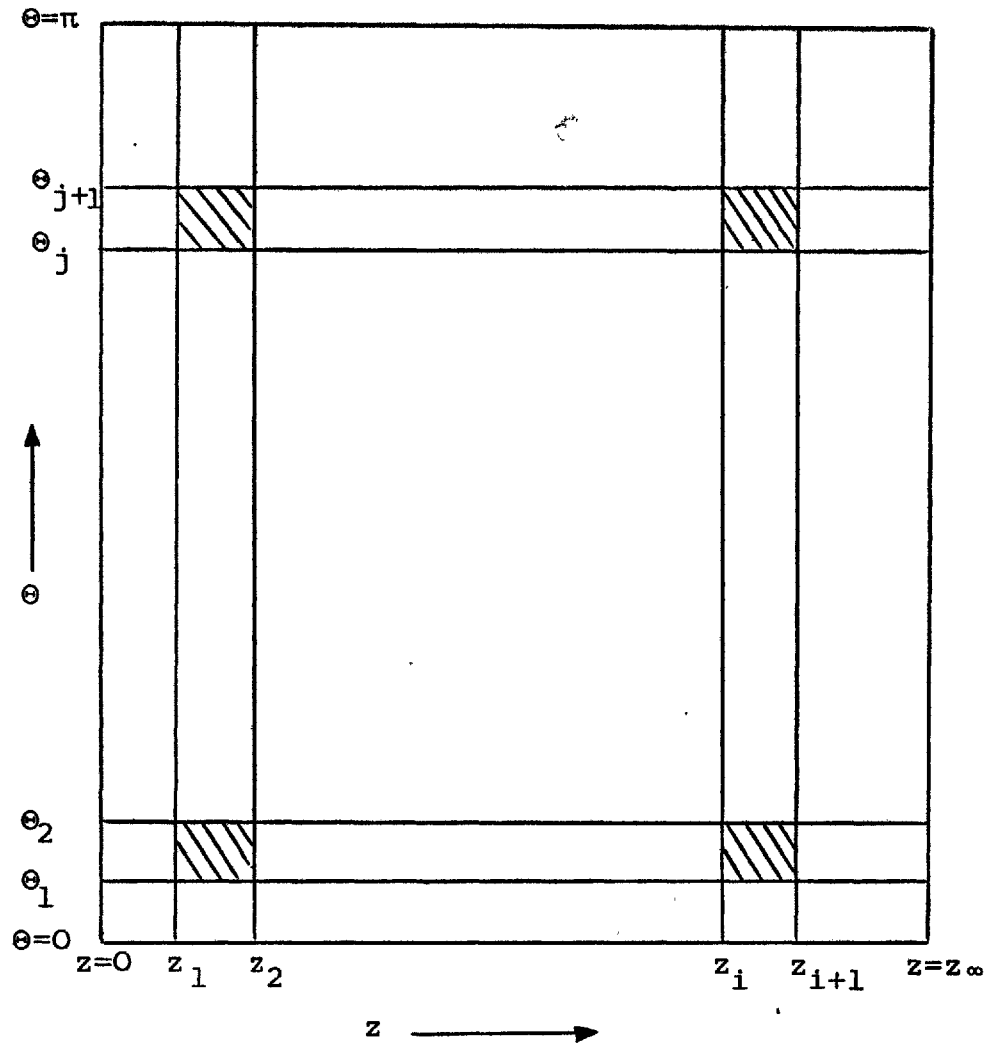

FIGURE A.4.3 MODIFIED POLAR COORDINATES (z,Θ)

and (A.4.8), one may write:

$$e^{Y_2 + iY_3} = e^{z + i\Theta} \qquad \text{(A.4.9)}$$

By equating the real and imaginary parts of relation (A.4.9), the following relation can be obtained:

$$Y_2 = z \quad \text{and} \quad Y_3 = \Theta \qquad \text{(A.4.10)}$$

However, by equating of $F = e^{z+i\Theta}$ and relation (A.4.2) one may write:

$$e^{z+i\Theta} = r\, e^{i\Theta}$$

so that:

$$r = e^{z}$$

The new coordinates (z,Θ) are plotted in figure A.4.3 which shows that the vertical lines z = constant and the horizontal lines Θ = constant correspond to the concentric circles and the radiating straight lines of figure A.4.2, respectively. The shaded areas in the two diagrams correspond , and the line z=0 corresponds to the surface of the solid sphere (r equal to unity). Hence, by the transformation $r=e^{z}$, the external region on the right hand side of figure A.4.2 is mapped onto the rectangle of figure A.4.3 which is bounded by the lines $\Theta=0$; $\Theta=\pi$; z=0, and $z=z_\infty$.

APPENDIX B

CALCULATION OF THE DIMENSIONLESS PRESSURES AT THE FRONT STAGNATION POINT AND AT THE SPHERE SURFACE

B.1 Introduction

The continuity equation, equation (2.3.3) and the time-dependent Navier-Stokes equation in polar coordinates, equations (2.3.20) and (2.3.21), for free convective heat transfer from a solid sphere are given in chapter 2. These equations are rewritten below as:

The continuity equation, equation (2.3.3)

$$\frac{1}{r^2}\frac{\partial}{\partial r}(r^2 u_r) + \frac{1}{r\sin\Theta}\frac{\partial}{\partial \Theta}(u_\Theta \sin\Theta) \qquad \text{(B.1.1)}$$

The Navier-Stokes equation:

r-component, equation (2.3.20):

$$\frac{\partial u_r}{\partial t} + u_r\frac{\partial u_r}{\partial r} + \frac{u_\Theta}{r}\frac{\partial u_r}{\partial \Theta} - \frac{u_\Theta^2}{r} = -\frac{1}{\rho_\infty}\frac{\partial P_d}{\partial r}$$

$$+\nu_\infty\left[\nabla^2 u_r - \frac{2}{r^2}u_r - \frac{2}{r^2}\frac{\partial u_\Theta}{\partial \Theta} - \frac{2}{r^2}u_\Theta\cot\Theta\right] - g\beta_\infty\cos\Theta\,(T-T_\infty) \qquad \text{(B.1.2)}$$

Θ-component, equation (2.3.21):

$$\frac{\partial u_\Theta}{\partial t} + u_r\frac{\partial u_\Theta}{\partial r} + \frac{u_\Theta}{r}\frac{\partial u_\Theta}{\partial \Theta} + \frac{u_r u_\Theta}{r} = -\frac{1}{\rho_\infty}\frac{1}{r}\frac{\partial P_d}{\partial \Theta}$$

$$+\nu_\infty\left[\nabla^2 u_\Theta + \frac{2}{r^2}\frac{\partial u_r}{\partial \Theta} - \frac{u_\Theta}{r^2\sin^2\Theta}\right] + g\beta_\infty\sin\Theta\,(T-T_\infty) \qquad \text{(B.1.3)}$$

where

$$\nabla^2 = \frac{1}{r^2}\frac{\partial}{\partial r}\left(r^2\frac{\partial}{\partial r}\right) + \frac{1}{r^2\sin\Theta}\frac{\partial}{\partial\Theta}\left(\sin\Theta\frac{\partial}{\partial\Theta}\right)$$

The vorticity, ζ, is defined by equation (2.4.5) as:

$$\zeta = \frac{1}{r}\left[\frac{\partial}{\partial r}(ru_\Theta) - \frac{\partial}{\partial\Theta}(u_r)\right] \qquad \text{(B.1.4)}$$

For convenience, the subscript d from the pressure terms will be omitted and P will be used exclusively on the understanding that the local pressure, P, will be measured relative to the undisturbed static-fluid pressure at the point considered.

B.2 Calculation of the Dimensionless Pressure at the Front Stagnation Point

As stated in chapter 2, along the axis of symmetry the velocity u_Θ, the stream function, ψ, and all their derivates with respect to r are zero. Therefore, along the axis of symmetry, equations (B.1.1), (B.1.2) and (B.1.4) become; respectively:

$$\frac{\partial u_r}{\partial r} + \frac{2u_r}{r} + \frac{1}{r}\frac{\partial u_r}{\partial\Theta} = 0 \qquad \text{(B.2.1)}$$

$$\frac{\partial u_r}{\partial t} + u_r\frac{\partial u_r}{\partial r} = -\frac{1}{\rho_\infty}\frac{\partial P}{\partial r} + \nu_\infty\left[\frac{\partial^2 u_r}{\partial r^2} + \frac{2}{r}\frac{\partial u_r}{\partial r} + \frac{1}{r^2}\frac{\partial^2 u_r}{\partial\Theta^2} + \frac{\cot\Theta}{r^2}\frac{\partial u_r}{\partial\Theta} - \frac{2u_r}{r^2} - \frac{2}{r^2}\frac{\partial u_\Theta}{\partial\Theta}\right] - \beta_\infty g\,(T-T_\infty) \qquad \text{(B.2.2)}$$

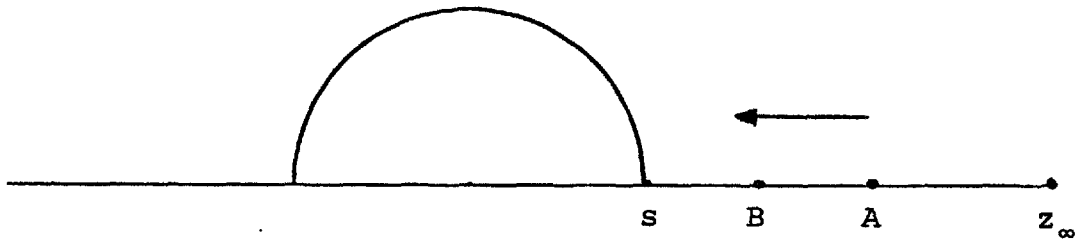

FIGURE B.2.1 INTEGRATION OF PRESSURE ALONG THE AXIS OF SYMMETRY

and,

$$\zeta = -\frac{1}{r}\frac{\partial u_r}{\partial \Theta} \tag{B.2.3}$$

Also, from equation (B.1.4)

$$\frac{\partial \zeta}{\partial \Theta} = \frac{\partial}{\partial \Theta}\left[\frac{\partial u_\Theta}{\partial r} + \frac{u_\Theta}{r} - \frac{1}{r}\frac{\partial u_r}{\partial \Theta}\right] = \frac{\partial^2 u_\Theta}{\partial \Theta \partial r} + \frac{1}{r}\frac{\partial u_\Theta}{\partial \Theta} - \frac{1}{r}\frac{\partial^2 u_r}{\partial \Theta^2} \tag{B.2.4}$$

By differentiation of equation (B.2.1) with respect to r and substitution into equation (B.2.2), the following equation can be obtained:

$$\frac{\partial u_r}{\partial t} + u_r\frac{\partial u_r}{\partial r} = -\frac{1}{\rho_\infty}\frac{\partial P}{\partial r} + \frac{\nu_\infty}{r}\left[-\frac{\partial^2 u_\Theta}{\partial r \partial \Theta} - \frac{1}{r}\frac{\partial u_\Theta}{\partial \Theta} + \frac{1}{r}\frac{\partial^2 u_r}{\partial \Theta^2} + \frac{\cot\Theta}{r}\frac{\partial u_r}{\partial \Theta}\right] - \beta_\infty g\,(T-T_\infty) \tag{B.2.5}$$

Now, by substitution of equations (B.2.3) and (B.2.4) into equation (B.2.5), one obtains:

$$\frac{\partial u_r}{\partial t} + u_r\frac{\partial u_r}{\partial r} = -\frac{1}{\rho_\infty}\frac{\partial P}{\partial r} + \frac{\nu_\infty}{r}\left[-\frac{\partial \zeta}{\partial \Theta} - \frac{\zeta}{\tan\Theta}\right] - \beta_\infty g\,(T-T_\infty) \tag{B.2.6}$$

But along the axis of symmetry, both tan Θ and ζ are zero. Therefore, using L'Hospital's rule;

$$\underset{\Theta \to 0}{\text{Limit}} \frac{\zeta}{\tan\Theta} = \frac{\partial \zeta}{\partial \Theta}$$

so that equation (B.2.6) becomes:

$$\frac{\partial u_r}{\partial t} + u_r \frac{\partial u_r}{\partial r} = - \frac{1}{\rho_\infty} \frac{\partial P}{\partial r} - \nu_\infty \frac{2}{r} \frac{\partial \zeta}{\partial \Theta} - g \beta_\infty (T-T_\infty) \qquad \text{(B.2.7)}$$

By integration of equation (B.2.7) along the axis of symmetry between points A and B shown in figure B.2.1, the following expression is obtained;

$$\frac{1}{2} \left[(u_r^2)_B - (u_r^2)_A \right] + \frac{1}{\rho_\infty} (P_B - P_A)$$

$$= - \int_A^B \nu_\infty \frac{2}{r} \frac{\partial \zeta}{\partial \Theta} dr - \int_A^B \frac{\partial u_r}{\partial t} dr - \int_A^B \beta_\infty g \, (T-T_\infty) dr \qquad \text{(B.2.8)}$$

By use of the dimensionless variables expressed by relation (2.5.1) and introduction of the dimensionless pressure, K, defined as follows:

$$K = \frac{P R^2}{\frac{1}{2} \rho_\infty \nu_\infty^2} \qquad \text{(B.2.9)}$$

equation (B.2.8) becomes:

$$\frac{1}{2} \left[(u_z^{*2})_B - (u_z^{*2})_A \right] + \frac{1}{2} (K_B - K_A)$$

$$= -2 \int_A^B \frac{\partial \zeta^*}{\partial \Theta} dz - \int_A^B \frac{\partial u_z^*}{\partial t^*} e^z dz - Gr \int_A^B T^* e^z dz \qquad \text{(B.2.10)}$$

Now, if point A is on the outer boundary and if point B is at the front stagnation point, then, at any time t:

$$(u_z^*)_A = u_z^* \Big|_{z=z_\infty} = 0 \quad ; \qquad (u_z^*)_B = u_z^* \Big|_{z=0} = 0 \quad ;$$

$$K_A = 0 \qquad \text{and } K_B = K_0$$

Thus:

$$K_0 = -4\int_{z_\infty}^{0} \frac{\partial \zeta^*}{\partial \Theta}\, dz - \int_{z_\infty}^{0} \frac{\partial u_z^*}{\partial t^*}\, e^z dz - Gr\int_{z_\infty}^{0} T^* e^z dz \qquad \text{(B.2.11)}$$

Now if u_z^* is expressed in terms of the stream function, equation (B.2.11) becomes:

$$K_0 = 4\int_{0}^{z_\infty} \frac{\partial \zeta^*}{\partial \Theta}\, dz - 2\int_{0}^{z_\infty} \frac{1}{e^z} \frac{\partial}{\partial t^*} \left(\frac{\partial^2 \psi^*}{\partial \Theta^2}\right) dz + Gr\int_{0}^{z_\infty} T^* e^z dz \qquad \text{(B.2.12)}$$

The integrands in equation (B.2.12) are evaluated at $\Theta=0$.

B.3 Calculation of the Dimensionless Pressure at the Sphere Surface

The pressure distribution on the sphere surface can be derived from the Θ-component of the time-dependent Navier-Stokes equation, equation (B.1.3) as follows. As stated in chapter 2 the following conditions apply at the sphere surface:

$$u_r = u_\Theta = \frac{\partial u_\Theta}{\partial t} = \frac{\partial u_\Theta}{\partial \Theta} = \frac{\partial u_r}{\partial \Theta} = \frac{\partial^2 u_\Theta}{\partial \Theta^2} = 0 \qquad \text{(B.3.1)}$$

Therefore, at the sphere surface, equation (B.1.3) may

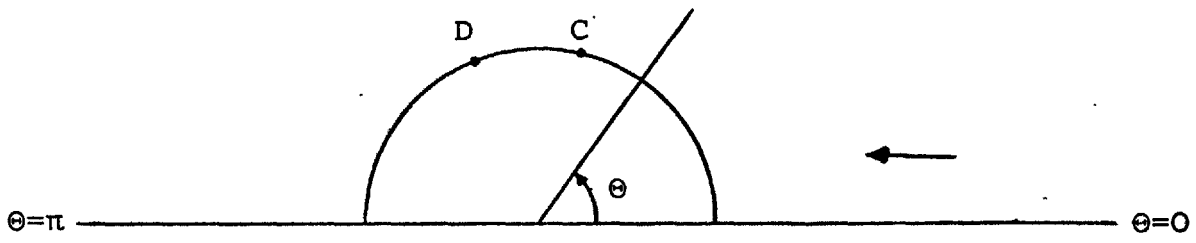

FIGURE B.3.1 INTEGRATION OF PRESSURE AT THE SPHERE SURFACE

be written as:

$$\frac{1}{\rho_\infty r}\frac{\partial P}{\partial \Theta} = \nu_\infty \nabla^2 u + g\beta_\infty \sin\Theta\,(T-T_\infty) \qquad (B.3.2)$$

or:

$$\frac{1}{\rho_\infty r}\frac{\partial P}{\partial \Theta} = \nu_\infty\left[\frac{\partial^2 u_\Theta}{\partial r^2} + \frac{2}{r}\frac{\partial u_\Theta}{\partial r}\right] + g\beta_\infty \sin\Theta\,(T-T_\infty) \qquad (B.3.3)$$

Also, from equation (B.1.4):

$$\frac{\partial \zeta_s}{\partial r} = \frac{\partial^2 u_\Theta}{\partial r^2} + \frac{1}{r}\frac{\partial u_\Theta}{\partial r}\,, \qquad (B.3.4)$$

and

$$\frac{\zeta_s}{r} = \frac{1}{r}\frac{\partial u_\Theta}{\partial r} \qquad (B.3.5)$$

By substitution of equations (B.3.4) and (B.3.5) into equation (B.3.3), one obtains:

$$\frac{1}{\rho_\infty r}\frac{\partial P}{\partial \Theta} = \nu_\infty\left(\frac{\partial \zeta_s}{\partial r} + \frac{\zeta_s}{r}\right) + \beta_\infty g\sin\Theta\,(T-T_\infty) \qquad (B.3.6)$$

By expressing equation (B.3.6) in dimensionless form and integrating between the points C and D shown in figure B.3.1, one obtains:

$$K_D = K_C - 2Gr\,(\cos\Theta_D - \cos\Theta_C) + 2\int_C^D \left(\frac{\partial \zeta_s^*}{\partial z} + \zeta^*\right)d\Theta \qquad (B.3.7)$$

If point D is at an angle Θ, and C is at the front stagnation point where $\Theta = 0$, then

$$K_C = K_O \quad \text{and} \quad K_D = K_\Theta$$

and equation (B.3.7), may be written as:

$$K_\Theta = K_O + 2\,Gr\,(1-\cos\Theta) + 2\int_0^\Theta \left(\frac{\partial \zeta_s^*}{\partial z} + \zeta^*\right) d\Theta \qquad (B.3.8)$$

The integrands in equation (B.3.8) are evaluated at the sphere surface, z=0. Equation (B.3.8) can be integrated in the above form or it can be rewritten in terms of stream function values as follows using the following relationships which were obtained in section 5 of chapter 2:

$$e^{2z} G^* = \frac{\partial^2 \psi^*}{\partial z^2} - \frac{\partial \psi^*}{\partial z} + \frac{\partial^2 \psi^*}{\partial \Theta^2} - \cot\Theta \frac{\partial \psi^*}{\partial \Theta}$$

and

$$G^* = \zeta^* e^z \sin\Theta$$

Thus; by substitution:

$$e^{3z} \sin\Theta \zeta^* = \frac{\partial^2 \psi^*}{\partial z^2} - \frac{\partial \psi^*}{\partial z} + \frac{\partial^2 \psi^*}{\partial \Theta^2} - \cot\Theta \frac{\partial \psi^*}{\partial \Theta} \qquad (B.3.9)$$

Differentiation of equation (B.3.9) with respect to z leads to:

$$e^{3z} \sin\Theta \left(3\zeta^* + \frac{\partial \zeta^*}{\partial z}\right) = \frac{\partial^3 \psi^*}{\partial z^3} - \frac{\partial^2 \psi^*}{\partial z^2} + \frac{\partial^3 \psi^*}{\partial^2 \Theta \partial z} - \cot\Theta \frac{\partial^2 \psi^*}{\partial z \partial \Theta} \qquad (B.3.10)$$

By application of the boundary conditions expressed in chapter 2, at the sphere surface, equation (B.3.10)

reduces to:

$$\sin\Theta\,(3\zeta^* + \frac{\partial\zeta^*}{\partial z})\Big|_{z=0} = \frac{\partial^3\psi^*}{\partial z^3} - \frac{\partial^2\psi^*}{\partial z^2} \qquad \text{(B.3.11)}$$

The surface vorticity is given in chapter 2 as:

$$\zeta^*\Big|_{z=0} = \frac{1}{\sin\Theta}\,\frac{\partial^2\psi^*}{\partial z^2} \qquad \text{(B.3.12)}$$

By substitution of equation (B.3.12) into (B.3.11) the following relationship can be obtained:

$$\frac{\partial\zeta^*}{\partial z}\Big|_{z=0} = \frac{1}{\sin\Theta}\,\frac{\partial^3\psi^*}{\partial z^3}\Big|_{Z=0} - 4\zeta^*\Big|_{z=0} \qquad \text{(B.3.13)}$$

Equation (B.3.8) can now be written as follows for the calculation of the surface pressure:

$$K_\Theta = K_O + 2\,Gr\,(1-\cos\Theta) + 2\int_O^\Theta (\frac{1}{\sin\Theta}\,\frac{\partial^3\psi^*}{\partial z^3} - 3\zeta^*)\,d\Theta \qquad \text{(B.3.14)}$$

The integrands in equation (B.3.14) are evaluated at the sphere surface, Z=O.

APPENDIX C

CALCULATION OF THE DRAG COEFFICIENTS

C.1 Introduction

The drag force on an immersed body is the resultant of the 'pressure drag' and 'frictional drag' forces exterted by the fluid on the surface of the body.

At every point on the sphere surface there is a force per unit area which acts perpendicularly to the sphere surface (see figure C.1.1). The drag force obtained by integration over the sphere surface of this force is known as the 'pressure drag' or 'form drag', D_P. Also, at every point there is a shear stress acting tangentially to the sphere surface. The drag force obtained by integration of the shear stress over the sphere surface is known as the 'frictional drag' or 'viscous drag', D_F.

It is customary to express the drag force in terms of a dimensionless coefficient, C_D, which for free convection at a given time, t, is defined in the present work as:

$$C_D = \frac{\text{DRAG FORCE}}{\text{CROSS-SECTIONAL AREA} \times \frac{1}{2} \frac{\rho_\infty \nu_\infty^2}{R^2}} \qquad \text{(C.1.1)}$$

The drag coefficient obtained from the pressure drag,

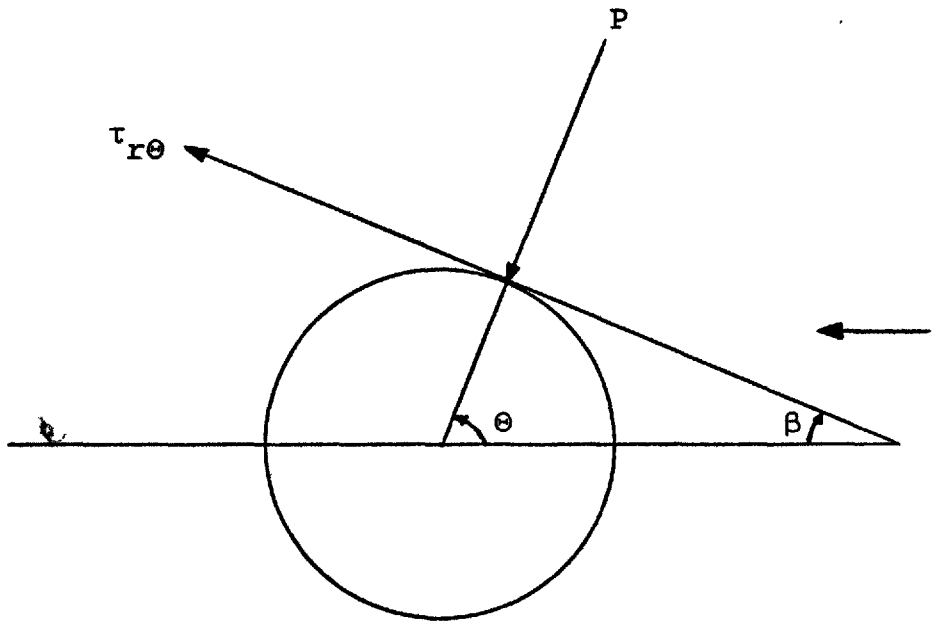

FIGURE C.1.1 FORCES ON THE SPHERE SURFACE

D_P, and the viscous drag, D_F; will be denoted by C_{DP} and C_{DF}, respectively. The total drag coefficient, C_{DT}, is the sum of the two drag coefficients, C_{DP} and C_{DF}.

$$C_{DT} = C_{DP} + C_{DF} \qquad (C.1.2)$$

C.2 Calculation of the Pressure Drag Coefficient

From equation (C.1.1), the pressure drag coefficient, C_{DP}, is defined as follows:

$$C_{DP} = \frac{D_P}{\pi R^2 \times \frac{1}{2} \frac{\rho_\infty v_\infty^2}{R^2}} \qquad (C.2.1)$$

With reference to figure C.1.1, the pressure drag force, D_P, can be calculated as follows:

$$D_P = \iint_S P \sin\beta \, dS \qquad (C.2.2)$$

where $\beta = \pi/2 - \Theta$

and $dS = 2\pi R^2 \sin\Theta \, d\Theta$

Therefore,

$$D_P = \pi R^2 \int_0^{\pi} P \sin 2\Theta \, d\Theta \qquad (C.2.3)$$

But, as before: $K = \dfrac{PR^2}{\frac{1}{2}\rho_\infty v_\infty^2}$

Therefore;

$$D_P = \pi R^2 \left(\tfrac{1}{2} \frac{\rho_\infty v_\infty^2}{R^2}\right) \int_0^{\pi} K_\Theta \sin 2\Theta \, d\Theta \qquad (C.2.4)$$

Hence, by application of equation (C.2.1):

$$C_{DP} = \int_0^{\pi} K_\Theta \sin 2\Theta \, d\Theta \qquad (C.2.5)$$

where K_Θ is calculated from equation (B.3.8) or from equation (B.3.14).

C.3 Calculation of the Viscous Drag Coefficient

From equation (C.1.1):

$$C_{DF} = \frac{D_F}{\pi R^2 \times \frac{1}{2} \frac{\rho_\infty v_\infty^2}{R^2}} \qquad (C.3.1)$$

With reference to figure C.1.1, the viscous drag force, D_F, can be calculated as follows:

$$D_F = \iint_S \tau_{r\Theta} \cos\beta \, dS \qquad (C.3.2)$$

where $\beta = \frac{\pi}{2} - \Theta$

$$dS = 2\pi R^2 \sin\Theta \, d\Theta$$

$$\tau_{r\Theta} = \mu_\infty \left[r \frac{\partial}{\partial r} \left(\frac{u_\Theta}{r}\right) + \frac{1}{r} \frac{\partial u_r}{\partial \Theta} \right] \qquad \text{(C.3.3)}$$

However, on the sphere surface:

$$u_\Theta = u_r = \frac{\partial u_r}{\partial \Theta} = 0$$

Therefore:

$$\tau_{r\Theta} = \mu_\infty \frac{\partial u_\Theta}{\partial r}$$

Also,

$$\zeta = \frac{\partial u_\Theta}{\partial r} + \frac{u_\Theta}{r} - \frac{1}{r} \frac{\partial u_r}{\partial \Theta}$$

again, on the sphere surface:

$$\zeta_s = \frac{\partial u_\Theta}{\partial r}$$

Therefore equation (c.3.2) reduces to:

$$D_F = 2\pi R^2 \mu_\infty \int_0^\pi \zeta_s \sin^2\Theta \, d\Theta \qquad \text{(C.3.4)}$$

The drag coefficient is defined by equation (C.2.1), so that when all functions are written in dimensionless form, the viscous drag coefficient is obtained as:

$$C_{DF} = 4 \int_0^\pi \zeta_s^* \sin^2\Theta \, d\Theta \qquad \text{(C.3.5)}$$

APPENDIX D

CALCULATION OF THE LOCAL AND THE AVERAGE NUSSELT NUMBERS

D.1 Calculation of the Local Nusselt Number

In convective heat transfer, the quantity of most practical importance is the rate at which heat transfer takes place from the surface of the body to the surrounding fluid.

In accordance with Fourier's law of heat condition, the heat flux q_r normal to the surface of a sphere, at any instant of time is given by:

$$q_r = - k_T \left.\frac{\partial T}{\partial r}\right|_{r=R} \qquad \text{(D.1.1)}$$

where k_T is the thermal conductivity of the fluid and $\frac{\partial T}{\partial r}$ is the local temperature gradient at the surface in the direction of the outward normal to the surface, r-direction.

The local heat flux may also be expressed in terms of the local heat transfer coefficient, h (Θ), as follows:

$$q_r = h\ (\Theta)\ (T_s - T_\infty) \qquad \text{(D.1.2)}$$

Equating equations (D.1.1) and (D.1.2) one obtains:

$$\frac{h\ (\Theta)}{k_T} = - \frac{1}{(T_s - T_\infty)} \left.\frac{\partial T}{\partial r}\right|_{r=R} \qquad \text{(D.1.3)}$$

The local Nusselt number, Nu_Θ , is defined as follows:

$$Nu_\Theta = \frac{h\ (\Theta)\ x\ 2R}{k_T} \qquad (D.1.4)$$

By substitution of equation (D.1.4) into equation (D.1.3), one obtains:

$$Nu_\Theta = \frac{-\ 2R}{(T_s - T_\infty)} \left.\frac{\partial T}{\partial r}\right|_{r=R} \qquad (D.1.5)$$

Equation (D.1.5) can be rewritten in dimensionless form as follows:

$$Nu_\Theta = -\ 2 \left.\frac{\partial T^*}{\partial z}\right|_{z=0} \qquad (D.1.6)$$

D.2 Calculation of the Average Nusselt Number

The average rate of heat transfer, from the sphere surface can be determined as follows:

The total heat flow rate from the sphere surface, Q_T, can be evaluated as follows:

$$Q_T = \iint_S q_r\ dS \qquad (D.2.1)$$

where q_r is the local heat flux and dS is an element of surface area on the sphere surface.

Q_T may also be expressed in terms of an average or overall heat transfer coefficient, $\bar{h}$, as follows:

$$Q_T = \bar{h}\ S\ (T_s - T_\infty) \qquad (D.2.2)$$

Therefore, by equating equation (D.2.1) and (D.2.2), one obtains:

$$\bar{h}\, S(T_s - T_\infty) = \iint_S q_r \, dS \qquad (D.2.3)$$

By substitution of q_r from equation (D.1.1), equation (D.2.3) can be expressed as:

$$\frac{\bar{h}}{k_T} = - \frac{1}{S(T_s - T_\infty)} \iint_S \frac{\partial T}{\partial r}\bigg|_{r=R} dS \qquad (D.2.4)$$

where for a sphere;

$$S = 4\pi R^2$$

and $dS = R^2 \sin\Theta \, d\Theta \, d\Phi$

therefore, equation (D.2.4) becomes:

$$\frac{\bar{h}}{k_T} = - \frac{1}{4\pi R^2 (T_s - T_\infty)} \int_0^{2\pi} \int_0^{\pi} \frac{\partial T}{\partial r}\bigg|_{r=R} R^2 \sin\Theta \, d\Theta d\Phi \qquad (D.2.5)$$

or

$$\frac{\bar{h}}{k_T} = - \frac{1}{2(T_s - T_\infty)} \int_0^{\pi} \frac{\partial T}{\partial r}\bigg|_{r=R} \sin\Theta d\Theta \qquad (D.2.6)$$

The overall or average Nusselt number, $\overline{Nu}$, is defined as follows:

$$\overline{Nu} = \frac{\bar{h}}{k_T} \times 2R \qquad (D.2.7)$$

By substitution of equation (D.2.7) into equation (D.2.6),

one obtains:

$$\overline{Nu} = - \frac{R}{(T_s - T_\infty)} \int_0^\pi \frac{\partial T}{\partial r}\bigg|_{r=R} \sin\Theta d\Theta \qquad (D.2.8)$$

Equation (d.2.8) can be rewritten in dimensionless form as follows:

$$\overline{Nu} = - \int_0^\pi \frac{\partial T^*}{\partial z}\bigg|_{z=0} \sin\Theta d\Theta \qquad (D.2.9)$$

But, from equation (D.1.6)

$$Nu_\Theta = - 2 \frac{\partial T^*}{\partial z}\bigg|_{z=0}$$

Thus, equation (D.2.9) can be rewritten in terms of the local Nusselt number as follows:

$$\overline{Nu} = \frac{1}{2}\int_0^\pi Nu_\Theta \sin\Theta d\Theta \qquad (D.2.10)$$

APPENDIX E

NUMERICAL INTEGRATION AND DEFFERENTIATION

E.1 Introduction

The solutions of the finite-difference equations derived in chapter 3 provide the numerical values of the stream function, vorticity, and temperature at each point in the flow region at any time.

From these distributions, other quantities, such as the surface pressure, the drag coefficients, and the local and the average Nusselt numbers can be obtained as described in appendices B, C and D, respectively. The calculation of these quantities requires numerical evaluations of the first derivatives of the dependent variables with respect to space variables or to time variable, and also the numerical evaluation of integrals over any range of the independent variables.

E.2 Numerical Integration

The integral of a general function W(X) over the limits $X = X_a$ and $X = X_b$ may be evaluated by the use of the 'trapezoidal rule'. The integration formula can be derived as follows:

The interval of integration, whose length is $X_b - X_a$, is subdivided into n equal parts of length ΔX, as shown

in figure E.2.1.

Therefore;

$$\Delta X = \frac{X_b - X_a}{n}$$

Then the n trapezoids in figure E.2.1 have the following areas:

$$\frac{1}{2}\left[W(X_a) + W(X_2)\right]\Delta X,\ \frac{1}{2}\left[W(X_2) + W(X_3)\right]\Delta X,\ \ldots,$$

$$\frac{1}{2}\left[W(X_{n-1}) + W(X_b)\right]\Delta X.$$

Thus,

$$\int_{X_a}^{X_b} W(X)\,dX \approx \Delta X \left[\frac{W(X_a)}{2} + W(X_2) + W(X_3) + \ldots + W(X_{n-1}) + \frac{W(X_b)}{2}\right] \qquad \text{(E.2.1)}$$

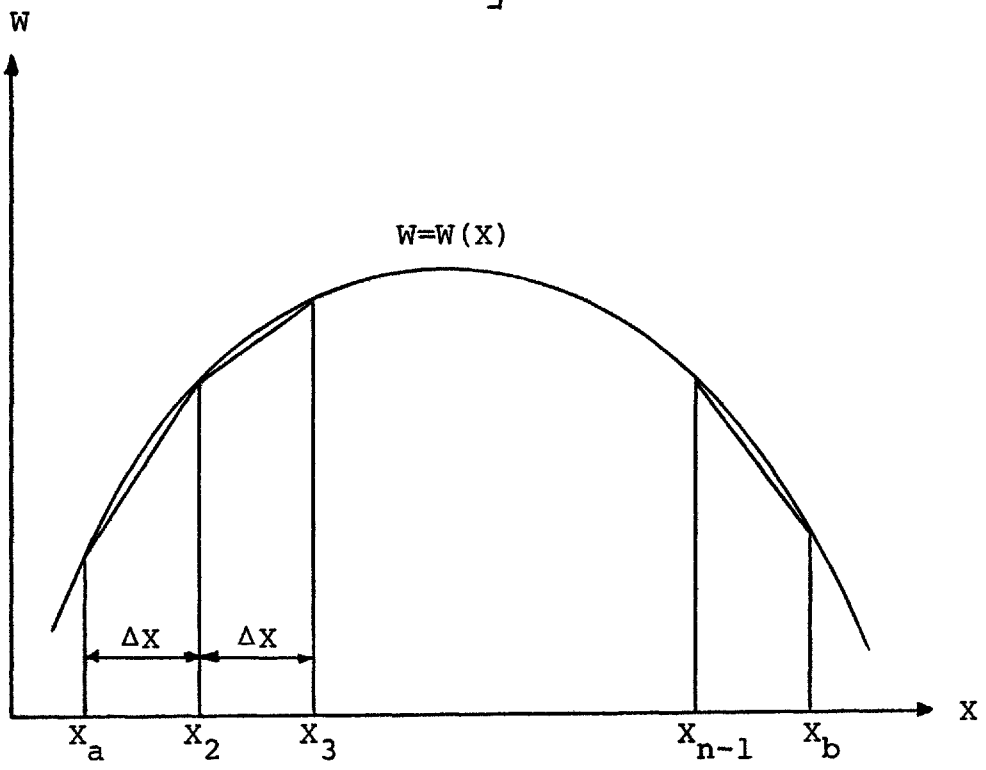

FIGURE E.2.1 THE TRAPEZOIDAL RULE

Equation (E.2.1) can be written in the following compact form:

$$\int_{X_a}^{X_b} W(X)dX \approx \Delta X\left[\frac{W(X_a) + W(X_b)}{2} + \sum_{J=2}^{n-1} W(X_J)\right] \qquad (E.2.2)$$

E.3 Numerical Differentiation

Consider a general function $W(X)$ and let $W(X_o)=W_1$ and $W(X_o+h)=W_2$, ... where $h=\Delta X$.

Define a forward difference operator Δ and a differentiation operator D as follows:

$$\Delta W_1 = W_2 - W_1 \qquad (E.3.1)$$

$$DW(X_o) = W'(X_o) = \left.\frac{\partial W}{\partial X}\right|_{X=X_o} \qquad (E.3.2)$$

From Taylor's series expansion, one can write:

$$W_2 = W(X_o+h) = W(X_o) + hW'(X_o) + \frac{h^2}{2!}W''(X_o) + \ldots \qquad (E.3.3)$$

By substitution of equations (E.3.2) into equation (E.3.3), and noting that $W(X_o) = W_1$, the following equation can be obtained:

$$W_2 = (1 + hD + \frac{h^2D^2}{2!} + \ldots)W_1 = e^{hD}W_1 \qquad (E.3.4)$$

Thus, from equations (E.3.1) and (E.3.4), the following

relationship can be obtained:

$$e^{hD} = 1 + \Delta \qquad \text{(E.3.5)}$$

or:

$$hD = \ln (1+\Delta)$$

$$= \Delta - \frac{1}{2}\Delta^2 + \frac{1}{3}\Delta^3 - \frac{1}{4}\Delta^4 + \ldots \qquad \text{(E.3.6)}$$

which on operating on W_1 gives the following relation:

$$hDW_1 = (\Delta - \frac{1}{2}\Delta^2 + \frac{1}{3}\Delta^3 - \frac{1}{4}\Delta^4 + \ldots)W_1 \qquad \text{(E.3.6)}$$

or:

$$hW_1' = \Delta W_1 - \frac{1}{2}\Delta^2 W_1 + \frac{1}{3}\Delta^3 W_1 - \frac{1}{4}\Delta^4 W_1 + \ldots \qquad \text{(E.3.7)}$$

where:

$$\Delta W_1 = W_2 - W_1 \qquad \text{(E.3.8)}$$

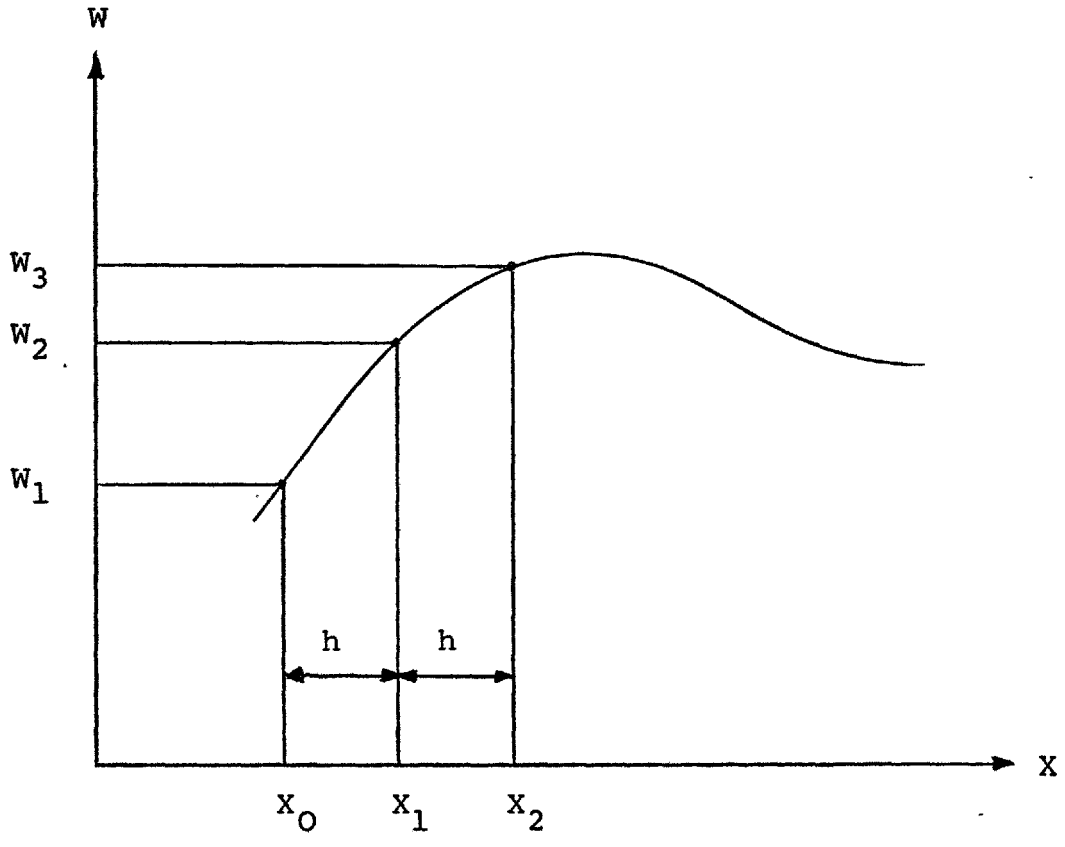

FIGURE E.3.1 NUMERICAL DIFFERENTIATION

$$\Delta^2 W_1 = W_3 - 2W_2 + W_1 \qquad \text{(E.3.9)}$$

$$\Delta^3 W_1 = W_4 - 3W_3 + 3W_2 - W_1 \qquad \text{(E.3.10)}$$

$$\Delta^4 W_1 = W_5 - 4W_4 + 6W_3 - 4W_2 + W_1 \qquad \text{(E.3.11)}$$

etc.....

By substitution of equations (E.3.8) to (E.3.11) into equation (E.3.7), the following equation is obtained when $\Delta^5 W_1$ and the higher difference terms are omitted:

$$\left.\frac{\partial W}{\partial X}\right|_{X=X_O} = W_1'$$

$$= \frac{1}{12h}\,(-25W_1 + 48W_2 - 36W_3 + 16W_4 - 3W_5) \qquad \text{(E.3.11)}$$

Thus, the derivative of the function W(X) can be evaluated at a given value of X in terms of five successively equally spaced values of the function.

APPENDIX F

COMPUTER PROGRAMME

F.1 User's Guide to the Computer Programme

The development of an accurate, stable and economical method of solving the equations governing the transfer of heat from a solid sphere by time-dependent free convection has been the central theme of the present study. A computer programme is a necessary link between the formal description of the method in terms of symbols and the practically useful predictions in terms of numbers.

The programme was written in the FORTRAN IV language and has been run on a CDC 7600 computer; with a few minor changes it can be run on CDC 6600 and CDC 6400 computers.

The listing of the computer programme is presented in section F.4. The skeleton of the present computer programme is very similar to that generated by Rafique (1971). The main function of each subroutine in the programme is described in the listing. Therefore, the user should not find it difficult to understand and use the programme. The main functions of the main subroutines can be summarised as follows.

The input data and output of the results are handled by two subroutines called INPUT and OUTPUT. The main computations described in Section 3.7 are performed by

two subroutines called UPDATE and VARBC. The various options built in the programme are controlled from a subroutine called CONTROL.

The main programme calls the above mentioned subroutines. The programme also consists of several auxillary subroutines which allow quick detection of errors.

To obtain all results presented in this thesis, the user needs only to specify appropriate counters and parameters in subroutine CONTROL.

F.2 List of FORTRAN Symbols

Given below is the list of the main FORTRAN symbols used in the programme. All the other symbols used in the programme are either defined in terms of these symbols or are self-explanatory.

FORTRAN SYMBOL	MEANING
A	a
AKNOT	k_0
AK(J)	k_Θ
ANUL(J)	Nu_Θ
ANUO	$\overline{Nu}$
B1(I)	b_{1i}
B2(I)	b_{2i}
B3(J)	b_{3j}

FORTRAN SYMBOL	MEANING
B4(J)	b_{4j}
C(I)	c_i
CCG	ε_G
CCTD	ε_T (downstream)
CCTU	ε_T (upstream)
CCU	ε_ψ
CDF	C_{DF}
CDP	C_{DP}
CDT	C_{DT}
CPT	The Central Processor time set for a CDC 7600 computer
CR	C_R
CS(J)	$\cos\Theta$
CT(J)	$\cot\Theta$
DFG	ω_G
DFTD	ω_T (downstream)
DFTU	ω_T (upstream)
DFU	ω_ψ
GO(I,J)	$G^n_{i,j}$
GN(I,J)	$G^{n+1}_{i,j}$
GR	Grashof number
H3(I,J)	h_{3ij}
II	Input magnetic tape unit number
IN1	IN1=total number of grid lines in the Z-direction

FORTRAN SYMBOL	MEANING
ISKIPN	Number of files to be skipped on the input magnetic tape.
ISKIPO	Number of files to be skipped on the output magnetic tape.
ITHETA(J)	Θ in degrees
IXSTEP	Number of line-printer steps to be used for plotting one quarter of the flow field. Normal setting as shown in programme lising.
JJ	Output magnetic tape unit number.
JN1	JN1=total number of grid lines in the Θ -direction.
KNT	Number of temperature contours to be plotted.
KNU	Number of stream-lines to be plotted.
KNV	Number of vorticity contours to be plotted.
KS	k in degrees

(All FORTRAN Symbols beginning with L are programme control contours)

LM1	If LM1=1, another step in time is taken. Otherwise iterations are performed on the existing solution.

FORTRAN SYMBOLE	MEANING
LM2	If LM2=1, the stream function equation is solved at the n+½ time step.
LNP1	If LNP1=1, the programme starts from t*=0. If LNP1=0, the operation of the programme is controlled by LNP2 or LNP3.
LNP2	If LNP2=1, the programme reads in a previously obtained converged solution from a magnetic tape and updates it in time. Otherwise set as zero.
LNP3	If LNP3=1, the programme reads in a previously obtained unconverged solution from a magnetic tape and performs the appropriate computations. Otherwise set as zero.
LOP1	If LOP1=1, a full output of results is produced and the current solution is transferred to a magnetic tape. Otherwise set as zero.
LOP2	If LOP2=1, only the Nusselt numbers, the surface pressures, and the drag coefficients are printed out and the current solution in the computer

FORTRAN SYMBOL	MEANING
	is transferred to a magnetic tape. Otherwise set as zero.
LOP3	If LOP3=1, a table of stream function, vorticity and temperature values together with the drag coefficients and Nusselt numbers are printed out. Otherwise set as zero.
M	The number of the sections (1-10) of the flow field that are to be searched when plotting contours.
MNPR	The maximum number of unconverged nodes acceptable in a solution. Normally set as zero.
MXITER	The maximum number of iterations allowed per time step for convergence of the time-dependent boundary conditons.
MXU	The maximum number of iterations allowed for convergence of the stream function values at the n+½ time step.
MXUP	The maximum number of iterations allowed for convergence of the stream function values at the n+½

FORTRAN SYMBOL	MEANING
	time step.
NPRG1	The total number of unconverged surface vorticity nodes.
NPRTD1	The total number of unconverged temperature nodes at the down-stream axis of symmetry.
NPRTU1	The total number of unconverged temperature nodes at the upstream axis of symmetry.
NPRU1	The total number of unconverged nodes in the stream function field.
NPRINT	The number of time-step after which a print out of the dependent variables is produced.
NTIMES	The total number of time steps by which the solution is advanced in time.
OPTIME	The approximate CDC 7600 central processor time required for output of results
PR	Prandtl number
RPLOTT	The radial distance upto which the isotherms plot is produced
RPLOTU	The radial distance upto which the streamlines plot is produced.

FORTRAN SYMBOL	MEANING
RPLOTV	The radial distance upto which the vorticity distribution plot is produced.
SH	Mesh size h
SK	Mesh size k
SN(J)	$\sin\theta$
ST	Time-step
THETA(J)	θ
TIME	t
TN(I,J)	$T_{i,j}^{n+1}$
TO(I,J)	$T_{i,j}^{n}$
UN(I,J)	$\psi_{i,j}^{n+1}$
UO(I,J)	$\psi_{i,j}^{n}$
VCT(K)	Values of the isotherm contours
VCU(K)	Values of the streamline contours
VCV(K)	Values of the vorticity contours
VN(I,J)	$\zeta_{i,j}^{n+1}$
VO(I,J)	$\zeta_{i,j}^{n}$
WT	ω_θ
WZ	ω_Z
Z(I)	Z_i, distance in z-direction

F.3 Flow Diagram and Listing of the Computer Programme

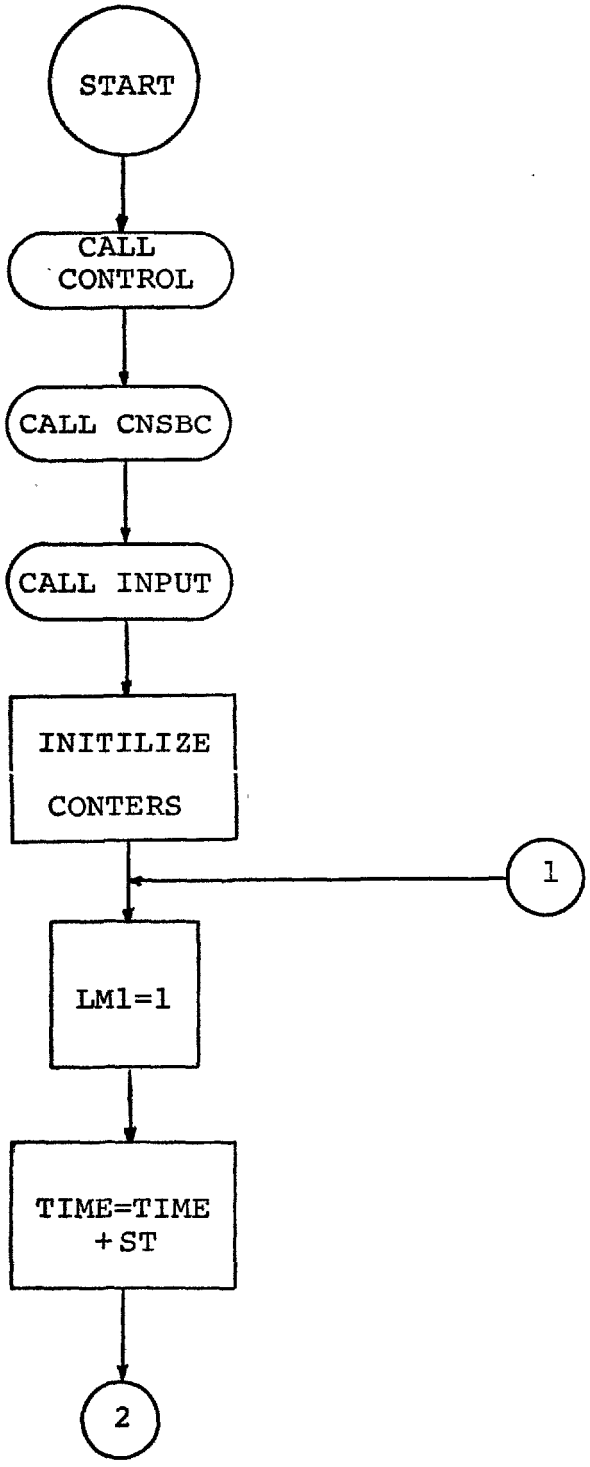

FIGURE F.3.1 FLOW DIAGRAM FOR THE MAIN PROGRAMME

FIGURE F.3.1 (CONTINUED)

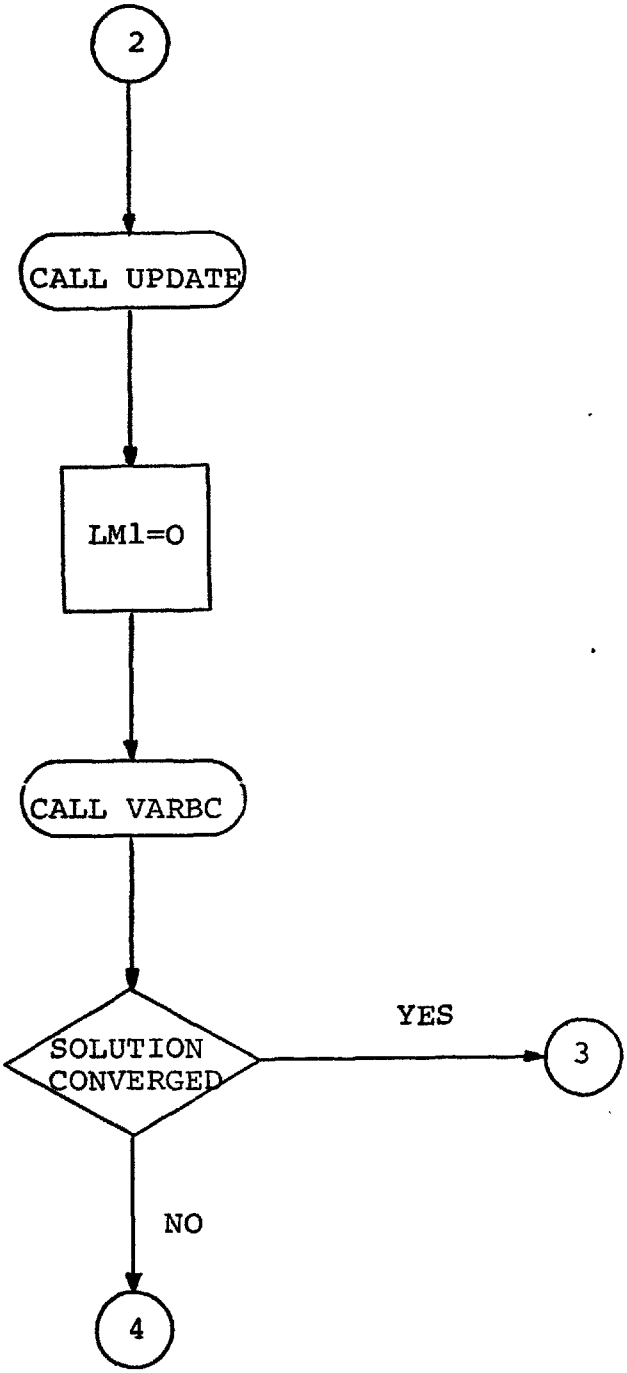

FIGURE F.3.1 (CONTINUED)

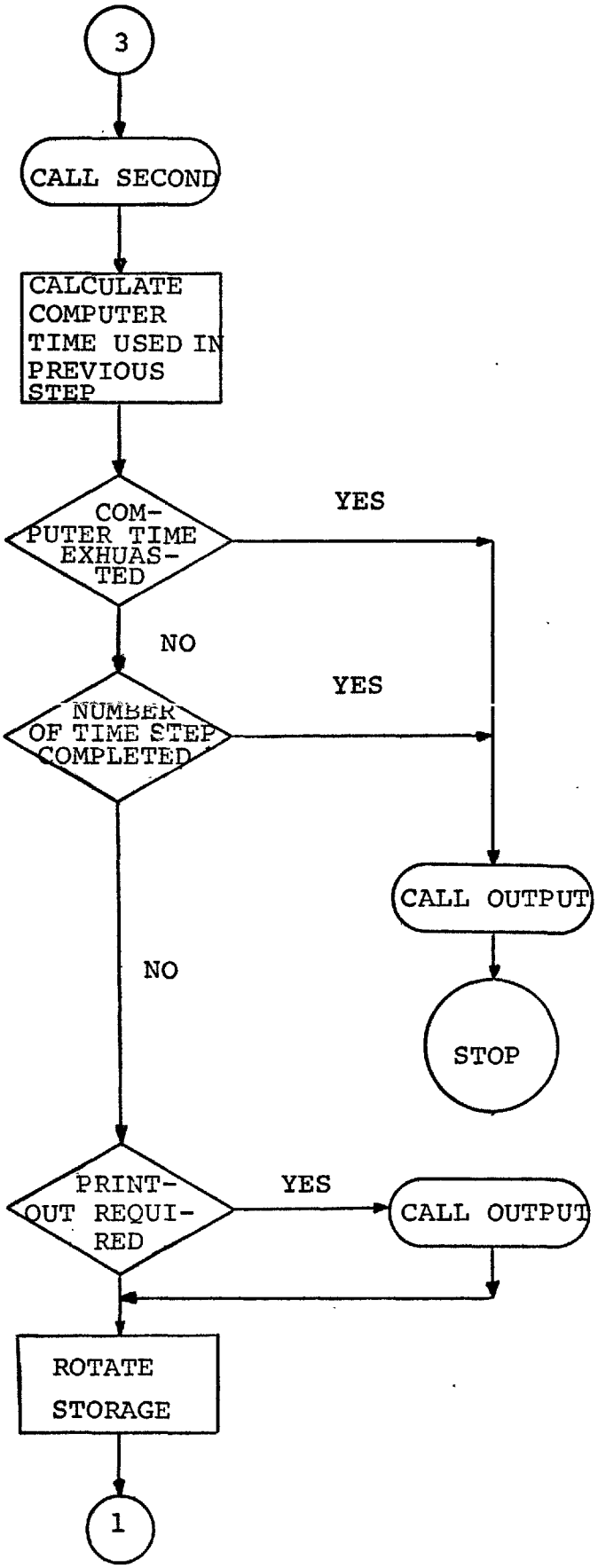

FIGURE F.3.1 (CONTINUED)

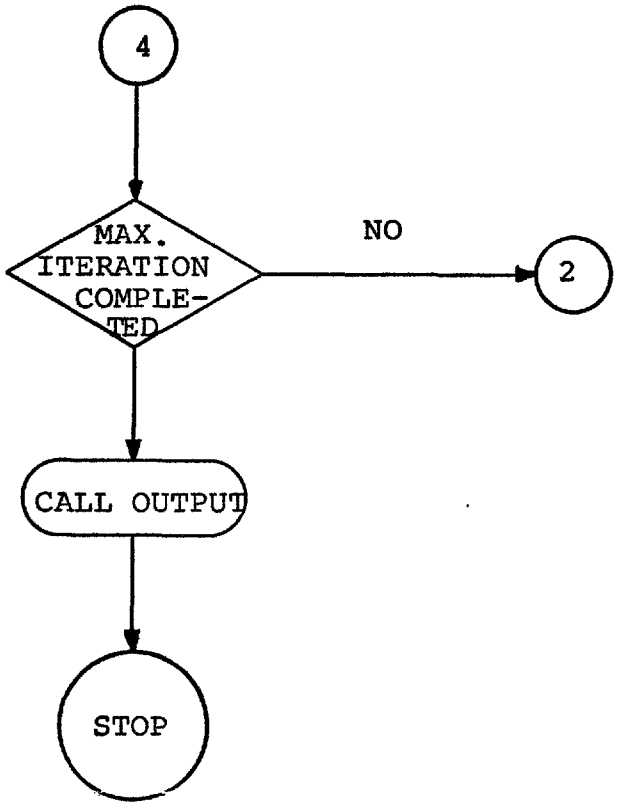

```
PROGRAM FREE       76/76   OPT=2                          FTN 4.2+178

      PROGRAM FREE(INPUT,OUTPUT,TAPE5=INPUT,TAPE6=OUTPUT,TAPE1,TAPE2)
C
C*****************************************************************
C
C     THIS PROGRAM SIMULATES FREE CONVECTIVE HEAT TRANSFER FROM A SOLI
C
C        SPHERE TO A VISCOUS INCOMPRESSIBLE NEWTONIAN MEDIUM BY
C
C           SOLVING TIME-DEPENDENT NAVIER-STOKES AND ENERGY
C
C              EQUATIONS SIMULTANEOUSLY USING PEACEMAN-
C
C                 RACHFORD ALTERNATING DIRECTION
C
C                   IMPLICIT ,ADI, METHOD.
C
C
C
C*****************************************************************
C
C****** ALL THE VARIABLES ARE IN DIMENSIONLESS FORMS
C
C*****************************************************************
C
C                              MAIN PROGRAM
C
C*****************************************************************
C
      COMMON /GRID/ Z(81),E(81),ITHETA(31),SN(31),CS(31),CT(31),H3(81,3
     1             ),THETA(31)
      COMMON /OLDV/ UO(81,31),GO(81,31),TO(81,31)
      COMMON /NEWV/ UN(81,31),GN(81,31),TN(81,31)
      COMMON /INJN/ IN1,JN1,IN,JN,SH,SK,ST,KS,GR,PR,CCJ,CCG,DFU,DFG
      COMMON /NPRC/ NPRJ1,NPRG1,NPRJ,NPRG,NTOTAL,MNPR,MXITER,NPRINT,
     1             NTIMES,MXU,MXUP
      COMMON /TSTEP/ RX(81),TIME
      COMMON /LOTPUT/ LOP1,LOP2,LOP3
      COMMON /LMAIN/ LM1,LM2
      COMMON /LRSTAB/ LRS1
      COMMON /CPTIME/ CPT,OPTIME
      COMMON /GRAF/ IGRAPH,NG
      COMMON /TEMP/ NPRTU1,NPRTD1,NPRTU,NPRTD,CCTJ,CCTD,DFTJ,DFTD
      LEVEL 2 ,Z,UO,UN,IN1,NPRU1,RX,LOP1,LM1,LRS1,CPT,IGRAPH,NPRTJ1
      WRITE(6,20)
C
C****** SET PROGRAM CONTROL PARAMETERS TO START COMPUTATION
C
      CALL CONTROL
C
C****** SET TIME-INDEPENDENT BOUNDARY CONDITIONS
C
      CALL CNSBC
C
C****** READ OR EVALUTE INPUT DATA
C
      CALL INPUT
      N=0$NPOLD=0$NPAGE=0$CPSECI=0.
```

```
PROGRAM FREE       76/76   OPT=2                          FTN 4.2+178

C*****************************************************************
C
C****** START PROCEEDING IN TIME
C
   10 CONTINUE
      NITER=0
      LM1=1
      TIME=TIME+ST
      IF(NPAGE.EQ.1) WRITE(6,20)
   20 FORMAT(1H1)
C*****************************************************************
C
   30 CONTINUE
C
C****** UPDATE TEMPERATURE AND VORTICITY FIELDS IN TIME--- AND SOLVE
C                          STREAM FUNCTION EQUATION
C
      CALL UPDATE
      LM1=0
C
C****** EVALUATE TIME-DEPENDENT BOUNDARY CONDITIONS AT THE NEW TIME-STE
C
      CALL VARBC
      NITER=NITER+1
      NTOTAL=NPRU+NPRG+NPRTU+NPRTD
      WRITE(6,40) NTOTAL,NPRU,NPRG,NPRTU,NPRTD
   40 FORMAT(1X,*NTOTAL=*,I4,5X,*NPRU=*,I4,5X,*NPRG=*,I4,5X,
     1       *NPRTU=*,I4,5X,*NPRTD=*,I4)
C
C****** TEST FOR CONVERGENCE
C
      IF(NTOTAL.LE.MNPR) GO TO 50
C
C****** TEST FOR MAXIMUM ITERATIONS
C
      IF(NITER.GE.MXITER) GOTO 110
      GOTO 30
   50 CONTINUE
C
C****** CHECK COMPUTER TIME USED
C
      CALL SECOND(CPSEC)
      WRITE(6,60) CPSEC,NITER
   60 FORMAT(1H0,*CPTIME = *,F12.5,10X,*NITER = *,I4)
      WRITE(6,120)
      TLEFT=CPT-CPSEC
      DLT1=TLEFT-OPTIME
      DLT2=CPSEC-CPSECI
      IF(DLT1.LE.DLT2) GOTO 100
      CPSECI=CPSEC
      N =N+1
C
C****** CHECK PRINT OUT OF RESULT
C
      IF(NTIMES.EQ.N) GO TO 100
      NPNEW=N/NPRINT
      IF((NPNEW-NPOLD).EQ.1) GO TO 90
```

```
PROGRAM FREE       76/76   OPT=2                          FTN 4.2+178

          NPAGE=0
       70 CONTINUE
          NPOLD=NPNEW
          DO 80 I=1,IN1
          DO 80 J=1,JN1
          UO(I,J)=UN(I,J)
          GO(I,J)=GN(I,J)
          TO(I,J)=TN(I,J)
       80 CONTINUE
          GO TO 10
       90 CONTINUE
          NPAGE=1
          LOP1=0$LOP2=0$LOP3=1
          CALL OUTPUT
          GO TO 70
      C*****************************************************************
      C
        100 CONTINUE
          LOP1=1$LOP2=0$LOP3=0
          IF(N.EQ.NTIMES) IGRAPH=1
          CALL OUTPUT
          IF(IGRAPH.EQ.0) WRITE(6,140)
          IGRAPH=0
          STOP
      C*****************************************************************
      C
        110 CONTINUE
          LOP1=0$LOP2=1$LOP3=0
          CALL OUTPUT
          WRITE(6,150)
          STOP
      C*****************************************************************
        120 FORMAT(35X,* ----------------------------------*)
        140 FORMAT(1H0,*------------SOLUTION CONVERGED AND TRANSFERRED ONTO
           1MAGNETIC TAPE-----REMEMBER TO SET LNP2=1 FOR NEXT RUN------*)
        150 FORMAT(1H0,*------------SOLUTION DIVERGED BUT TRANSFERRED ONTO
           1AGNETIC TAPE-----REMEMBER TO SET LNP3=1 FOR NEXT RUN------*)
          END
```

```
UBROUTINE CONTROL    76/76   OPT=2                          FTN 4.2+178

      SUBROUTINE CONTROL
C
C******
C       THIS SUBROUTINE SUPPLIES ALL PROGRAM CONTROL PARAMETERS
C******
C
      COMMON /GRID/ Z(81),E(81),ITHETA(31),SN(31),CS(31),CT(31),H3(81,3
     1              ),THETA(31)
      COMMON /NPRC/ NPRJ1,NPRG1,NPRU,NPRG,NTOTAL,MNPR,MXITER,NPRINT,
     1              NTIMES,MXU,MXUP
      COMMON /INJN/ IN1,JN1,IN,JN,SH,SK,ST,KS,GR,PR,CCJ,CCG,DFU,DFG
      COMMON /TSTEP/ RX(81),TIME
      COMMON /PLTPCN/ VCU(10),VCV(10),VCT(10),KNU,KNV,KNT,M
      COMMON /PLOTC/ XX1(31,10),YY1(31,10),XX2(31,10),YY2(31,10),IYS,
     1               IXSTEP,JNH1,JNH,KNP,RPLOT,RPLOTU,RPLOTV,RPLOTT
      COMMON /LMAIN/ LM1,LM2
      COMMON /LNPUT/ LNP1,LNP2,LNP3
      COMMON /LNTAPE/ ISKIPN,II
      COMMON /LOTAPE/ ISKIPO,JJ
      COMMON /CPTIME/ CPT,OPTIME
      COMMON /GRAF/ IGRAPH,NG
      COMMON /TEMP/ NPRTU1,NPRTD1,NPRTU,NPRTD,CCTJ,CCTD,DFTJ,DFTD
      LEVEL 2 ,Z,NPRU1,IN1,RX,VCU,XX1,LM1,LNP1,ISKIPN,ISKIPO,
     1        CPT,IGRAPH,NPRTU1
C
C****** SET GRASHOF NUMBER, PRANDTL NUMBER, MESH SIZES AND TIME-INTERVA
C
      GR=1.
      PR=0.72
      TIME=0.
      SH=0.04£KS=6
      SK=3.14159*FLOAT(KS)/180.
      ST=0.001
      IN1=81£JN1=31
      IN=IN1-1
      JN=JN1-1
      JNHH=JN/2
      JNHH2=JNHH+2
C*************************************************************************
C
C****** SET APPROPRIATE INITIAL CONDITION
C
      LNP1=1£LNP2=0£LNP3=0
      II=1£JJ=2
      ISKIPN=0£ISKIPO=0
      LM2=1
C*************************************************************************
C
C****** SET CONVERGENCE CRITERIA AND RELAXATION FACTORS
C
      CCU=0.000001£DFU=1.6
      CCG=0.001£DFG=0.65
      CCTJ=0.000001£DFTJ=1.5
      CCTD=0.000001£DFTD=1.5
      MNPR=0
      MXITER=50
      MXUP=200£MXU=200
```

```
UBROUTINE CONTROL    76/76   OPT=2                          FTN 4.2+178

      C*************************************************************************
      C
      C****** SET OUTPUT PARAMETERS
      C
            CPT=1200.
            OPTIME=10.
            NPRINT=100
            NTIMES=2
            IGRAPH=0
      C*************************************************************************
      C
      C****** SET PARAMETERS FOR STREAM FUNCTION,VORTICITY AND TEPERATURE
      C                          CONTOUR PLOTS
      C
            RPLOTU=24.5325$RPLOTV=24.5325$RPLOTT=24.5325$M=10$IXSTEP=60
            IYS=1.6666*FLOAT(IXSTEP-1)+1.5
            KNU=3$KNV=3$KNT=3
            VCU(1)=0.05$VCU(2)=0.1$VCU(3)=0.2
            VCV(1)=0.015$VCV(2)=-0.00025$VCV(3)=-0.001
             VCT(1)=0.7$VCT(2)=0.25$VCT(3)=0.01
            WRITE(6,10)
         10 FORMAT(1X,//,60X,*CONVERGENCE CRITERION          RELAXATION FACTO
           1*)
            WRITE(6,20) CCU,DFU,CCG,DFG,CCTU,DFTU,CCTD,DFTD
         20 FORMAT(1X,//,5X,*STREAM FUNCTION*,45X,F11.8,21X,F5.3,///,5X,
           1*SURFACE VORTICITY*,43X,F11.8,21X,F5.3,///,5X,*AXIS OF SYMMETRY T
           2MPERATURE--UPSTREAM*,22X,F11.8,21X,F5.3,///,5X,*AXIS OF SYMMETRY
           3EMPERATURE--DOWNSTREAM*,20X,F11.8,21X,F5.3)
            WRITE(6,30) SH,KS,ST,IN1,JN1,TIME
         30 FORMAT(1X,////,5X,*MESH SIZE IN RADIAL DIRECTION*,15X,F6.4,//,5X,
           1 *MESH SIZE IN ANGULAR DIRECTION(DEGREES)*,9X,I2,//,5X,*TIME INTE
           2VAL*,30X,F6.4,//,5X,*NUMBER OF GRID POINTS IN RADIAL DIRECTION*,
           36X,I3,//,5X,*NUMBER OF GRID POINTS IN ANGULAR DIRECTION*,5X,I3,
           4//,5X,*STARTING TIME FOR THIS RUN*,18X,F6.4)
            RETURN
            END
```

```
SUBROUTINE CNSBC      76/76   OPT=2                    FTN 4.2+178

      SUBROUTINE CNSBC
C
C******
C       THIS SUBROUTINE SETS TIME-INDEPENDENT BOUNDARY CONDITIONS
C******
C
      COMMON /GRID/ Z(81),E(81),ITHETA(31),SN(31),CS(31),CT(31),H3(81,3
     1              ),THETA(31)
      COMMON /NEWV/ UN(81,31),GN(81,31),TN(81,31)
      COMMON /VOO/ VO(81,31)
      COMMON /VON/ VN(81,31)
      COMMON /INJN/ IN1,JN1,IN,JN,SH,SK,ST,KS,GR,PR,CCU,CCG,DFU,DFG
      LEVEL 2 ,Z,UN,VO,VN,IN1
C
      DO 10 I=1,IN1
      UN(I,1)=0.
      UN(I,JN1)=0.
      GN(I,1)=0.
      GN(I,JN1)=0.
      VO(I,1)=0.
      VO(I,JN1)=0.
      VN(I,1)=0.
      VN(I,JN1)=0.
   10 CONTINUE
      DO 20 J=1,JN1
      TN(1,J)=1.
      TN(IN1,J)=0.
   20 CONTINUE
      DO 30 J=2,JN
      UN(1,J)=0.
      UN(IN1,J)=0.
      GN(IN1,J)=0.
      VO(IN1,J)=0.
      VN(IN1,J)=0.
   30 CONTINUE
      RETURN
      END
```

```
UBROUTINE INPUT      76/76   OPT=2                          FTN 4.2+178

      SUBROUTINE INPUT
C
C******
C       THIS SUBROUTINE CONTROLS ALL INPUT DATA REQUIRES TO START OFF
C                       SOLUTION PROCEDURE
C******
C
      COMMON /GRID/ Z(81),E(81),ITHETA(31),SN(31),CS(31),CT(31),H3(81,3
     1              ),THETA(31)
      COMMON /OLDV/ UO(81,31),GO(81,31),TO(81,31)
      COMMON /NEWV/ UN(81,31),GN(81,31),TN(81,31)
      COMMON /IJCOEF/ ASH,ASK,RSH,RSK,CR,A
      COMMON /COEF/ B1(81),B2(81),B3(81),B4(81),C(81),ESQ(81)
      COMMON /TSTEP/ RX(81),TIME
      COMMON /INJN/ IN1,JN1,IN,JN,SH,SK,ST,KS,GR,PR,CCJ,CCG,DFU,DFG
      COMMON /NPRC/ NPRJ1,NPRG1,NPRU,NPRG,NTOTAL,MNPR,MXITER,NPRINT,
     1              NTIMES,MXU,MXUP
      COMMON /LNPUT/ LNP1,LNP2,LNP3
      COMMON /TEMP/ NPRTU1,NPRTD1,NPRTU,NPRTD,CCTJ,CCTD,DFTJ,DFTD
      COMMON /LRSTAB/ LRS1
      LEVEL 2 ,Z,UO,UN,ASH,B1,RX,IN1,NPRU1,LNP1,NPRTU1,LRS1
C
      NPRU1=(IN-1)*(JN-1)
      NPRG1=JN-1
      NPR1=NPRU1+NPRG1
      NPRTU1=IN-1
      NPRTD1=IN-1
      IF(LNP1.EQ.1) GO TO 20
      IF(LNP2.EQ.1) GO TO 30
      IF(LNP3.EQ.1) GO TO 50
      WRITE(6,10)
   10 FORMAT(1X,* INCORRECT CONTROL PARAMETERS----EXECUTION TERMINATED*
      STOP
C*************************************************************************
C
   20 CONTINUE
      CALL GRID
      CALL COEFF
      CALL INTVAL
      WRITE(6,90)
      GO TO 60
C*************************************************************************
C
   30 CONTINUE
      CALL INTAPE
      DO 40 J=1,JN1
      DO 40 I=1,IN1
      UO(I,J)=UN(I,J)
      GO(I,J)=GN(I,J)
      TO(I,J)=TN(I,J)
   40 CONTINUE
      WRITE(6,100)
      GO TO 60
C*************************************************************************
C
   50 CONTINUE
      CALL INTAPE
```

```
UBROUTINE INPUT      76/76   OPT=2                          FTN 4.2+178

      WRITE(6,110)
C*****************************************************************
C
   60 CONTINUE
C
C****** EVALUATE CONSTANT COEFFICIENTS FOR TRANSPORT EQJATIONS
C
      A=2.*((1./SH**2)+(1./SK**2))
      ASH=1./(A*SH*SH)
      ASK=1./(A*SK*SK)
      RSH=1./(A*SH)
      RSK=1./(A*SK)
      CR=1./(2.*A*SH*SK)
      DO 70 I=1,IN1
      ESQ(I)=(E(I)*E(I))/A
      RX(I)=(2.*ESQ(I))/ST
   70 CONTINUE
C
      WRITE(6,80) E(IN1)
   80 FORMAT(1X,///,5X,*RATIO OF THE DIAMETER OF THE OJTER BOUNDARY TO
     1HE SPHERE DIAMETER =*,F10.6)
C
C****** LRS1=1 WRITE OLD VALUES OTHERWISE WRITE NEW VALJES
C
      LRS1=1
      CALL RESTAB
C
   90 FORMAT(1X,///,20X,*COMPUTATION STARTS FROM CONDJCTION SOLJTION*)
  100 FORMAT(1X,///,20X,*COMPUTATION STARTS FROM CONVERGED RESULTS OF P
     1EVIOUS RUN*)
  110 FORMAT(1X,///,20X,*COMPUTATION STARTS FROM DIVERGED RESULTS OF PR
     1VIOUS RUN*)
C
      RETURN
      END
```

SUBROUTINE GRID 76/76 OPT=2 FTN 4.2+178

```
      SUBROUTINE GRID
C
C******
C       THIS SUBROUTINE SUPPLIES GRID INFORMATION AT EACH NODE
C******
C
      COMMON /GRID/ Z(81),E(81),ITHETA(31),SN(31),CS(31),CT(31),H3(81,3
     1              ),THETA(31)
      COMMON /INJN/ IN1,JN1,IN,JN,SH,SK,ST,KS,GR,PR,CCJ,CCG,DFU,DFG
      LEVEL 2 ,Z,IN1
C
      DO 10 J=2,JN
      ITHETA(J)=KS*(J-1)
      THETA(J)=SK*FLOAT(J-1)
      SN(J)=SIN(THETA(J))
      CS(J)=COS(THETA(J))
      CT(J)=CS(J)/SN(J)
   10 CONTINUE
      ITHETA(1)=0
      ITHETA(JN1)=180
      THETA(1)=0.
      THETA(JN1)=SK*FLOAT(JN)
      SN(1)=0.
      SN(JN1)=0.
      CS(1)=1.
      CS(JN1)=-1.
      DO 20 I=2,IN
      Z(I)=SH*FLOAT(I-1)
      E(I)=EXP(Z(I))
   20 CONTINUE
      Z(1)=0.
      Z(IN1)=SH*FLOAT(IN)
      E(1)=1.
      E(IN1)=EXP(Z(IN1))
      DO 30 J=1,JN1
      DO 30 I=1,IN1
      H3(I,J)=E(I)*SN(J)
   30 CONTINUE
      RETURN
      END
```

UBROUTINE COEFF 76/76 OPT=2 FTN 4.2+178

```
      SUBROUTINE COEFF
C
C******
C       THIS SUBROUTINE EVALUATES CONSTANT COEFFICIENTS IN
C                  FINITE-DIFFERENCE EQUATIONS
C******
C
      COMMON /GRID/ Z(81),E(81),ITHETA(31),SN(31),CS(31),CT(31),H3(81,3
     1            ),THETA(31)
      COMMON /COFF/ B1(81),B2(81),B3(81),B4(81),C(81),ESQ(81)
      COMMON /INJN/ IN1,JN1,IN,JN,SH,SK,ST,KS,GR,PR,CCJ,CCG,DFU,DFG
      LEVEL 2 ,Z,B1,IN1
C
      A=2.*((1./SH**2)+(1./SK**2))
      BA=((1./SH**2)-0.5/SH)/A
      BB=((1./SH**2)+0.5/SH)/A
      DO 10 I=2,IN
      B1(I)=BA
      B2(I)=BB
      C(I)=(E(I)*E(I))/A
   10 CONTINUE
      DO 20 J=2,JN
      B3(J)=((1./SK**2)-0.5*CT(J)/SK)/A
      B4(J)=((1.0/SK**2)+0.5*CT(J)/SK)/A
   20 CONTINUE
      RETURN
      END
```

```
UBROUTINE INTVAL     76/76   OPT=2                          FTN 4.2+178

      SUBROUTINE INTVAL
C
C******
C       THIS SUBROUTINE SETS APPROPRIATE INITIAL CONDITIONS
C******
C
      COMMON /GRID/ Z(81),E(81),ITHETA(31),SN(31),CS(31),CT(31),H3(81,3
     1             ),THETA(31)
      COMMON /OLDV/ UO(81,31),GO(81,31),TO(81,31)
      COMMON /NEWV/ UN(81,31),GN(81,31),TN(81,31)
      COMMON /INJN/ IN1,JN1,IN,JN,SH,SK,ST,KS,GR,PR,CCJ,CCG,DFU,DFG
      LEVEL 2 ,Z,UO,UN,IN1
C
C****** INITIAL CONDITIONS OF VORTICITY AND STREAM FUNCTION
C
      DO 10 J=1,JN1
      DO 10 I=1,IN1
      GO(I,J)=0.
      UO(I,J)=0.
   10 CONTINUE
C
C****** INITIAL CONDITION OF TEMPERATURE --- PURE RADIAL CONDUCTION
C
      ER=1./E(IN1)
      ER1=1.-ER
      DO 20 J=1,JN1
      DO 20 I=2,IN
      TO(I,J)=1./(E(I)*ER1)-1./(E(IN1)*ER1)
   20 CONTINUE
      DO 30 J=1,JN1
      TO(1,J)=1.
      TO(IN1,J)=0.
   30 CONTINUE
      DO 40 J=1,JN1
      DO 40 I=1,IN1
      UN(I,J)=UO(I,J)
      GN(I,J)=GO(I,J)
      TN(I,J)=TO(I,J)
   40 CONTINUE
      RETURN
      END
```

```
UBROUTINE JPDATE     76/76   OPT=2                          FTN 4.2+178

      SUBROUTINE UPDATE
C
C******
C       THIS SUBROUTINE UPDATES TEMPERATURE AND VORTICITY FIELDS IN
C       TIME USING PEACEMAN RACHFORD ALTERNATING DIRECTION IMPLICIT
C       ,ADI, METHOD AND SOLVES STREAM FUNCTION EQUATION USING
C       SUCCESSIVE OVER RELAXATION,SOR, METHOD
C******
C
      COMMON /GRID/ Z(81),E(81),ITHETA(31),SN(31),CS(31),CT(31),H3(81,3
     1          ),THETA(31)
      COMMON /OLDV/ UO(81,31),GO(81,31),TO(81,31)
      COMMON /NEWV/ UN(81,31),GN(81,31),TN(81,31)
      COMMON /VON/ VN(81,31)
      COMMON /IJCOEF/ ASH,ASK,RSH,RSK,CR,A
      COMMON /INJN/ IN1,JN1,IN,JN,SH,SK,ST,KS,GR,PR,CCJ,CCG,DFU,DFG
      COMMON /NPRC/ NPRJ1,NPRG1,NPRU,NPRG,NTOTAL,MNPR,MXITER,NPRINT,
     1          NTIMES,MXU,MXUP
      COMMON /COFF/ B1(81),B2(81),B3(81),B4(81),C(81),ESQ(81)
      COMMON /SLVCF/ C1(81),C2(81),C3(81),D(81),P(81),LSV1
      COMMON /TSTEP/ RX(81),TIME
      COMMON /LMAIN/ LM1,LM2
      COMMON /LRSTAB/ LRS1
      LEVEL 2 ,Z,UO,UN,VN,ASH,IN1,NPRU1,B1,C1,RX,LM1,LRS1
C
      C1(1)=0.
      C2(1)=1.
      C3(1)=0.
      IF(LM1.EQ.0) GO TO 120
C*************************************************************************
C
C****** UPDATE VALUES OF VORTICITY AND TEMPERATURE AT THE HALF TIME STE
C       ----COLUMN WISE
C
      C1(JN1)=0.
      C2(JN1)=1.
      C3(JN1)=0.
C
C****** LSV1=1 UPDATE COLUMN BY COLUMN OTHERWISE UPDATE ROW BY ROW
C
      LSV1=1
C*************************************************************************
C
C****** UPDATE VALUES OF TEMPERATURE
C
      DO 30 I=2,IN
      D(1)=TN(I,1)
      D(JN1)=TN(I,JN1)
      DO 10 J=2,JN
      SKG=CR/H3(I,J)
      DIFUJ=UO(I,J+1)-UO(I,J-1)
      DIFUI=UO(I+1,J)-UO(I-1,J)
      IF(DIFUI) 2,3,4
    2 WZ=1.
      GO TO 5
    3 WZ=0.5
      GO TO 5
```

```
UBROUTINE JPDATE     76/76   OPT=2                              FTN 4.2+178

      4 WZ=0.
      5 CONTINUE
        IF(DIFUJ)6,7,8
      6 WT=0.
        GO TO 9
      7 WT=0.5
        GO TO 9
      8 WT=1.
      9 CONTINUE
        C1(J)=B1(I)-PR*SKG*DIFUJ*(1.-WT)
        C2(J)=PR*RX(I)-2.*ASH+PR*SKG*DIFUJ*(1.-2.*WT)
        C3(J)=B2(I)+PR*SKG*DIFUJ*WT
        D(J)=C1(J)*TO(I-1,J)+C2(J)*TO(I,J)+C3(J)*TO(I+1,J)
        C1(J)=-B3(J)-PR*SKG*DIFUI*(1.-WZ)
        C2(J)=PR*RX(I)+2.*ASK+PR*SKG*DIFUI*(1.-2.*WZ)
        C3(J)=-B4(J)+PR*SKG*DIFUI*WZ
     10 CONTINUE
        CALL SOLVE
        DO 20 J=1,JN1
        TN(I,J)=P(J)
     20 CONTINUE
     30 CONTINUE
        DO 40 J=1,JN1
        DO 40 I=1,IN1
        TO(I,J)=TN(I,J)
     40 CONTINUE
C*************************************************************************
C
C****** UPDATE VALUES OF VORTICITY
C
        DO 70 I=2,IN
        D(1)=GN(I,1)
        D(JN1)=GN(I,JN1)
        DO 50 J=2,JN
        SKG=CR/H3(I,J)
        SKT=CR*H3(I,J)*H3(I,J)
        DIFTI=TO(I+1,J)-TO(I-1,J)
        DIFTJ=TO(I,J+1)-TO(I,J-1)
        DIFUJ=UO(I,J+1)-UO(I,J-1)
        DIFUI=UO(I+1,J)-UO(I-1,J)
        IF(DIFUI) 41,42,43
     41 WZ=1.
        GO TO 45
     42 WZ=0.5
        GO TO 45
     43 WZ=0.
     45 CONTINUE
        IF(DIFUJ)46,47,48
     46 WT=0.
        GO TO 49
     47 WT=0.5
        GO TO 49
     48 WT=1.
     49 CONTINUE
        C1(J)=B2(I)-SKG*DIFUJ*(1.-WT)
        C2(J)=RX(I)-2.*ASH+SKG*DIFUJ*(1.-2.*WT-2.*SH)
        C3(J)=B1(I)+ KG*DIFUJ*WT
```

```
UBROUTINE JPDATE     76/76   OPT=2                          FTN 4.2+178

          C4J=SKT*GR*(SH*CT(J)*DIFTJ+SK*DIFTI)
          D(J)=C1(J)*GO(I-1,J)+C2(J)*GO(I,J)+C3(J)*GO(I+1,J)+C4J
          C1(J)=-B4(J)-SKG*DIFUI*(1.-WZ)
          C2(J)=RX(I)+2.*ASK+SKG*DIFUI*(1.-2.*WZ-2.*SK*CT(J))
          C3(J)=-B3(J)+SKG*DIFUI*WZ
       50 CONTINUE
          CALL SOLVE
          DO 60 J=1,JN1
          GN(I,J)=P(J)
       60 CONTINUE
       70 CONTINUE
          DO 80 J=1,JN1
          DO 80 I=1,IN1
          GO(I,J)=GN(I,J)
       80 CONTINUE
          IF(LM2.EQ.0) GO TO 120
      C*****************************************************************
      C
      C****** SOLVE STREAM FUNCTION AT THE HALF TIME STEP
      C
          N=0
       90 CONTINUE
          NPRU=NPRU1
          DO 100 J=2,JN
          DO 100 I=2,IN
          UTGN=B1(I)*UN(I+1,J)+B2(I)*UN(I-1,J)+B3(J)*UN(I,J+1)
         1      +B4(J)*UN(I,J-1)-C(I)*GN(I,J)
          UTGN=UN(I,J)+DFU*(UTGN-UN(I,J))
          ERRORU=UTGN-UN(I,J)
          IF(ABS(ERRORU).LE.CCU) NPRU=NPRU-1
          UN(I,J)=UTGN
      100 CONTINUE
          N=N+1
          IF(NPRU.EQ.0) GO TO 110
          IF(N.EQ.MXU) STOP
          GO TO 90
      110 CONTINUE
          WRITE(6,220) N
          CALL VARBC
      C
      C*****************************************************************
      C*****************************************************************
      C*****************************************************************
      C
      C****** UPDATE VALUES OF TEMPERATURE AND VORTICITY AT THE NEW TIME STEP
      C                              ROW BY ROW
      C
      120 CONTINUE
          C1(IN1)=0.
          C2(IN1)=1.
          C3(IN1)=0.
          LSV1=0
      C*****************************************************************
      C
      C****** UPDATE VALUES OF TEMPERATURE
      C
          DO 150 J=2,JN
```

```
UBROUTINE JPDATE     76/76   OPT=2                          FTN 4.2+178

      D(1)=TN(1,J)
      D(IN1)=TN(IN1,J)
      DO 130 I=2,IN
      SKG=CR/H3(I,J)
      DIFUI=UN(I+1,J)-UN(I-1,J)
      DIFUJ=UN(I,J+1)-UN(I,J-1)
      IF(DIFUI) 121,122,123
  121 WZ=1.
      GO TO 125
  122 WZ=0.5
      GO TO 125
  123 WZ=0.
  125 CONTINUE
      IF(DIFUJ)126,127,128
  126 WT=0.
      GO TO 129
  127 WT=0.5
      GO TO 129
  128 WT=1.
  129 CONTINUE
      C1(I)=B3(J)+PR*SKG*DIFUI*(1.-WZ)
      C2(I)=PR*RX(I)-2.*ASK-PR*SKG*DIFUI*(1.-2.*WZ)
      C3(I)=B4(J)-PR*SKG*DIFUI*WZ
      D(I)=C1(I)*TO(I,J-1)+C2(I)*TO(I,J)+C3(I)*TO(I,J+1)
      C1(I)=-B1(I)+PR*SKG*DIFUJ*(1.-WT)
      C2(I)=PR*RX(I)+2.*ASH-PR*SKG*DIFUJ*(1.-2.*WT)
      C3(I)=-B2(I)-PR*SKG*DIFUJ*WT
  130 CONTINUE
      CALL SOLVE
      DO 140 I=1,IN1
      TN(I,J)=P(I)
  140 CONTINUE
  150 CONTINUE
C*************************************************************************
C
C****** UPDATE VALUES OF VORTICITY
C
      DO 180 J=2,JN
      D(1)=GN(1,J)
      D(IN1)=GN(IN1,J)
      DO 160 I=2,IN
      SKG=CR/H3(I,J)
      SKT=CR*H3(I,J)*H3(I,J)
      DIFTI=TN(I+1,J)-TN(I-1,J)
      DIFTJ=TN(I,J+1)-TN(I,J-1)
      DIFUI=UN(I+1,J)-UN(I-1,J)
      DIFUJ=UN(I,J+1)-UN(I,J-1)
      IF(DIFUI) 151,152,153
  151 WZ=1.
      GO TO 155
  152 WZ=0.5
      GO TO 155
  153 WZ=0.
  155 CONTINUE
      IF(DIFUJ)156,157,158
  156 WT=0.
      GO TO 159
```

```
UBROUTINE JPDATE     76/76   OPT=2                          FTN 4.2+178

      157 WT=0.5
          GO TO 159
      158 WT=1.
      159 CONTINUE
          C1(I)=B4(J)+SKG*DIFUI*(1.-WZ)
          C2(I)=RX(I)-2.*ASK-SKG*DIFUI*(1.-2.*WZ-2.*SK*CT(J))
          C3(I)=B3(J)-SKG*DIFUI*WZ
          C4I=SKT*GR*(SH*CT(J)*DIFTJ+SK*DIFTI)
          D(I)=C1(I)*GO(I,J-1)+C2(I)*GO(I,J)+C3(I)*GO(I,J+1)+C4I
          C1(I)=-B2(I)+SKG*DIFUJ*(1.-WT)
          C2(I)=RX(I)+2.*ASH-SKG*DIFUJ*(1.-2.*WT-2.*SH)
          C3(I)=-B1(I)-SKG*DIFUJ*WT
      160 CONTINUE
          CALL SOLVE
          DO 170 I=1,IN1
          GN(I,J)=P(I)
      170 CONTINUE
      180 CONTINUE
      185 CONTINUE
C*************************************************************************
C
C****** SOLVE STREAM FUNCTION AT NEW TIME STEP
C
          N=0
      190 CONTINUE
          N=N+1
          NPRU=NPRU1
          DO 200 J=2,JN
          DO 200 I=2,IN
          UTGN=B1(I)*UN(I+1,J)+B2(I)*UN(I-1,J)+B3(J)*UN(I,J+1)
         1     +B4(J)*UN(I,J-1)-C(I)*GN(I,J)
          UTGN=UN(I,J)+DFU*(UTGN-UN(I,J))
          ERRORU=UTGN-UN(I,J)
          IF(ABS(ERRORU).LE.CCU) NPRU=NPRU-1
          UN(I,J)=UTGN
      200 CONTINUE
          IF(NPRU.EQ.0) GO TO 210
          IF(N.EQ.MXUP) GO TO 230
          GO TO 190
      210 CONTINUE
          WRITE(6,220) N
      220 FORMAT(10X,2HN=,I4)
          RETURN
      230 CONTINUE
          DO 240 J=2,JN
          DO 240 I=1,IN1
          VN(I,J)=GN(I,J)/H3(I,J)
      240 CONTINUE
          LRS1=0
          CALL RESTAR
          GO TO 185
          END
```

```
SUBROUTINE VARBC      76/76   OPT=2                    FTN 4.2+178

      SUBROUTINE VARBC
C
C******
C      THIS SUBROUTINE EVALUATES TIME-DEPENDENT BOUNDARY CONDITIONS
C******
C
      COMMON /GRID/ Z(81),E(81),ITHETA(31),SN(31),CS(31),CT(31),H3(81,
     1              ),THETA(31)
      COMMON /NEWV/ UN(81,31),GN(81,31),TN(81,31)
      COMMON /INJN/ IN1,JN1,IN,JN,SH,SK,ST,KS,GR,PR,CCJ,CCG,DFU,DFG
      COMMON /NPRC/ NPRJ1,NPRG1,NPRU,NPRG,NTOTAL,MNPR,MXITER,NPRINT,
     1              NTIMES,MXU,MXUP
      COMMON /LMAIN/ LM1,LM2
      COMMON /TEMP/ NPRTU1,NPRTD1,NPRTU,NPRTD,CCTJ,CCTD,DFTJ,DFTD
      LEVEL 2 ,Z,UN,IN1,NPRU1,LM1,NPRTU1
C
      RSH2=0.5/(SH*SH)
      IF(LM1.EQ.1) GO TO 30
C*************************************************************************
C
C****** EVALUATE AT THE NEW TIME-STEP
C
      NPRG=NPRG1
      NPRTU=NPRTU1
      NPRTD=NPRTD1
C
C****** EVALUATE SURFACE VORTICITY
C
      DO 10 J=2,JN
      UTGN=RSH2*(8.*UN(2,J)-UN(3,J))
      UTGN=GN(1,J)+DFG*(UTGN-GN(1,J))
      ERRORG=(UTGN-GN(1,J))/H3(1,J)
      IF(ABS(ERRORG).LE.CCG) NPRG=NPRG-1
      GN(1,J)=UTGN
   10 CONTINUE
C
C****** EVALUATE TEMPERATURE ALONG THE AXIS OF SYMMETRY
C
      DO 20 I=2,IN
      UTGN=(18.*TN(I,2)-9.*TN(I,3)+2.*TN(I,4))/11.
      UTGN=TN(I,1)+DFTU*(UTGN-TN(I,1))
      ERRORT=UTGN-TN(I,1)
      IF(ABS(ERRORT).LE.CCTU) NPRTU=NPRTU-1
      TN(I,1)=UTGN
      UTGN=(18.*TN(I,JN)-9.*TN(I,JN-1)+2.*TN(I,JN-2))/11.
      UTGN=TN(I,JN1)+DFTD*(UTGN-TN(I,JN1))
      ERRORT=UTGN-TN(I,JN1)
      IF(ABS(ERRORT).LE.CCTD) NPRTD=NPRTD-1
      TN(I,JN1)=UTGN
   20 CONTINUE
      RETURN
C
C*************************************************************************
C*************************************************************************
C
C****** EVALUATE AT THE HALF TIME-STEP
C
```

SUBROUTINE VARBC 76/76 OPT=2 FTN 4.2+178

```
   30 CONTINUE
C
C****** EVALUATE SURFACE VORTICITY
C
      DO 40 J=2,JN
      GN(1,J)=(8.*UN(2,J)-UN(3,J))*RSH2
   40 CONTINUE
C
C****** EVALUATE TEMPERATURE ALONG THE AXIS OF SYMMETRY
C
      DO 50 I=2,IN
      TN(I,1)=(18.*TN(I,2)-9.*TN(I,3)+2.*TN(I,4))/11.
      TN(I,JN1)=(1 .*TN(I,JN)-9.*TN(I,JN-1)+2.*TN(I,JN-2))/11.
   50 CONTINUE
      RETURN
      END
```

```
UBROUTINE SOLVE      76/76   OPT=2                          FTN 4.2+178

      SUBROUTINE SOLVE
C
C******
C       THIS SUBROUTINE SOLVES TRIDIAGONAL MATRICES FOR TEMPERATURE
C                          AND VORTICITY VALUES
C******
C
      DIMENSION  W(81),G(81)
      COMMON /GRID/ Z(81),E(81),ITHETA(31),SN(31),CS(31),CT(31),H3(81,3
     1              ),THETA(31)
      COMMON /INJN/ IN1,JN1,IN,JN,SH,SK,ST,KS,GR,PR,CCJ,CCG,DFU,DFG
      COMMON /SLVCF/ C1(81),C2(81),C3(81),D(81),P(81),LSV1
      LEVEL 2 ,Z,IN1,C1
C
      IF(LSV1.EQ.1) GO TO 30
      W(1)=C2(1)
      G(1)=D(1)/W(1)
      DO 10 I=2,IN1
      W(I)=C2(I)-C1(I)*C3(I-1)/W(I-1)
      G(I)=(D(I)-C1(I)*G(I-1))/W(I)
   10 CONTINUE
      P(IN1)=G(IN1)
      I=IN
      DO 20 K=1,IN
      P(I)=G(I)-C3(I)*P(I+1)/W(I)
      I=I-1
   20 CONTINUE
      RETURN
C
C*************************************************************************
C
   30 CONTINUE
      W(1)=C2(1)
      G(1)=D(1)/W(1)
      DO 40 J=2,JN1
      W(J)=C2(J)-C1(J)*C3(J-1)/W(J-1)
      G(J)=(D(J)-C1(J)*G(J-1))/W(J)
   40 CONTINUE
      P(JN1)=G(JN1)
      J=JN
      DO 50 K=1,JN
      P(J)=G(J)-C3(J)*P(J+1)/W(J)
      J=J-1
   50 CONTINUE
      RETURN
      END
```

```
UBROUTINE OUTPUT     76/76   OPT=2                          FTN 4.2+178

      SUBROUTINE OUTPUT
C******
C       THIS SUBROUTINE CONTROLS OUTPUT OF RESULTS
C******
C
      COMMON /GRID/ Z(81),E(81),ITHETA(31),SN(31),CS(31),CT(31),H3(81,3
     1              ),THETA(31)
      COMMON /INJN/ IN1,JN1,IN,JN,SH,SK,ST,KS,GR,PR,CCJ,CCG,DFU,DFG
      COMMON /LOTPUT/ LOP1,LOP2,LOP3
      COMMON /LRSTAB/ LRS1
      LEVEL 2 ,Z,IN1,LOP1,LRS1
C
      LRS1=0
      IF(LOP1.EQ.1) GO TO 20
      IF(LOP2.EQ.1) GO TO 30
      IF(LOP3.EQ.1) GO TO 40
      WRITE(6,10)
   10 FORMAT(1X,*INCORRECT GENERATION OF OUTPUT CONTROL PARAMETERS*)
      RETURN
C*************************************************************************
C
   20 CONTINUE
      CALL PDNCOEF
      CALL RESTAB
      CALL CNPLTP
      CALL OUTAPE
      RETURN
C*************************************************************************
C
   30 CONTINUE
      CALL PDNCOEF
      CALL OUTAPE
      RETURN
C*************************************************************************
C
   40 CONTINUE
      CALL PDNCOEF
      CALL RESTAB
      RETURN
      END
```

```
UBROUTINE INTAPE     76/76   OPT=2                          FTN 4.2+178

      SUBROUTINE INTAPE
C
C******
C       THIS SUBROUTINE READS IN DATA FROM MAGNETIC TAPE
C******
C
      COMMON /GRID/ Z(81),E(81),ITHETA(31),SN(31),CS(31),CT(31),H3(81,3
     1              ),THETA(31)
      COMMON /OLDV/ UO(81,31),GO(81,31),TO(81,31)
      COMMON /NEWV/ UN(81,31),GN(81,31),TN(81,31)
      COMMON /INJN/ IN1,JN1,IN,JN,SH,SK,ST,KS,GR,PR,CCJ,CCG,DFU,DFG
      COMMON /COEF/ B1(81),B2(81),B3(81),B4(81),C(81),ESQ(81)
      COMMON /LNTAPE/ ISKIPN,II
      LEVEL 2 ,Z,UO,UN,IN1,B1,ISKIPN
C
      REWIND II
      IF(ISKIPN.GT.0) CALL SKPFILE(ISKIPN,II)
C
      READ(II)(Z(I),E(I),I=1,IN1)
      READ(II)(ITHETA(J),THETA(J),SN(J),CS(J),CT(J),J=1,JN1)
      READ(II)(B1(I),B2(I),C(I),I=1,IN1)
      READ(II)(B3(J),B4(J),J=1,JN1)
      READ(II)((H3(I,J),I=1,IN1),J=1,JN1)
      READ(II)((UO(I,J),I=1,IN1),J=1,JN1)
      READ(II)((GO(I,J),I=1,IN1),J=1,JN1)
      READ(II)((TO(I,J),I=1,IN1),J=1,JN1)
      READ(II)((UN(I,J),I=1,IN1),J=1,JN1)
      READ(II)((GN(I,J),I=1,IN1),J=1,JN1)
      READ(II)((TN(I,J),I=1,IN1),J=1,JN1)
      RETURN
      END
```

```
UBROUTINE OUTAPE     76/76   OPT=2                          FTN 4.2+178

      SUBROUTINE OUTAPE
C
C******
C       THIS SUBROUTINE WRITES OUT DATA ON MAGNETIC TAPE
C******
C
      COMMON /GRID/ Z(81),E(81),ITHETA(31),SN(31),CS(31),CT(31),H3(81,3
     1              ),THETA(31)
      COMMON /OLDV/ UO(81,31),GO(81,31),TO(81,31)
      COMMON /NEWV/ UN(81,31),GN(81,31),TN(81,31)
      COMMON /INJN/ IN1,JN1,IN,JN,SH,SK,ST,KS,GR,PR,CCJ,CCG,DFU,DFG
      COMMON /COFF/ B1(81),B2(81),B3(81),B4(81),C(81),ESQ(81)
      COMMON /LOTAPE/ ISKIPO,JJ
      LEVEL 2 ,Z,UO,UN,IN1,B1,ISKIPO
C
      REWIND JJ
      IF(ISKIPO.GT.0) CALL SKPFILE(ISKIPO,JJ)
      WRITE(JJ)(Z(I),E(I),I=1,IN1)
      WRITE(JJ)(ITHETA(J),THETA(J),SN(J),CS(J),CT(J),J=1,JN1)
      WRITE(JJ)(B1(I),B2(I),C(I),I=1,IN1)
      WRITE(JJ)(B3(J),B4(J),J=1,JN1)
      WRITE(JJ)((H3(I,J),I=1,IN1),J=1,JN1)
      WRITE(JJ)((UO(I,J),I=1,IN1),J=1,JN1)
      WRITE(JJ)((GO(I,J),I=1,IN1),J=1,JN1)
      WRITE(JJ)((TO(I,J),I=1,IN1),J=1,JN1)
      WRITE(JJ)((UN(I,J),I=1,IN1),J=1,JN1)
      WRITE(JJ)((GN(I,J),I=1,IN1),J=1,JN1)
      WRITE(JJ)((TN(I,J),I=1,IN1),J=1,JN1)
      END FILE JJ
      RETURN
      END
```

UBROUTINE SKPFILE 76/76 OPT=2 FTN 4.2+178

```
      SUBROUTINE SKPFILE (ISKIP,I)
C
C******
C       THIS SUBROUTINE SKIPS FILES ON MAGNETIC TAPE *** CDC 7600
C******
C
      LEVEL 2 ,ISKIP,I
C
      N=0
   10 CONTINUE
      READ(I) DUMMY
      IF(EOF(I)) 20,30
   20 N=N+1
      IF(N.EQ.ISKIP) RETURN
   30 GO TO 10
      END
```

```
UBROUTINE CNPLTP     76/76   OPT=2                          FTN 4.2+178

      SUBROUTINE CNPLTP
C
C******
C       THIS SUBROUTINE EVALUATES PLOT POSITIONS OF CONTOURS AND CALLS
C                 THE LINE-PRINTER PLOTTING ROUTINE
C******
C
      DIMENSION ZVC1(10),ZVC2(10),LVC(10)
      COMMON /GRID/ Z(81),E(81),ITHETA(31),SN(31),CS(31),CT(31),H3(81,3
     1              ),THETA(31)
      COMMON /PLTPCN/ VCU(10),VCV(10),VCT(10),KNU,KNV,KNT,M
      COMMON /NEWV/ UN(81,31),GN(81,31),TN(81,31)
      COMMON /VON/ VN(81,31)
      COMMON /PLOTC/ XX1(31,10),YY1(31,10),XX2(31,10),YY2(31,10),IYS,
     1               IXSTEP,JNH1,JNH,KNP,RPLOT,RPLOTU,RPLOTV,RPLOTT
      COMMON /INJN/ IN1,JN1,IN,JN,SH,SK,ST,KS,GR,PR,CCJ,CCG,DFU,DFG
       LEVEL 2 ,Z,VCU,UN,VN,XX1,IN1
C
      WRITE(6,240)
      WRITE(6,250)
      WRITE(6,260)  (VCU(K),K=1,KNU)
      DO 10 K=1,KNU
      ZVC1(K)=0.
      ZVC2(K)=0.
      LVC(K)=1
   10 CONTINUE
      IIN1=(IN*M/10)+1
      IIN=IIN1-1
      JNH=JN/2
      JNH1=JNH+1
C*************************************************************************
C
C****** SEARCH AND INTERPOLATE BETWEEN TWO I-LINES---
C                                          ---STREAM FUNCTION CONTOURS
C
      DO 70 J=2,JN
      DO 40 I=2,IIN1
      DO 40 K=1,KNU
      IF(UN(I-1,J).LE.VCU(K).AND.UN(I,J).GE.VCU(K)) GO TO 20
      IF(UN(I-1,J).GE.VCU(K).AND.UN(I,J).LE.VCU(K)) GO TO 20
      GO TO 40
   20 IF(LVC(K).EQ.0) GO TO 30
      ZVC1(K)=SH*(FLOAT(I-2)+(VCU(K)-UN(I-1,J))/(UN(I,J)-UN(I-1,J)))
      ZVC2(K)=0.
      LVC(K)=0
      GO TO 40
   30 ZVC2(K)=SH*(FLOAT(I-2)+(VCU(K)-UN(I-1,J))/(UN(I,J)-UN(I-1,J)))
   40 CONTINUE
      DO 50 K=1,KNU
      ZVC1(K)=EXP(ZVC1(K))
      ZVC2(K)=EXP(ZVC2(K))
      IF(ZVC1(K).LE.1.) ZVC1(K)=0.
      IF(ZVC2(K).LE.1.) ZVC2(K)=0.
      YY1(J-1,K)=ZVC1(K)*SN(J)
      XX1(J-1,K)=ZVC1(K)*CS(J)
      YY2(J-1,K)=ZVC2(K)*SN(J)
      XX2(J-1,K)=ZVC2(K)*CS(J)
```

```
BROUTINE CNPLTP     76/76   OPT=2                          FTN 4.2+178

      50 CONTINUE
         WRITE(6,270) ITHETA(J),(ZVC1(K),K=1,KNU)
         WRITE(6,280) (ZVC2(K),K=1,KNU)
         DO 60 K=1,KNU
         ZVC1(K)=0.
         ZVC2(K)=0.
         LVC(K)=1
      60 CONTINUE
      70 CONTINUE
C
C****** PLOT STREAM FUNCTION CONTOURS
C
         RPLOT=RPLOTU
         KNP=KNU
         CALL CNPLOT
      80 CONTINUE
         WRITE(6,290)
         WRITE(6,250)
         WRITE(6,260) (VCV(K),K=1,KNV)
         DO 90 K=1,KNV
         ZVC1(K)=0.
         ZVC2(K)=0.
         LVC(K)=1
      90 CONTINUE
C*************************************************************************
C
C****** SEARCH AND INTERPOLATE BETWEEN TWO I-LINES---
C                                          ---VORTICITY CONTOURS
C
         DO 150 J=2,JN
         DO 120 I=2,IIN1
         DO 120 K=1,KNV
         IF(VN(I-1,J).LE.VCV(K).AND.VN(I,J).GE.VCV(K)) GOTO 100
         IF(VN(I-1,J).GE.VCV(K).AND.VN(I,J).LE.VCV(K)) GO TO 100
         GO TO 120
     100 IF(LVC(K).EQ.0) GO TO 110
         ZVC1(K)=SH*(FLOAT(I-2)+(VCV(K)-VN(I-1,J))/(VN(I,J)-VN(I-1,J)))
         ZVC2(K)=0.
         LVC(K)=0
         GO TO 120
     110 ZVC2(K)=SH*(FLOAT(I-2)+(VCV(K)-VN(I-1,J))/(VN(I,J)-VN(I-1,J)))
     120 CONTINUE
         DO 130 K=1,KNV
         ZVC1(K)=EXP(ZVC1(K))
         ZVC2(K)=EXP(ZVC2(K))
         IF(ZVC1(K).LE.1.) ZVC1(K)=0.
         IF(ZVC2(K).LE.1.)ZVC2(K)=0.
         YY1(J-1,K)=ZVC1(K)*SN(J)
         XX1(J-1,K)=ZVC1(K)*CS(J)
         YY2(J-1,K)=ZVC2(K)*SN(J)
         XX2(J-1,K)=ZVC2(K)*CS(J)
     130 CONTINUE
         WRITE(6,270) ITHETA(J),(ZVC1(K),K=1,KNV)
         WRITE(6,280)  (ZVC2(K),K=1,KNV)
         DO 140 K=1,KNV
         ZVC1(K)=0.
         ZVC2(K)=0.
```

```
UBROUTINE CNPLTP     76/76   OPT=2                          FTN 4.2+178

          LVC(K)=1
  140 CONTINUE
  150 CONTINUE
C
C****** PLOT VORTICITY CONTOURS
C
      RPLOT=RPLOTV
      KNP=KNV
      CALL CNPLOT
C*************************************************************************
C
C****** SEARCH AND INTERPOLATE BETWEEN TWO I-LINES---
C                                          ---TEMPERATURE CONTOURS
C
  160 CONTINUE
      WRITE(6,300)
      WRITE(6,250)
      WRITE(6,260) (VCT(K),K=1,KNT)
      DO 170 K=1,KNT
      ZVC1(K)=0.
      ZVC2(K)=0.
      LVC(K)=1
  170 CONTINUE
      DO 230 J=2,JN
      DO 200 I=2,IIN1
      DO 200 K=1,KNT
      IF(TN(I-1,J).LE.VCT(K).AND.TN(I,J).GE.VCT(K)) GO TO 180
      IF(TN(I-1,J).GE.VCT(K).AND.TN(I,J).LE.VCT(K)) GO TO 180
      GO TO 200
  180 IF(LVC(K).EQ.0) GO TO 190
      ZVC1(K)=SH*(FLOAT(I-2)+(VCT(K)-TN(I-1,J))/(TN(I,J)-TN(I-1,J)))
      ZVC2(K)=0.
      LVC(K)=0
      GO TO 200
  190 ZVC2(K)=SH*(FLOAT(I-2)+(VCT(K)-TN(I-1,J))/(TN(I,J)-TN(I-1,J)))
  200 CONTINUE
      DO 210 K=1,KNT
      ZVC1(K)=EXP(ZVC1(K))
      ZVC2(K)=EXP(ZVC2(K))
      IF(ZVC1(K).LE.1.) ZVC1(K)=0.
      IF(ZVC2(K).LE.1.) ZVC2(K)=0.
      YY1(J-1,K)=ZVC1(K)*SN(J)
      XX1(J-1,K)=ZVC1(K)*CS(J)
      YY2(J-1,K)=ZVC2(K)*SN(J)
      XX2(J-1,K)=ZVC2(K)*CS(J)
  210 CONTINUE
      WRITE(6,270)  ITHETA(J),(ZVC1(K),K=1,KNT)
      WRITE(6,280) (ZVC2(K),K=1,KNT)
      DO 220 K=1,KNT
      ZVC1(K)=0.
      ZVC2(K)=0.
      LVC(K)=1
  220 CONTINUE
  230 CONTINUE
C
C****** PLOT TEMPERATURE CONTOURS
C
```

```
UBROUTINE CNPLTP     76/76   OPT=2                    FTN 4.2+178

      RPLOT=RPLOTT
      KNP=KNT
      CALL CNPLOT
  240 FORMAT(1H1,35X,*----- COORDINATES OF STREAM FUNCTION CONTOURS ---
     1-*)
  250 FORMAT(1H0,/,5X,5HANGLE,10X,1X,9HCONTOUR 1,1X,9HCONTOUR 2,1X,9HCO
     1TOUR 3,1X,9HCONTOUR 4,1X,9HCONTOUR 5,1X,9HCONTOUR 6,1X,9HCONTOUR
     2,1X,9HCONTOUR 8,1X,9HCONTOUR 9,1X,10HCONTOUR 10)
  260 FORMAT(20X,10F10.7)
  270 FORMAT(1H0,4X,I5,10X,10F10.4)
  280 FORMAT(20X,10F10.4)
  290 FORMAT(1H1,38X,*----- COORDINATES OF VORTICITY CONTOURS -----*)
  300 FORMAT(1H1,36X,*----- COORDINATES OF TEMPERATURE CONTOURS -----*)
      RETURN
      END
```

```
UBROUTINE CNPLOT     76/76   OPT=2                          FTN 4.2+178

      SUBROUTINE CNPLOT
C
C******
C       THIS SUBROUTINE PLOTS STREAM FUNCTION , VORTICITY AND TEMPERATUR
C                                    CONTOURS
C******
C
      DIMENSION CHAR(120)
      COMMON /GRID/ Z(81),E(81),ITHETA(31),SN(31),CS(31),CT(31),H3(81,3
     1              ),THETA(31)
      COMMON /PLOTC/ XX1(31,10),YY1(31,10),XX2(31,10),YY2(31,10),IYS,
     1               IXSTEP,JNH1,JNH,KNP,RPLOT,RPLOTU,RPLOTV,RPLOTT
      COMMON /INJN/ IN1,JN1,IN,JN,SH,SK,ST,KS,GR,PR,CCJ,CCG,DFU,DFG
      LEVEL 2 ,Z,XX1,IN1
      DATA BLANK,PLOT/1H ,1H./
C
      DX=RPLOT/(FLOAT(IXSTEP-1))
      DXHLF=DX/2.
      DO 10 L=1,120
      CHAR(L)=PLOT
   10 CONTINUE
      WRITE(6,20) CHAR
   20 FORMAT(1H1,120A1)
      DO 30 L=1,119
      CHAR(L)=BLANK
   30 CONTINUE
C*************************************************************************
C
C****** PLOT CONTOURS IN THE UPSTREAM SECTION
C
      XPLOT=RPLOT
   40 CONTINUE
      DO 60 JJ=1,JNH
      DO 60 K=1,KNP
      IF(ABS(XPLOT-XX1(JJ,K)).LE.DXHLF) GO TO 50
      GO TO 52
   50 LL=(FLOAT(IYS)/RPLOT)*YY1(JJ,K)+0.5
      IF(LL.EQ.0.OR.LL.GT.IYS) GO TO 52
      CHAR(LL)=PLOT
   52 IF(ABS(XPLOT-XX2(JJ,K)).LE.DXHLF) GO TO 55
      GO TO 60
   55 LL=(FLOAT(IYS)/RPLOT)*YY2(JJ,K)+0.5
      IF(LL.EQ.0.OR.LL.GT.IYS) GO TO 60
      CHAR(LL)=PLOT
   60 CONTINUE
      IF(XPLOT.LT.1.) GO TO 100
      WRITE(6,70) CHAR
   70 FORMAT(1X,1H.,120A1)
   80 CONTINUE
      DO 90 L=1,IYS
      CHAR(L)=BLANK
   90 CONTINUE
      IF(XPLOT.LE.(DX/1000.)) GO TO 130
      XPLOT=XPLOT-DX
      GO TO 40
  100 CONTINUE
      CL=1.-((XPLOT)**2)
```

```
UBROUTINE CNPLOT     76/76   OPT=2                          FTN 4.2+178

          LC=(FLOAT(IYS)/RPLOT)*SQRT(CL)+0.5
          IF(LC.EQ.0.OR.LC.GT.IYS) GO TO 110
          CHAR(LC)=PLOT
      110 CONTINUE
          WRITE(6,120) CHAR
      120 FORMAT(2X,120A1)
          GO TO 80
      130 CONTINUE
C*************************************************************************
C
C****** PLOT CONTOURS IN THE DOWN-STREAM SECTION
C
          XPLOT=DX
          NHJ=JNH-1
          NJ=JN-1
      140 CONTINUE
          DO 180 JJ=JNH,NJ
          DO 180 K=1,KNP
          IF(ABS(XPLOT+XX1(JJ,K)).LE.DXHLF) GO TO 150
          GO TO 160
      150 LL=(FLOAT(IYS)/RPLOT)*YY1(JJ,K)+0.5
          IF(LL.EQ.0.OR.LL.GT.IYS) GO TO 160
          CHAR(LL)=PLOT
      160 IF(ABS(XPLOT+XX2(JJ,K)).LE.DXHLF) GO TO 170
          GO TO 180
      170 LL=(FLOAT(IYS)/RPLOT)*YY2(JJ,K)+0.5
          IF(LL.EQ.0.OR.LL.GT.IYS) GO TO 180
          CHAR(LL)=PLOT
      180 CONTINUE
          IF(XPLOT.LT.1.) GO TO 210
          WRITE(6,70) CHAR
      190 CONTINUE
          IF(XPLOT.GE.(RPLOT-DX/1000.)) RETURN
          DO 200 L=1,IYS
          CHAR(L)=BLANK
      200 CONTINUE
          XPLOT=XPLOT+DX
          GO TO 140
      210 CONTINUE
          CL=1.-((XPLOT)**2)
          LC=(FLOAT(IYS)/RPLOT)*SQRT(CL)+0.5
          IF(LC.EQ.0.OR.LC.GT.IYS) GO TO 220
          CHAR(LC)=PLOT
      220 CONTINUE
          WRITE(6,120) CHAR
          GO TO 190
          END.
```

```
UBROUTINE PDNCOEF    76/76  OPT=2                    FTN 4.2+178

      SUBROUTINE PDNCOEF
C******
C      THIS SUBROUTINE EVALUATS SURFACE PRESSURE , DRAG COEFFICIENTS
C              AND LOCAL AND AVERAGE NUSSELT NUMBERS
C******
      DIMENSION  VTH(31),VTH2(31),AK(31),AK2(31),ANUL(31)
      DIMENSION  ANUL2(31)
      COMMON /GRID/ Z(81),E(81),ITHETA(31),SN(31),CS(31),CT(31),H3(81,3
     1             ),THETA(31)
      COMMON /OLDV/ UO(81,31),GO(81,31),TO(81,31)
      COMMON /NEWV/ UN(81,31),GN(81,31),TN(81,31)
      COMMON /VON/ VN(81,31)
      COMMON /INJN/ IN1,JN1,IN,JN,SH,SK,ST,KS,GR,PR,CCJ,CCG,DFU,DFG
      COMMON /GRAF/ IGRAPH,NG
      COMMON /TSTEP/ RX(81),TIME
      LEVEL 2 ,Z,UO,UN,VN,IN1,IGRAPH,RX
C
      DO 10 J=2,JN
      DO 10 I=1,IN1
      VN(I,J)=GN(I,J)/H3(I,J)
   10 CONTINUE
      S1=1./(12.*SH)
      S2=1./(12.*SK)
      S3=2./(SK*SK*ST)
C*************************************************************************
C
C****** EVALUATE FRONT STAGNATION PRESSURE COEFFICIENT
C
C****** AT I=1,J=1  T=1 AND AT I=IN1,J=1. T=0.
C****** ON SYMMETRY AXIS (J=1) STREAM FUNCTION IS ZERO
C****** AT OUTER BOUNDARY VORTICITY IS ZERO
C
      YUZ=0.
      YVZ=0.5*S2*(48.*VN(1,2)-36.*VN(1,3)+16.*VN(1,4)-3.*VN(1,5))
      YTZ=0.5*1.
      DO 20 I=2,IN
      VZ=S2*(48.*VN(I,2)-36.*VN(I,3)+16.*VN(I,4)-3.*VN(I,5))
      UZ=S3*(UN(I,2)-UO(I,2))/E(I)
      TZ=TN(I,1)*E(I)
      YVZ=YVZ+VZ
      YUZ=YUZ+UZ
      YTZ=YTZ+TZ
   20 CONTINUE
      A1=SH*YVZ
      A2=SH*YUZ
      A3=SH*YTZ
      AKNOT=4.*A1+2.*GR*A3
C
C*************************************************************************
C
C****** EVALUATE SURFACE PRESSURE COEFFICIENT
C
C****** AT I=I AND J=1 (J=JN1) VOTICITY IS ZERO
C
      RSH3=6./(SH*SH*SH)
      RSHP4=3./SH+4.
      VTH(1)=0.$VTH(JN1)=0.
```

```
SUBROUTINE PDNCOEF    76/76   OPT=2                          FTN 4.2+178

      VTH2(1)=0.$VTH2(JN1)=0.
      DO 30 J=2,JN
      YY=S1*(-25.*VN(1,J)+48.*VN(2,J)-36.*VN(3,J)+16.*VN(4,J)-3.*VN(5,J
     1)
C
C****** EVALUATION OF SURFACE PRESSUR USING STREAM FUNCTION VALJES
C
      Y2=RSH3*UN(2,J)/SN(J)-RSHP4*VN(1,J)
      VTH(J)=2.*(YY+VN(1,J))
      VTH2(J)=2.*(Y2+VN(1,J))
   30 CONTINUE
      AK(1)=AKNOT
      AK2(1)=AKNOT
      DO 40 J=2,JN1
      AK(J)=AK(J-1)+0.5*SK*(VTH(J-1)+VTH(J))-2.*GR*(CS(J)-CS(J-1))
      AK2(J)=AK2(J-1)+0.5*SK*(VTH2(J-1)+VTH2(J))-2.*GR*(CS(J)-CS(J-1))
   40 CONTINUE
C
C*************************************************************************
C
C****** EVALUATE VISCOUS AND FORM DRAG COEFFICIENTS
C
      CF=0.
      CP=0.
      CP2=0.
      DO 50 J=2,JN
      SNS=SN(J)*SN(J)
      SN2=2.*SN(J)*CS(J)
      CF=CF+VN(1,J)*SNS
      CP=CP+AK(J)*SN2
      CP2=CP2+AK2(J)*SN2
   50 CONTINUE
      CDF=4.*SK*CF
      CDP=SK*CP
      CDP2=SK*CP2
      CDT=CDF+CDP
      CDT2=CDF+CDP2
C*************************************************************************
C
C****** EVALUATE LOCAL AND OVERALL NUSSELT NUMBER
C
      ANU0=0.
      DO 60 J=1,JN1
      ANUL(J)=S1*(-25.+48.*TN(2,J)-36.*TN(3,J)+16.*TN(4,J)-3.*TN(5,J))
      ANU0=ANU0+ANUL(J)*SN(J)
      ANUL(J)=-2.*ANUL(J)
      ANUL2(J)=ANUL(J)/ANUL(1)
   60 CONTINUE
      ANU0=-(ANU0*SK)
      WRITE(6,70)
   70 FORMAT(1H1,5X,5HANGLE,6X,3HVTH,11X,4HVTH2,10X,2HK ,10X,2HK2
     1,11X,2HKC,11X,3HVNS,10X,4HANUL,8X,5HRAANU)
      DO 90 J=1,JN1
      AKC=AK(J)-2.*A2
      WRITE(6,80) ITHETA(J),VTH(J),VTH2(J),AK(J),AK2(J),AKC,VN(1,J),
     1ANUL(J),ANUL2(J)
   80 FORMAT(5X,I4,8(2X,F11.5))
```

```
UBROUTINE PDNCOEF    76/76   OPT=2                          FTN 4.2+178

     90 CONTINUE
        WRITE(6,100)
    100 FORMAT(1X,///,10X,2HGR,10X,2HPR,10X,2HA1,10X,2HA2,9X,2HA3,10X,
       13HCDF,9X,3HCDP,7X,3HCDT,7X,4HCDP2,7X,4HCDT2)
        WRITE(6,110) GR,PR,A1,A2,A3,CDF,CDP,CDT,CDP2,CDT2
    110 FORMAT(4X,F9.3,4X,9(F11.5))
    120 CONTINUE
        AKNOT=AK(1)-2.*A2
        WRITE(6,130) TIME,AKNOT,ANUO
    130 FORMAT(10X,//,5X,*TOTAL TIME=  *,F12.5,5X,*AKNOT=  *,F10.5,
       15X,*OVERALL NUSSELT NO.=  *,F10.5)
        RETURN
        END
```

```
UBROUTINE RESTAB     76/76   OPT=2                              FTN 4.2+178

      SUBROUTINE RESTAB
C
C******
C      THIS SUBROUTINE PRINTS OUT STREAM FUNCTION , VORTICITY AND
C            TEMPERATURE FIELDS IN TABULAR FORM
C******
C
      COMMON /GRID/ Z(81),E(81),ITHETA(31),SN(31),CS(31),CT(31),H3(81,3
     1             ),THETA(31)
      COMMON /OLDV/ UO(81,31),GO(81,31),TO(81,31)
      COMMON /NEWV/ UN(81,31),GN(81,31),TN(81,31)
      COMMON /VOO/ VO(81,31)
      COMMON /VON/ VN(81,31)
      COMMON /TSTEP/ RX(81),TIME
      COMMON /INJN/ IN1,JN1,IN,JN,SH,SK,ST,KS,GR,PR,CCJ,CCG,DFU,DFG
      COMMON /NPRC/ NPRJ1,NPRG1,NPRU,NPRG,NTOTAL,MNPR,MXITER,NPRINT,
     1             NTIMES,MXU,MXUP
      COMMON /LRSTAB/ LRS1
      COMMON /GRAF/ IGRAPH,NG
      LEVEL 2 ,Z,UO,UN,VO,VN,RX,IN1,NPRU1,LRS1,IGRAPH
C
C****** LRS1=1 WRITE OLD VALUES OTHERWISE WRITE NEW VALUES
C
      IF(LRS1.EQ.1) GO TO 60
      WRITE(6,130)
      INN=IN1-10
      DO 10 K=1,INN,10
      K1=K+9
      WRITE(6,140) ((UN(I,J),I=K,K1),J=1,JN1)
      WRITE(6,150)
   10 CONTINUE
      WRITE(6,160) ((UN(I,J),I=IN1,IN1),J=1,JN1)
      WRITE(6,170)
   20 CONTINUE
      DO 30 K=1,INN,10
      K1=K+9
      WRITE(6,140)  ((VN(I,J),I=K,K1),J=1,JN1)
      WRITE(6,150)
   30 CONTINUE
      WRITE(6,160) ((VN(I,J),I=IN1,IN1),J=1,JN1)
   40 CONTINUE
      WRITE(6,180)
      DO 50 K=1,INN,10
      K1=K+9
      WRITE(6,140) ((TN(I,J),I=K,K1),J=1,JN1)
      WRITE(6,150)
   50 CONTINUE
      WRITE(6,160) ((TN(I,J),I=IN1,IN1),J=1,JN1)
      RETURN
C*************************************************************************
C
   60 CONTINUE
      TIME=TIME-ST
      IF(TIME.LT.0.0) TIME=0.
      WRITE(6,120) GR,PR,TIME
      WRITE(6,130)
      INN=IN1-10
```

```
BROUTINE RESTAB     76/76   OPT=2                          FTN 4.2+178

      DO 70 K=1,INN,10
      K1=K+9
      WRITE(6,140) ((UO(I,J),I=K,K1),J=1,JN1)
      WRITE(6,150)
   70 CONTINUE
      WRITE(6,160) ((UO(I,J),I=IN1,IN1),J=1,JN1)
      WRITE(6,170)
      DO 80  J=2,JN
      DO 80  I=1,IN1
      VO(I,J)=GO(I,J)/H3(I,J)
   80 CONTINUE
      DO 90 K=1,INN,10
      K1=K+9
      WRITE(6,140) ((VO(I,J),I=K,K1),J=1,JN1)
      WRITE(6,150)
   90 CONTINUE
      WRITE(6,160) ((VO(I,J),I=IN1,IN1),J=1,JN1)
  100 CONTINUE
      WRITE(6,180)
      DO 110 K=1,INN,10
      K1=K+9
      WRITE(6,140) ((TO(I,J),I=K,K1),J=1,JN1)
      WRITE(6,150)
  110 CONTINUE
      WRITE(6,160)  ((TO(I,J),I=IN1,IN1),J=1,JN1)
      RETURN
  120 FORMAT(1H0,///,15X,*GRASHOF NO. = *,F12.5,10X,*PRANDTL NO. = *,
     1F8.3,10X,*TOTAL TIME = *,F12.5)
  130 FORMAT(1H1,34X,*         STREAM FUNCTION              *)
  140 FORMAT(5X,10G12.5)
  150 FORMAT(1H0,56X,* ---------- *)
  160 FORMAT(5X,G12.5)
  170 FORMAT(1H1,30X,*         VORTCITY DISTRIBUTION        *)
  180 FORMAT(1H1,30X,*         TEMPERATURE DISTRIBJTION     *)
      END
```

TABLES

Gr	Pr	r_∞	h	k	Δt	ε_ψ	ε_G	ε_T
0.05	0.72	24.53	0.04	6^o	0.01	10^{-6}	10^{-3}	10^{-6}
1	0.72	24.53	0.04	6^o	0.01	10^{-6}	10^{-3}	10^{-6}
10	0.72	24.53	0.04	6^o	0.005	$5X10^{-6}$	$5X10^{-3}$	10^{-6}
25	0.72	24.53	0.04	6^o	0.001	$7.5X10^{-6}$	$7.5X10^{-3}$	10^{-6}
50	0.72	24.53	0.04	6^o	0.001	$2.5X10^{-5}$	10^{-2}	10^{-5}
125	0.72	24.53	0.04	6^o	0.001	$5X10^{-5}$	$5X10^{-2}$	$5X10^{-5}$
1250	10	24.53	0.04	6^o	0.0005	10^{-3}	10^{-1}	10^{-4}

TABLE 1: MAIN RESULTS AS THE SOLUTIONS OF THE TIME - DEPENDENT EQUATIONS APPROACH LATE-TIME STEADY STATE

ω_ψ	ω_G	ω_T	$\overline{Nu}$	K_o	K_π	C_{DF}	C_{DP}	C_{DT}
1.9	1.2	1.5	2.09	0.49	-0.40	1.13	0.59	1.72
1.6	0.65	1.5	2.34	6.32	-5.69	15.75	7.95	23.70
1.5	0.5	1.5	2.92	37.44	-33.60	78.25	42.36	120.21
1.5	0.5	1.5	3.30	81.59	-46.05	146.39	82.62	229.01
1.5	0.5	1.5	3.82	141.26	-54.43	236.11	138.18	374.29
1.5	0.5	1.5	4.25	297.28	-61.53	448.31	276.20	724.51
1.5	0.3	1.2	9.98	1988.35	-71.10	1958.01	1386.11	3344.12

TABLE 1 (CONTINUED)

Pr=0.72

Gr	0.05	1	10	25	50
$\overline{Nu}$	2.09	2.39	2.96	3.32	3.96
K_o	0.50	5.97	36.07	76.23	118.30
K_π	-0.40	-5.40	-31.26	-48.68	-12.66
C_{DF}	1.17	16.42	74.88	143.70	211.20
C_{DP}	0.58	7.58	41.29	87.08	105.45
C_{DT}	1.75	24.00	116.17	230.73	316.65

h=0.04 , k=6° , r_∞=24.53

TABLE 2: MAIN RESULTS OF THE SOLUTIONS OF THE TIME-INDEPENDENT EQUATIONS

$\overline{Nu}$ / Gr	PRESENT STUDY; TIME-DEPENDENT NUMERCIAL SOLUTION	PRESENT STUDY; TIME-INDEPENDENT NUMERICAL SOLUTION	HOSSAIN (1966); ANALYTICAL SOLUTION	YUGE (1961); EXPERIMENTAL METHOD	TSUBOUCHI AND SATO (1960); EXPERIMENTAL METHOD	MATHERS et-al (1957); EXPERIMENTAL METHOD	RANZ AND MARSHALL (1952); EXPERIMENTAL METHOD
0.05	2.09	2.09	2.05	2.32	2.43	2.18	2.42
1	2.34	2.39		2.67	2.90	2.54	2.90
10	2.92	2.96		3.20		3.26	
25	3.30	3.32		3.51		3.73	
50	3.82	3.96		3.80		4.05	
125	4.25			4.26		4.59	
1250	6.12			6.03		6.60	
12500	9.32			9.10		10.19	

TABLE 3: COMPARISON OF AVERAGE NUSSELT NUMBER FOR DIFFERENT GRASHOF NUMBERS FOR A PRANDTL NUMBER OF 0.72

RESULTS QUATED AT t=1.5

r_∞	h	k	$\overline{Nu}$	K_o	K_π	C_{DF}	C_{DP}	C_{DT}
24.53	0.04	6^o	2.175	32.90	-14.38	65.01	33.39	98.40
24.53	0.04571	6^o	2.10	29.18	-12.98	58.19	27.90	86.09
24.53	0.04	9^o	2.12	30.71	-13.53	59.43	29.29	88.72
16.44	0.04	6^o	2.10	29.98	-15.21	60.41	29.83	90.24

TABLE 4: EFFECTS OF VARIATIONS OF MESH SIZES AND PROXIMETY OF THE OUTER BOUNDARY ON THE RESULTS OF GRASHOF NUMBER OF 10 AND PRANDTL NUMBER OF 0.72 SOLUTION

	Gr=25 , Pr=0.72		Gr=50 , Pr=0.72	
	r_∞=24.53	r_∞=20.08	r_∞=24.53	r_∞=16.44
h	0.04	0.04	0.04	0.04
k	6°	6°	6°	6°
$\overline{Nu}$	3.30	3.11	3.82	3.32
K_o	81.59	75.15	141.26	130.19
K_π	-46.05	-50.26	-54.43	-57.62
C_{DF}	146.39	138.24	236.11	217.98
C_{DP}	82.62	78.95	138.18	130.75
C_{DT}	229.01	217.19	374.29	348.73

TABLE 5: EFFECT OF PROXIMETY OF THE OUTER BOUNDARY ON THE RESULTS OF GRASHOF NUMBERS OF 25 AND 50 FOR A PRANDTL NUMBER OF 0.72

	Gr=50, Pr=100	Gr=12500, Pr=10
r_∞	24.53	11.02
h	0.04	0.04
k	6^o	6^o
$\overline{Nu}$	8.21	16.82
K_o	122.6	12077.34
K_π	-57.37	3904.00
C_{DF}	195.04	8700.77
C_{DP}	114.61	6606.85
C_{DT}	309.65	15307.62

TABLE 6: LATE-TIME STEADY STATE RESULTS FOR A GRASHOF NUMBER OF 50 AND A PRANDTL NUMBER OF 100, AND FOR A GRASHOF NUMBER OF 12500 AND A PRANDTL NUMBER OF 10 SOLUTIONS

TIME ,t	VARIABLE	ANGLE (DEGREES), Θ			
		0	60	120	180
28	Nu_Θ	2.127	2.107	2.066	2.044
	ζ_s	0.000	0.176	0.177	0.000
	K_Θ	0.452	0.249	-0.157	-0.360
30	Nu_Θ	2.130	2.109	2.065	2.041
	ζ_s	0.000	0.181	0.183	0.000
	K_Θ	0.463	0.254	-0.164	-0.373
32	Nu_Θ	2.131	2.110	2.064	2.041
	ζ_s	0.000	0.184	0.187	0.000
	K_Θ	0.473	0.260	-0.170	-0.383
34	Nu_Θ	2.132	2.110	2.064	2.040
	ζ_s	0.000	0.185	0.191	0.000
	K_Θ	0.481	0.264	-0.175	-0.394
36	Nu_Θ	2.132	2.110	2.064	2.040
	ζ_s	0.000	0.186	0.192	0.000
	K_Θ	0.489	0.267	-0.179	-0.402

TABLE 7: VALUES OF LOCAL NUSSELT NUMBER, SURFACE VORTICITY AND SURFACE PRESSURE AS THE SOLUTIONS OF THE EQUATIONS APPROACH LATE-TIME CONDITION FOR A GRASHOF NUMBER OF 0.05 AND A PRANDTL NUMBER OF 0.72

TIME, t	VARIABLE	ANGLE (DEGREES), θ			
		0	60	120	180
11	Nu_θ	2.575	2.426	2.040	1.783
	ζ_s	0.000	2.394	2.416	0.000
	K_θ	5.955	2.982	-2.670	-4.250
12	Nu_θ	2.651	2.488	2.089	1.812
	ζ_s	0.000	2.501	2.551	0.000
	K_θ	6.157	3.092	-2.912	-5.011
13	Nu_θ	2.687	2.523	2.114	1.824
	ζ_s	0.000	2.559	2.632	0.000
	K_θ	6.277	3.135	-3.023	-5.446
14	Nu_θ	2.695	2.539	2.123	1.828
	ζ_s	0.000	2.573	2.642	0.000
	K_θ	6.309	3.140	-3.073	-5.586
15	Nu_θ	2.700	2.540	2.125	1.828
	ζ_s	0.000	2.573	2.642	0.000
	K_θ	6.320	3.141	-3.075	-5.691

TABLE 8: VALUES OF LOCAL NUSSELT NUMBER, SURFACE VORTICITY AND SURFACE PRESSURE AS THE SOLUTIONS OF THE EQUATIONS APPROACH LATE-TIME CONDITION FOR A GRASHOF NUMBER OF 1 AND A PRANDTL NUMBER OF 0.72

TIME, t	VARIABLE	ANGLE (DEGREES), θ			
		0	60	120	180
3.5	Nu_θ	3.62	3.32	2.40	1.61
	ζ_s	0.00	12.81	11.84	0.00
	K_θ	35.08	14.08	-19.24	-24.44
4	Nu_θ	3.69	3.38	2.47	1.69
	ζ_s	0.00	12.99	12.02	0.00
	K_θ	36.47	13.05	-23.87	-29.64
4.5	Nu_θ	3.73	3.42	2.51	1.73
	ζ_s	0.00	13.09	12.11	0.00
	K_θ	37.10	12.41	-26.65	-32.99
5	Nu_θ	3.76	3.45	2.54	1.76
	ζ_s	0.00	13.14	12.15	0.00
	K_θ	37.31	12.15	-27.91	-33.40
6	Nu_θ	3.78	3.47	2.55	1.78
	ζ_s	0.00	13.15	12.15	0.00
	K_θ	37.44	12.01	-28.72	-33.60

TABLE 9: VALUES OF LOCAL NUSSELT NUMBER, SURFACE VORTICITY AND SURFACE PRESSURE AS THE SOLUTIONS OF THE EQUATIONS APPROACH LATE-TIME CONDITION FOR A GRASHOF NUMBER OF 10 AND A PRANDTL NUMBER OF 0.72

TIME, t	VARIABLE	ANGLE (DEGREES), θ			
		0	60	120	180
1	Nu_θ	3.49	3.14	2.10	1.26
	ζ_s	0.00	22.69	19.98	0.00
	K_θ	71.82	31.86	-25.24	-28.06
1.25	Nu_θ	3.81	3.45	2.35	1.40
	ζ_s	0.00	24.18	21.36	0.00
	K_θ	76.74	29.94	-37.41	-37.51
1.5	Nu_θ	3.99	3.64	2.48	1.47
	ζ_s	0.00	24.85	21.22	0.00
	K_θ	79.75	28.86	-43.15	-42.80
1.75	Nu_θ	4.09	3.72	2.56	1.49
	ζ_s	0.00	25.15	22.03	0.00
	K_θ	80.85	28.26	-46.59	-45.51
2	Nu_θ	4.14	3.76	2.58	1.50
	ζ_s	0.00	25.25	22.06	0.00
	K_θ	81.59	28.37	-47.29	-46.05

TABLE 10: VALUES OF LOCAL NUSSELT NUMBER, SURFACE VORTICITY AND SURFACE PRESSURE AS THE SOLUTIONS OF THE EQUATIONS APPROACH LATE-TIME CONDITION FOR A GRASHOF NUMBER OF 25 AND A PRANDTL NUMBER OF 0.72

TIME, t	VARIABLE	ANGLE (DEGREES), θ			
		0	60	120	180
0.6	Nu_θ	3.69	3.28	2.08	1.15
	ζ_s	0.00	36.55	30.99	0.00
	K_θ	127.53	56.70	-36.54	-30.59
0.85	Nu_θ	4.30	3.87	2.51	1.39
	ζ_s	0.00	39.08	32.40	0.00
	K_θ	135.12	52.47	-57.18	-46.73
1.1	Nu_θ	4.66	4.20	2.78	1.50
	ζ_s	0.00	40.31	33.21	0.00
	K_θ	139.46	50.65	-65.69	-52.32
1.35	Nu_θ	4.78	4.32	2.90	1.53
	ζ_s	0.00	41.08	33.83	0.00
	K_θ	140.10	49.81	-69.49	-54.16
1.60	Nu_θ	4.82	4.36	2.91	1.54
	ζ_s	0.00	41.29	33.96	0.00
	K_θ	141.26	49.95	-70.00	-54.43

TABLE 11: VALUES OF LOCAL NUSSELT NUMBER, SURFACE VORTICITY AND SURFACE PRESSURE AS THE SOLUTIONS OF THE EQUATIONS APPROACH LATE-TIME CONDITION FOR A GRASHOF NUMBER OF 50 AND A PRANDTL NUMBER OF 0.72

TIME, t	VARIABLE	ANGLE (DEGREES), Θ			
		0	60	120	180
0.75	Nu_Θ	5.45	4.89	3.09	1.35
	ζ_s	0.00	81.45	63.70	0.00
	K_Θ	296.23	101.59	-124.35	-61.45
0.8	Nu_Θ	5.59	5.02	3.18	1.42
	ζ_s	0.00	81.69	63.70	0.00
	K_Θ	296.55	100.76	-125.37	-61.49
0.85	Nu_Θ	5.64	5.07	3.23	1.45
	ζ_s	0.00	81.78	63.71	0.00
	K_Θ	296.83	100.25	-126.00	-61.51
0.9	Nu_Θ	5.68	5.11	3.25	1.47
	ζ_s	0.00	81.82	63.71	0.00
	K_Θ	297.10	99.90	-126.19	-61.52
0.95	Nu_Θ	5.70	5.12	3.26	1.47
	ζ_s	0.00	81.82	63.71	0.00
	K_Θ	297.28	99.73	-126.29	-61.53

TABLE 12: VALUES OF LOCAL NUSSELT NUMBER, SURFACE VORTICITY AND SURFACE PRESSURE AS THE SOLUTIONS OF THE EQUATIONS APPROACH LATE-TIME CONDITION FOR A GRASHOF NUMBER OF 125 AND A PRANDTL NUMBER OF 0.72

TIME, t	VARIAVLE	ANGLE (DEGREES), Θ			
		0	60	120	180
0.15	Nu_Θ	12.93	11.39	5.62	0.45
	ζ_s	0.00	323.42	235.53	0.00
	K_Θ	1854.46	664.73	-578.8	243.21
0.17	Nu_Θ	14.79	13.17	7.18	0.49
	ζ_s	0.00	340.63	254.54	0.00
	K_Θ	1932.70	544.77	-607.41	68.73
0.19	Nu_Θ	15.75	14.11	7.93	0.52
	ζ_s	0.00	348.87	264.77	0.00
	K_Θ	1970.01	473.32	-623.30	-31.68
0.21	Nu_Θ	16.27	14.69	8.32	0.53
	ζ_s	0.00	351.71	270.45	0.00
	K_Θ	1986.48	432.85	-631.92	-69.88
0.24	Nu_Θ	16.53	14.83	8.42	0.54
	ζ_s	0.00	352.68	271.46	0.00
	K_Θ	1988.35	430.75	-632.72	-71.10

TABLE 13: VALUES OF LOCAL NUSSELT NUMBER, SURFACE VORTICITY AND SURFACE PRESSURE AS THE SOLUTIONS OF THE EQUATIONS APPROACH LATE-TIME CONDITION FOR A GRASHOF NUMBER OF 1250 AND A PRANDTL NUMBER OF 10

BIBLIOGRAPHY

Al-Taha, T.R.,
Ph.D. Thesis, University of London (1969)

Ames, W.F.,
"Nonlinear Partial Differential Equation in Engineering",
Academic Press, N.Y. (1965)

Aris, R.,
"Vector, Tensors and Basic Equations of Fluid Dynamics",
Prentice Hall, London (1962)

Batchelor, G.K.,
"An Introduction to Fluid Mechanics",
Camb. Univ. Press (1970)

Bird, R.B., Stewart, W.E., and Lightfoot, E.N.,
"Transport Phenomena", John Wiley, N.Y. (1960)

Birkhoff, G.,
"Hydrodynamic, A Study in Logic, Fact and Similitude",
Revised Edition, Princton Univ. Press, N.J. (1960)

Bruce, G.H., Peaceman, D.W., Rachford, H.H., Jr.,
Petroleum Transactions, AIME, 198, 79 (1953)

Chiang, T., Ossin, A., and Tien, C.L.,
Trans. ASME, J. Ht. Transfer
84, 537 (1964)

Crank, J., and Nicolson, P.,
Proc. Camb. Phil. Soc., 43 , 50 (1947)

Douglas, J., and Rachford, H.H.,
Trans. of the American Mathematical Soc., 82, 421 (1956)

Dufort, E.C., and Frankel, S.P.,
Maths. Tables and Other Aids to Computation,
7, 135 (1953)

Elenbaas, W.,
Physica, 9, 285 (1942)

Farzetdinov, M.M.,
PMM, 22, 393 (1958)

Fendell, F.E.,
J. Fluid Mech., 34, 163 (1968)

Forsythe, G.E., and Wasow, W.,
"Finite - Difference Methods for Partial Differential
Equations", Wiley, N.Y. (1960)

Forsythe, G.E.,
Rep. No. CS-147 Computer Science Dept.,
Stanford Univ. (1970)

Garner, F.H., and Hofman, J.M.,
J.A.I.Ch.E., 7, 148 (1961)

Gebhart, B.,
"Heat Transfer", McGraw Hill, N.Y. (1961)

Gosman, A.D., Pun, W.W., Runchal, A.K., Spalding, D.B., and Wolfshtein, M.,
"Heat and Mass Transfer in Recirculating Flow"
Academic Press, London (1969)

Hatim, M.H.,
Ph.D. Thesis, University of London (1975)

Hellums, J.D.,
Ph.D. Thesis, University of Michigan (1960)

Hellums, J.D., and Churchill, S.W.,
Chem. Eng. Prog. Symp. Series. 57, 75 (1961)

Hicks, D.L.,
SC-RR-69-728, Sandia Laboratories, Albuquerque,
New Mexico (1969)

Hossain, M.A.,
Ph.D. Thesis, Cornell Univeristy (1966)

Howarth, L.,
"Modern Developments in Fluid Dynamics",
Vol. 1, Oxford University Press (1953)

Jakob, M.,
"Heat Transfer", Vol. 1, John Wiley (1949)

Kreyszig, E.,
"Advanced Engineering Mathematics", 2nd Ed.,
John Wiley (1967)

Lamb, H.,
"Hydrodynamics", 6th Ed., Camb. Univ. Press (1932)

Lilly, D.K.,
U.S. Weather Bureau, Monthly Weather Review,
93, No. 1, 11 (1965)

Mahony, J.J.,
Proc. Roy. Soc. London, A, 238, 412 (1956-'57)

Mathers, W.G., Madden, A.G., and Piret, E.,
Ind. Eng. Chem. 49, 961 (1957)

McAdams, W.H.,
"Heat Transmission", 3rd Ed., McGraw Hill (1954)

Merk, H.J., and Prins, J.A.,
Appl. Sci. Res. A 4, 11 (1953)

Meyer, P.,
Institution of Chem. Engs 15, 127 (1937)

Mitchell, A.R.,
"Computational Methods in Partial Differential Equations"
John Wiley (1969)

Navier, "Memoire sur les Lois du Movement des Fluids",
Mem. de L'Acad.
des Sciences, VI, 389 (1822)

Pandya, D.V.,
Ph.D. Thesis, University of London (1967)

Peaceman, D.W., and Rachford, H.H. Jr.,
J. Soc. Indust. Applied Maths., 3, No. 1, 28 (1965)

Phillips, H., and Wiener, N.,
J. Mathematics and Physics, 2. 105 (1923)

Prandtl, L.,
Proc. 3rd Intern. Math. Congr. Heidelberg (1904)
Translated NACA TM 452 (1928)

Rafique, K.,
Ph.D. Thesis, University of London (1971)

Ranz, W.E., and Marshall, W.R., Jr.,
Chem. Eng. Prog. 48, 173 (1952)

Richardson, L.F.,
Trans. Roy. Soc. London, Ser. A, 210, 307 (1910)

Richtmyer, R.D., and Morton, K.W.,
"Difference Methods for Initial-Value Problems"
2nd Ed., John Wiley N.Y. (1967)

Roache, P.J.,
"Computational Fluid Dynamics" Hermosa Publishers (1972)

Sandoval, A.H.,
DIC Thesis, Imperial College (1965)

Schlichting, H.,
"Boundary Layer Theory", 6th Ed., McGraw Hill (1968)

Schutz, G.,
Int. J. Ht. Mass Tr., 6, 873 (1963)

Smith, G.D.,
"Numerical Solution of Partial Differential Equations"
Oxford University Press London (1965)

Sommerfield, A.,
"Partial Differential Equations in Physics"
Translated from German, Academic Press (1949)

Spiegel, M.R.,
"Vector Analysis", Schum Publication N.Y. (1959)

Stokes, G.G.,
Camb. Trans. VIII (Paper i, 75), 287 (1845)

Stokes, G.G.,
Trans. Camb. Phil. Soc., 9, 2, 8 (1851)

Thom, A.
Aero Res. Council Rep. and Memo. No. 1194 (1928)

Tsubouchi, T., and Sato, S.,
Rep. of the Inst. of High Speed Mech.,
Tohoku University, 12, 127 (1960-61)

Wolfshtein, M.,
Rep. SF/R/2, Mech. Eng. Dept., Imperial College,
London (1967)

Yamagata, K.,

Trans. Soc. Mech. Engrs. Japan, 9, 37, 132 (1943)

Yang, K.T., and Jerger, E.W.,

J. Ht. Transfer, Trans. ASME, 86, Ser. C,

1, 107 (1964)

Yuge, T.,

Trans. AMSE, C82, 214 (1960)